University of Alberta

The Role of TIMP3 in Diabetic Nephropathy, Cardiac and Vascular Diseases

by

Ratnadeep Basu

A thesis submitted to the Faculty of Graduate Studies and Research

in partial fulfillment of the requirements for the degree of

Doctor of Philosophy

Department of Physiology

Fall 2013

Edmonton, Alberta

ABSTRACT

Chronic diseases such as diabetes, cardiovascular and renal diseases are major health concerns globally. Cardiovascular diseases with diabetes comprise more than 50% of all deaths attributed to non-communicable diseases worldwide. Acquiring more than one of these diseases at the same time results in poorer prognosis compared to any individual disease. Pathological changes in cellular metabolism and extracellular matrix (ECM) remodelling that result in structural and functional damage are among the common and essential mechanisms that underlie diabetic nephropathy, diabetic cardiomyopathy, focal and systemic vascular diseases. ECM is the structural framework of an organ, and maintaining its integrity is essential for optimal structure and function of the cardiovascular and the renal system. A balance in the function of matrix metalloproteases (MMPs) and their four physiological inhibitors (TIMPs 1-4) is required for optimal ECM turnover. This balance is disrupted in pathological conditions. In addition to being a potent inhibitor of a number of MMPs, TIMP3 is the only ECM-bound TIMP whereby it can exert tissue-specific effects. TIMP3-deficiency has been linked to several cardiovascular and renal diseases, and this effect has been shown to be organ specific and stimulus dependant. We found that TIMP3 was protective in diabetic nephropathy without any contribution to diabetic cardiomyopathy, diastolic dysfunction associated with myocardial metabolic changes and impaired calcium handling. We found a novel role of TIMP3 in both focal (Abdominal aortic aneurysm, AAA) and systemic (Hypertension) vascular pathologies associated with ECM remodelling. In response to Ang II, TIMP3-deficiency

resulted in a pathologically suppressed hypertensive response due to excess degradation of vascular ECM which culminated to development of AAA upon prolonged exposure. Targeting MMP2 alone in TIMP3$^{-/-}$ mice exacerbated AAA with heightened inflammation and increased MMP9, however, a broad spectrum MMP inhibitor proved to be a successful approach in preventing AAA. In summary, my thesis explores the essential and optimal role of TIMP3 in the context of pathological ECM remodeling in cardiac, vascular and kidney diseases.

This Thesis Is Dedicated

In loving memory of my mother, Dr. Gouri Basu who inculcated in me the following……..

"Once you start working on something, don't be afraid of failure and don't abandon it. People who work sincerely are the happiest"

Chanakya
(Indian philosopher and teacher; 350-275 BC)

ACKNOWLEDGEMENTS

I would like to express my deepest gratitude to my supervisor, Dr. Zamaneh Kassiri without whom I could not have accomplished the work laid out this thesis. Her constant pursuit of brilliant ideas, trust in my abilities, mentorship and perseverance has shaped me both as a researcher and a better person.

I would like to sincerely thank all my collaborators especially; Dr. Gavin Oudit for entrusting me with various projects, independent from this thesis, and gave me immense confidence and has diversified my experience in science. His uncanny ability at translational research has helped me to link my scientific projects to deadly global diseases that continue to plague the world.

Special thanks to my supervisory committee members, Dr. Gary Lopaschuck and Dr. Peter Light for their invaluable suggestions and constant support throughout the course of my doctoral programme that guided my projects to its present state.

A heartfelt gratitude goes to all my present and past lab members, especially Dr. Vijay Kandalam and Dr. Sue Wang for their hard work as a team and support from the very beginning in this doctoral programme. I would also like to thank Donna Becker, for sharing with me her knowledge of echocardiography on small animals and being available at times of need.

Last but not least I would thank my family who made immense sacrifices for letting me pursue my ambition and encouraging me throughout this amazing and cherished journey of science.

CONTENTS

LIST OF FIGURES

LIST OF TABLES

LIST OF ABBREVIATIONS

A	late diastolic filling velocity during atrial contraction
A’	late diastolic myocardial velocity using tissue Doppler
AAA	abdominal aortic aneurysm
ADAMs	a disintegrin and metalloproteinase
AF	atrial fibrillation
AHA	American Heart Association
ANF	atrial natriuretic factor
ApoE	apolipoprotein E
Ar	pulmonary venous atrial reversal wave
AT1	angiotensin type-1 receptor
ATP	adenosine triphosphate
AV	atrioventricular
BNP	brain natriuretic peptide
BP	blood pressure
BW	body weight
CAD	coronary artery disease
CCRC	cumulative concentration response curve
CKD	chronic kidney disease
CO	cardiac output
COPD	chronic obstructive pulmonary disease
CP	creatine phosphate
CSA	cross-sectional area
CT	cycle threshold

CTGF	connective tissue growth factor
DC	diabetic cardiomyopathy
DHF	diastolic heart failure
DN	diabetic nephropathy
DNA	deoxyribonucleic acid
DOCA	deoxycorticosterone
DT	deceleration time
E	early diastolic filling wave velocity
E’	early diastolic myocardial velocity
EBM	endothelial cell basal media
ECM	extracellular matrix
EF	ejection fraction
ET	ejection time
ESRD	end stage renal disease
ETC	electron transport chain
EWDR	E wave deceleration rate
$FADH_2$	reduced flavin adenine dinucleotide
FB	fibroblast
FBS	fetal bovine serum
FDA	food and drug administration
FITC	fluorescein isothiocyanate
FS	fractional shortening
GFR	glomerular filtration rate
GPCR	G-protein coupled receptor

HBSS	Hank’s buffered salt solution
HDL	high density lipoprotein
HF	heart failure
HPLC	high performance liquid chromatography
HPRT	hypoxanthine-guanine phosphoribosyltransferase-1
HR	heart rate
IDDM	insulin dependant diabetes mellitus
IHD	ischemic heart disease
IVRT	isovolumic relaxation time
JGA	juxtaglomerular apparatus
1K1C	one-kidney, one clip
2K1C	two-kidney, one clip
LA	left atrium
LDL	low density lipoprotein
L-NAME	L-NG nitroarginine methyl ester
LV	left ventricle
LVEDP	left ventricle end-diastolic pressure
LVEDV	left ventricle end-diastolic volume
LVESV	left ventricular end-systolic volume
MCP	monocyte chemotactic protein
MCh	methacholine
MHC	myosin heavy chain
MI	myocardial infarction
MMP	matrix metalloproteinase

MMPi	matrix metalloproteinase inhibitor (pharmacological)
MPEF	multiphoton excitation fluorescence
mRNA	messenger RNA
MT1-MMP	membrane type 1-matrix metalloproteinase
NADH	reduced nicotinamide adenine dinucleotide
NADPH	reduced nicotinamide adenine dinucleotide phosphate
NCD	non communicable diseases
NCX	sodium calcium exchanger
NIDDM	noninsulin-dependant diabetes mellitus
NOX	NADPH oxidase
PBS	phosphate buffered saline
PCR	polymerase chain reaction
PCPE	procollagen C-terminal proteinase enhancer
PDGF	platelet-derived growth factor
PE	phenylephrine
PI3K	phosphatidylinositol-3-kinase
PKC	protein kinase C
PLB	phospholamban
PSP	peak systolic perfusion pressure
PV	pulmonary vein
PVs	pulmonary venous flow velocity in systole
PVd	pulmonary venous flow velocity in diastole
PVAr	pulmonary venous atrial flow reversal
RAAS	renin-angiotensin-aldosterone system

RNA	ribonucleic acid
RNS	reactive nitrogen species
ROS	reactive oxygen species
ROCK	*rho*-associated kinase
RT-PCR	real-time polymerase chain reaction
RV	right ventricle
S’	peak systolic annular motion
SERCA	sarco (endo) plasmic reticulum Ca^{2+} ATPase
SHR	spontaneous hypertensive rat
SkMA	skeletal muscle actin
SMC	smooth muscle cell
SR	sarcoplasmic reticulum
SV	stroke volume
TC-SBP	tail-cuff systolic blood pressure
TDI	tissue Doppler imaging
TFPI-2	tissue factor pathway inhibitor-2
TGF-β	transforming growth factor
TIMP	tissue inhibitor of metalloproteinase
TNF	tumor necrosis factor
TPR	total peripheral resistance
uPA	urokinase-type plasminogen activator
VcFc	velocity of circumferential fibre shortening
VEGF	vascular endothelial growth factor
VEGFR	vascular endothelial growth factor receptor

Vp	mitral inflow of propagation velocity
VSMC	vascular smooth muscle cells
VVG	Verhoeff-Van Geison staining
WHO	World Health Organization
WT	wild-type
WT-1	Wilms tumor 1 protein

LIST OF PREFIX

M	mega (10^{6})
k	kilo (10^{3})
c	centi (10^{-2})
m	milli (10^{-3})
μ	micro (10^{-6})
n	nano (10^{-9})

LIST OF UNITS

Hz	hertz
L	litre
m	metre
g	gram
Da	dalton
℃	degree Celsius
wk	week
d	day

LIST OF SYMBOLS

α	alpha
β	beta
γ	gamma

CHAPTER ONE

LITERATURE REVIEW

1.1 GENERAL INTRODUCTION

As scientific advances have been successful in eradicating or controlling most of the infectious diseases and increasing life expectancy, chronic non communicable diseases (NCD) have emerged as the major cause of mortality in the 21st century. NCD is defined as a slow progressive chronic, non-transmissible disease which is derived mainly from both modifiable (poor diet, physical inactivity, tobacco and alcohol consumption) and non-modifiable (racial or ethnic distribution) risk factors. The NCD comprise of a plethora of medical conditions such as cardiovascular diseases (CVD), diabetes, chronic kidney diseases (CKD), chronic respiratory diseases, cancer and mental illnesses (depression, schizophrenia). In 2010, the world health organization (WHO) reported NCD as the main cause of death globally (approximately 63% of all deaths worldwide). Among these, CVD (48%) and diabetes (3%) together contributed to more than half of all mortalities (more than 36 million) from NCDs worldwide [1].

CVD, diabetes and CKD are components of NCDs which impose a serious threat in terms of mortality and morbidity to the aging population in the developing and the developed countries (for Canadian statistics refer to **Fig. 1.1**). These diseases share a complex causal relationship in terms of etiology and/or complication. Obesity, old age and sedentary life style serve as common risk factors for all these three diseases which enhances the likelihood of individuals suffering from the three diseases at the same time, which are referred to as comorbidities. Recent

pathological and epidemiological studies have demonstrated common links between these diseases [2]. Though these common links are poorly understood, the quest for revealing these associations is the focus of my work.

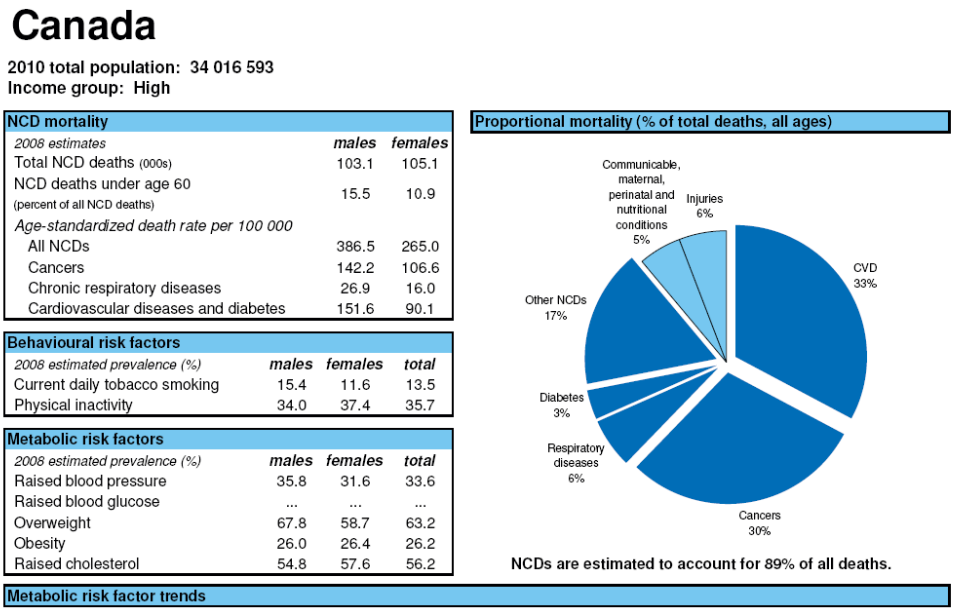

Canada

2010 total population: 34 016 593
Income group: High

NCD mortality

2008 estimates	*males*	*females*
Total NCD deaths (000s)	103.1	105.1
NCD deaths under age 60 (percent of all NCD deaths)	15.5	10.9
Age-standardized death rate per 100 000		
All NCDs	386.5	265.0
Cancers	142.2	106.6
Chronic respiratory diseases	26.9	16.0
Cardiovascular diseases and diabetes	151.6	90.1

Behavioural risk factors

2008 estimated prevalence (%)	*males*	*females*	*total*
Current daily tobacco smoking	15.4	11.6	13.5
Physical inactivity	34.0	37.4	35.7

Metabolic risk factors

2008 estimated prevalence (%)	*males*	*females*	*total*
Raised blood pressure	35.8	31.6	33.6
Raised blood glucose	...	...	...
Overweight	67.8	58.7	63.2
Obesity	26.0	26.4	26.2
Raised cholesterol	54.8	57.6	56.2

Proportional mortality (% of total deaths, all ages)

NCDs are estimated to account for 89% of all deaths.

Metabolic risk factor trends

Figure 1.1 NCD profile in Canada extracted from WHO Noncommunicable diseases profile 2011[2]

1.2 STRUCTURE AND FUNCTION OF THE CARDIOVASCULAR SYSTEM

1.2.1 Cardiovascular System

The mammalian cardiovascular system is comprised of a four chambered heart, and a network of vessels either arising from the ventricles (arteries) or terminating to the atria (veins). The heart and the network of blood vessels work as a closed unit which together forms the cardiovascular system.

Structure and function of the heart

The heart is a single, muscular organ with the right and left side separated by a muscular wall, septum. Each side of the heart functions as a separate pump and is further divided into an atrium and a ventricle. The heart wall consists of three layers, the inner layer composed of endothelial tissue (endocardium), the predominant muscular middle layer (myocardium) and a thin external layer (epicardium). The right atrium (RA) receives partially deoxygenated blood from the systemic circulation through the two major veins, the superior and inferior venae cavae. Deoxygenated blood flows from RA into the right ventricle (RV) during ventricular diastole (relaxation) through the right atrio-ventricular valve (tricuspid valve), which maintains a unidirectional flow via a pressure gradient from RA to RV. The RV then pumps the blood out through the pulmonary artery to the lungs for re-oxygenation. The oxygen rich blood enters the left atrium (LA) via the pulmonary veins and further flows into the LV through the bicuspid valve (also known as the mitral valve). The LV pumps the oxygenated blood into the systemic circulation through the largest artery of the body, the aorta which branches into a network of progressively smaller vessels and facilitates tissue perfusion. Even though both the RV and the LV simultaneously pump equal amounts of blood into the pulmonary and systemic circulation respectively during the contraction phase (ventricular systole), the LV performs a greater work as it pumps the blood into the systemic circulation with a higher resistance and a higher pressure compared to the pulmonary circulation (a low pressure and a low resistance system.

Structure and physiology of the arterial system

The arterial system consists of blood vessels (and their branches) which emerge from the ventricles and carry oxygen rich blood (except for the pulmonary artery) to the organs and tissues. The aorta is the largest artery that originates from the LV and gives rise to small arteries, which further divide into arterioles and capillaries in their decreasing order of lumen size. The large arteries, which conduct blood away from the heart and serve as pressure reservoirs. They impose minimal resistance, due to their larger lumen size, to facilitate forward flow of blood and as such, are referred to as conduit arteries. The arterioles and capillaries are responsible for the resistance of the arterial system. According to the Poiseuille Law ($R = 8L\eta/\pi r^4$, where R = resistance, L = length of the tube, η = viscocity of the fluid and r = vascular internal radius), resistance is inversely proportional to the fourth power of the radius. This highlights the impact of the lumen size in the arterial system on the blood pressure as even a small change in the arterial radius can manifest into a marked change in vascular resistance and subsequently the blood pressure. The peripheral resistance of the arterial system is equal to the sum of the resistances of all peripheral blood vessels in the circulatory network, and is referred to as total peripheral resistance (TPR). The arterial system is a part of a closed circulatory system where large arteries are an essential component to maintain circulatory homeostasis by undergoing large volume changes with minimal changes in pressure. This is owing to the property of the large arteries to act as elastic reservoirs to facilitate a transition of the

cardiac cycle from the systolic phase to its diastolic phase without a rapid fall in systemic blood pressure. These elastic arteries are able to accommodate a fraction of the blood volume ejected during cardiac systole and facilitate forward flow during diastole using the windkessel effect[3].

The arterial wall is comprised of 3 layers. The innermost layer (tunica intima) forms the luminal surface and is made up of a cellular monolayer called the endothelium. These endothelial cells are attached to a basal lamina which in order is held by an internal elastic lamina. The medial layer (tunica media) is comprised of smooth muscle cells (SMC) and connective tissue fibres, predominantly collagen and elastin. Collagen and elastin deposited by the SMCs of the media account for the mechanical properties of the arterial system and represents approximately 50% of the vessel's dry weight [4]. Elastin is arranged in the form of fenestrated sheets (lamellae) to allow for a uniform distribution of the aortic wall stress, whereas the collagen fibres arranged between these lamellar layers provide the tensile strength to overcome the high blood pressure and restrict aortic distension (passive wall tension). Surprisingly, the number of lamellar units (defined as an elastic lamella together with the SMCs attached to it) in a given arterial segment is directly proportional to the wall tension force [5] and remains unchanged after birth [6]. The outermost layer of the arterial wall, tunica adventitia, is separated from the adjacent medial layer by the external elastic lamina. This layer has abundant collagen in its extracellular matrix produced mainly by a varied population of native myofibroblast cells [7]. High content of collagen in

tunica adventitia provides structural strength against the extreme high blood pressures endured by the arterial wall and prevents their rupture. Apart from its protective effects, studies have shown that this outer compartment is extremely important for regenerative properties of the vascular wall. Recently, it has been shown that mature blood vessels contain residential progenitor cells that can differentiate into SMCs in response to stress or injury[8]. Nutrition to the aortic wall is provided in two ways. The sub-intimal avascular region equivalent to 29 laminar units of tunica media derive nutrition by transitional filtration from the lumen[9]. Outside this zone, nutrition is provided by fine feeding vessels (for nutrition and oxygen) called vasa vasorum located in the outer layer of the aortic wall. Though, in mice and other small mammals with fewer than 29 lamellar units in the medial region of the aortic wall have no discernable vasa vasorum [9], however, the tunica adventitia remains an important site of inflammation due to the presence of these feeding vessels restricted to this layer

1.2.2 Echocardiography on Small Animals

Cardiac performance within the physiological range involves systolic function, an adequate stroke volume ejected by the LV at a normal arterial pressure, and diastolic function, optimal filling of the LV without requiring elevation in LA pressure [10]. Echocardiographic imaging provides a non-invasive assessment of the systolic and diastolic cardiac function. In addition to the commonly used parameters to evaluate systolic function such as the ejection fraction (EF) and fractional shortening (FS), a number of measurements have been reported to

indicate diastolic function. These include left atrial size, pulmonary vein velocity, mitral Doppler flow, tissue Doppler and myocardial strain. It must be noted that the size of the subject is a critical factor in selecting appropriate parameters to accurately assess the diastolic dysfunction. For instance, certain parameters which have been proven to be useful in patients, cannot be used in rodent models due to the small size of the heart in these animals which can restrict the spatial resolution at times.

1.2.2.1 Analysis of the Systolic Function

Assessment of the LV contraction phase (referred to as cardiac systole) is essential in the understanding of LV hemodynamics in normal and disease states. LV contractile function can be reported by different parameters, such as ejection fraction (EF) which is defined as the percentage of the blood volume that is ejected out of the LV during a single contraction compared to the total volume of blood in the LV: EF(%) = (LVEDV-LDESV/LVEDV) x 100; where LVEDV= left ventricular end diastolic volume, LDESV= left ventricular end systolic volume. EF remains an ideal parameter for assessing LV contractility due to its easy applicability and lack of complex calculation. The physiological range of EF is > 50% but usually remains higher than 60% in small animals. The second widely used parameter that evaluates systolic function is LV fractional shortening (FS) and is defined as the percentage change in LV diameter during systole and diastole; FS(%) =(LVEDd-LVEDs/LVEDd)x100; where LVEDd= left ventricular diameter during diastole, LVEDs= left ventricular diameter during systole. These

parameters are acquired from motion mode images (M mode) of the LV in either short axis or long axis parasternal view (illustrated in Chapter 2, **Fig. 2.5**). A third derived parameter from FS is widely used to assess systolic function and known as velocity of circumferential shortening (VcFc) which relates to instantaneous velocity of fibre shortening to maximum wall tension during LV contraction[11].

1.2.2.2 Analysis of Cardiac Diastolic Function

As opposed to the systolic function, evaluation of the diastolic function remains controversial and difficult to interpret. Invasive methods of LV pressure-volume relationship during a cardiac cycle and measurement of the rate of LV pressure decline during isovolumetric relaxation using catheters have been regarded as the gold standard technique in assessing diastolic function. However, the advent of Doppler studies has allowed to evaluate many aspects of LV filling (diastolic function), besides being a non-invasive and more practical method for routine clinical use. The echocardiographic parameters used to evaluate LV filling pressure and remain as surrogate measurements of diastolic function in patients and in small animals are obtained from various ways that include left atrial size, mitral flow profile (isovolumic relaxation time, deceleration time, ratio of velocity during early (E wave) and atrial filling phase (A wave), pulmonary venous flow profile and tissue Doppler imaging.

Left Atrial (LA) Size

LA volume is a marker for chronic elevated left ventricular (LV) filling pressure and is used to assess diastolic dysfunction in humans[12, 13] and large and small

animals. In patients, it has been proposed that LA volume provides a more accurate prognostic compared to LA diameter, and should be included in routine clinical evaluations[14]. Measurement of the LA volume or diameter in rodents, although feasible, requires attention for accurate measurements given the small size of LA in these animals. M-mode images (motion modulation images) (**Fig. 1.2**) in the parasternal long axis view can be used to measure the maximal antero-posterior left atrial diameter and is used as left atrial size in rodents[15]. A progressive increase in LA size in association with changes in other parameters could indicate persistent elevation in LV filling pressure and can be used a marker for diastolic dysfunction.

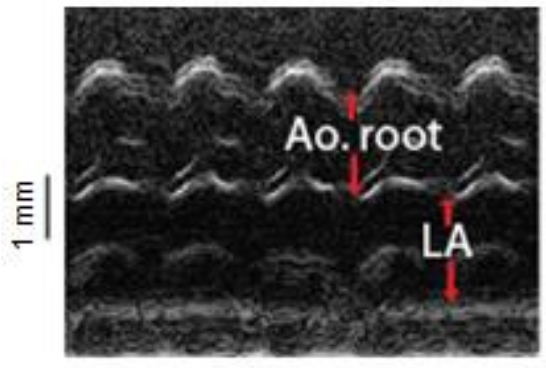

Figure 1.2 Representative Image of the murine left atrium (LA) with aortic root (Ao. Root)

LA and aortic root shown in red arrows, in M mode images taken from parasternal long axis view.

Mitral Flow Profile

Mitral flow is comprised of two wave forms, the E-wave and the A-wave (illustrated in Chapter 2, **Fig. 2.6**), and provides information about the LV filling dynamics. The E-wave represents the blood flow through the bicuspid valves

during the early filling phase of the LV, and as such can be affected by the rate of relaxation and compliance of the LV. The A-wave represents the blood flow during the active filling phase of LV and can be influenced by LA contractility and compliance of LV[16]. The ratio of E-wave to A-wave (E/A) is routinely used as a measurement of diastolic dysfunction. The time from the peak of the E-wave to the baseline is referred to as the Deceleration Time (DT), and represents the time required for equilibration between the LV pressure and LA pressure. In early stages of impaired LV relaxation, DT is prolonged, but as this impairment persists, DT shortens. Mitral flow profile can also provide information about the isovolumetric relaxation time (IVRT), the time from the closure of the aortic valve to the opening of the mitral valve. IVRT has been used for assessment of diastolic dysfunction in patients[17] as well as in rodents[15].

Although these measurements provide valuable information on kinetics of LV filling, it should be noted that these parameters can be influenced by a number of factors, such as preload, arrhythmia, and diseases that cause a hyperdynamic state of the heart. Moreover, it has been shown that DT and E/A ratio correlate better with mean LV diastolic pressure when EF < 50% but fails to sustain such correlation with preserved systolic functions (>50%)[18]. Myocardial relaxation disorder (i.e., decreased longitudinal velocity of the mitral annulus during early diastole and decreased propagation velocity mitral inflow), decreased compliance (shortened mitral A-wave duration and mitral deceleration time), and increased filling pressure (shortened IVRT and increased ratio between early diastolic mitral

and mitral annular velocities) have been known as the echocardiographic hall marks of diastolic dysfunction[19].

Tissue Doppler imaging (TDI)

Doppler echocardiography of left ventricular inflow has been widely used to assess LV diastolic function in humans[20] and in mice[21]. It depicts the mitral annular motion in the form of 2 waves, E'or Ea-wave and A'-wave, (**Fig. 2.7**) representing the tissue velocities during passive LV filling (E') and active LV filling and LA contraction (A'). These measurements can be made at the septal or the medial annulus. However, unlike the mitral flow, it is independent from confounding factors such as atrial and ventricular compliance, the rate of ventricular relaxation and left atrial pressure[19, 22]. The E'/A' and E/E' ratios have been used to monitor the progression of the disease states contributing to elevated LV filling pressures[23]. Septal annular velocities or the average of septal and lateral annular velocities could correlate better with mean LV diastolic pressure even in individuals with preserved systolic function (EF> 50%), thus providing an important parameter for evaluating diastolic dysfunction regardless of systolic function [24]. Boluyt et al (2004) reported that the age-associated differences in diastolic dysfunction include an increase in IVRT and a decrease in peak E-wave at the septal annulus and at the lateral annulus of the mitral valve[25]. Tissue Doppler has also been recently used to measure regional myocardial velocities by measuring endocardial versus epicardial velocities in a short axis view and were used to obtain strain rates to evaluate the rate of fractional deformity due to force

during systole [26]. The indices like myocardial velocities (wall motion velocity measured by Doppler imaging), deformity (strain) and the rate of deformity (strain rate) have been validated in mice using TDI[26]. Both myocardial velocities and strain rate have been found to be valid in assessing LV systolic function in mice. Prediction of LV remodeling using novel parameter such as peak radial strain rate obtained from TDI in murine model of myocardial infarction has been recently vaidated[27]. The Tei index is an echocardiography-defined Doppler index mmcalculated from the formula, Tei index= (IVRT + IVCT)/ET; where IVRT= isovolumic relaxation time, IVCT= isovolumic contraction time, ET= ejection time). Tei index can also be affected by heart rate changes induced by anaesthesia. Therefore, Tissue Doppler Tei index is more suitable for assessing overall LV function[28].

Pulmonary Venous (PV) Flow

As discussed earlier, LA size can serve as a marker of chronic diastolic dysfunction. The pulmonary venous (PV) flow (**Fig. 1.3**) that leads to LA, can also be measured by Doppler imaging. This measurement constitutes one retrograde and two anterograde waves, the A reversal (Ar)-, PVS- and PVD-wave, respectively[29]. Abnormal PV flow pattern as a consequence of increased atrial pressure can be observed in many types of diastolic dysfunction[30]. A major anatomical difference between human and mouse left atrium is that in humans, the LA has four pulmonary vein orifices compared to a single orifice in mice[29]. This difference in anatomy along with the markedly higher heart rate in mice (500-600

bpm) compared to humans (60-80 bpm), underlie the differently shaped PV flow wave in these two species. In mice, a small A-wave reversal (Ar) is followed by a S-wave that is smaller than the D-wave. In humans, however, the S-wave is larger than the D-wave. Thus, a normal pulmonary venous waveform in mouse could appear as a restrictive pattern by human standards. Impaired LV relaxation and reduced compliance result in decreased D-wave without altering the S-wave such that the S- to D-wave ratio increases and is indicative of early diastolic dysfunction. Interestingly, this change in the S-wave to D-wave ratio occurs in both, humans and mice, and as such is a reliable measure of diastolic dysfunction in both species.

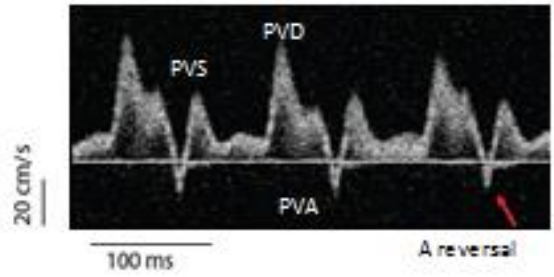

Figure 1.3 Representative image of the pulmonary venous flow in mouse heart

Corresponding pulmonary venous systolic wave (PVS), pulmonary venous diastolic wave (PVD) and pulmonary venous atrial wave (PVA) or A reversal (shown by a red arrow).

In humans and large mammals, the ratio of pulmonary vein A-reversal duration (PVAR) to mitral atrial duration is a distinct marker for elevated LV end diastolic pressure (LVEDP). In patients with LVEDP exceeding 15 mm Hg, PVAR duration exceeds mitral A wave duration [31] and can be an indicator of increased LV late diastolic pressure. However this ratio and its significant correlation with

diastolic dysfunction is yet to be established in rodents. In patients, the ratio of S-velocity to D-velocity is used to monitor progression of diastolic dysfunction as an increase in S/D velocity ratio is indicative of progression of diastolic dysfunction.

Mitral inflow of propagation velocity (Vp):

During ventricular diastole, a wave of relaxation starts from the apex and progresses further towards the base resulting in a apex-to-base pressure difference[32]. Impaired diastolic relaxation can blunt or obliterate the apex-to-base pressure gradient. Mitral inflow of propagation velocity (Vp) is used to assess the direct effects of the pressure gradient changes on the mitral inflow observed in a color Doppler and can be measured in more than one way. Few studies in mice have used this parameter which has shown correlation with elevated LV filling pressure. Similar to other echocardiagraphic parameteres, Vp has been shown to be affected by anesthesia in murine models which could result in misinterpretation of LV function in healthy hearts[21].

1.3 BASICS OF THE RENAL SYSTEM

The renal system (also known as the urinary system) consists of two kidneys as the main functional organs for the formation of urine, together with other components (ureters, urethra and urinary bladder) as accessory structures to guide the formed urine outside the body. Kidneys help maintaining the circulatory homeostasis of the body primarily by regulating plasma ionic composition, volume, osmolarity and pH. They act as a filter to eliminate metabolic waste

products (urea and uric acid from protein and nucleic acid catabolism) and foreign compounds (such as drugs, pesticides, food additives, etc.). Apart from being an important organ of excretion, kidneys perform secondary endocrine function by producing erythropoietin (a hormone that stimulates formation of red blood cells) and renin (an enzymatic hormone that regulates long term blood pressure by maintaining salt and water balance).

1.3.1 Structure and Function of the Kidneys

Macroscopically, each kidney is made up of an outer (cortex) and an inner (medulla) layer consisting of a number of striated triangles called the renal pyramids and formed by a specific arrangement of approximately 1 million microscopic structural and functional units, known as nephrons. Each nephron is made up of two components, i) a tuft of capillaries called the glomerulus arising from the afferent arteriole, which itself is a part of the renal artery. In addition to the endothelial cells of the capillaries, other cell types such as podocytes (surrounding epithelial cell layer with foot processes) and mesangial cells are associated with the glomerular capillaries and form a unit that regulates glomerular function. Mesangial cells provide structural sustenance to the capillaries by maintaining the structure of the mesangial matrix (**Fig. 1.4**) that holds the cells together and possess contractile properties provided by anchoring filaments attached to the glomerular basement membrane. Moreover, mesangial cells facilitate matrix to cell signalling and respond to capillary stretch by producing various signalling molecules and cytokines such as TGF-β1

(transforming growth factor isoform)[33], VEGF (vascular endothelial growth factor)[34], CTGF (connective tissue growth factor)[35] that mediate activation of PKC (protein kinase C)[36] and PI3K (phosphatidylinositol-3kinase)/Akt[37] intracellular signalling pathways. However, alterations in these pathways during pathological states and impaired cross talk between podocytes, endothelial cells and mesangial cells can adversely affect glomerular capillary growth and function. These capillaries re-join to form efferent arteriole of relatively smaller lumen compared to the afferent arteriole. This is the only case in the body where capillaries arising from an arteriole join to form another arteriole instead of a venule. A tubular component made up of a single layer of epithelial cells that begins with a double wall invagination around the glomerulus as a cup known as the Bowman's capsule and continues to form the proximal tubule, the loop of Henle, distal tubule and the collecting duct. The capsule together with the proximal tubule and the distal tubule is in the cortex while the loop of Henle is located exclusively in the medullary layer of the kidney. The vascular component and tubular components of the nephron are responsible for the formation of urine by three basic mechanisms in the order of their occurrence, i) glomerular filtration of protein free plasma in the glomerulus derived by a pressure gradient known as glomerular filtration pressure (GFP). Theoretically it can be calculated as the sum of the starling forces in the renal corpuscle such as glomerular capillary hydrostatic pressure (depends on mean arterial pressure), Bowman's capsule osmotic pressure that favours filtration counteracted by an opposing force created

by Bowman's capsule hydrostatic pressure and glomerular osmotic pressure. The glomerular filtration rate (GFR) is the volume of fluid that traverses from the glomerular capillaries into the Bowman's space per unit time. Approximately 20% of the plasma is filtered (filtration fraction) to form glomerular filtrate which passes through 3 layers also known as the glomerular membrane (the fenestrations in the wall of the glomerular capillaries, the basement membrane and the intrinsic glomerular cells (podocytes and mesangial cells) to enter the Bowman's capsule and further transported by the above mentioned tubular components. ii) On its way through the tubules, the molecules needed by the body (glucose, amino acids, vitamins etc.) and water is reabsorbed into the blood by a process known as tubular reabsorption. iii) A third process known as the tubular secretion allows the movement of certain ions (H^+, K^+) from the peritubular capillaries back into the tubules by diffusion and active transport, thereby forming urine that is excreted from the body.

The endocrine function of the kidney is carried out by a group of specialized vascular and tubular cells known as the juxtaglomerular apparatus (JGA) at the region where the distal tubule proximates the afferent and efferent arterioles of the same nephron. The granulated cells of the JGA secrete a hormone called renin into the blood which in turn activates angiotensinogen (a plasma protein synthesized in the liver) to angiotensin I. Subsequently, Angiotensin converting enzyme converts angiotensin I into angiotensin II (predominantly in the pulmonary capillaries) which further stimulates secretion of a hormone called the

aldosterone from the adrenal cortex. These hormones together form the renin-angiotensin-aldosterone system (RAAS) which is responsible for the regulation of blood pressure.

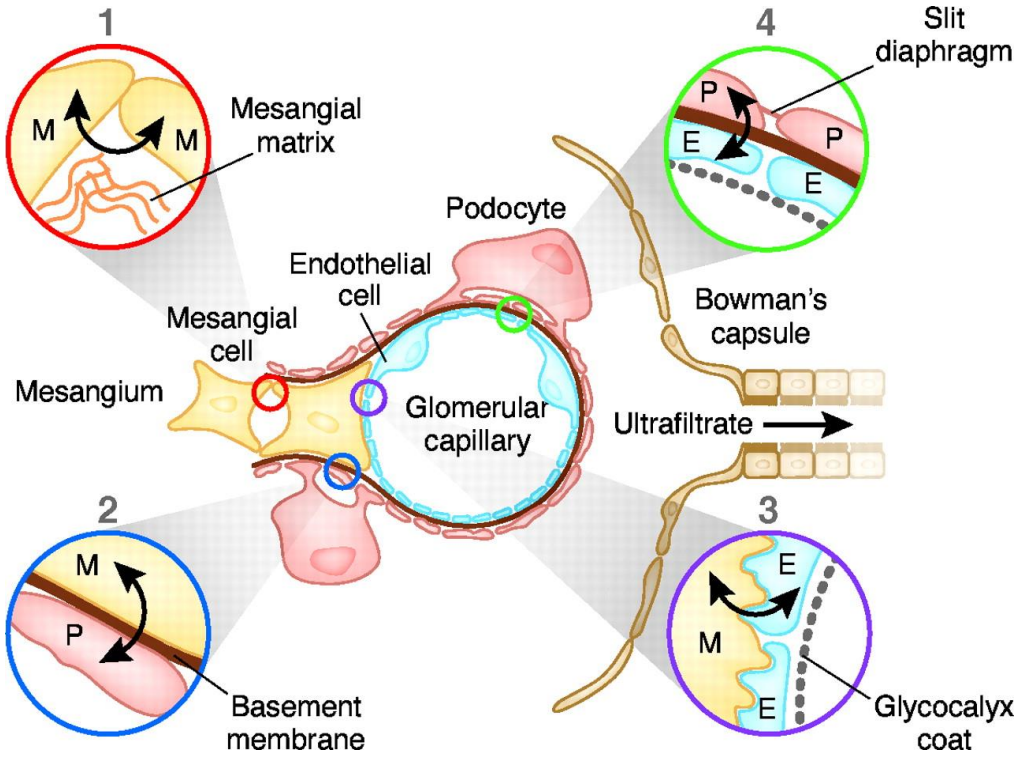

Figure 1.4 Intrinsic cells of the glomerulus which regulate GFR

Extracted from Schlöndorff *et al.* [38]

1.4 MAJOR NONCOMMUNICABLE DISEASES OF THE 21ST CENTURY

In recent years WHO has recognized that the NCDs are the primary cause of premature death and a major source of loss of productivity and growth in both developed and developing countries. In 2008, 36 million, out of 57 million global deaths were attributed to NCDs and this number is expected to rise (to 52 million)

by the year 2030[1]. Diseases caused by infections, nutritional deficiencies, maternal and perinatal conditions has benefited the most from modern medical advancements and are on a decline by 7 million a year during the same period where deaths from NCDs continue to surge[39]. Cardiovascular disease and diabetes are recognised among the 5 key NCDs targeted by WHO, while chronic kidney disease remains an important determinant of adverse health outcomes and a risk multiplier in these diseases [40].

1.4.1 Diabetes Mellitus

Diabetes mellitus is primarily a metabolic disorder that is associated with long-term micro and macro-vascular complications that lead to end organ damage (cardiac, vascular and renal, predominantly). Despite great advances in modern therapies, it has remained the fastest growing NCD globally. Though the pathophysiology of diabetes is multifactorial, the nature of end organ complications is comparable among the different types of diabetes. The classification of diabetes has changed enormously since the introduction of insulin dependent (IDDM) and non-insulin-dependent diabetes mellitus (NIDDM) criteria in 1979 by the National diabetes data group, primarily based on the pharmacological therapy applied. The current classification proposed by the American Diabetes Association in 1997 is based on the pathogenesis as oppose to therapy, and comprises of Type 1 DM, Type 2 DM, other types and gestational diabetes[41]. Type 1 DM previously known as IDDM (also known as juvenile diabetes) accounts for approximately 5-10% of all diabetics and is caused by an

autoimmune destruction of beta cells responsible for secretion of insulin in the pancreas. On the contrary, Type 2 DM affects more than 90-95% of people with diabetes and is caused by insulin resistance in tissues that leads to relative insulin deficiency. An intermediate state that lies between a normal glycemic state and frank diabetes that can exist for many years is known as pre-diabetes. According to the WHO, pre-diabetic state comprises of people with impaired fasting glucose (IFG, glucose > 110 mg/dl and < 126 mg/dl) and impaired glucose tolerance (IGT, 2hrs plasma glucose level on 75 g oral glucose tolerance test > 140 mg/dl and < 200 mg/dl)[42]. Pre-diabetes is regarded as a high risk state for developing frank diabetes. Irrespective of the cause, high plasma glucose largely underlies the long term risks of micro and macro-vascular complications in pre-diabetic and overt diabetic states.

1.4.1.1 Diabetic Cardiomyopathy

The effects of diabetes mellitus on cardiovascular diseases are well-established and it is estimated that the increase in the global diabetic populace in the next two decades will result in an upsurge in cardiovascular diseases[43, 44]. Diabetic cardiomyopathy was specifically identified for the first time by Rubler et al. in 1972 based on autopsy data from 4 diabetic patients[45]. However, diabetic cardiomyopathy remained an under recognized clinical entity due to the lack of conclusive consensus over its clinical symptoms, diagnostics and pathogenesis. Clinically, it is defined as abnormal myocardial function concomitant with diabetes in the absence of any co-morbidities such as epicardial or coronary artery

diseases, hypertension or valvular diseases[46]. The advent of improved diagnostics and non-invasive techniques (echocardiography and Doppler imaging) over the past two decades has demonstrated a mixed clinical scenario of Type 2 diabetic cardiomyopathy with LV hypertrophy[47], isolated diastolic dysfunction[48-51], systolic dysfunction in subclinical diabetics[52] along with asymptomatic early diabetics[53] and both concurrently[54]. The cardiomyopathy associated with type 2 diabetes is characterized by increased myocardial interstitial fibrosis, inflammation, vasoconstriction and endothelial dysfunction[55-57]. However, type 1 diabetic cardiomyopathy has been poorly studied. Studies using experimental rodent models of type1 diabetes suggest a wide plethora of cardiac phenotype from systolic dysfunction in isolated hearts of streptozotocin (STZ) induced diabetic mice[58], isolated diastolic dysfunction in bio breeding (BB) rats[59-61] to a combined (systolic and diastolic) dysfunction in STZ treated mice[62, 63] and rat[64] hearts. Most studies on animal models of Type 1 diabetes utilize streptozotocin (STZ)-induced diabetes models. STZ is a beta cell toxin which, in addition to eliminating pancreatic beta cells, it induces a strong inflammatory response[65, 66] which can result in diabetes-independent effects. Thus, it is important to explore the cardiac phenotype in a genetic model of Type1 diabetes without any compounding effects of external toxicity.

Pathophysiology and molecular basis of diabetic cardiomyopathy (DC)

Studies suggest that the cardiac complication in diabetes is a consequence of the direct effects of hyperglycaemia and hyperinsulinemia on the myocardial cells[67, 68].

Cultured rat cardiac myocytes and fibroblasts showed differential responses to high glucose and high insulin concentrations[69]. High glucose concentrations increased collagen synthesis and mRNA expression of fibronectin and TGF-β1 only in cardiac fibroblast, whereas high insulin concentrations increased DNA and collagen synthesis in fibroblasts and elevated protein synthesis and ANP secretion in cardiomyocytes[69]. Irrespective of the initial trigger, the mechanisms involving cardiac dysfunction in diabetic cardiomyopathy are multifactorial and can be broadly divided into 5 categories. These are i) myocyte structural loss and fibrosis, ii) myocardial hypertrophy, iii) impaired myocyte calcium handling and iv) impaired cardiac metabolism.

DC: Myocyte Structural Loss and Fibrosis

Healthy myocardial ECM is primarily comprised of collagen type I and collagen type III which is more specific to the heart [70]. In the myocardium of type I and II diabetic patients, collagen type III but not type I is found to increase [71]. region[72] Myocardial fibrosis involves diffuse accumulation of collagen in the interstitial and perivascular region, which is partly responsible for the replacement of functional contractile fibres post myocyte loss that leads to suppressed myocardial function in diabetic cardiomyopathy. An alteration in myocardial ultrastructure involves contractile protein loss, myocytolysis, vacuolization, and loss of contractile proteins as reported in STZ (streptozotocin) induced diabetic rat heart [73]. Nonetheless, alterations in the myocardial ultrastructure do not necessarily

precede cardiac dysfunction and reiterate the presence of other mechanisms responsible for cardiac dysfunction in early stages of diabetes.

DC: Myocardial Hypertrophy

Myocardial hypertrophy involves an increase in the size of individual myocytes that is associated with increased intracellular protein synthesis and accumulation of contractile units via activation of a number of signalling pathways. Hyperinsulinemia, a cardinal feature of type 2 diabetes prior to gradual beta cell failure enhances insulin exposure in the myocardium as it remains a major insulin responsive site during the early phase of diabetes, while other tissues become insulin resistant[74, 75]. Similar to growth factors, insulin bind to its membrane bound tyrosine kinase receptor to activate phosphoinositide 3-kinase (PI3K)/protein kinase B (Akt) mediated inactivation of glycogen synthases kinase-3β (GSK3β) to induce nuclear transcriptions such as nuclear factor of activated T-cells (NFAT-3) which regulate hypertrophic processes[76]. This PI3K mediated pathway also plays a key role in exercise induced physiological hypertrophy as mice with dominant negative PI3K expressed specifically in cardiac tissue failed to develop cardiac hypertrophy in response to exercise but not to pressure overload[77]. Myocyte hypertrophy is associated with transcriptional reactivation of fetal genes (ANF, βMHC) and cardiac myosin undergo transition from an adult to fetal isoform[78]. However, expression of constitutively active PI3K specific to cardiac tissue resulted in myocyte hypertrophy without any contractile dysfunction or activation of fetal genes[79]. This suggests that alternative

pathways might be predominant in diabetic cardiomyopathy which facilitates myocardial hypertrophy mediated cardiac dysfunction. Mitogenic activity of insulin via the PI3Kα-Akt-1 activation of mammalian target of rapamycin (mTOR) can lead to enhanced protein sysnthesis[80] seen in myocardial hypertrophy but do not sustain in states of chronic hyperinsulinemia where activation of Akt-1 is maintained indirectly by higher sympathetic activity[81].

DC: Impaired Myocyte Calcium Handling

A key feature of diabetic cardiomyopathy is impaired relaxation as indicated by investigations on various patients and animal models of diabetes[82-84]. Under physiological conditions, myocyte contraction is facilitated by a T-tubule action potential that activates voltage gated (L type) Ca^{2+} channels (with some contribution from the sodium calcium-exchanger (NCX))[85] and marks the onset of calcium induced calcium-release. Ca^{2+} influx through L-type calcium channels in turn activates the ryanodine receptors embedded in the sarcoplasmic reticulum (SR) that mediates the release of sarcoplasmic calcium in to the cytosol. The increase in cytosolic Ca^{2+} triggers the contraction coupling by binding to troponin and exposing myosin binding sites on the thin filaments of the sarcomere. This enables the sarcomere to contract which extrapolates to contraction of the muscle fibre and thereby generating the systolic phase of the heart. At the end of the muscle contraction, the cytosolic Ca^{2+} is pumped into the SR by Ca^{2+} ATPases located in the SR membrane (SERCA), or sent out of the cardiomyocyte by NCX. However, the contribution of the Na/Ca exchanger in the removal of cytosolic

Ca^{2+} is species dependent (approximately 30% in humans and rabbits but only 7% in rodent hearts) [86]. This uptake of Ca^{2+} marks the beginning of cardiac relaxation and requires ATP for the SR pumps to work efficiently. SERCA in turn is modulated by reversible phosphorylation at 3 different sites (serine 10 by protein kinase C, serine 16 by cAMP or cGMP dependant protein kinase and threonine 17 by Ca^{2+}-calmodulin dependant protein kinase) of an inhibitory protein called phospholamban (PLB) [87, 88]. Impaired relaxation in animal models of diabetic cardiomyopathy is associated with anomalous Ca^{2+} handling due to abnormal sarcolemma transport process [89-91], defective SR [92-94], impaired SERCA pump uptake due to impaired PLB phosphorylation [92], modification of the membrane structure [95], reparation by free radicals [96], reduced availability of ATP[97] and suppressed expression levels of SERCA [98-100].

DC: Impaired Cardiac Metabolism

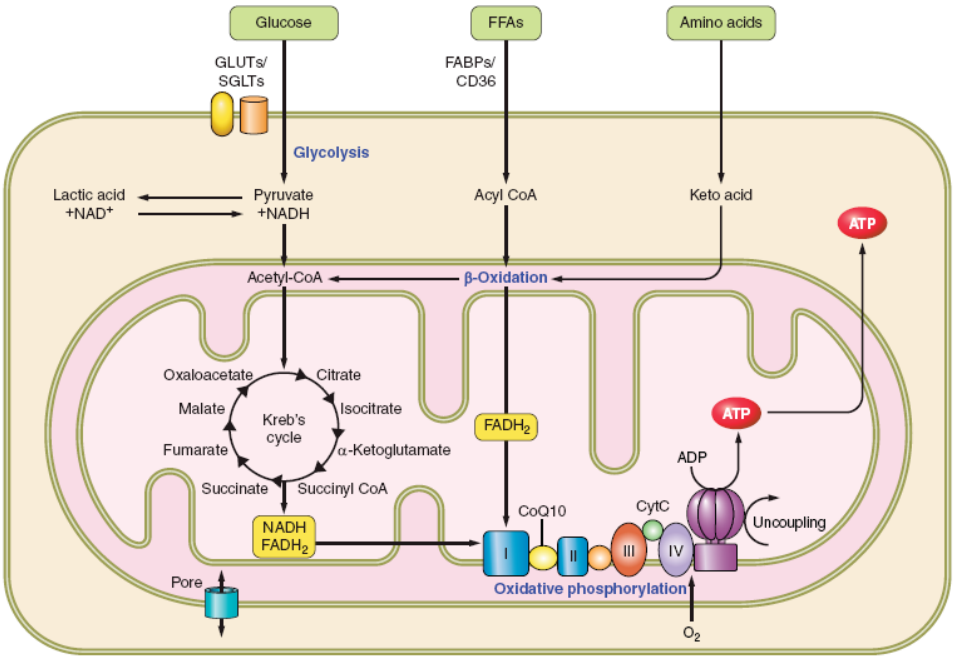

Figure 1.5 Metabolism of major sources of fuels for cellular energy

Extracted from Forbes *et al.* [101]

Under normal physiological conditions, predominantly fatty acid (FA) oxidation (60-90%) followed by glycolysis (refer to **Fig. 1.5**) derived pyruvate oxidation and other sources (lactate)[102] provide energy for the heart. Cardiac function under physiological condition requires a constant supply of adenosine triphosphate (ATP) which is resynthesized primarily by mitochondrial oxidative phosphorylation and a lesser proportion from glycolysis [103]. Diabetic myocardium in patients relies primarily on FA and ketones rather than glucose and lactate uptake compared to non-diabetic populace[104]. Anomalous FA metabolism has been implicated by many studies as the primary pathogenetic factor underlying diabetes-associated cardiovascular disease as evident by elevated rates of cardiac FA oxidation in db/db mice (a model of obesity induced diabetes)[105]. Glucose

transport in the diabetic myocardium in experimental animals with insulin deficiency is impaired[106-108] partially due to suppressed mRNA expression and protein levels of 2 main glucose transporters GLUT1 and GLUT4[106] which can be restored by insulin treatment in diabetic rats[109].

However, in a diabetic swine model, in spite of the decreased concentration of glucose transporters in the diabetic myocardium, the rates of glucose uptake remained comparable to non-diabetic, normoglycemic swine heart which is partly compensated by an elevated glucose gradient across the myocyte membrane due to high levels of extracellular glucose[110]. Additionaly, higher levels of plasma FFA causes a lower consumption of glucose and lactate such that the heart relies mainly on FA oxidation[104]. This shift of fuel is partly due to the inhibition of the pyruvate dehydrogenase complex (PDC) by acetyl CoA (generated in abundance from β oxidation of FA in the mitochondrial matrix) which mediates phosphorylation and inactivation of pyruvate dehydrogenase [111]. Experiments on perfused diabetic rat hearts, have shown to have low levels of glucose oxidation, even in the absence of exogenous fatty acids. This further suggests the importance of additional ways of suppressing glucose metabolism in diabetic hearts, such as PDH kinase mediated inhibition of pyruvate decarboxylation without affecting the ability of the enzyme PDH [112]. The FAs in the heart are derived from circulating free FA bound to albumin in the plasma, fatty esters in chylomicrons and very low density lipoproteins which remains elevated in diabetic state [113]. Once FA enters a myocyte, it either gets converted into fatty acyl CoA which further forms fatty

acyl carnitine to enter the mitochondria for β-oxidation, or it gets stored in the cell as triacylglycerol (TAG). Diabetes is associated with high contents of myocardial TAG [114] which could partly be due to elevated concentrations of free FA in the plasma and increased levels of myocardial CoA as found in diabetic "BB" Wistar rats [115]. TAG can be readily converted into esterified fatty acids and transported into the mitochondrial matrix for β oxidation. Esterified fatty acids, also known as long chain acyl CoA, are assisted by a triad of carnitine dependant enzymes (carnitine palmitoyltransferase I, carnitine: acyl carnitine translocase and carnitine palmitoyltransferase II) to enter the mitochondrial matrix where CPT I is the rate limiting enzyme for the uptake of FA [116].

In the light of these excess FA accumulation and myocardial energy substrate switch from carbohydrate to FA metabolism in the diabetic myocardium, many studies on experimental animals have associated diabetic cardiomyopathy to changes in myocardial energetics [117, 118] and improved cardiac function by controlling the glycemic status in patients [119].

1.4.1.2 Diabetic Nephropathy

Diabetic nephropathy (DN) remains the major cause of end stage renal disease (ESRD) which continues to increase in incidence and prevalence[120]. In patients with diabetes, excretion of low levels of albumin (microalbuminuria) concomitant with glomerular mesangial expansion and matrix deposition serve as the early signs before the onset of overt nephropathy.It takes about 10 years (or longer) before the actual onset of overt nephropathy and the development of

macroalbuminuria associated with decline in the GFR[121]. In order to investigate the pathogenesis of these crippling diabetic complications, animal models of diabetes serve as useful tools with advantages of genetic mouse models such as Akita mice (a genetic mouse model of type 1 diabetes) that closely recapitulates human DN over chemically induced diabetic models have been thoroughly verified [122]. DN-associated changes, such as kidney hypertrophy, glomerular basement membrane thickening, mesangial expansion and progressive proteinuria are well recognised structural and functional alterations associated with changes primarily in the glomerulus and the proximal tubules, which account for more than 90% of the cortical mass in the kidney [123, 124].

The onset of overt DN and its progression is a very complex process given the diversity of renal cellular structure and function. The symptoms vary from a state of hyperfiltration to a decline in GFR over the course of the disease. Moreover, pathological changes such as oxidative stress, tubulointerstitial fibrosis, cellular hypertrophy and inflammation affect a variety of renal cells including the endothelial and the smooth muscle cells of the renal microvasculature, mesangial cells and podocytes of the glomerulus, epithelial cells of the tubular and collecting duct.

DN: Renal hypertrophy and glomerular matrix remodelling

An early feature of a diabetic kidney is its enlargement that is associated with hypertrophy and hyperplasia of resident renal cells [125]. DN involves structural changes that involve renal hypertrophy in the early stages of the disease and

progresses to a more distinctive, irreversible feature of extracellular matrix accumulation in the glomerulus, called the nodular glomerulosclerosis, in its more advanced stages of diabetes. Evidence from morphometric studies performed in patients with type 1 diabetes [126] and experimental diabetic animals [127] revealed that thickening of glomerular basement membrane and hypertrophy closely accompany thickening of the tubular basement membrane and tubuloepithelial hypertrophy, and mark the advent of an irreversible alteration in the form of tubulointerstitial fibrosis and atrophy [127, 128]. Moreover, animal studies on DN have shown that renal cells along the entire nephron that undergo hypertrophy, possess the ability to proliferate at any point of time in the disease process depending on the availability of growth factors, growth factor receptors and their specific genetic predisposition [129, 130]. However, ex vivo cell culture of mesangial cells from mouse[131] and human[132] exposed to pathological concentration of glucose, simulating diabetic condition had proliferative effects in the first 48 hours of exposure but gets inhibited with prolonged exposure.

The initial proliferative response is attributed to the stimulation of PDGF-B (platelet-derived growth factor-B) whereas the activation of endogenous TGFβ in the later phase of glucose exposure inhibits cellular proliferation and induces hypertrophy that progresses to inflammation and fibrosis mediated renal injury. These processes are accompanied by an increase in glomerular capillary size that leads to alterations in glomerular hemodynamics (increased intraglomerular pressure and capillary wall stress), release of growth factors and cytokines

(TGFβ)[133] along with several vasoactive molecules (Ang II, endothelin-1) [134] which mediate imbalance of matrix proteins and eventually leads to mesangial matrix expansion.

DN: Protein kinase C mediated renal injury

Hyperglycemia, irrespective of the type of diabetes, induces tissue damage due to high intracellular levels of glucose particularly in cell types which are unable to control uptake of glucose efficiently. Though most cell types are able to reduce glucose uptake when exposed to hyperglycemia, a few are prone to damage and mediate end stage diabetic complications such as capillary endothelial, mesangial and Schwann cells[135, 136]. Increased intracellular glucose induces synthesis of diacylglycerol (DAG) which in turn activates different isoforms of protein kinase C in a cell specific manner in the kidneys[137, 138]. Renal activation of PKC occurs within a few days of induction of diabetes[138] and has also been demonstrated in ex vivo studies of cultured renal cells exposed to high concentrations of glucose[139].

Various isoforms of PKC are grouped based on their activation profile, such as classical (PKC, -β, -γ and -α) which require both intracellular calcium and DAG, novel (PKC, -δ, -ε, -η, -θ) that need only DAG and atypical (PKC, -ζ, -λ) which do not require DAG for their activation. However, various studies have revealed that hyperglycemia-induced activation of diverse isoforms of PKC in renal cells is tissue specific such as PKCα and PKCβ in glomerular membrane fraction[140], and membrane linked PKCδ and PKCε in diabetic rat glomerular cells[141], could partly elucidate the differential growth response of specific renal resident cells during

the progression of diabetes. Moreover, growth factors and vasoactive components (such as Ang II, endothelin I and prostanoids or thromboxane) resulting from hemodynamic changes in the capillaries mediate activation of PKC together with hyperglycemia. This results in the instigation of various downstream pathways such as activation of TGFβ and mitogen activated protein kinase (MAPK) [142] pathways that lead to alteration of renal matrix protein synthesis and cell growth respectively. Studies involving mouse models deficient in various PKC isoforms have shined light on the role of PKC in diabetic renal damage. Renal hypertrophy was completely abrogated in diabetic PKCβ-KO due to reduced expression of TGFβ[143] and markers of oxidative stress without any alteration in the expression of subunits that constitute NADPH oxidase[144]. On the contrary, diabetic PKCα-KO mice revealed reduction in albuminuria[145] associated with decreased VEGF expression, an important growth factor implicated in the loss of albumin in the glomerular filtrate associated with nephrin protein in the podocytes[146]. Interestingly, development of pathological changes of DN such as albuminuria, mesangial matrix expansion and tubulointerstitial fibrosis in PKCε-KO mice even without the induction of diabetes reveal the protective effect of this isoform and is consistent with its increase in diabetic nephropathy[147].

DN: Oxidative stress

Hyperglycemia induces the production of intracellular oxidative agents in renal cells that belong to a large family of reactive oxygen species (ROS) which are oxygen containing chemically active molecules that includes the superoxide anion,

hydrogen peroxide, hydroxyl radical, and peroxynitrite [148]. Under physiological conditions, ROS is generated and degraded efficiently to maintain cellular homeostasis. In conditions such as hyperglycemia, ROS are produced at supra physiological concentrations which induce alterations of signalling pathways and mediate end organ damage[149]. Majority of the ROS are produced during oxidative phosphorylation in the mitochondria, though contributions from other sources such as the enzyme complex, NADPH-oxidase bound to plasma membrane and to some extent from xanthine oxidase[150, 151], play an important role[152].

The mitochondrial electron transport chain (ETC) consists of 4 complexes (Complex I-IV) which receive electrons from donors such as NADH (donor for complex I) and $FADH_2$ (donates to complex II) that are generated in the Krebs cycle. Electrons donated in complex I and II are transferred to coenzyme Q and then to complex III-cytochrome C-complex IV and then taken up by molecular oxygen and reduced to form water. A part of the energy from this electron transport is used to pump protons through the mitochondrial membrane only at complexes I, III and IV. This generates a voltage gradient across the membrane which drives ATP production via ATP synthase. The generation of ATP is specifically regulated by a group of uncoupling proteins that use the voltage gradient to produce heat in a healthy cell. However, increased cellular levels of glucose in a diabetic kidney are oxidized to produce higher concentrations of electron donors, generating voltage gradients to a threshold where the electrons

are unable to transfer in complex III [153] and gets backed up in the coenzyme Q to produce superoxide oxidant from molecular oxygen[154].

Another important source of ROS in the kidney is a group of components of the phagocytic enzyme known as NADPH oxidase (Nox) as they are expressed constitutively in renal vessels, glomeruli, podocytes, tubules and interstitial fibroblast along with the homologues Nox-1, Nox-4. The enzyme consists of membrane bound subunit Nox-2 (also known as gp91^{phox}), p22^{phox} and cytosolic components p47 ^{phox}, p67 ^{phox}, p40 ^{phox} and Rac1 which assemble together to activate the enzyme[155, 156]. PKC is a well-known activator of NADPH oxidase which generates ROS that acts as a second messenger for numerous transcription factors known to be altered in renal disease[157], such as nuclear factor -κB (NF-κB)[158], Akt/PKB[159] and ERK1/2[160].

The physiological balance of ROS in the cell is maintained by several endogenous antioxidants, most notably cytoplasmic Cu/Zn superoxide dismutase (SOD), glutathione peroxidise, mitochondrial manganese SOD and heme oxygenase-1 which have been found to be induced by hyperglycemia[161]. Studies involving overexpression of cytoplasmic Cu/Zn SOD has been shown to reduce glomerular damage in both type 1 and 2 diabetic mouse models[162, 163]. Moreover, disruption of the fine balance between ROS and antioxidants, as a result of inconsistent oxidative reactions at supra-physiological levels, may cause renal tissue damage via several redox sensitive phenomena such as cell survival, growth, apoptosis, migration and ECM remodelling[164].

1.4.2 Hypertension

It is estimated that approximately 1 billion people are affected by hypertension globally, and this incidence is predicted to increase by 60% in the year 2025 [165]. The aetiology of hypertension still remains ambiguous as only 5-10% of hypertensive patients have a discernible cause (known as secondary hypertension) where as majority of it without an identifiable basis is known as primary or essential hypertension. An adequate systemic arterial pressure is essential for proper tissue perfusion. The blood pressure varies significantly during the ventricular systolic phase (systolic blood pressure) and its relaxation phase (diastolic blood pressure), such that it maintains a sufficient mean arterial pressure irrespective of the phase of cardiac cycle. The physiological range of the blood pressure is species specific and varies with age and is regulated by an intricate relationship of heart and the vasculature. Hypertension involves a state where the blood pressure (systolic, diastolic or both) exceeds the species specific physiological range and acts as a silent killer without any early symptoms that involves multiple-organ diseases such as chronic kidney disease, cardiac hypertrophy and stroke.

1.4.2.1 Hypertension: A Vascular Perspective

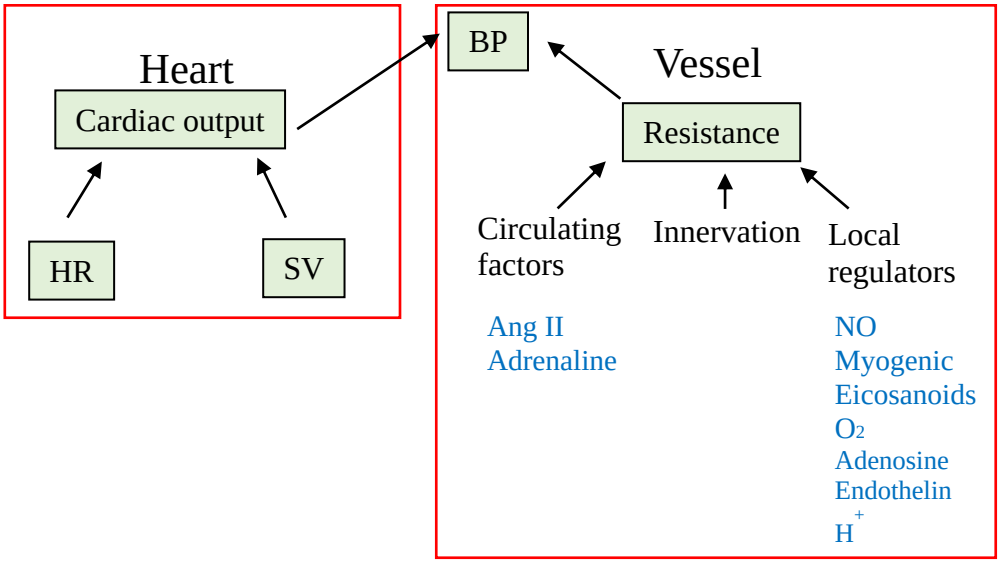

Figure 1.6 Factors affecting Blood pressure.

Extracted and modified from Mayet et al.[166]

It is an established fact that flow dynamics involved in generating blood pressure differences are determined mainly by cardiac output and peripheral vascular resistance (**Fig. 1.6**) according to Darcy's law (analogous to Ohm's law):

$$\Delta P = Q \times R$$

where ΔP = pressure difference, Q = bulk flow, and R= resistance. This law can be applied to the entire vascular circulation:

$$MAP = CO \times PR$$

Where, MAP = mean arterial pressure , C.O = cardiac output, and PR=peripheral resistance . CO is maintained by LV function that depends on preload (LV end diastolic volume), ventricular contractility and afterload which in turn depends on peripheral vascular resistance. Moreover, resistance in the circulatory system can

be determined by Hagen-Poiseulle's equation: $R=8L\eta/\pi r^4$; where R= resistance, L= length of the tube, η= viscocity of the fluid and r= tube's internal radius. Hence, peripheral resistance is inversely proportional to the vascular radius which is regulated by the constriction/ dilation of peripheral arteries. Therefore, a small change in the arterial radius can result in a much larger change in blood pressure. Thus, it is essential to study the factors that impact the vascular structure, such as vascular ECM remodelling and alterations of signalling cascades in the cells comprising the vascular wall, in order to elucidate the contribution of vascular pathology in the development of hypertension and its complications.

Vascular remodelling and cellular basis of Hypertension

Hypertension is associated with vascular remodelling characterized by rearrangement of cellular and structural components of vascular wall. Vascular remodelling is a physiological process that helps the body to adapt during injury and growth, however, under certain conditions, it can form the basis for pathological remodelling. Both physiological and pathological vascular remodeling entail degradation and reorganization of the ECM. Arterial ECM is primarily comprised of elastin and collagen, the main structural component of the ECM that provide significant structural support and recoil properties for the arteries[6, 167]. Alterations in the structure of small arteries primarily involves inward eutrophic and hypertrophic remodelling [168]. Eutrophic remodelling is associated with a decrease in outer arterial diameter and lumen diameter without any change in the cross sectional area of the tunica media. Hypertrophic

remodelling, on the other hand, accompanies thickening of the media, resulting in decreased lumen size and increased media to lumen ratio. Irrespective of the type of remodelling, the media-to-lumen ratio increases, however eutrophic alteration is not associated with stiffening of the remodelled vessel as seen in mild or early stages of hypertension. Animal models of hypertension such as spontaneously hypertensive rats (SHR)[169, 170] and 2 kidney-1 clip (2K1C) Goldblatt rats [171] revealed eutrophic vascular remodelling mimicking mild primary hypertensive patients[172]. Conversely, models of severe hypertension are associated with hypertrophic vascular remodelling as reported in Dahl salt sensitive rats[173], 1 kidney 1 clip Goldblatt rats (1K1C)[174], deoxycorticosterone acetate (DOCA) salt rats[175] similar to patients with secondary hypertension[176]. Furthermore, it is hypothesized that mechanisms such as SMC apoptosis restricted to the outer border which compensate the inward growth (towards the lumen), are responsible for preservation of medial thickness in eutrophic remodelling [177]. Contribution of SMC apoptosis as the primary phenomenon or a compensatory effect on growth in vascular remodelling, remains uncertain since apoptotic factors such as Ang II (via AT2 receptor) [178] and endothelin (ET-1) (via endothelin B receptors) [179] have additional pressor and growth promoting effects. Nevertheless, SHR rats treated with an ACE inhibitor (antagonist of AT1 receptor) and Ca^{2+} channel blockers revealed SMC apoptosis in thoracic aorta [180], although simple hypotensive treatment of hydralazine did not affect SMCs in these rats [181].

Apart from growth and apoptosis of the cellular components, ECM alteration and vascular fibrosis plays an equivocally important role in hypertension-related vascular remodelling. Hypertension is associated with enhanced collagen synthesis in the arterial wall as revealed in aorta and mesenteric arteries of SHR and DOCA-salt rats[182]. Though fibrillar collagen I and III are abundant in all three layers of the vascular wall, collagen III but not I was found to be increased in specific SHR strains[183]. Arterial stiffness characterizing hypertensive vessels is driven by recruitment of collagen fibres at an elevated distending pressure and not necessarily due to an increase in total collagen amount, as evident from small arteries of patients with mild hypertension[184]. Vascular remodelling follows a temporal pattern with arterial wall stiffening becoming predominant during the later stages [185] of advanced hypertension but absent during early stages due to alterations in SMC-ECM anchoring[186] and degradation of ECM[187] to compensate for the increased wall stress. However, these compensatory mechanisms aimed to counter hemodynamic changes early in the disease lead to arterial stiffness and fibrosis that mark the hallmarks of advanced hypertension as a consequence of disruption of an intricate balance between the two vascular wall structural proteins, collagen and elastin, which is maintained by dynamic processes of protein production and degradation[188]. The main structural proteins, collagen (that imparts tensile strength) and elastin (essential for elasticity and recoil function of arteries), together with laminin, fibronectin and proteoglycans (as adhesive proteins) are essential for the integrity of the vascular wall. Elastin remains more susceptible to

damage and breakdown due to a decreased turnover rate and less susceptible to reparation compared to collagen[189, 190]. Although loss of elastin combined with accumulation of collagen have been speculated as a mechanism underlying vascular stiffening[191], pathogenic effects of elastin loss alone is evident from studies using elastin haplosufficient mice that revealed decreased vascular compliance leading to increased systemic blood pressure[192].

Degradation of vascular ECM is carried out primarily by a group of proteases known as metalloproteinases that include matrix metalloproteinases (MMPs), adamalysins, papalysins together with serine and cysteine proteases. The activity of MMPs are inhibited by several inhibitors among which a group of 4 tissue inhibitors of metalloproteinases (TIMP1-4) are of prime importance[193] whose expressions are altered in vascular remodelling[194]. Structural and functional details of these proteases will be discussed in Section 1.6.1.

1.4.2.2 Experimental Models of Hypertension and Its Complications

Animal models used to study hypertension can be broadly divided into genetic and non-genetic models[195]. In mice, genotype driven genetic models primarily include transgenic mice with targeted specific genes involved in the pathogenomic mechanism of hypertension. These include receptors for renal ion channels and transporters[196], transgenic and knock out models of specific components of the renin angiotensin aldosterone system (RAAS)[197, 198] along with other protein or molecules including allelic variants and ablation of ANP receptor[199], nitric oxide (NO, Glu298Asp variant ofeNOS)[200]. Endothelin receptor

(ET-BKO)[201], bradykinin receptor B2[202] and prostaglandin (PGE2) receptors [203]. Non-genetic models are representative of secondary hypertension with an identifiable cause and often involve surgical manipulation to the renovascular system. The first such model was developed by Goldblatt et al by unilateral occlusion of renal artery in dogs and called the 2K1C model [204]. Further variations to enhance the effects of renal artery occlusion have been since developed by nephrectectomy of the contralateral kidney in a model known as 1K1C [205]. Other types of non-genetic non-surgical induced hypertension include administration of mineralocorticoid DOCA[206], chronic inhibition of NO[207], high fructose diet in rats[208], and infusion of Ang II either by subcutaneous implantation of osmotic pumps[209] or direct intra renal administration[210]. Hypertensive models involving Ang II infusion recapitulates a wide range of hypertensive processes and mechanisms in patient given that majority of modern anti-hypertensive (ACEI, ARB) medicines involve antagonism of this pathway.

1.4.3 Abdominal Aortic Aneurysm (AAA)

An aortic aneurysm is traditionally defined as a focal dilation of more than 50% of its original diameter that involves all the layers of the concerned vessel. One of the criteria for classifying aneurysm is based on its anatomic site. If it involves the aortic region that extends below the diaphragm, it is referred to as abdominal aortic aneurysm (AAA). In humans, AAA most often develops in the infrarenal regions as oppose to suprarenal in experimental animal models. AAA is the most common form of aneurysm with prevalence of approximately 2.5% among people

of 60 years of age or older more[211]. AAA shows sexual bias and is more prevalent in men (8% of men over the age of 65 years) than women with epidemiological risk factors such as hypertension (weak association), cigarette smoking, increasing age, dyslipidemia (low HDL cholesterol), coronary artery disease (CAD) and chronic obstructive pulmonary disease (COPD), while some studies suggest an opposite association with diabetes [211]. However, the prognosis of AAA in women remains worse than in men with higher rupture rates[212] and an upsurge in mortality and hospital admission rate over the past few decades[213, 214]. AAA shows genetic predisposition in approximately 12-19% of patients with the disease but lacks any trace of a specific mutation or accords with family history of first degree relative affected with it[215].

Aetiology and pathogenesis of Abdominal Aortic Aneurysm (AAA)

Irrespective of the cause of AAA which can be degenerative, infectious, traumatic, inflammatory and congenital in nature, it may or may not be associated with dissection or rupture. Studies in experimental animal models and patients suggest that AAA is mainly characterized by vascular ECM damage in the tunica media and adventitia, SMC loss, inflammation with infiltration of lymphocytes and macrophages in the aortic wall and altered hemodynamics leading to biochemical stress and dilatation of lumen diameter. Although the pathological processes with relevance to AAA such as degradation of structural proteins (elastin and collagen)[216], inflammation and SMC apoptosis are focal in nature, mounting

evidence suggest that AAA is a manifestation of a systemic disease of the vascular system[217].

Vascular ECM remodelling in Abdominal Aortic Aneurysm (AAA)

Vascular remodelling is a continuous process defined as turnover in the vascular ECM proteins and cellular components within the aortic wall, whereby it adapts to any change in the vascular environment (size, composition of a matured vessel) to accommodate repair and to maintain a homeostatic environment to facilitate normal function. On the contrary, improper adaptation of the cellular components and the ECM framework leads to pathological remodelling which underlies abnormal dilatation of the abdominal aorta. Vascular ECM of a large elastic artery such as aorta, which is responsible for the mechanical properties of the aortic wall, is predominantly synthesized by the vascular SMC[6]. The SMCs of the aortic wall do not contribute towards the passive mechanical properties as oppose to small and resistant arteries[192]. The mechanical properties of the aortic wall vary from tensile strength (collagens), required for the inflation of the wall during ventricular systole, and its complete recovery by elastic recoil (elastin) during the diastolic phase. Elasticity of the aortic wall is nonlinear to accommodate the increasing pressure and to avoid rupture of the aortic wall during cardiac systole.

In AAA, these mechanical properties of the aortic wall are disrupted primarily due to the proteolysis of the structural proteins of the ECM, elastin and collagen. Proteolysis remains as one of the key mechanisms underlying the pathogenesis of AAA primarily due to loss of ECM proteins and accretion of proteolytic enzymes

in the concerned aneurysmal tissue[218]. Different classes of proteases that can contribute to aneurysm formation (matrix metalloproteinase, serine proteases and cysteine proteases[219-221] , members of the MMP family have been more linked to aneurysm formation[222].

MMPs consist of a family of 26 extracellular and transmembrane enzymes which play an important role in maintaining the integrity of the vascular ECM together in balance with their physiological inhibitors, the tissue inhibitor of metalloproteinase (TIMP1-4). Impairment of this delicate balance between these groups of enzymes is fundamental to the pathogenesis of aneurysm formation[223], expansion[224] and rupture[225] due to the abnormal lysis and arrangement of structural ECM proteins[216]. MMPs at post translational level are predominantly inhibited by a group of endogenous inhibitors known as TIMPs which are of 4 subtypes, TIMPs 1-4. MMPs and TIMPs will be further described in Section 1.6.

Imaging of aorta in AAA

Changes in aortic luminal diameter not only define AAA (an increase in more than 50% of its original diameter) but remain an essential determinant for risk of rupture of the aneurysmal aorta. Although different validated methods to measure aortic diameter in murine models of AAA (calibrated ocular grid to evaluate external aortic diameter, shrinkage index by histomorphometry to estimate internal luminal diameter) [226, 227] exists in the literature, they lack the ability to quantify AAA progression adequately[228]. However, recent advances in high frequency ultrasound imaging technique with increased spatial resolution,

adequately measures luminal aortic diameter non-invasively in live, small animals [228, 229]. In addition to the simplicity of the procedure, ultrasound imaging allows serial estimation of luminal diameter that is essential to study temporal progression of AAA. A detailed discussion on the methodology and parameter can be found in section 2.5.6 of Chapter 2.

1.5 EXPERIMENTAL MOUSE MODELS OF ABDOMINAL AORTIC ANEURYSM (AAA)

Experimental mouse models of AAA include genetically and chemically induced disease that recapitulate features of the disease in patients, such as medial degeneration, inflammation, adverse ECM remodelling, thrombus formation and rupture[230]. Mouse models have gained dominance over other mammalian and avian models in biomedical research of AAA due to ready access to perturbation and ability to overexpression or deletion of genes, smaller size and smaller gestation period.

1.5.1 Genetically Induced Mouse Models of AAA

Genetically induced mouse models include mice either harbouring a spontaneous or specifically engineered mutation, with either deficiency or over expression of a particular gene of interest. Blotchy mouse is a model of AAA that harbours a mutation on the X chromosome that causes impaired intestinal absorption of copper. As copper is an essential co-factor for lysyl oxidase (Lox) mediated crosslinking of elastin and collagen, decreased levels of Lox makes these mice susceptible to AAA with increase in rupture rates in males[231]. The major

limitation of this model that restricts its use is the aneurysmal formation in other regions of the vasculature and emphysema [232]. Moreover, development of mice lacking Lox are not viable due to high rupture rates of thoracic rather than abdominal aneurysm[233]. Other genetically engineered mice comprising deficiency of genes of the protease system such as MMP3KO[234] and TIMP1KO[235] in combination with apolipoprotein E deficiency and high fat diet only, developed dissection and small thoracic and abdominal aneurysms, but lacked focal damage of ECM at the abdominal aorta and specificity for AAA[230]. Mice deficient in apolipoproteinE (apoE)[236] and LDL receptors[237] were developed to study atherosclerotic plaque formation, and it was dicovered that when fed a high fat diet, these mice developed pseudo-micro aneurysms (in the suprarenal aspect of the aorta)[238]. Moreover, urokinase deficiency, via inactivation of MMP12, abrogated aortic pathology in apoE deficient mice[239]. AAA was once considered as a focal manifestation of an advanced atherosclerotic disease[240], however recent evidence has defied this conventional understanding[241]. Besides, lower incidence of AAA in the population with diabetes mellitus[242], normally regarded as the risk comparable to atherosclerosis, suggests that atherosclerotic lesions are coincidence rather than pathogenic in AAA. One of the most interesting transgenic mouse models known as Tsukuba hypertensive mouse was produced by cross breeding strains that expressed renin and angiotensinogen transgenes[243]. Surprisingly neither of these transgenic mice expressing peptides of the RAAS individually developed hypertension, however the double transgenic mouse had

elevated blood pressure and upon fed with 1% NaCl in drinking water developed aortic aneurysm (thoracic and abdominal) and increased rate of rupture[244]. Nevertheless, these models revealed the importance of RAAS peptides in the induction of AAA in experimental mice and served as a rationale behind the use of Angiotensin II infusions to study the pathogenesis of AAA.

1.5.2 Chemically Induced Mouse Models of AAA

Three most common chemical induced experimental models of AAA include transient intraluminal infusion of elastase (a pancreatic extract) [245], adventitial exposure of a high concentration $CaCl_2$ solution [246], or chronic subcutaneous infusion of a hypertensive dose of Ang II in a hypercholestremic [247] or normocholestremic background [248]. The Ang II infusion model allows for detection of aneurysm throughout the aorta while the elastase infusion and $CaCl_2$ exposure models provide information exclusively about focal aortic susceptibility. Histological evidence of disrupted elastin in the aortic wall of patients and experimental models of AAA provided rationale for the use of elastase infusions in rats and subsequently in mice through a catheter introduced at the iliac bifurcation followed by a distal suture thereby isolating a segment of the abdominal aorta and restoration of blood flow after 5 min of incubation [249]. Subsequently an immediate dilatation of the area is formed due to the mechanical pressure of the experimental procedure and a constant degree of dilation is maintained for 7 days without any damage to the elastin fibres. Additionally, infusion of elastase maintained the dilation by day 14 due to the immense damage

to the elastic lamellae concomitant with inflammatory infiltration in the adventitial layer. Mice treated with vehicle do not show these destructive changes, nor any dilation at day 14. Doxycycline treatment attenuates such changes which was attributed to its MMP inhibitory function and further supported by MMP-9 deficient mice that failed to develop aneurysms after elastase infusion[245]. Reports of elevated levels of Angiotensin converting enzyme (ACE) in aneurysmal tissue of elastase infused rats, increased levels of Ang II in human aneurysmal tissue[250], prevention of AAA development by three commonly used ACE inhibitors (captopril, lisinopril and enalapril) in models of elastase infusion without any contribution from hemodynamic alteration[251]

Another model of chemical induced AAA was developed by the peri-aortic placement of a gauze soaked in a high concentration calcium chloride solution, or direct application of the concentrated calcium chloride solution on the aorta between the renal artery and the iliac bifurcation[252]. Exposure of the abdominal aorta calcium chloride results in dilation secondary to disruption of the media and inflammation. The advantage of this model over the elastase infusion model is that it does not involve luminal dilation caused by mechanical pressure of infusion. Mice deficient in either MMP-2 or MMP-9 failed to develop aortic aneurysm when treated with calcium chloride, however introduction of wildtype macrophages led to the development of AAA in MMP-9 deficient but not in MMP-2 deficient mice[246]. Thus, it was concluded that the macrophage-derived

MMP-9 and the MMP-2 from native SMCs are required simultaneously for the promotion of AAA.

Salt induced promotion of AAA in angiotensinogen and renin double transgenic mice[244], and the inability of aldosterone infusion to generate AAA in apoE deficient mice, support a key role for Ang II in the pathogenesis of AAA. Infusion of Ang II (subcutaneous, by osmotic pumps) in apoE and LDL receptor deficient mice has successfully generated reproducible phenotype of AAA associated with atherosclerotic lesions. Apart from these hyperlipidemia associated models of AAA, a small percentage of normolipidemic mice deficient in Urokinase-type plasminogen activator (uPA)[253], that converts plasminogen into active serine protease and can thereby potentiate MMP activation and ECM destruction[254], developed AAA. Thus, studies of direct effects of Ang II in the activation of proteases (such as MMPs) and ECM degradation associated with AAA needs further investigation without any confounding effects of hyperlipidemia.

1.6 MATRIX METEALLOPROTEINASE (MMPS) AND THEIR ENDOGENOUS INHIBITORS IN THE VASCULATURE.

1.6.1 Matrix Metalloproteinases (MMPs)

MMPs are a family of approximately 26 zinc endo-peptidases, 23 of which are found in humans with close structural homology (**Fig. 1.7**). MMPs have been traditionally classified on the basis of their substrate specificity, although there is evidence of overlapping substrate specificity or numbered in the order of their discovery. MMPs are key proteases responsible for the degradation of ECM and

connective tissue by their proteolytic effects and play a vital role in vascular remodelling including turnover of the ECM[255-257]. Apart from proteolytic degradations, MMPs are capable of activating cell surface receptors and cellular cytoskeleton proteins thereby modulating cell–ECM and cell-cell interactions.

Structure of MMPs

MMPs are usually made up of five-domain proteins (**Fig. 1.8**), with an exception of the additional transmembrane segment in membrane-type class of MMPs (MT-MMPs) and absence of hinge or hemopexin domains in MMP-7 and MMP-26 (matrilysin 1 and 2 respectively) [258, 259]. The five domains, from the (N)-terminus to the carboxyl (C)-terminus are: signal domain, pro-domain, catalytic domain, hinge region, and hemopexin domain. All proteinases in the MMP family have 3 molecular specificities such as: sequence homology with collagenase-1, a cysteine switch motif PRCGXPD that connects the pro domain to the catalytic domain and chelates the embedded zinc site thereby maintaining MMPs in their latent zymogen form (MMP-23 is an exception that lacks this motif), and 3 histidine bound zinc binding motif with conserved sequence in the catalytic domain [260]. MMPs can be divided into 6 groups broadly on the basis of their specificity (collagenases, gelatinases A and B, stromelysins 1 and 2, matrilysin 1, stromelysin 3 and epilysin). A variety of cells in the vessel wall synthesize MMPs, such as neutrophils, eosinophils, macrophages, fibroblasts and predominantly SMCs.

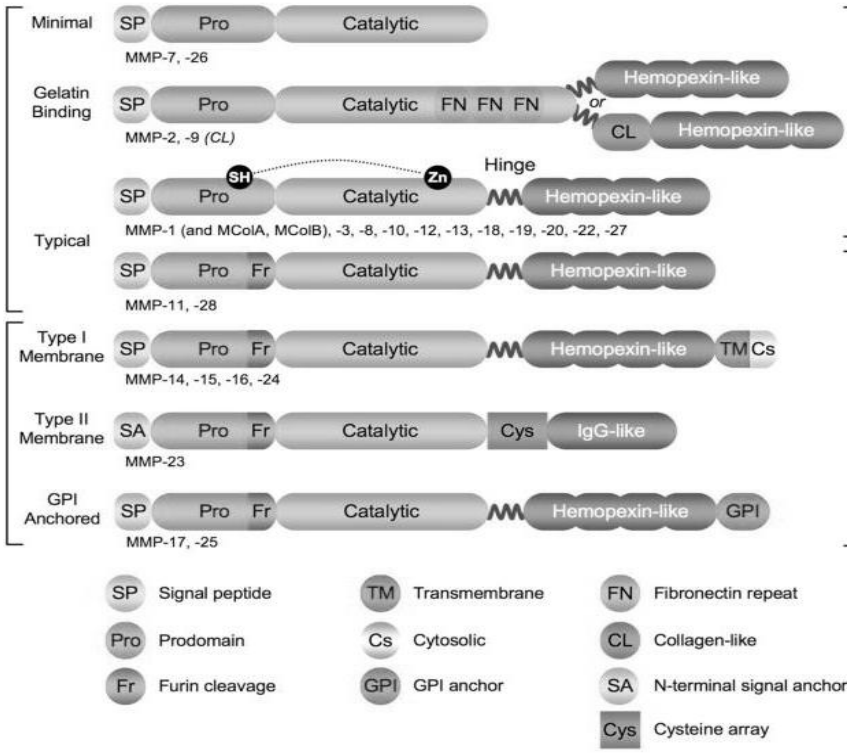

Figure1.7 Biochemical Structure and classification of MMPs

Extracted from Ra & Parks [261].

Characteristics of the 6 groups of MMPs

MMPs can be broadly divided into 6 groups on the basis of their specificity originally discovered substrate specificity:

1) MMP-1, -8, -13 and -18 (xenopus) are known as collagenases that cleave interstitial collagen I, II and III. However, it has been reported that in addition to cleaving other ECM molecules, these MMPs have proteolytic functions over several non-ECM molecules [262].

2) MMP2 (gelatinaseA) and MMP9 (gelatinaseB) are known as gelatinases as they were initially discovered to cleave denatured collagen, gelatin. Their catalytic domain consists of 3 repeats of a type II fibronectin domain which facilitates binding to gelatin, collagen and laminin[263], while MMP9 has also been reported to be a potent elastase [264].

3) MMP3 (stromelysin-1) and MMP10 (stromelysin-2) are known as stromelysins and share similar substrate specificity, although MMP10 possesses more potent proteolytic activities over MMP3. MMP7 (matrilysin-1) and MMP26 (matrilysin-2 or endometase) lack the hemopexin domain.

4) MMP14 (MT1-MMP), MMP15 (MT2-MMP), MMP16 (MT3-MMP) and MMP24 (MT4-MMP) are all membrane-type MMPs that consist of type I transmembrane proteins. Particularly MT1-MMP has the ability to cleave collagen type I, II and III and simultaneously can activate other MMPs[265].

5) MMP11 (stromelysin-3 but differs in substrate specificity from other stromelysins), -12, -19, -20, -22, -23 and -28 are other MMPs among which MMP12 (metalloelastase) can cleave elastin and has been shown to have a role in vascular remodelling.

6) The last member to be added in the family of MMPs is MMP28 (Epilysin) [266].

MMPs relevant to vascular remodelling in AAA

AAA is known to be associated with elevated synthesis or/and activation of MMPs[222, 267]. Studies on patients with AAA impending rupture, have shown increases in both plasma and tissue (aortic wall) MMP levels suggesting a key role played by MMPs in the fatal complication of AAA[268-271]. Of all MMPs found in vascular tissue, gelatinases MMP-2 and -9 possess the ability to degrade gelatin (denatured collagen), elastin and collagen I, IV, V and VII[272] and have been implicated the most in the pathogenesis of AAA[273-275]. Studies on patient samples and animal models of AAA have successfully demonstrated elevated levels and potential role of MMP-1[276], MMP-2[277], MMP-3[234], MMP-8[278], MMP-9[246], MMP-12[279], MMP-13[280] and MMP-14(MT-1MMP)[281] underlying aberrant matrix remodelling in AAA. Moreover concentrations of gelatinases in abdominal aortic

tissue homogenates from patients with AAA have been shown to be 0.04 g/ml for MMP2[277], and 0.5 g/gm for MMP9[282]. Plasma levels of MMP2 and MMP9 have also been found to be elevated in patients with AAA[283, 284]. In addition to their proteolytic effect on ECM structural proteins, gelatinases can alter aortic SMC contraction which has been speculated to underlie early aneurysm development[285].

MMP activation

MMPs are regulated at 3 levels: transcription, activation (exposure of their catalytic subunit), and inhibition of activated MMPs by their inhibitors. MMP activation involves the cleavage of the pro-domain, and shortening of the molecule in a periodic process[286], thereby uncovering the catalytic site for proteolytic action on substrates. The main process of MMP activation involves exposure of the catalytic site for proteolytic degradation of the substrate. Although activated MMPs can be inhibited modestly by domains of netrins, the procollagen C-terminal proteinase enhancer (PCPE), the reversion-inducing cysteine-rich protein with Kazal motifs (RECK), or tissue factor pathway inhibitor (TFPI-2), their predominant inhibitors are the endogenous group of 4 proteinases known as TIMPs [287]

1.6.2 Tissue Inhibitors of Metalloproteinases (TIMPs) and Their Role in AAA

TIMPs are a family of 4 members, of molecular weights ranging from 21-30 kDa with 37-51% homology, and are endogenous inhibitors of MMPs. All four TIMPs

(TIMP1-TIMP4) are found in vertebrates with the predominance of TIMP4 in the vascular tissue and their expression levels are modulated during tissue remodelling or development[194]. The N-terminal and the C-terminal domains of TIMPs (**Fig. 1.8**) consist of 3 conserved disulphide bonds, while the N-terminal domain is capable of folding as a distinct unit that can inhibit MMPs[288]. TIMPs can inhibit all MMPs verified to date except for TIMP1 which cannot inhibit MT1-MMP[289]. TIMP3 is unique as it is the only TIMP bound to the ECM via its C terminal domain that provides extra reservoir by prolonging its half life[290] and possesses a broader range of inhibitory properties, which differs from the other TIMPs, as it can inhibit a a number of disintigrin and metalloproteinase (ADAMs)[291]. TIMPs have also been reported to influence cell growth[292], migration and apoptosis [293] independent from their MMP-inhibitory function[287]. Apart from TIMP4, all the other TIMPs have been implicated in the pathogenesis of AAA[294]. TIMP1 has been shown to play an important role in vascular pathology, and its levels have been shown to both increase[295] and decrease[296] in aneurysmal tissues from AAA patients. To overcome such inconsistencies in the levels of TIMP1, the ratio of MMP9 to TIMP1 levels was used as an index of proteolytic activity in the ECM [295]. The role of TIMP2 in AAA is complex as it can inhibit a number of MMPs, and simultaneously can activate MMP2, through a tri-molecular activation complex involving MT1-MMP. TIMP2 levels were found to be reduced in patients with AAA[297], while another study demonstrated elevation of TIMP3, and not TIMP1 or TIMP2 levels in aortic samples from

patients with AAA [296]. The ratio of MMP2 to TIMP2 levels has also been reported as as index of proteolysis in the ECM[295, 298]. The definitive role of elevated TIMP3 levels in AAA remains inconclusive and needs further investigation to determine its causal or protective function in AAA.

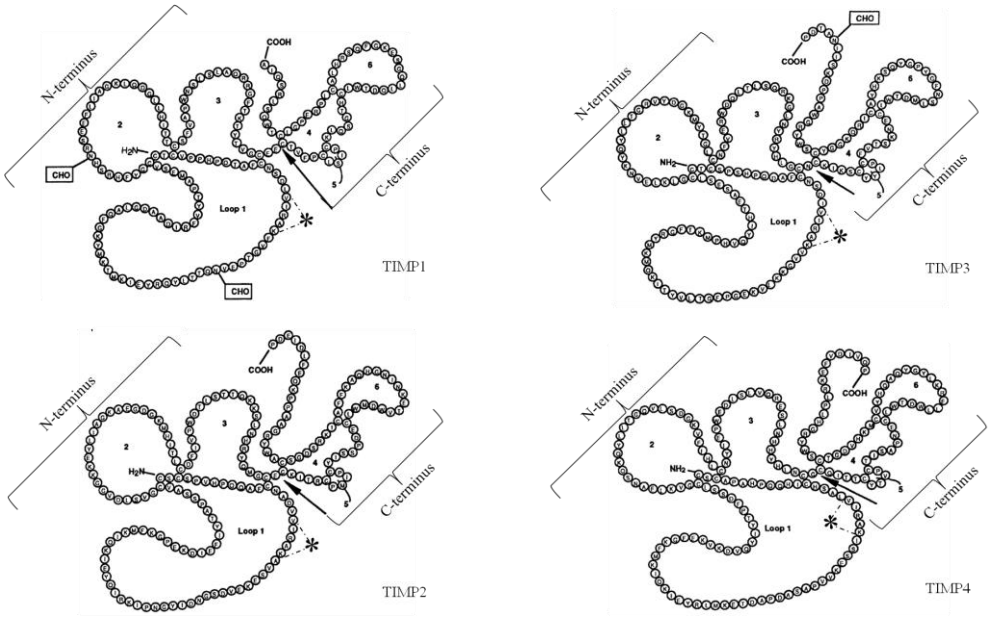

Figure 1.8 Basic structure of TIMP1 to TIMP4.

TIMP1 –4 sequences. N- and C-terminus junction indicated by arrows. Adapted from Moore et al. [289].

1.6.3 Tetracycline as a Pharmacological Inhibitor of MMPs.

Golub and colleagues, during their mechanistic work on periodontal disease in diabetic rats made the first discovery of the potential MMP inhibitory role of tetracycline[299]. Tetracyclines are naturally occurring pleiotropic agents that can also be synthesized. They are essentially broad spectrum antibiotics that alter ribosomal function and interfere with protein synthesis. They improve SMC cell-cell and cell-substrate adhesions by direct inhibition of MMPs at the catalytic

site[300]. An analog of tetracycline that has been used most widely in patients as an MMP inhibitor is Metastat (COL-3), a chemically modified version of tetracycline which lacks its antibacterial property. However, doxycycline is the only known compound that is approved by FDA as an inhibitor of MMPs in periodontal disease [301] via its beneficial effects on ECM remodelling [302]. Petrinec et al. and Curci et al. were the first to show the beneficial effects of doxycycline in experimental AAA model of rats in an elastase infusion model [303, 304]. Recently doxycycline has been used in clinical trials [290] for therapeutic effects on AAA, although their clinical efficiency is this vascular pathology is still unknown . Although it is suggested that the mechanism underlying MMP inhibitory property of tetracycline is similar to that of TIMPs, it still remains to be understood.

1.7 HYPOTHESES AND OBJECTIVE

1.7.1 Hypotheses

1) The cardiomypathy associated with Type 1 diabetes is primarily diastolic dysfuntion with preserved systolic function.

2) TIMP3, an essential ECM-bound physiological inhibitor of MMPs, plays an essential role in the progression of diabetic nephrapathy but not diabetic cardiomyopahty.

3) TIMP3 plays a critical role in agonist induced vascular remodelling thereby influencing hypertension, and leading to aortic aneurysm in the long term.

1.7.2 Objectives of the Thesis

Since TIMP3 is highly expressed in the kidneys, heart and the arteries, we aimed to investigate the multifaceted role of TIMP3 in modulating pathologies in these organs which often occur as comorbid diseases.

1.8 REFERENCES

1. Robinson HM, Hort K. Non-communicable diseases and health systems reform in low-and-middle-income countries. *Pac Health Dialog*.18:179-190

2. Kanda T, Wakino S, Hayashi K, Plutzky J. Cardiovascular disease, chronic kidney disease, and type 2 diabetes mellitus: Proceeding with caution at a dangerous intersection. *J Am Soc Nephrol*. 2008;19:4-7

3. Dobrin PB. Mechanical properties of arterises. *Physiol Rev*. 1978;58:397-460

4. Harkness ML, Harkness RD, McDonald DA. The collagen and elastin content of the arterial wall in the dog. *Proc R Soc Lond B Biol Sci*. 1957;146:541-551

5. Clark JM, Glagov S. Transmural organization of the arterial media. The lamellar unit revisited. *Arteriosclerosis*. 1985;5:19-34

6. Wagenseil JE, Mecham RP. Vascular extracellular matrix and arterial mechanics. *Physiol Rev*. 2009;89:957-989

7. Karrer HE. An electron microscope study of the aorta in young and in aging mice. *J Ultrastruct Res*. 1961;5:1-27

8. Stenmark KR, Davie N, Frid M, Gerasimovskaya E, Das M. Role of the adventitia in pulmonary vascular remodeling. *Physiology (Bethesda)*. 2006;21:134-145

9. Wolinsky H, Glagov S. Nature of species differences in the medial distribution of aortic vasa vasorum in mammals. *Circ Res*. 1967;20:409-421

10. Tschope C, Paulus WJ. Is echocardiographic evaluation of diastolic function useful in determining clinical care? Doppler echocardiography yields dubious estimates of left ventricular diastolic pressures. *Circulation*. 2009;120:810-820; discussion 820

11. Karliner JS, Gault JH, Eckberg D, Mullins CB, Ross J, Jr. Mean velocity of fiber shortening. A simplified measure of left ventricular myocardial contractility. *Circulation*. 1971;44:323-333

12. Jorge AJ, Ribeiro ML, Rosa ML, Licio FV, Fernandes LC, Lanzieri PG, Jorge BA, Brito FO, Mesquita ET. Left atrium measurement in patients

suspected of having heart failure with preserved ejection fraction. *Arq Bras Cardiol*.

13. Pritchett AM, Mahoney DW, Jacobsen SJ, Rodeheffer RJ, Karon BL, Redfield MM. Diastolic dysfunction and left atrial volume: A population-based study. *J Am Coll Cardiol*. 2005;45:87-92

14. Tsang TS, Abhayaratna WP, Barnes ME, Miyasaka Y, Gersh BJ, Bailey KR, Cha SS, Seward JB. Prediction of cardiovascular outcomes with left atrial size: Is volume superior to area or diameter? *J Am Coll Cardiol*. 2006;47:1018-1023

15. Basu R, Oudit GY, Wang X, Zhang L, Ussher JR, Lopaschuk GD, Kassiri Z. Type 1 diabetic cardiomyopathy in the akita (ins2wt/c96y) mouse model is characterized by lipotoxicity and diastolic dysfunction with preserved systolic function. *Am J Physiol Heart Circ Physiol*. 2009;297:H2096-2108

16. Lester SJ, Tajik AJ, Nishimura RA, Oh JK, Khandheria BK, Seward JB. Unlocking the mysteries of diastolic function: Deciphering the rosetta stone 10 years later. *J Am Coll Cardiol*. 2008;51:679-689

17. Hamlin SK, Villars PS, Kanusky JT, Shaw AD. Role of diastole in left ventricular function, ii: Diagnosis and treatment. *Am J Crit Care*. 2004;13:453-466; quiz 467-458

18. Nagueh SF, Appleton CP, Gillebert TC, Marino PN, Oh JK, Smiseth OA, Waggoner AD, Flachskampf FA, Pellikka PA, Evangelisa A. Recommendations for the evaluation of left ventricular diastolic function by echocardiography. *Eur J Echocardiogr*. 2009;10:165-193

19. Oh JK, Hatle L, Tajik AJ, Little WC. Diastolic heart failure can be diagnosed by comprehensive two-dimensional and doppler echocardiography. *J Am Coll Cardiol*. 2006;47:500-506

20. Isaaz K. Tissue doppler imaging for the assessment of left ventricular systolic and diastolic functions. *Curr Opin Cardiol*. 2002;17:431-442

21. Tsujita Y, Kato T, Sussman MA. Evaluation of left ventricular function in cardiomyopathic mice by tissue doppler and color m-mode doppler echocardiography. *Echocardiography*. 2005;22:245-253

22. Yamamoto K, Nishimura RA, Chaliki HP, Appleton CP, Holmes DR, Jr., Redfield MM. Determination of left ventricular filling pressure by doppler echocardiography in patients with coronary artery disease: Critical role of left ventricular systolic function. *J Am Coll Cardiol*. 1997;30:1819-1826

23. Dokainish H, Zoghbi WA, Lakkis NM, Al-Bakshy F, Dhir M, Quinones MA, Nagueh SF. Optimal noninvasive assessment of left ventricular filling pressures: A comparison of tissue doppler echocardiography and b-type natriuretic peptide in patients with pulmonary artery catheters. *Circulation*. 2004;109:2432-2439

24. Ommen SR, Nishimura RA, Appleton CP, Miller FA, Oh JK, Redfield MM, Tajik AJ. Clinical utility of doppler echocardiography and tissue doppler imaging in the estimation of left ventricular filling pressures: A comparative simultaneous doppler-catheterization study. *Circulation*. 2000;102:1788-1794

25. Boluyt MO, Converso K, Hwang HS, Mikkor A, Russell MW. Echocardiographic assessment of age-associated changes in systolic and diastolic function of the female f344 rat heart. *J Appl Physiol*. 2004;96:822-828

26. Sebag IA, Handschumacher MD, Ichinose F, Morgan JG, Hataishi R, Rodrigues AC, Guerrero JL, Steudel W, Raher MJ, Halpern EF, Derumeaux G, Bloch KD, Picard MH, Scherrer-Crosbie M. Quantitative assessment of regional myocardial function in mice by tissue doppler imaging: Comparison with hemodynamics and sonomicrometry. *Circulation*. 2005;111:2611-2616

27. Thibault H, Gomez L, Donal E, Augeul L, Scherrer-Crosbie M, Ovize M, Derumeaux G. Regional myocardial function after myocardial infarction in mice: A follow-up study by strain rate imaging. *J Am Soc Echocardiogr*. 2009;22:198-205

28. Schaefer A, Meyer GP, Hilfiker-Kleiner D, Brand B, Drexler H, Klein G. Evaluation of tissue doppler tei index for global left ventricular function in mice after myocardial infarction: Comparison with pulsed doppler tei index. *Eur J Echocardiogr*. 2005;6:367-375

29. Stypmann J. Doppler ultrasound in mice. *Echocardiography*. 2007;24:97-112

30. Steen T, Voss BM, Smiseth OA. Influence of heart rate and left atrial pressure on pulmonary venous flow pattern in dogs. *Am J Physiol*. 1994;266:H2296-2302

31. Rossvoll O, Hatle LK. Pulmonary venous flow velocities recorded by transthoracic doppler ultrasound: Relation to left ventricular diastolic pressures. *J Am Coll Cardiol*. 1993;21:1687-1696

32. Brun P, Tribouilloy C, Duval AM, Iserin L, Meguira A, Pelle G, Dubois-Rande JL. Left ventricular flow propagation during early filling is related to wall relaxation: A color m-mode doppler analysis. *J Am Coll Cardiol*. 1992;20:420-432

33. Riser BL, Cortes P, Heilig C, Grondin J, Ladson-Wofford S, Patterson D, Narins RG. Cyclic stretching force selectively up-regulates transforming growth factor-beta isoforms in cultured rat mesangial cells. *Am J Pathol*. 1996;148:1915-1923

34. Gruden G, Thomas S, Burt D, Zhou W, Chusney G, Gnudi L, Viberti G. Interaction of angiotensin ii and mechanical stretch on vascular endothelial growth factor production by human mesangial cells. *J Am Soc Nephrol*. 1999;10:730-737

35. Riser BL, Denichilo M, Cortes P, Baker C, Grondin JM, Yee J, Narins RG. Regulation of connective tissue growth factor activity in cultured rat mesangial cells and its expression in experimental diabetic glomerulosclerosis. *J Am Soc Nephrol*. 2000;11:25-38

36. Ingram AJ, James L, Ly H, Thai K, Scholey JW. Stretch activation of jun n-terminal kinase/stress-activated protein kinase in mesangial cells. *Kidney Int*. 2000;58:1431-1439

37. Krepinsky JC, Li Y, Chang Y, Liu L, Peng F, Wu D, Tang D, Scholey J, Ingram AJ. Akt mediates mechanical strain-induced collagen production by mesangial cells. *J Am Soc Nephrol*. 2005;16:1661-1672

38. Schlondorff D, Banas B. The mesangial cell revisited: No cell is an island. *J Am Soc Nephrol*. 2009;20:1179-1187

39. Morabia A, Abel T. The who report "preventing chronic diseases: A vital investment" and us. *Soz Praventivmed*. 2006;51:74

40. Couser WG, Remuzzi G, Mendis S, Tonelli M. The contribution of chronic kidney disease to the global burden of major noncommunicable diseases. *Kidney Int*.80:1258-1270

41. Maraschin Jde F. Classification of diabetes. *Adv Exp Med Biol*.771:12-19

42. Ryden L, Mellbin L. Joint esc/easd guidelines on diabetes, where are we now and where should we go? *Curr Vasc Pharmacol*. 2012;10:690-692

43. Roglic G, Unwin N, Bennett PH, Mathers C, Tuomilehto J, Nag S, Connolly V, King H. The burden of mortality attributable to diabetes: Realistic estimates for the year 2000. *Diabetes Care*. 2005;28:2130-2135

44. Wild S, Roglic G, Green A, Sicree R, King H. Global prevalence of diabetes: Estimates for the year 2000 and projections for 2030. *Diabetes Care*. 2004;27:1047-1053

45. Rubler S, Dlugash J, Yuceoglu YZ, Kumral T, Branwood AW, Grishman A. New type of cardiomyopathy associated with diabetic glomerulosclerosis. *Am J Cardiol*. 1972;30:595-602

46. Aneja A, Tang WH, Bansilal S, Garcia MJ, Farkouh ME. Diabetic cardiomyopathy: Insights into pathogenesis, diagnostic challenges, and therapeutic options. *Am J Med*. 2008;121:748-757

47. Teupe C, Rosak C. Diabetic cardiomyopathy and diastolic heart failure -- difficulties with relaxation. *Diabetes Res Clin Pract*.97:185-194

48. Zabalgoitia M, Ismaeil MF, Anderson L, Maklady FA. Prevalence of diastolic dysfunction in normotensive, asymptomatic patients with well-controlled type 2 diabetes mellitus. *Am J Cardiol*. 2001;87:320-323

49. Poirier P, Bogaty P, Garneau C, Marois L, Dumesnil JG. Diastolic dysfunction in normotensive men with well-controlled type 2 diabetes: Importance of maneuvers in echocardiographic screening for preclinical diabetic cardiomyopathy. *Diabetes Care*. 2001;24:5-10

50. Boyer JK, Thanigaraj S, Schechtman KB, Perez JE. Prevalence of ventricular diastolic dysfunction in asymptomatic, normotensive patients with diabetes mellitus. *Am J Cardiol*. 2004;93:870-875

51. Di Bonito P, Moio N, Cavuto L, Covino G, Murena E, Scilla C, Turco S, Capaldo B, Sibilio G. Early detection of diabetic cardiomyopathy: Usefulness of tissue doppler imaging. *Diabet Med*. 2005;22:1720-1725

52. Fang ZY, Schull-Meade R, Downey M, Prins J, Marwick TH. Determinants of subclinical diabetic heart disease. *Diabetologia*. 2005;48:394-402

53. Fang ZY, Yuda S, Anderson V, Short L, Case C, Marwick TH. Echocardiographic detection of early diabetic myocardial disease. *J Am Coll Cardiol*. 2003;41:611-617

54. Von Bibra H, Thrainsdottir IS, Hansen A, Dounis V, Malmberg K, Ryden L. Tissue doppler imaging for the detection and quantitation of myocardial dysfunction in patients with type 2 diabetes mellitus. *Diab Vasc Dis Res*. 2005;2:24-30

55. Aragno M, Mastrocola R, Alloatti G, Vercellinatto I, Bardini P, Geuna S, Catalano MG, Danni O, Boccuzzi G. Oxidative stress triggers cardiac fibrosis in the heart of diabetic rats. *Endocrinology*. 2008;149:380-388

56. King GL. The role of inflammatory cytokines in diabetes and its complications. *Journal of periodontology*. 2008;79:1527-1534

57. Hotamisligil GS. Inflammatory pathways and insulin action. *Int J Obes Relat Metab Disord*. 2003;27 Suppl 3:S53-55

58. Trost SU, Belke DD, Bluhm WF, Meyer M, Swanson E, Dillmann WH. Overexpression of the sarcoplasmic reticulum ca(2+)-atpase improves myocardial contractility in diabetic cardiomyopathy. *Diabetes*. 2002;51:1166-1171

59. Broderick TL, Poirier P. Cardiac function and ischaemic tolerance during acute loss of metabolic control in the diabetic bb wor rat. *Acta Diabetol*. 2005;42:171-178

60. Rodrigues B, McNeill JH. Cardiac dysfunction in isolated perfused hearts from spontaneously diabetic bb rats. *Can J Physiol Pharmacol*. 1990;68:514-518

61. Broderick TL, Hutchison AK. Cardiac dysfunction in the euglycemic diabetic-prone bb wor rat. *Metabolism*. 2004;53:1391-1394

62. Kajstura J, Fiordaliso F, Andreoli AM, Li B, Chimenti S, Medow MS, Limana F, Nadal-Ginard B, Leri A, Anversa P. Igf-1 overexpression inhibits the development of diabetic cardiomyopathy and angiotensin ii-mediated oxidative stress. *Diabetes*. 2001;50:1414-1424

63. Nielsen LB, Bartels ED, Bollano E. Overexpression of apolipoprotein b in the heart impedes cardiac triglyceride accumulation and development of cardiac dysfunction in diabetic mice. *J Biol Chem*. 2002;277:27014-27020

64. Joffe, II, Travers KE, Perreault-Micale CL, Hampton T, Katz SE, Morgan JP, Douglas PS. Abnormal cardiac function in the streptozotocin-induced non-insulin-dependent diabetic rat: Noninvasive assessment with doppler echocardiography and contribution of the nitric oxide pathway. *J Am Coll Cardiol*. 1999;34:2111-2119

65. Eddouks M, Chattopadhyay D, Zeggwagh NA. Animal models as tools to investigate antidiabetic and anti-inflammatory plants. *Evidence-based complementary and alternative medicine : eCAM*. 2012;2012:142087

66. Paik SG, Fleischer N, Shin SI. Insulin-dependent diabetes mellitus induced by subdiabetogenic doses of streptozotocin: Obligatory role of cell-mediated autoimmune processes. *Proc Natl Acad Sci U S A*. 1980;77:6129-6133

67. Mizushige K, Yao L, Noma T, Kiyomoto H, Yu Y, Hosomi N, Ohmori K, Matsuo H. Alteration in left ventricular diastolic filling and accumulation of myocardial collagen at insulin-resistant prediabetic stage of a type ii diabetic rat model. *Circulation*. 2000;101:899-907

68. Palmieri V, Bella JN, Arnett DK, Liu JE, Oberman A, Schuck MY, Kitzman DW, Hopkins PN, Morgan D, Rao DC, Devereux RB. Effect of type 2 diabetes mellitus on left ventricular geometry and systolic function in hypertensive subjects: Hypertension genetic epidemiology network (hypergen) study. *Circulation*. 2001;103:102-107

69. Tokudome T, Horio T, Yoshihara F, Suga S, Kawano Y, Kohno M, Kangawa K. Direct effects of high glucose and insulin on protein synthesis in cultured cardiac myocytes and DNA and collagen synthesis in cardiac fibroblasts. *Metabolism*. 2004;53:710-715

70. Bishop JE, Laurent GJ. Collagen turnover and its regulation in the normal and hypertrophying heart. *Eur Heart J*. 1995;16 Suppl C:38-44

71. Shimizu M, Umeda K, Sugihara N, Yoshio H, Ino H, Takeda R, Okada Y, Nakanishi I. Collagen remodelling in myocardia of patients with diabetes. *J Clin Pathol*. 1993;46:32-36

72. van Hoeven KH, Factor SM. A comparison of the pathological spectrum of hypertensive, diabetic, and hypertensive-diabetic heart disease. *Circulation*. 1990;82:848-855

73. Malhotra A, Penpargkul S, Fein FS, Sonnenblick EH, Scheuer J. The effect of streptozotocin-induced diabetes in rats on cardiac contractile proteins. *Circ Res*. 1981;49:1243-1250

74. Utriainen T, Takala T, Luotolahti M, Ronnemaa T, Laine H, Ruotsalainen U, Haaparanta M, Nuutila P, Yki-Jarvinen H. Insulin resistance characterizes glucose uptake in skeletal muscle but not in the heart in niddm. *Diabetologia*. 1998;41:555-559

75. Jagasia D, Whiting JM, Concato J, Pfau S, McNulty PH. Effect of non-insulin-dependent diabetes mellitus on myocardial insulin responsiveness in patients with ischemic heart disease. *Circulation*. 2001;103:1734-1739

76. O'Neill BT, Abel ED. Akt1 in the cardiovascular system: Friend or foe? *J Clin Invest*. 2005;115:2059-2064

77. McMullen JR, Shioi T, Zhang L, Tarnavski O, Sherwood MC, Kang PM, Izumo S. Phosphoinositide 3-kinase(p110alpha) plays a critical role for the induction of physiological, but not pathological, cardiac hypertrophy. *Proc Natl Acad Sci U S A*. 2003;100:12355-12360

78. Izumo S, Nadal-Ginard B, Mahdavi V. Protooncogene induction and reprogramming of cardiac gene expression produced by pressure overload. *Proc Natl Acad Sci U S A*. 1988;85:339-343

79. Shioi T, Kang PM, Douglas PS, Hampe J, Yballe CM, Lawitts J, Cantley LC, Izumo S. The conserved phosphoinositide 3-kinase pathway determines heart size in mice. *EMBO J*. 2000;19:2537-2548

80. Khamzina L, Veilleux A, Bergeron S, Marette A. Increased activation of the mammalian target of rapamycin pathway in liver and skeletal muscle of obese rats: Possible involvement in obesity-linked insulin resistance. *Endocrinology*. 2005;146:1473-1481

81. Morisco C, Condorelli G, Trimarco V, Bellis A, Marrone C, Sadoshima J, Trimarco B. Akt mediates the cross-talk between beta-adrenergic and insulin receptors in neonatal cardiomyocytes. *Circ Res*. 2005;96:180-188

82. Choi KM, Zhong Y, Hoit BD, Grupp IL, Hahn H, Dilly KW, Guatimosim S, Lederer WJ, Matlib MA. Defective intracellular ca(2+) signaling contributes to cardiomyopathy in type 1 diabetic rats. *Am J Physiol Heart Circ Physiol*. 2002;283:H1398-1408

83. Pereira L, Matthes J, Schuster I, Valdivia HH, Herzig S, Richard S, Gomez AM. Mechanisms of [ca2+]i transient decrease in cardiomyopathy of db/db type 2 diabetic mice. *Diabetes*. 2006;55:608-615

84. Zhao XY, Hu SJ, Li J, Mou Y, Chen BP, Xia Q. Decreased cardiac sarcoplasmic reticulum ca2+ -atpase activity contributes to cardiac dysfunction in streptozotocin-induced diabetic rats. *Journal of physiology and biochemistry*. 2006;62:1-8

85. Sipido KR, Maes M, Van de Werf F. Low efficiency of ca2+ entry through the na(+)-ca2+ exchanger as trigger for ca2+ release from the sarcoplasmic reticulum. A comparison between l-type ca2+ current and reverse-mode na(+)-ca2+ exchange. *Circ Res*. 1997;81:1034-1044

86. Shigekawa M, Iwamoto T. Cardiac na(+)-ca(2+) exchange: Molecular and pharmacological aspects. *Circ Res*. 2001;88:864-876

87. Simmerman HK, Collins JH, Theibert JL, Wegener AD, Jones LR. Sequence analysis of phospholamban. Identification of phosphorylation sites and two major structural domains. *J Biol Chem*. 1986;261:13333-13341

88. Raeymaekers L, Hofmann F, Casteels R. Cyclic gmp-dependent protein kinase phosphorylates phospholamban in isolated sarcoplasmic reticulum from cardiac and smooth muscle. *Biochem J*. 1988;252:269-273

89. Hattori Y, Matsuda N, Kimura J, Ishitani T, Tamada A, Gando S, Kemmotsu O, Kanno M. Diminished function and expression of the cardiac na+-ca2+ exchanger in diabetic rats: Implication in ca2+ overload. *J Physiol*. 2000;527 Pt 1:85-94

90. Makino N, Dhalla KS, Elimban V, Dhalla NS. Sarcolemmal ca2+ transport in streptozotocin-induced diabetic cardiomyopathy in rats. *Am J Physiol*. 1987;253:E202-207

91. Wang DW, Kiyosue T, Shigematsu S, Arita M. Abnormalities of k+ and ca2+ currents in ventricular myocytes from rats with chronic diabetes. *Am J Physiol*. 1995;269:H1288-1296

92. Ganguly PK, Pierce GN, Dhalla KS, Dhalla NS. Defective sarcoplasmic reticular calcium transport in diabetic cardiomyopathy. *Am J Physiol*. 1983;244:E528-535

93. Penpargkul S, Fein F, Sonnenblick EH, Scheuer J. Depressed cardiac sarcoplasmic reticular function from diabetic rats. *J Mol Cell Cardiol*. 1981;13:303-309

94. Lopaschuk GD, Katz S, McNeill JH. Studies on the mechanism by which diabetes alters cardiac sarcoplasmic reticulum function. *Proc West Pharmacol Soc*. 1982;25:47-50

95. Han X, Abendschein DR, Kelley JG, Gross RW. Diabetes-induced changes in specific lipid molecular species in rat myocardium. *Biochem J*. 2000;352 Pt 1:79-89

96. Dhalla NS, Liu X, Panagia V, Takeda N. Subcellular remodeling and heart dysfunction in chronic diabetes. *Cardiovasc Res*. 1998;40:239-247

97. Xu KY, Zweier JL, Becker LC. Functional coupling between glycolysis and sarcoplasmic reticulum ca2+ transport. *Circ Res*. 1995;77:88-97

98. Netticadan T, Temsah RM, Kent A, Elimban V, Dhalla NS. Depressed levels of ca2+-cycling proteins may underlie sarcoplasmic reticulum dysfunction in the diabetic heart. *Diabetes*. 2001;50:2133-2138

99. Teshima Y, Takahashi N, Saikawa T, Hara M, Yasunaga S, Hidaka S, Sakata T. Diminished expression of sarcoplasmic reticulum ca(2+)-atpase and ryanodine sensitive ca(2+)channel mrna in streptozotocin-induced diabetic rat heart. *J Mol Cell Cardiol*. 2000;32:655-664

100. Depre C, Young ME, Ying J, Ahuja HS, Han Q, Garza N, Davies PJ, Taegtmeyer H. Streptozotocin-induced changes in cardiac gene expression in the absence of severe contractile dysfunction. *J Mol Cell Cardiol*. 2000;32:985-996

101. Forbes JM, Cooper ME. Mechanisms of diabetic complications. *Physiol Rev*.93:137-188

102. Neely JR, Morgan HE. Relationship between carbohydrate and lipid metabolism and the energy balance of heart muscle. *Annu Rev Physiol*. 1974;36:413-459

103. Stanley WC, Lopaschuk GD, Hall JL, McCormack JG. Regulation of myocardial carbohydrate metabolism under normal and ischaemic conditions. Potential for pharmacological interventions. *Cardiovasc Res*. 1997;33:243-257

104. Stanley WC, Lopaschuk GD, McCormack JG. Regulation of energy substrate metabolism in the diabetic heart. *Cardiovasc Res*. 1997;34:25-33

105. Belke DD, Larsen TS, Gibbs EM, Severson DL. Altered metabolism causes cardiac dysfunction in perfused hearts from diabetic (db/db) mice. *Am J Physiol Endocrinol Metab*. 2000;279:E1104-1113

106. Garvey WT, Hardin D, Juhaszova M, Dominguez JH. Effects of diabetes on myocardial glucose transport system in rats: Implications for diabetic cardiomyopathy. *Am J Physiol*. 1993;264:H837-844

107. Morgan HE, Cadenas E, Regen DM, Park CR. Regulation of glucose uptake in muscle. Ii. Rate-limiting steps and effects of insulin and anoxia in heart muscle from diabetic rats. *J Biol Chem*. 1961;236:262-268

108. Barrett EJ, Schwartz RG, Francis CK, Zaret BL. Regulation by insulin of myocardial glucose and fatty acid metabolism in the conscious dog. *J Clin Invest*. 1984;74:1073-1079

109. Camps M, Castello A, Munoz P, Monfar M, Testar X, Palacin M, Zorzano A. Effect of diabetes and fasting on glut-4 (muscle/fat) glucose-transporter expression in insulin-sensitive tissues. Heterogeneous response in heart, red and white muscle. *Biochem J*. 1992;282 (Pt 3):765-772

110. Stanley WC, Hall JL, Smith KR, Cartee GD, Hacker TA, Wisneski JA. Myocardial glucose transporters and glycolytic metabolism during ischemia in hyperglycemic diabetic swine. *Metabolism*. 1994;43:61-69

111. Hansford RG, Cohen L. Relative importance of pyruvate dehydrogenase interconversion and feed-back inhibition in the effect of fatty acids on pyruvate oxidation by rat heart mitochondria. *Arch Biochem Biophys*. 1978;191:65-81

112. McCormack JG, Edgell NJ, Denton RM. Studies on the interactions of ca2+ and pyruvate in the regulation of rat heart pyruvate dehydrogenase activity. Effects of starvation and diabetes. *Biochem J*. 1982;202:419-427

113. Lopaschuk GD. Abnormal mechanical function in diabetes: Relationship to altered myocardial carbohydrate/lipid metabolism. *Coron Artery Dis*. 1996;7:116-123

114. Murthy VK, Shipp JC. Accumulation of myocardial triglycerides ketotic diabetes; evidence for increased biosynthesis. *Diabetes*. 1977;26:222-229

115. Lopaschuk GD, Tsang H. Metabolism of palmitate in isolated working hearts from spontaneously diabetic "bb" wistar rats. *Circ Res*. 1987;61:853-858

116. McGarry JD, Leatherman GF, Foster DW. Carnitine palmitoyltransferase i. The site of inhibition of hepatic fatty acid oxidation by malonyl-coa. *J Biol Chem*. 1978;253:4128-4136

117. Tahiliani AG, McNeill JH. Diabetes-induced abnormalities in the myocardium. *Life Sci*. 1986;38:959-974

118. Shapiro LM. Specific heart disease in diabetes mellitus. *Br Med J (Clin Res Ed)*. 1982;284:140-141

119. Bellodi G, Manicardi V, Malavasi V, Veneri L, Bernini G, Bossini P, Distefano S, Magnanini G, Muratori L, Rossi G, et al. Hyperglycemia and prognosis of acute myocardial infarction in patients without diabetes mellitus. *Am J Cardiol*. 1989;64:885-888

120. Gilbertson DT, Liu J, Xue JL, Louis TA, Solid CA, Ebben JP, Collins AJ. Projecting the number of patients with end-stage renal disease in the united states to the year 2015. *J Am Soc Nephrol*. 2005;16:3736-3741

121. Cooper ME. Pathogenesis, prevention, and treatment of diabetic nephropathy. *Lancet*. 1998;352:213-219

122. Gurley SB, Clare SE, Snow KP, Hu A, Meyer TW, Coffman TM. Impact of genetic background on nephropathy in diabetic mice. *Am J Physiol Renal Physiol*. 2006;290:F214-222

123. Dorup J, Morsing P, Rasch R. Tubule-tubule and tubule-arteriole contacts in rat kidney distal nephrons. A morphologic study based on computer-assisted three-dimensional reconstructions. *Lab Invest*. 1992;67:761-769

124. Seyer-Hansen K, Hansen J, Gundersen HJ. Renal hypertrophy in experimental diabetes. A morphometric study. *Diabetologia*. 1980;18:501-505

125. Rasch R, Norgaard JO. Renal enlargement: Comparative autoradiographic studies of 3h-thymidine uptake in diabetic and uninephrectomized rats. *Diabetologia*. 1983;25:280-287

126. Mogensen CE, Andersen MJ. Increased kidney size and glomerular filtration rate in early juvenile diabetes. *Diabetes*. 1973;22:706-712

127. Seyer-Hansen K. Renal hypertrophy in experimental diabetes mellitus. *Kidney Int*. 1983;23:643-646

128. Ziyadeh FN. The extracellular matrix in diabetic nephropathy. *Am J Kidney Dis*. 1993;22:736-744

129. Schwieger J, Fine LG. Renal hypertrophy, growth factors, and nephropathy in diabetes mellitus. *Semin Nephrol*. 1990;10:242-253

130. Wolf G. Cellular mechanisms of tubule hypertrophy and hyperplasia in renal injury. *Miner Electrolyte Metab*. 1995;21:303-316

131. Wolf G, Sharma K, Chen Y, Ericksen M, Ziyadeh FN. High glucose-induced proliferation in mesangial cells is reversed by autocrine tgf-beta. *Kidney Int*. 1992;42:647-656

132. Nahman NS, Jr., Leonhart KL, Cosio FG, Hebert CL. Effects of high glucose on cellular proliferation and fibronectin production by cultured human mesangial cells. *Kidney Int*. 1992;41:396-402

133. Kolm-Litty V, Sauer U, Nerlich A, Lehmann R, Schleicher ED. High glucose-induced transforming growth factor beta1 production is mediated by the hexosamine pathway in porcine glomerular mesangial cells. *J Clin Invest*. 1998;101:160-169

134. Wolf G, Mueller E, Stahl RA, Ziyadeh FN. Angiotensin ii-induced hypertrophy of cultured murine proximal tubular cells is mediated by endogenous transforming growth factor-beta. *J Clin Invest*. 1993;92:1366-1372

135. Kaiser N, Sasson S, Feener EP, Boukobza-Vardi N, Higashi S, Moller DE, Davidheiser S, Przybylski RJ, King GL. Differential regulation of glucose transport and transporters by glucose in vascular endothelial and smooth muscle cells. *Diabetes*. 1993;42:80-89

136. Heilig CW, Concepcion LA, Riser BL, Freytag SO, Zhu M, Cortes P. Overexpression of glucose transporters in rat mesangial cells cultured in a normal glucose milieu mimics the diabetic phenotype. *J Clin Invest*. 1995;96:1802-1814

137. Koya D, King GL. Protein kinase c activation and the development of diabetic complications. *Diabetes*. 1998;47:859-866

138. Derubertis FR, Craven PA. Activation of protein kinase c in glomerular cells in diabetes. Mechanisms and potential links to the pathogenesis of diabetic glomerulopathy. *Diabetes*. 1994;43:1-8

139. Sharma K, Ziyadeh FN. Biochemical events and cytokine interactions linking glucose metabolism to the development of diabetic nephropathy. *Semin Nephrol*. 1997;17:80-92

140. Ishii H, Koya D, King GL. Protein kinase c activation and its role in the development of vascular complications in diabetes mellitus. *J Mol Med (Berl)*. 1998;76:21-31

141. Babazono T, Kapor-Drezgic J, Dlugosz JA, Whiteside C. Altered expression and subcellular localization of diacylglycerol-sensitive protein kinase c isoforms in diabetic rat glomerular cells. *Diabetes*. 1998;47:668-676

142. Haneda M, Araki S, Togawa M, Sugimoto T, Isono M, Kikkawa R. Activation of mitogen-activated protein kinase cascade in diabetic glomeruli and mesangial cells cultured under high glucose conditions. *Kidney Int Suppl*. 1997;60:S66-69

143. Meier M, Park JK, Overheu D, Kirsch T, Lindschau C, Gueler F, Leitges M, Menne J, Haller H. Deletion of protein kinase c-beta isoform in vivo reduces renal hypertrophy but not albuminuria in the streptozotocin-induced diabetic mouse model. *Diabetes*. 2007;56:346-354

144. Ohshiro Y, Ma RC, Yasuda Y, Hiraoka-Yamamoto J, Clermont AC, Isshiki K, Yagi K, Arikawa E, Kern TS, King GL. Reduction of diabetes-induced oxidative stress, fibrotic cytokine expression, and renal dysfunction in protein kinase cbeta-null mice. *Diabetes*. 2006;55:3112-3120

145. Menne J, Park JK, Boehne M, Elger M, Lindschau C, Kirsch T, Meier M, Gueler F, Fiebeler A, Bahlmann FH, Leitges M, Haller H. Diminished loss of proteoglycans and lack of albuminuria in protein kinase c-alpha-deficient diabetic mice. *Diabetes*. 2004;53:2101-2109

146. Tossidou I, Teng B, Menne J, Shushakova N, Park JK, Becker JU, Modde F, Leitges M, Haller H, Schiffer M. Podocytic pkc-alpha is regulated in murine and human diabetes and mediates nephrin endocytosis. *PLoS One*.5:e10185

147. Meier M, Menne J, Park JK, Holtz M, Gueler F, Kirsch T, Schiffer M, Mengel M, Lindschau C, Leitges M, Haller H. Deletion of protein kinase c-epsilon signaling pathway induces glomerulosclerosis and tubulointerstitial fibrosis in vivo. *J Am Soc Nephrol*. 2007;18:1190-1198

148. Djordjevic VB. Free radicals in cell biology. *Int Rev Cytol*. 2004;237:57-89

149. Lee HB, Yu MR, Yang Y, Jiang Z, Ha H. Reactive oxygen species-regulated signaling pathways in diabetic nephropathy. *J Am Soc Nephrol*. 2003;14:S241-245

150. Gonzalez DR, Treuer AV, Castellanos J, Dulce RA, Hare JM. Impaired s-nitrosylation of the ryanodine receptor caused by xanthine oxidase activity contributes to calcium leak in heart failure. *The Journal of biological chemistry*. 2010;285:28938-28945

151. Hayashi K, Kimata H, Obata K, Matsushita A, Fukata A, Hashimoto K, Noda A, Iwase M, Koike Y, Yokota M, Nagata K. Xanthine oxidase inhibition improves left ventricular dysfunction in dilated cardiomyopathic hamsters. *Journal of cardiac failure*. 2008;14:238-244

152. Gill PS, Wilcox CS. Nadph oxidases in the kidney. *Antioxid Redox Signal*. 2006;8:1597-1607

153. Korshunov SS, Skulachev VP, Starkov AA. High protonic potential actuates a mechanism of production of reactive oxygen species in mitochondria. *FEBS Lett*. 1997;416:15-18

154. Brownlee M. The pathobiology of diabetic complications: A unifying mechanism. *Diabetes*. 2005;54:1615-1625

155. Asaba K, Tojo A, Onozato ML, Goto A, Quinn MT, Fujita T, Wilcox CS. Effects of nadph oxidase inhibitor in diabetic nephropathy. *Kidney Int*. 2005;67:1890-1898

156. Etoh T, Inoguchi T, Kakimoto M, Sonoda N, Kobayashi K, Kuroda J, Sumimoto H, Nawata H. Increased expression of nad(p)h oxidase subunits, nox4 and p22phox, in the kidney of streptozotocin-induced diabetic rats and its reversibity by interventive insulin treatment. *Diabetologia*. 2003;46:1428-1437

157. Wilcox CS. Oxidative stress and nitric oxide deficiency in the kidney: A critical link to hypertension? *Am J Physiol Regul Integr Comp Physiol*. 2005;289:R913-935

158. Ruiz-Ortega M, Lorenzo O, Ruperez M, Blanco J, Egido J. Systemic infusion of angiotensin ii into normal rats activates nuclear factor-kappab and ap-1 in the kidney: Role of at(1) and at(2) receptors. *Am J Pathol*. 2001;158:1743-1756

159. Gorin Y, Ricono JM, Kim NH, Bhandari B, Choudhury GG, Abboud HE. Nox4 mediates angiotensin ii-induced activation of akt/protein kinase b in mesangial cells. *Am J Physiol Renal Physiol*. 2003;285:F219-229

160. Gorin Y, Block K, Hernandez J, Bhandari B, Wagner B, Barnes JL, Abboud HE. Nox4 nad(p)h oxidase mediates hypertrophy and fibronectin expression in the diabetic kidney. *J Biol Chem*. 2005;280:39616-39626

161. Koya D, Hayashi K, Kitada M, Kashiwagi A, Kikkawa R, Haneda M. Effects of antioxidants in diabetes-induced oxidative stress in the glomeruli of diabetic rats. *J Am Soc Nephrol*. 2003;14:S250-253

162. Craven PA, Melhem MF, Phillips SL, DeRubertis FR. Overexpression of cu2+/zn2+ superoxide dismutase protects against early diabetic glomerular injury in transgenic mice. *Diabetes*. 2001;50:2114-2125

163. Kitiyakara C, Chabrashvili T, Chen Y, Blau J, Karber A, Aslam S, Welch WJ, Wilcox CS. Salt intake, oxidative stress, and renal expression of nadph oxidase and superoxide dismutase. *J Am Soc Nephrol*. 2003;14:2775-2782

164. Phillips AO. The role of renal proximal tubular cells in diabetic nephropathy. *Curr Diab Rep*. 2003;3:491-496

165. Kearney PM, Whelton M, Reynolds K, Muntner P, Whelton PK, He J. Global burden of hypertension: Analysis of worldwide data. *Lancet*. 2005;365:217-223

166. Mayet J, Hughes A. Cardiac and vascular pathophysiology in hypertension. *Heart*. 2003;89:1104-1109

167. Cummins PM, von Offenberg Sweeney N, Killeen MT, Birney YA, Redmond EM, Cahill PA. Cyclic strain-mediated matrix metalloproteinase regulation within the vascular endothelium: A force to be reckoned with. *Am J Physiol Heart Circ Physiol*. 2007;292:H28-42

168. Intengan HD, Schiffrin EL. Vascular remodeling in hypertension: Roles of apoptosis, inflammation, and fibrosis. *Hypertension*. 2001;38:581-587

169. Deng LY, Schiffrin EL. Effects of endothelin-1 and vasopressin on resistance arteries of spontaneously hypertensive rats. *Am J Hypertens*. 1992;5:817-822

170. Mulvany MJ, Baumbach GL, Aalkjaer C, Heagerty AM, Korsgaard N, Schiffrin EL, Heistad DD. Vascular remodeling. *Hypertension*. 1996;28:505-506

171. Li JS, Knafo L, Turgeon A, Garcia R, Schiffrin EL. Effect of endothelin antagonism on blood pressure and vascular structure in renovascular hypertensive rats. *Am J Physiol*. 1996;271:H88-93

172. Korsgaard N, Aalkjaer C, Heagerty AM, Izzard AS, Mulvany MJ. Histology of subcutaneous small arteries from patients with essential hypertension. *Hypertension*. 1993;22:523-526

173. d'Uscio LV, Barton M, Shaw S, Moreau P, Luscher TF. Structure and function of small arteries in salt-induced hypertension: Effects of chronic endothelin-subtype-a-receptor blockade. *Hypertension*. 1997;30:905-911

174. Deng LY, Schiffrin EL. Morphological and functional alterations of mesenteric small resistance arteries in early renal hypertension in rats. *Am J Physiol*. 1991;261:H1171-1177

175. Schiffrin EL, Deng LY, Larochelle P. Morphology of resistance arteries and comparison of effects of vasoconstrictors in mild essential hypertensive patients. *Clin Invest Med*. 1993;16:177-186

176. Rizzoni D, Porteri E, Castellano M, Bettoni G, Muiesan ML, Muiesan P, Giulini SM, Agabiti-Rosei E. Vascular hypertrophy and remodeling in secondary hypertension. *Hypertension*. 1996;28:785-790

177. Intengan HD, Schiffrin EL. Structure and mechanical properties of resistance arteries in hypertension: Role of adhesion molecules and extracellular matrix determinants. *Hypertension*. 2000;36:312-318

178. Tea BS, Der Sarkissian S, Touyz RM, Hamet P, deBlois D. Proapoptotic and growth-inhibitory role of angiotensin ii type 2 receptor in vascular smooth muscle cells of spontaneously hypertensive rats in vivo. *Hypertension*. 2000;35:1069-1073

179. Cattaruzza M, Dimigen C, Ehrenreich H, Hecker M. Stretch-induced endothelin b receptor-mediated apoptosis in vascular smooth muscle cells. *FASEB J*. 2000;14:991-998

180. Sharifi AM, Schiffrin EL. Apoptosis in vasculature of spontaneously hypertensive rats: Effect of an angiotensin converting enzyme inhibitor and a calcium channel antagonist. *Am J Hypertens*. 1998;11:1108-1116

181. deBlois D, Tea BS, Than VD, Tremblay J, Hamet P. Smooth muscle apoptosis during vascular regression in spontaneously hypertensive rats. *Hypertension*. 1997;29:340-349

182. Ooshima A, Fuller GC, Cardinale GJ, Spector S, Udenfriend S. Increased collagen synthesis in blood vessels of hypertensive rats and its reversal by antihypertensive agents. *Proc Natl Acad Sci U S A*. 1974;71:3019-3023

183. Chamiot Clerc P, Renaud JF, Blacher J, Legrand M, Samuel JL, Levy BI, Sassard J, Safar ME. Collagen i and iii and mechanical properties of conduit arteries in rats with genetic hypertension. *J Vasc Res*. 1999;36:139-146

184. Intengan HD, Deng LY, Li JS, Schiffrin EL. Mechanics and composition of human subcutaneous resistance arteries in essential hypertension. *Hypertension*. 1999;33:569-574

185. Mulvany MJ. A reduced elastic modulus of vascular wall components in hypertension? *Hypertension*. 1992;20:7-9

186. Thybo NK, Mulvany MJ, Jastrup B, Nielsen H, Aalkjaer C. Some pharmacological and elastic characteristics of isolated subcutaneous small arteries from patients with essential hypertension. *J Hypertens*. 1996;14:993-998

187. Flamant M, Placier S, Dubroca C, Esposito B, Lopes I, Chatziantoniou C, Tedgui A, Dussaule JC, Lehoux S. Role of matrix metalloproteinases in early hypertensive vascular remodeling. *Hypertension*. 2007;50:212-218

188. Lemarie CA, Tharaux PL, Lehoux S. Extracellular matrix alterations in hypertensive vascular remodeling. *J Mol Cell Cardiol*.48:433-439

189. Hu JJ, Ambrus A, Fossum TW, Miller MW, Humphrey JD, Wilson E. Time courses of growth and remodeling of porcine aortic media during hypertension: A quantitative immunohistochemical examination. *J Histochem Cytochem*. 2008;56:359-370

190. O'Rourke MF. Arterial aging: Pathophysiological principles. *Vasc Med*. 2007;12:329-341

191. Wilkinson IB, McEniery CM. Arterial stiffness, endothelial function and novel pharmacological approaches. *Clin Exp Pharmacol Physiol*. 2004;31:795-799

192. Faury G, Pezet M, Knutsen RH, Boyle WA, Heximer SP, McLean SE, Minkes RK, Blumer KJ, Kovacs A, Kelly DP, Li DY, Starcher B, Mecham RP. Developmental adaptation of the mouse cardiovascular system to elastin haploinsufficiency. *J Clin Invest*. 2003;112:1419-1428

193. Baker AH, Edwards DR, Murphy G. Metalloproteinase inhibitors: Biological actions and therapeutic opportunities. *J Cell Sci*. 2002;115:3719-3727

194. Brew K, Dinakarpandian D, Nagase H. Tissue inhibitors of metalloproteinases: Evolution, structure and function. *Biochim Biophys Acta*. 2000;1477:267-283

195. Lerman LO, Chade AR, Sica V, Napoli C. Animal models of hypertension: An overview. *J Lab Clin Med*. 2005;146:160-173

196. Kuro-o M, Hanaoka K, Hiroi Y, Noguchi T, Fujimori Y, Takewaki S, Hayasaka M, Katoh H, Miyagishi A, Nagai R, et al. Salt-sensitive hypertension in transgenic mice overexpressing na(+)-proton exchanger. *Circ Res*. 1995;76:148-153

197. Kimura S, Mullins JJ, Bunnemann B, Metzger R, Hilgenfeldt U, Zimmermann F, Jacob H, Fuxe K, Ganten D, Kaling M. High blood pressure in transgenic mice carrying the rat angiotensinogen gene. *EMBO J*. 1992;11:821-827

198. Ohkubo H, Kawakami H, Kakehi Y, Takumi T, Arai H, Yokota Y, Iwai M, Tanabe Y, Masu M, Hata J, et al. Generation of transgenic mice with elevated blood pressure by introduction of the rat renin and angiotensinogen genes. *Proc Natl Acad Sci U S A*. 1990;87:5153-5157

199. Pitzalis MV, Sarzani R, Dessi-Fulgheri P, Iacoviello M, Forleo C, Lucarelli K, Pietrucci F, Salvi F, Sorrentino S, Romito R, Guida P, Rappelli A, Rizzon P. Allelic variants of natriuretic peptide receptor genes are associated with family history of hypertension and cardiovascular phenotype. *J Hypertens*. 2003;21:1491-1496

200. Shoji M, Tsutaya S, Saito R, Takamatu H, Yasujima M. Positive association of endothelial nitric oxide synthase gene polymorphism with hypertension in northern japan. *Life Sci*. 2000;66:2557-2562

201. Telemaque-Potts S, Kuc RE, Maguire JJ, Ohlstein E, Yanagisawa M, Davenport AP. Elevated systemic levels of endothelin-1 and blood pressure correlate with blunted constrictor responses and downregulation of endothelin(a), but not endothelin(b), receptors in an animal model of hypertension. *Clin Sci (Lond)*. 2002;103 Suppl 48:357S-362S

202. Alfie ME, Yang XP, Hess F, Carretero OA. Salt-sensitive hypertension in bradykinin b2 receptor knockout mice. *Biochem Biophys Res Commun*. 1996;224:625-630

203. Breyer MD, Breyer RM. Prostaglandin receptors: Their role in regulating renal function. *Curr Opin Nephrol Hypertens*. 2000;9:23-29

204. Goldblatt H, Lynch J, Hanzal RF, Summerville WW. Studies on experimental hypertension : I. The production of persistent elevation of systolic blood pressure by means of renal ischemia. *J Exp Med*. 1934;59:347-379

205. Thurston H, Swales JD. Influence of sodium restriction upon two models of renal hypertension. *Clin Sci Mol Med*. 1976;51:275-279

206. Selye H. Production of nephrosclerosis by overdosage with desoxycorticosterone acetate. *Can Med Assoc J*. 1942;47:515-519

207. Lahera V, Salazar J, Salom MG, Romero JC. Deficient production of nitric oxide induces volume-dependent hypertension. *J Hypertens Suppl*. 1992;10:S173-177

208. Hwang IS, Ho H, Hoffman BB, Reaven GM. Fructose-induced insulin resistance and hypertension in rats. *Hypertension*. 1987;10:512-516

209. Rizkalla B, Forbes JM, Cooper ME, Cao Z. Increased renal vascular endothelial growth factor and angiopoietins by angiotensin ii infusion is mediated by both at1 and at2 receptors. *J Am Soc Nephrol*. 2003;14:3061-3071

210. Edgley A, Kett M, Anderson W. 'Slow pressor' hypertension from low-dose chronic angiotensin ii infusion. *Clin Exp Pharmacol Physiol*. 2001;28:1035-1039

211. Lederle FA, Johnson GR, Wilson SE, Chute EP, Littooy FN, Bandyk D, Krupski WC, Barone GW, Acher CW, Ballard DJ. Prevalence and associations of abdominal aortic aneurysm detected through screening. Aneurysm detection and management (adam) veterans affairs cooperative study group. *Ann Intern Med*. 1997;126:441-449

212. Wanhainen A, Lundkvist J, Bergqvist D, Bjorck M. Cost-effectiveness of screening women for abdominal aortic aneurysm. *J Vasc Surg*. 2006;43:908-914; discussion 914

213. Best VA, Price JF, Fowkes FG. Persistent increase in the incidence of abdominal aortic aneurysm in scotland, 1981-2000. *Br J Surg*. 2003;90:1510-1515

214. Filipovic M, Goldacre MJ, Roberts SE, Yeates D, Duncan ME, Cook-Mozaffari P. Trends in mortality and hospital admission rates for abdominal aortic aneurysm in england and wales, 1979-1999. *Br J Surg*. 2005;92:968-975

215. Verloes A, Sakalihasan N, Koulischer L, Limet R. Aneurysms of the abdominal aorta: Familial and genetic aspects in three hundred thirteen pedigrees. *J Vasc Surg*. 1995;21:646-655

216. Dobrin PB, Mrkvicka R. Failure of elastin or collagen as possible critical connective tissue alterations underlying aneurysmal dilatation. *Cardiovasc Surg*. 1994;2:484-488

217. Nordon IM, Hinchliffe RJ, Loftus IM, Thompson MM. Pathophysiology and epidemiology of abdominal aortic aneurysms. *Nat Rev Cardiol*.8:92-102

218. Mata KM, Prudente PS, Rocha FS, Prado CM, Floriano EM, Elias J, Jr., Rizzi E, Gerlach RF, Rossi MA, Ramos SG. Combining two potential causes of metalloproteinase secretion causes abdominal aortic aneurysms in rats: A new experimental model. *Int J Exp Pathol*.92:26-39

219. Shi GP, Sukhova GK, Grubb A, Ducharme A, Rhode LH, Lee RT, Ridker PM, Libby P, Chapman HA. Cystatin c deficiency in human atherosclerosis and aortic aneurysms. *J Clin Invest*. 1999;104:1191-1197

220. Shimizu K, Mitchell RN, Libby P. Inflammation and cellular immune responses in abdominal aortic aneurysms. *Arterioscler Thromb Vasc Biol*. 2006;26:987-994

221. Subramanian V, Uchida HA, Ijaz T, Moorleghen JJ, Howatt DA, Balakrishnan A. Calpain inhibition attenuates angiotensin ii-induced abdominal aortic aneurysms and atherosclerosis in low-density lipoprotein receptor-deficient mice. *Journal of cardiovascular pharmacology*. 2012;59:66-76

222. Thompson RW, Parks WC. Role of matrix metalloproteinases in abdominal aortic aneurysms. *Ann N Y Acad Sci*. 1996;800:157-174

223. Brophy CM, Marks WH, Reilly JM, Tilson MD. Decreased tissue inhibitor of metalloproteinases (timp) in abdominal aortic aneurysm tissue: A preliminary report. *J Surg Res*. 1991;50:653-657

224. McMillan WD, Tamarina NA, Cipollone M, Johnson DA, Parker MA, Pearce WH. Size matters: The relationship between mmp-9 expression and aortic diameter. *Circulation*. 1997;96:2228-2232

225. Wilson WR, Anderton M, Schwalbe EC, Jones JL, Furness PN, Bell PR, Thompson MM. Matrix metalloproteinase-8 and -9 are increased at the site of abdominal aortic aneurysm rupture. *Circulation*. 2006;113:438-445

226. Bergoeing MP, Arif B, Hackmann AE, Ennis TL, Thompson RW, Curci JA. Cigarette smoking increases aortic dilatation without affecting matrix metalloproteinase-9 and -12 expression in a modified mouse model of aneurysm formation. *J Vasc Surg*. 2007;45:1217-1227

227. Sho E, Sho M, Nanjo H, Kawamura K, Masuda H, Dalman RL. Hemodynamic regulation of cd34+ cell localization and differentiation in experimental aneurysms. *Arterioscler Thromb Vasc Biol*. 2004;24:1916-1921

228. Martin-McNulty B, Vincelette J, Vergona R, Sullivan ME, Wang YX. Noninvasive measurement of abdominal aortic aneurysms in intact mice by a high-frequency ultrasound imaging system. *Ultrasound Med Biol*. 2005;31:745-749

229. Barisione C, Charnigo R, Howatt DA, Moorleghen JJ, Rateri DL, Daugherty A. Rapid dilation of the abdominal aorta during infusion of

angiotensin ii detected by noninvasive high-frequency ultrasonography. *J Vasc Surg*. 2006;44:372-376

230. Daugherty A, Cassis LA. Mouse models of abdominal aortic aneurysms. *Arterioscler Thromb Vasc Biol*. 2004;24:429-434

231. Brophy CM, Tilson JE, Braverman IM, Tilson MD. Age of onset, pattern of distribution, and histology of aneurysm development in a genetically predisposed mouse model. *J Vasc Surg*. 1988;8:45-48

232. Carrell TW, Smith A, Burnand KG. Experimental techniques and models in the study of the development and treatment of abdominal aortic aneurysm. *Br J Surg*. 1999;86:305-312

233. Maki JM, Rasanen J, Tikkanen H, Sormunen R, Makikallio K, Kivirikko KI, Soininen R. Inactivation of the lysyl oxidase gene lox leads to aortic aneurysms, cardiovascular dysfunction, and perinatal death in mice. *Circulation*. 2002;106:2503-2509

234. Silence J, Lupu F, Collen D, Lijnen HR. Persistence of atherosclerotic plaque but reduced aneurysm formation in mice with stromelysin-1 (mmp-3) gene inactivation. *Arterioscler Thromb Vasc Biol*. 2001;21:1440-1445

235. Silence J, Collen D, Lijnen HR. Reduced atherosclerotic plaque but enhanced aneurysm formation in mice with inactivation of the tissue inhibitor of metalloproteinase-1 (timp-1) gene. *Circ Res*. 2002;90:897-903

236. Zhang SH, Reddick RL, Piedrahita JA, Maeda N. Spontaneous hypercholesterolemia and arterial lesions in mice lacking apolipoprotein e. *Science*. 1992;258:468-471

237. Ishibashi S, Goldstein JL, Brown MS, Herz J, Burns DK. Massive xanthomatosis and atherosclerosis in cholesterol-fed low density lipoprotein receptor-negative mice. *J Clin Invest*. 1994;93:1885-1893

238. Tangirala RK, Rubin EM, Palinski W. Quantitation of atherosclerosis in murine models: Correlation between lesions in the aortic origin and in the entire aorta, and differences in the extent of lesions between sexes in ldl receptor-deficient and apolipoprotein e-deficient mice. *J Lipid Res*. 1995;36:2320-2328

239. Carmeliet P, Moons L, Lijnen R, Baes M, Lemaitre V, Tipping P, Drew A, Eeckhout Y, Shapiro S, Lupu F, Collen D. Urokinase-generated plasmin activates matrix metalloproteinases during aneurysm formation. *Nat Genet*. 1997;17:439-444

240. Patel MI, Hardman DT, Fisher CM, Appleberg M. Current views on the pathogenesis of abdominal aortic aneurysms. *J Am Coll Surg*. 1995;181:371-382

241. Nordon I, Brar R, Taylor J, Hinchliffe R, Loftus IM, Thompson MM. Evidence from cross-sectional imaging indicates abdominal but not thoracic aortic aneurysms are local manifestations of a systemic dilating diathesis. *J Vasc Surg*. 2009;50:171-176 e171

242. Shantikumar S, Ajjan R, Porter KE, Scott DJ. Diabetes and the abdominal aortic aneurysm. *Eur J Vasc Endovasc Surg*.39:200-207

243. Fukamizu A, Sugimura K, Takimoto E, Sugiyama F, Seo MS, Takahashi S, Hatae T, Kajiwara N, Yagami K, Murakami K. Chimeric renin-angiotensin system demonstrates sustained increase in blood pressure of transgenic mice carrying both human renin and human angiotensinogen genes. *J Biol Chem*. 1993;268:11617-11621

244. Nishijo N, Sugiyama F, Kimoto K, Taniguchi K, Murakami K, Suzuki S, Fukamizu A, Yagami K. Salt-sensitive aortic aneurysm and rupture in hypertensive transgenic mice that overproduce angiotensin ii. *Lab Invest*. 1998;78:1059-1066

245. Pyo R, Lee JK, Shipley JM, Curci JA, Mao D, Ziporin SJ, Ennis TL, Shapiro SD, Senior RM, Thompson RW. Targeted gene disruption of matrix metalloproteinase-9 (gelatinase b) suppresses development of experimental abdominal aortic aneurysms. *J Clin Invest*. 2000;105:1641-1649

246. Longo GM, Xiong W, Greiner TC, Zhao Y, Fiotti N, Baxter BT. Matrix metalloproteinases 2 and 9 work in concert to produce aortic aneurysms. *J Clin Invest*. 2002;110:625-632

247. Daugherty A, Manning MW, Cassis LA. Angiotensin ii promotes atherosclerotic lesions and aneurysms in apolipoprotein e-deficient mice. *J Clin Invest*. 2000;105:1605-1612

248. Basu R, Fan D, Kandalam V, Lee J, Das SK, Wang X, Baldwin TA, Oudit GY, Kassiri Z. Loss of timp3 gene leads to abdominal aortic aneurysm formation in response to angiotensin ii. *J Biol Chem*. 2012;287:44083-44096

249. Anidjar S, Salzmann JL, Gentric D, Lagneau P, Camilleri JP, Michel JB. Elastase-induced experimental aneurysms in rats. *Circulation*. 1990;82:973-981

250. Nishimoto M, Takai S, Fukumoto H, Tsunemi K, Yuda A, Sawada Y, Yamada M, Jin D, Sakaguchi M, Nishimoto Y, Sasaki S, Miyazaki M. Increased local angiotensin ii formation in aneurysmal aorta. *Life Sci*. 2002;71:2195-2205

251. Liao S, Miralles M, Kelley BJ, Curci JA, Borhani M, Thompson RW. Suppression of experimental abdominal aortic aneurysms in the rat by treatment with angiotensin-converting enzyme inhibitors. *J Vasc Surg*. 2001;33:1057-1064

252. Chiou AC, Chiu B, Pearce WH. Murine aortic aneurysm produced by periarterial application of calcium chloride. *J Surg Res*. 2001;99:371-376

253. Deng GG, Martin-McNulty B, Sukovich DA, Freay A, Halks-Miller M, Thinnes T, Loskutoff DJ, Carmeliet P, Dole WP, Wang YX. Urokinase-type plasminogen activator plays a critical role in angiotensin ii-induced abdominal aortic aneurysm. *Circ Res*. 2003;92:510-517

254. Lijnen HR, Lupu F, Moons L, Carmeliet P, Goulding D, Collen D. Temporal and topographic matrix metalloproteinase expression after vascular injury in mice. *Thromb Haemost*. 1999;81:799-807

255. Visse R, Nagase H. Matrix metalloproteinases and tissue inhibitors of metalloproteinases: Structure, function, and biochemistry. *Circ Res*. 2003;92:827-839

256. Galis ZS, Khatri JJ. Matrix metalloproteinases in vascular remodeling and atherogenesis: The good, the bad, and the ugly. *Circ Res*. 2002;90:251-262

257. Liu YE, Wang M, Greene J, Su J, Ullrich S, Li H, Sheng S, Alexander P, Sang QA, Shi YE. Preparation and characterization of recombinant tissue inhibitor of metalloproteinase 4 (timp-4). *J Biol Chem*. 1997;272:20479-20483

258. Uria JA, Lopez-Otin C. Matrilysin-2, a new matrix metalloproteinase expressed in human tumors and showing the minimal domain organization required for secretion, latency, and activity. *Cancer research*. 2000;60:4745-4751

259. de Coignac AB, Elson G, Delneste Y, Magistrelli G, Jeannin P, Aubry JP, Berthier O, Schmitt D, Bonnefoy JY, Gauchat JF. Cloning of mmp-26. A novel matrilysin-like proteinase. *European journal of biochemistry / FEBS*. 2000;267:3323-3329

260. Raffetto JD, Khalil RA. Matrix metalloproteinases and their inhibitors in vascular remodeling and vascular disease. *Biochem Pharmacol*. 2008;75:346-359

261. Ra HJ, Parks WC. Control of matrix metalloproteinase catalytic activity. *Matrix biology : journal of the International Society for Matrix Biology*. 2007;26:587-596

262. Somerville RP, Oblander SA, Apte SS. Matrix metalloproteinases: Old dogs with new tricks. *Genome Biol*. 2003;4:216

263. Allan JA, Docherty AJ, Barker PJ, Huskisson NS, Reynolds JJ, Murphy G. Binding of gelatinases a and b to type-i collagen and other matrix components. *Biochem J*. 1995;309 (Pt 1):299-306

264. McMillan WD, Patterson BK, Keen RR, Shively VP, Cipollone M, Pearce WH. In situ localization and quantification of mrna for 92-kd type iv collagenase and its inhibitor in aneurysmal, occlusive, and normal aorta. *Arterioscler Thromb Vasc Biol*. 1995;15:1139-1144

265. d'Ortho MP, Will H, Atkinson S, Butler G, Messent A, Gavrilovic J, Smith B, Timpl R, Zardi L, Murphy G. Membrane-type matrix metalloproteinases 1 and 2 exhibit broad-spectrum proteolytic capacities comparable to many matrix metalloproteinases. *Eur J Biochem*. 1997;250:751-757

266. Marchenko GN, Strongin AY. Mmp-28, a new human matrix metalloproteinase with an unusual cysteine-switch sequence is widely expressed in tumors. *Gene*. 2001;265:87-93

267. Boyle JR, McDermott E, Crowther M, Wills AD, Bell PR, Thompson MM. Doxycycline inhibits elastin degradation and reduces metalloproteinase activity in a model of aneurysmal disease. *J Vasc Surg*. 1998;27:354-361

268. Newman KM, Malon AM, Shin RD, Scholes JV, Ramey WG, Tilson MD. Matrix metalloproteinases in abdominal aortic aneurysm: Characterization, purification, and their possible sources. *Connect Tissue Res*. 1994;30:265-276

269. Hovsepian DM, Ziporin SJ, Sakurai MK, Lee JK, Curci JA, Thompson RW. Elevated plasma levels of matrix metalloproteinase-9 in patients with abdominal aortic aneurysms: A circulating marker of degenerative aneurysm disease. *J Vasc Interv Radiol*. 2000;11:1345-1352

270. Lindholt JS, Vammen S, Fasting H, Henneberg EW, Heickendorff L. The plasma level of matrix metalloproteinase 9 may predict the natural history

of small abdominal aortic aneurysms. A preliminary study. *Eur J Vasc Endovasc Surg*. 2000;20:281-285

271. Sangiorgi G, D'Averio R, Mauriello A, Bondio M, Pontillo M, Castelvecchio S, Trimarchi S, Tolva V, Nano G, Rampoldi V, Spagnoli LG, Inglese L. Plasma levels of metalloproteinases-3 and -9 as markers of successful abdominal aortic aneurysm exclusion after endovascular graft treatment. *Circulation*. 2001;104:I288-295

272. Zervoudaki A, Economou E, Stefanadis C, Pitsavos C, Tsioufis K, Aggeli C, Vasiliadou K, Toutouza M, Toutouzas P. Plasma levels of active extracellular matrix metalloproteinases 2 and 9 in patients with essential hypertension before and after antihypertensive treatment. *J Hum Hypertens*. 2003;17:119-124

273. Sakalihasan N, Delvenne P, Nusgens BV, Limet R, Lapiere CM. Activated forms of mmp2 and mmp9 in abdominal aortic aneurysms. *J Vasc Surg*. 1996;24:127-133

274. Crowther M, Goodall S, Jones JL, Bell PR, Thompson MM. Localization of matrix metalloproteinase 2 within the aneurysmal and normal aortic wall. *Br J Surg*. 2000;87:1391-1400

275. Petersen E, Gineitis A, Wagberg F, Angquist KA. Activity of matrix metalloproteinase-2 and -9 in abdominal aortic aneurysms. Relation to size and rupture. *Eur J Vasc Endovasc Surg*. 2000;20:457-461

276. Irizarry E, Newman KM, Gandhi RH, Nackman GB, Halpern V, Wishner S, Scholes JV, Tilson MD. Demonstration of interstitial collagenase in abdominal aortic aneurysm disease. *J Surg Res*. 1993;54:571-574

277. Goodall S, Crowther M, Hemingway DM, Bell PR, Thompson MM. Ubiquitous elevation of matrix metalloproteinase-2 expression in the vasculature of patients with abdominal aneurysms. *Circulation*. 2001;104:304-309

278. Wilson WR, Schwalbe EC, Jones JL, Bell PR, Thompson MM. Matrix metalloproteinase 8 (neutrophil collagenase) in the pathogenesis of abdominal aortic aneurysm. *Br J Surg*. 2005;92:828-833

279. Longo GM, Buda SJ, Fiotta N, Xiong W, Griener T, Shapiro S, Baxter BT. Mmp-12 has a role in abdominal aortic aneurysms in mice. *Surgery*. 2005;137:457-462

280. Mao D, Lee JK, VanVickle SJ, Thompson RW. Expression of collagenase-3 (mmp-13) in human abdominal aortic aneurysms and

vascular smooth muscle cells in culture. *Biochem Biophys Res Commun*. 1999;261:904-910

281. Xiong W, Knispel R, MacTaggart J, Greiner TC, Weiss SJ, Baxter BT. Membrane-type 1 matrix metalloproteinase regulates macrophage-dependent elastolytic activity and aneurysm formation in vivo. *J Biol Chem*. 2009;284:1765-1771

282. Nagashima H, Aoka Y, Sakomura Y, Sakuta A, Aomi S, Ishizuka N, Hagiwara N, Kawana M, Kasanuki H. A 3-hydroxy-3-methylglutaryl coenzyme a reductase inhibitor, cerivastatin, suppresses production of matrix metalloproteinase-9 in human abdominal aortic aneurysm wall. *J Vasc Surg*. 2002;36:158-163

283. McMillan WD, Pearce WH. Increased plasma levels of metalloproteinase-9 are associated with abdominal aortic aneurysms. *J Vasc Surg*. 1999;29:122-127; discussion 127-129

284. Knox JB, Sukhova GK, Whittemore AD, Libby P. Evidence for altered balance between matrix metalloproteinases and their inhibitors in human aortic diseases. *Circulation*. 1997;95:205-212

285. Chew DK, Conte MS, Khalil RA. Matrix metalloproteinase-specific inhibition of ca2+ entry mechanisms of vascular contraction. *J Vasc Surg*. 2004;40:1001-1010

286. Vanhoutte D, Heymans S. Timps and cardiac remodeling: 'Embracing the mmp-independent-side of the family'. *J Mol Cell Cardiol*.48:445-453

287. Lambert E, Dasse E, Haye B, Petitfrere E. Timps as multifacial proteins. *Crit Rev Oncol Hematol*. 2004;49:187-198

288. Murphy G, Houbrechts A, Cockett MI, Williamson RA, O'Shea M, Docherty AJ. The n-terminal domain of tissue inhibitor of metalloproteinases retains metalloproteinase inhibitory activity. *Biochemistry*. 1991;30:8097-8102

289. Will H, Atkinson SJ, Butler GS, Smith B, Murphy G. The soluble catalytic domain of membrane type 1 matrix metalloproteinase cleaves the propeptide of progelatinase a and initiates autoproteolytic activation. Regulation by timp-2 and timp-3. *J Biol Chem*. 1996;271:17119-17123

290. Dodd BR, Spence RA. Doxycycline inhibition of abdominal aortic aneurysm growth: A systematic review of the literature. *Curr Vasc Pharmacol*.9:471-478

291. Kashiwagi M, Tortorella M, Nagase H, Brew K. Timp-3 is a potent inhibitor of aggrecanase 1 (adam-ts4) and aggrecanase 2 (adam-ts5). *J Biol Chem*. 2001;276:12501-12504

292. Yang TT, Hawkes SP. Role of the 21-kda protein timp-3 in oncogenic transformation of cultured chicken embryo fibroblasts. *Proc Natl Acad Sci U S A*. 1992;89:10676-10680

293. Baker AH, Zaltsman AB, George SJ, Newby AC. Divergent effects of tissue inhibitor of metalloproteinase-1, -2, or -3 overexpression on rat vascular smooth muscle cell invasion, proliferation, and death in vitro. Timp-3 promotes apoptosis. *J Clin Invest*. 1998;101:1478-1487

294. Theruvath TP, Jones JA, Ikonomidis JS. Matrix metalloproteinases and descending aortic aneurysms: Parity, disparity, and switch. *J Card Surg*.27:81-90

295. Tamarina NA, McMillan WD, Shively VP, Pearce WH. Expression of matrix metalloproteinases and their inhibitors in aneurysms and normal aorta. *Surgery*. 1997;122:264-271; discussion 271-262

296. Annabi B, Shedid D, Ghosn P, Kenigsberg RL, Desrosiers RR, Bojanowski MW, Beaulieu E, Nassif E, Moumdjian R, Beliveau R. Differential regulation of matrix metalloproteinase activities in abdominal aortic aneurysms. *J Vasc Surg*. 2002;35:539-546

297. McMillan WD, Patterson BK, Keen RR, Pearce WH. In situ localization and quantification of seventy-two-kilodalton type iv collagenase in aneurysmal, occlusive, and normal aorta. *J Vasc Surg*. 1995;22:295-305

298. Crowther M, Goodall S, Jones JL, Bell PR, Thompson MM. Increased matrix metalloproteinase 2 expression in vascular smooth muscle cells cultured from abdominal aortic aneurysms. *J Vasc Surg*. 2000;32:575-583

299. Golub LM, Lee HM, Lehrer G, Nemiroff A, McNamara TF, Kaplan R, Ramamurthy NS. Minocycline reduces gingival collagenolytic activity during diabetes. Preliminary observations and a proposed new mechanism of action. *J Periodontal Res*. 1983;18:516-526

300. Franco C, Ho B, Mulholland D, Hou G, Islam M, Donaldson K, Bendeck MP. Doxycycline alters vascular smooth muscle cell adhesion, migration, and reorganization of fibrillar collagen matrices. *Am J Pathol*. 2006;168:1697-1709

301. Kivela-Rajamaki M, Maisi P, Srinivas R, Tervahartiala T, Teronen O, Husa V, Salo T, Sorsa T. Levels and molecular forms of mmp-7

(matrilysin-1) and mmp-8 (collagenase-2) in diseased human peri-implant sulcular fluid. *J Periodontal Res*. 2003;38:583-590

302. Sapadin AN, Fleischmajer R. Tetracyclines: Nonantibiotic properties and their clinical implications. *J Am Acad Dermatol*. 2006;54:258-265

303. Petrinec D, Liao S, Holmes DR, Reilly JM, Parks WC, Thompson RW. Doxycycline inhibition of aneurysmal degeneration in an elastase-induced rat model of abdominal aortic aneurysm: Preservation of aortic elastin associated with suppressed production of 92 kd gelatinase. *J Vasc Surg*. 1996;23:336-346

304. Curci JA, Petrinec D, Liao S, Golub LM, Thompson RW. Pharmacologic suppression of experimental abdominal aortic aneurysms: Acomparison of doxycycline and four chemically modified tetracyclines. *J Vasc Surg*. 1998;28:1082-1093

CHAPTER TWO

MATERIALS AND METHODS

2.1 ANIMAL CARE

Wild-type (WT), diabetic heterozygous Akita (*Ins2*$^{WT/C96Y}$), were purchased from Jackson Laboratories (Bar Harbor, USA), TIMP3-deficient (TIMP3$^{-/-}$)[1] and MMP2-deficient mice (MMP2$^{-/-}$)[2] were generated as described. All mice were in C57BL/6 background. Mice were housed and bred in the animal facility at the University of Alberta. All animal experiments were conducted in accordance with the guidelines of the University of Alberta Animal care and Canadian Council on Animal Care Guidelines and regulations of Animal Policy and Welfare (protocol 633 AUP). Throughout the period of study, animals were provided with free access to water and standard rodent chow (Harlan Teklad, Madison, WI).

2.1.1 Genetic Mouse Model of Diabetes Type I (Akita)

The Ins2WT/C96Y (Akita) mouse is a well-established, non-obese model of type 1 diabetes. It has been adopted by Animal Models of Diabetic Complications Consortium. (AMDCC) as an important animal model to study the chronic type 1 diabetic complications[3]. The Akita mouse model harbours a spontaneous mutation of C96Y in the insulin gene resulting in impaired pro-insulin folding in the endoplasmic reticulum creating protein aggregates in the ER. This initiates ER stress responses resulting in severe β-cell dysfunction and impaired insulin secretion[4-7]. These heterozygous mice develop severe hyperglycemia due to lack of plasma insulin as early as 3 to 4 weeks of age [3]. Thus, the Akita mouse has the

characteristics to study chronic type 1 diabetic complications as it recapitulates effects of various genetic manipulations on progression of diabetic cardiovascular complications [8-15] and diabetic nephropathy [16-30] in humans.

2.1.1.1 Breeding of Heterozygous Akita Mice

To generate the male mice heterozyote for Ins2 mutation (*Ins2*$^{WT/C96Y}$), we bred male heterozygous Akita mice with wild type females (**Fig. 2.1**). We chose the heterozygote mice since they exhibit a more gradual rise in blood glucose level starting at 3-4 weeks of age, whereas the hyperglycemia is markedly more severe in the homozygote mice.

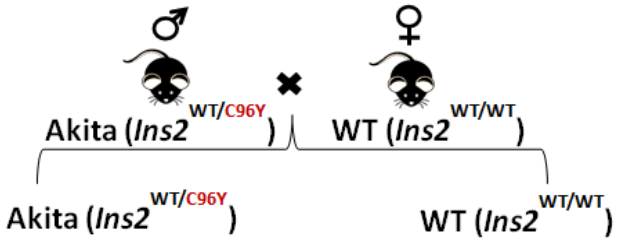

Figure 2.1 Flow chart for breeding of heterozygous Akita mice

The offsprings were genotyped using the DNA isolated from tail samples using the sodium dodecyl sulphate-potassium method. Using a standard PCR protocol, the region of the *Ins2* gene that contained the mutation was amplified using appropriate foraward and reverse primers 5'-TGCTGATGCCCTGGCCTGCT-3' and 5'-TGGTCCC -ACATATGCACATG-3'(ACGT Corp., Toronto, Ont.). The polymerase chain reaction (PCR) protocol was as follows: cycling conditions of 94°C for 3 minutes, 12 cycles of 94°C for 20 seconds, 64°C for 30 seconds, 72°C for 35 seconds and 72°C for 2 minutes. The amplification product (280-bp)

in both mutant and control (WT) alleles were treated with a restriction enzyme, FnU4H1, (1 U/0.2 µl; New England Biolabs, Pickering, ON, Canada) for 3 hours. This restriction enzyme would cleave the PCR product at 280 basepair (bp), resulting in 140 bp fragments in WT mice, whereas presence of *Ins2*$^{WT/C96Y}$ mutation would prevent this cleavage. Thus, the PCR product in the heterozygote Akita mice was comprised of a 280bp (mutant allele) and a 140 bp (WT allele) band, whereas the WT mice only showed a 140 bp product. The heterozygote Akita males and their litter-mate WT male were used for experiments.

2.1.2 Generation of the Diabetic Model with TIMP3 Deficiency

TIMP3-deficient (TIMP3$^{-/-}$/*Ins2*$^{WT/WT}$) mice were generated on a C57BL/6J background as described earlier[1, 31]. TIMP3-deficiency in diabetic heterozygous Akita mice (TIMP3$^{-/-}$/*Ins2*$^{WT/C96Y}$) was achieved by three generations of breeding (**Fig. 2.2)**.

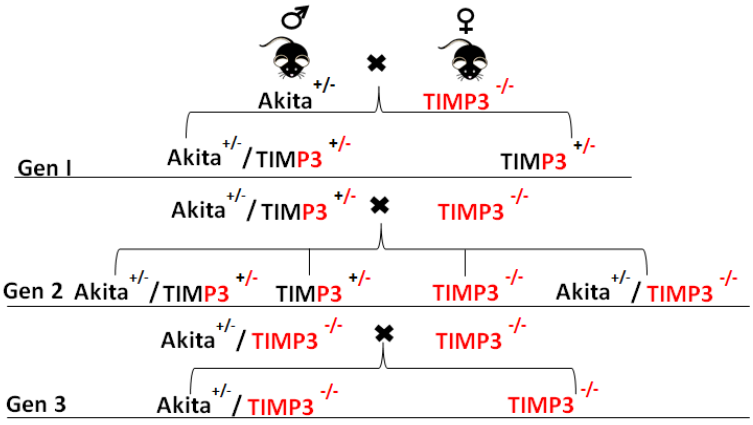

Figure 2.2 Flow chart for breeding of heterozygous Akita and TIMP3 double knock out mice in 3 generations.

Initially TIMP3-deficient ($TIMP3^{-/-}$) females were bred with Akita ($Ins2^{WT/C96Y}$) male mice. This breeding pair produced Akita/$TIMP3^{+/-}$ ($TIMP3^{+/-}$/$Ins2^{WT/C96Y}$) heterozygous and $TIMP3^{+/-}$ ($TIMP3^{+/-}$/ $Ins2^{WT/WT}$) mice in the first generation. We further crossed Akita/$TIMP3^{+/-}$ males with $TIMP3^{-/-}$ female mice and generated double transgenic Akita/$TIMP3^{-/-}$ along with Akita/$TIMP3^{+/-}$, $TIMP3^{+/-}$ and $TIMP3^{-/-}$ mice and verified by genotyping for both Akita and TIMP3 mutations. Finally, we continued breeding male Akita/$TIMP3^{-/-}$ with $TIMP3^{-/-}$ female mice which generated only double transgenic Akita/$TIMP3^{-/-}$ and littermate $TIMP3^{-/-}$ mice. Only Male Akita/$TIMP3^{-/-}$and littermate $TIMP3^{-/-}$, Akita and their littermate WT mice were used in our studies.

2.1.3 Generation of MMP2 and TIMP3 Double Deficient Transgenic Mice

$MMP2^{-/-}$ male and $TIMP3^{-/-}$ female mice were cross bred to generate $MMP2^{+/-}$ /$TIMP3^{+/-}$ transgenic mice (**Fig. 2.3)**. All mice were on the C57BL/6J background and genotyped to confirm the hetero status of both genes. Subsequently $MMP2^{+/-}$/$TIMP3^{+/-}$ male and a $MMP2^{+/-}$/$TIMP3^{+/-}$ female were crossed to generate a variant of possible genetic manipulations shown in Fig. 2.3 including MMP2 and TIMP3 double knock out ($MMP2^{-/-}$/$TIMP3^{-/-}$). However, the probability of generating this DKO is very low (apprx. 11.1%) in the first cross-breeding of hetero parents and required at least 4 crosses before a DKO could be generated. Thereafter, DKO males were crossed with DKO females to generate more offsprings for experimental procedures.

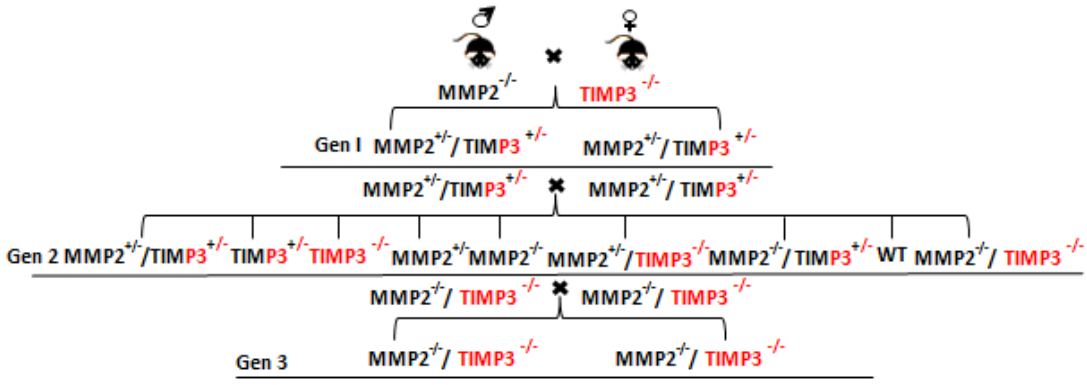

Figure 2.3 Schematic illustration for breeding of MMP2 and TIMP3 double knock out (DKO) mice in 3 generations
(Practically it takes 4 crosses for a DKO generation as the probability of getting it in Gen 2 is approximately 11.1%).

2.2 EXPERIMENTAL MURINE MODELS OF DISEASES STUDIED

To study molecular mechanisms involving diabetic complications, we used transgenic and diabetic mice harbouring a spontaneous mutation without any surgical or chemical intervention. The Akita mouse model was used to elucidate temporal changes (at 3 and 6 months of age) and insights into the mechanism of diabetic complications. Angiotensin II induced hypertension and abdominal aneurysm studies involved implantation of micro-osmotic pumps (Model 1002, Durect Co.) subcutaneously in male mice of concerned genotypes to deliver Ang II at the rate of 1.5 mg/kg/day[31, 32].

2.2.1 Implantation of Micro-osmotic Pumps

Ten-week old male WT, TIMP3$^{-/-}$ and TIMP3$^{-/-}$/MMP2$^{-/-}$ mice were anesthetised with 1% isoflurane and 1 L/min 100% oxygen on spontaneous breathing without intubation, and laid out in a supine position on a heated pad to maintain normal

body temperature at 36-37^{0}C. A 1 cm x 1 cm area on dorsal region (between the shoulder blades) was shaved with an electric razor and remnant hair removed with a depilatory cream (Nair; Church & Dwilight Co, Inc; Princeton, NJ). A small incision of approximately 2-3 mm was made along the natural fold of the skin under sterile conditions (using 1% povidone solution). With the aid of a trocar, a pocket was made subcutaneously and a micro-osmotic pump (Model 1002, Duract Co.) prefilled with Ang II or saline was implanted such that the opening of the pump was directed towards the caudal end of the animal. This micro-osmotic pump allowed an infusion rate of 0.25 µL/day for 14 days to deliver 1.5 mg.kg^{-1}.d^{-1} of Ang II (Sigma) or saline (control). Once the pump was implanted, the skin was closed with the use of a 6-0 silk suture and the mice were allowed to recover on a warming pad until they were fully awake. The pumps were replaced at day 14 to allow for continuous infusion for 28 days.

2.3 TISSUE COLLECTION

2.3.1 Mortality and Autopsy

Each mouse housed in the animal facility was monitored daily for morbidities and mortalitiest throughout the experimental protocol. Mice from various genotypes receiving Ang II were particularly observed twice daily due to their higher risk of mortality. Each incidence of mortality was recorded and an autopsy was performed on each mouse found dead throughout the course of the study. Percent survival was reported in the form of Kepleir Meyer curve. Aortic rupture was confirmed by the presence of blood clot in the peritoneal cavity

(abdominal) or in the chest cavity (thoracic), and simultaneously confirmed by direct visualization of the aorta under a stereomicroscope, subsequently the aorta was isolated and fixed in formalin for reference. Frequency of aortic rupture-related mortality was recorded and reported separately.

2.3.2 Tissue Collection from Akita and Akita/TIMP3$^{-/-}$ (and Parallel WT) Mice

Mice of different genotypes involved in diabetic cardiomyopathy and nephropathy studies were sacrificed at 3 months or 6 months of age after being anesthetized with a cocktail of ketamine (90mg/Kg body weight) and xylazine (4.5mg/Kg body weight). Hearts and kidneys were excised, weighed after removal of excess blood, visceral fat and connective tissue, and either formalin-fixed or flash-frozen in liquid nitrogen. Formalin-fixed organs were used for structural and histological analyses (Periodic acid Schiff to detect glomerular protein and characterize lesions in kidneys), Masson Trichrome to visualize interstitial fibrosis and Picosirius red staining to determine collagen accumulation), while flash-frozen tissue were processed molecular analyses such as mRNA, protein and enzymatic activities in the myocardium, or cortex and the medulla in kidneys.

To obtain LV weight, the hearts were quickly excised, the atria and right ventricle (RV) were removed and discarded and the remaining LV was weighed before stored by flash-freezing. For histology and immunohistochemical analyses, whole hearts were arrested in diastole with 1 M KCl and then fixed in

10% neutral buffered formalin for a minimum of 48 hours. This method was employed to arrest the heart in diastole such that end-diastolic maximum dimensions of the ventricle was maintained for qualitative histological assessment of chamber and ventricular wall properties.

Thorough records were maintained for each mouse including date of birth, identification number, genotype, body weight, heart weight, LV weight, kidney weight and tibial length (**Table 2.0**)

Table 2.0 Data collection sheet for mice

Date of Exp. DOB	Genotype	Time point	BW	HW	LVW	TL	KW		Notes
							Rt	Lt	

BW= Body weight; HW= Heart weight; LVW= Left ventricle weight; TL=Tibial length; KW= Kidney weight; Rt= Right, Lt= Left; DOB= Date of Birth

2.3.3 Tissue Collection from Mice with Ang II Pump Implantation

At 2 weeks or 4 weeks post implantation of micro-osmotic pump containing either Ang II or saline, mice from various genotype were injected with 0.05 ml of 1000USP/ml heparin for 15 min and then sub-lethally anesthetized using a ketamine/xylazine cocktail as described in Section 2.3.2. After exposing the abdominal and thoracic cavity (using a pair of scissors), the entire aorta was dissected, from the root (attached to the heart) until beyond the renal bifurcation using a stereomicroscope (Leica DM4000B microscope). The entire aorta comprising of both thoracic and abdominal part was rinsed thoroughly in PBS to

get rid of excess blood, and para-aortic fatty tissue attached to the aortic wall was carefully removed with the aid of small iris scissors without damaging the vessel. Subsequently, the attached heart and kidneys were excised and images of the entire aorta were taken with the aid of a stereomicroscope (Olympus, SZ61) at 6.7× resolution. Additionally, carotid and mesenteric artery was excised and either flash-frozen in liquid nitrogen (including fixation in cryoprotective embedding medium-OCT) and stored in -80 ℃, or were arrested with 1M KCl in relaxation phase prior to formalin-fixation in 10% buffered formalin for molecular and histological experiments respectively.

2.4 MEASUREMENTS OF METABOLIC PARAMETERS

2.4.1 Plasma Glucose Measurement

Animals were fasted but allowed free water for 8 hours before being restrained in a plexi-glass restrainer to obtain approximately 3 µl of blood (one drop) from tail vein via venous puncture from conscious mice. Blood glucose levels were measured every month starting (4 weeks till 24 weeks of age) between 8 and 9 AM using Ascensia Contour glucometer (Bayer, Canada).

2.4.2 Plasma Insulin Measurement

Mouse plasma insulin levels were measured using the sandwich type immunoassay (ALPCO mouse ultrasensitive insulin ELISA, 26G keewaydin drive, salem, NH 03079) kit for the quantitative determination of mouse insulin in plasma according to manufacturer's instructions. Mouse plasma was obtained from blood collected by tail tip snipping and centrifuged for 10 minutes at 1,000-

2,000 $\times g$ using a refrigerated centrifuge. In a clear 96-well microplate coated with a monoclonal antibody specific for insulin, 5 µl plasma was added with 75 µl of conjugate, incubated for 2 hours on a shaker (700-900 rpm), the wells were washed three times with a wash buffer (350 µl) provided in the kit, and blotted dry. Subsequently, 100 µl of TMB substrate (provided in the kit) was added and incubated for 30 mins before the reaction was arrested by a stop solution provided by the manufacturer. The optical density (OD) was recorded by a spectrophotometer at 450 and 640 nm wavelengfhs and the concentration was calculated by a standard curve with known concentrations of standards and OD provided by the manufacturer (**Fig. 2.4**)

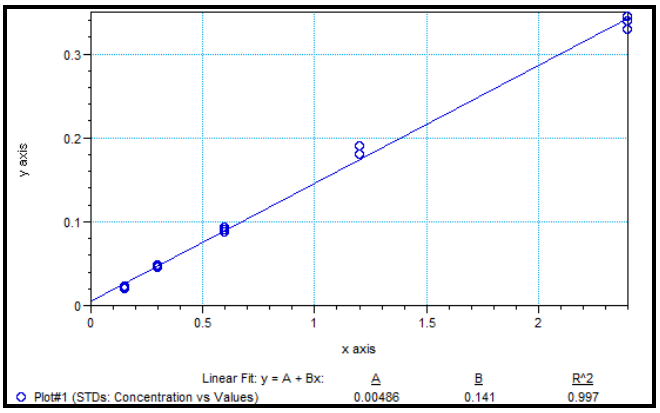

Figure 2.4 A typical standard curve obtained with corresponding OD.

2.4.3 Determination of Myocardial Triacylglycerol

Intramyocardial lipids were extracted from 5 mg of flash-frozen freshly excised heart tissue (not perfused) as described previously[33]. The dried lipids were redissolved in 50 µL of 3:2 *tert*-butyl alcohol:Triton X-100/methyl alcohol (1:1, vol/vol) mixture, and cardiac triacylglycerol content was measured with the

Wako L-Type TG-H kit (Wako Diagnostics, Osaka, Japan) as per manufacturer's instructions.

2.4.4 Myocardial Long-chain Fatty Acids and Ceramide

Identification and quantification of the major long-chain acyl CoA molecular species were performed by high-performance liquid chromatography (HPLC), as described previously[33]. The sum of all major peaks identified by HPLC (C16:0, C18:0, C18:1, C18:2) were considered as total long chain fatty acyl CoAs. Myocardial ceramide levels were detemined by the use of HPLC as described previously[34].

2.5 ISOLATED WORKING HEART PREPARATION

The isolated working heart preparation was used to compare the basal *ex vivo* systolic performance between Akita and WT hearts under controlled conditions (using 1.2mM palmitate, 11mM glucose and no insulin) as previously described[35].

2.5.1 Working Heart Apparatus Set-up

Thoracotomy was performed on completely anesthetized (with a cocktail of ketamine (90mg/Kg BW) and xylazine (4.5mg/Kg BW)) animal and the heart excised with the aid of scissors and retained in a separate container with freshly prepared cold (4°C) Krebs-Hensleit solution. The heart was trimmed of any epicardial fat and rinsed to avoid excess blood before being rapidly attached to 2 cannulas via the aorta and the left atrium. Hearts were aerobically perfused with oxygenated Krebs-Hensleit solution in an anterograde fashion, with an inflow of

perfusate initialized from the cannulated left atrium at a preload of 7 mmHg, and ejected out of the cannulated aorta against a predetermined afterload pressure of 50 mmHg for 30 min. The Krebs-Hensleit solution consisted of 1.2 mM palmitate, 3% bovine serum albumin (BSA) fraction V, 11 mM glucose, 2.5 mM Ca^{2+} and oxygenated with 95% O_2/ 5% CO_2 without insulin to simulate diabetic condition.

2.5.2 Assessment of *ex vivo* Cardiac Function

Coronary flows were measured using a transonic flow probe system and the heart function *ex-vivo* was assessed using an inline pressure transducer attached to a BIOPAC data collection system which was used for data acquisition and analysis. Cardiac function was monitored in the isolated working heart using a pressure transducer in the aortic inflow and outflow lines. Temperature of the Krebs-Hensleit solution was measured by an immersed thermocouple throughout the length of the experimental procedure. The parameters obtained from the isolated working heart included chamber pressure (CP), preload, afterload, heart rate, peak systolic perfusion pressure (PSP), end diastolic perfusion pressure (EDP), cardiac output (CO), stroke volume (SV), aortic flow (A_oF), coronary flow (derived from CO- A_oF), cardiac work (derived from (PSP-CP)*CO_{max}) / dry wt.) and cardiac work ((PSP- max preload) *CO* 0.13) / dry wt, whereby 0.13 is a factor for conversion of mmHg to kPa and dry wt implies to total cardiac dry weight.

2.5.3 Assessment of Cardiovascular Physiology (*In vivo)*

Transthoracic echocardiography was performed as described previously with a Vevo 770 high-resolution imaging system equipped with a 30-MHz transducer (RMV-707B; VisualSonics, Toronto, Canada)[33, 36]. Prior to echo mice were anesthetized using 1.0-1.5% isoflurane (3% induction) mixed with 1% oxygen and laid in supine position on a heated animal handling platform with all legs taped to ECG electrodes for heart rate and respiration monitoring. A heat lamp was directed towards the animal to maintain normal body temperature at 36-37°C (monitored continuously using a rectal temperature probe). Hair was removed from the abdominal area with a depilatory cream (Nair; Church & Dwilight Co, Inc; Princeton, NJ) to optimize ultrasound signal. Pre-warmed ultrasound transmission gel was used between the skin and the scan head as a coupling agent. M-mode images were obtained for measurements of LV wall thickness (LVWT), LV end-diastolic diameter (LVEDD), and LV end-systolic diameter (LVESD). LV fractional shortening (FS), a measure of systolic function, was calculated using the following equation: FS(%)=(LVEDD–LVESD/LVEDD)x100 from M mode images (**Fig 2.5**) .

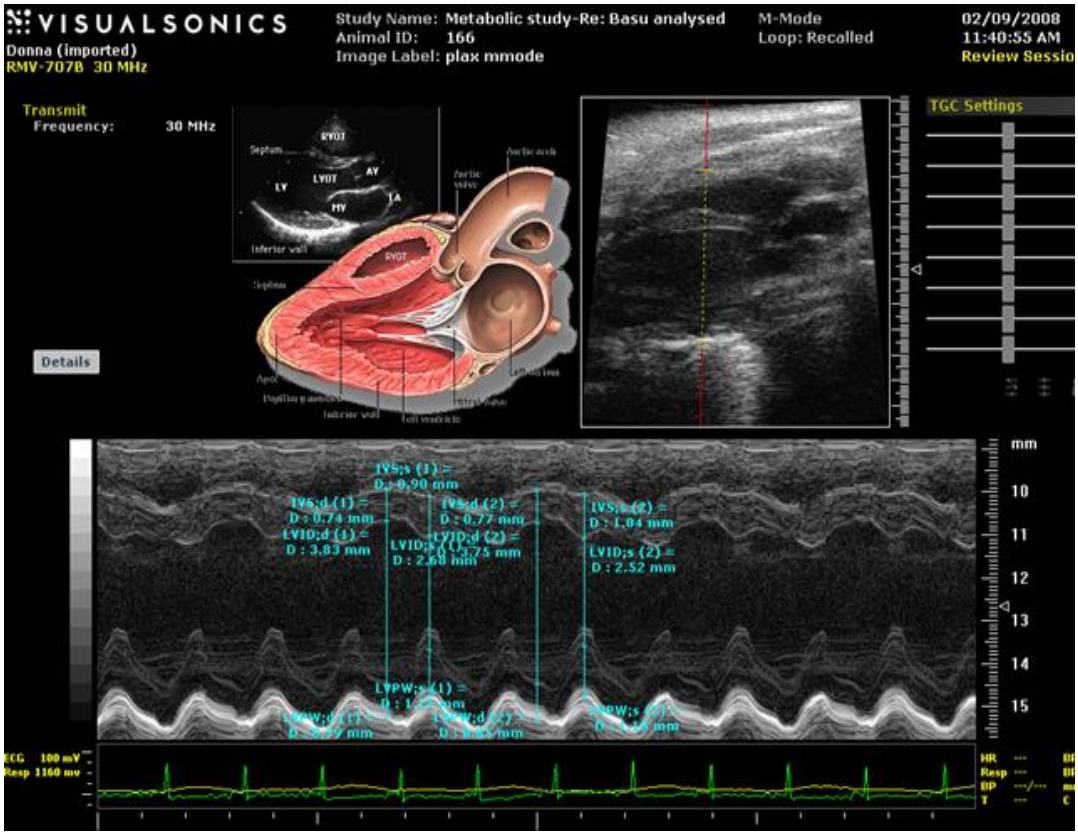

Figure 2.5 Echocardiogram M-mode imaging from parasternal long axis view for cardiac wall structure and systolic function assessment.
Inset image extracted from Yale atlas of Echo (www.yale.edu)

2.5.4 Transmitral Doppler (TMD)

Doppler imaging of the transmitral filling pattern with the early transmitral filling wave (E-wave) followed by the late filling wave due to atrial contraction (A-wave) was used to assess diastolic function. Isovolumic relaxation time (IVRT) and deceleration time (DT) of the early (E) filling wave were determined with pulsed-wave Doppler (**Fig. 2.6**)

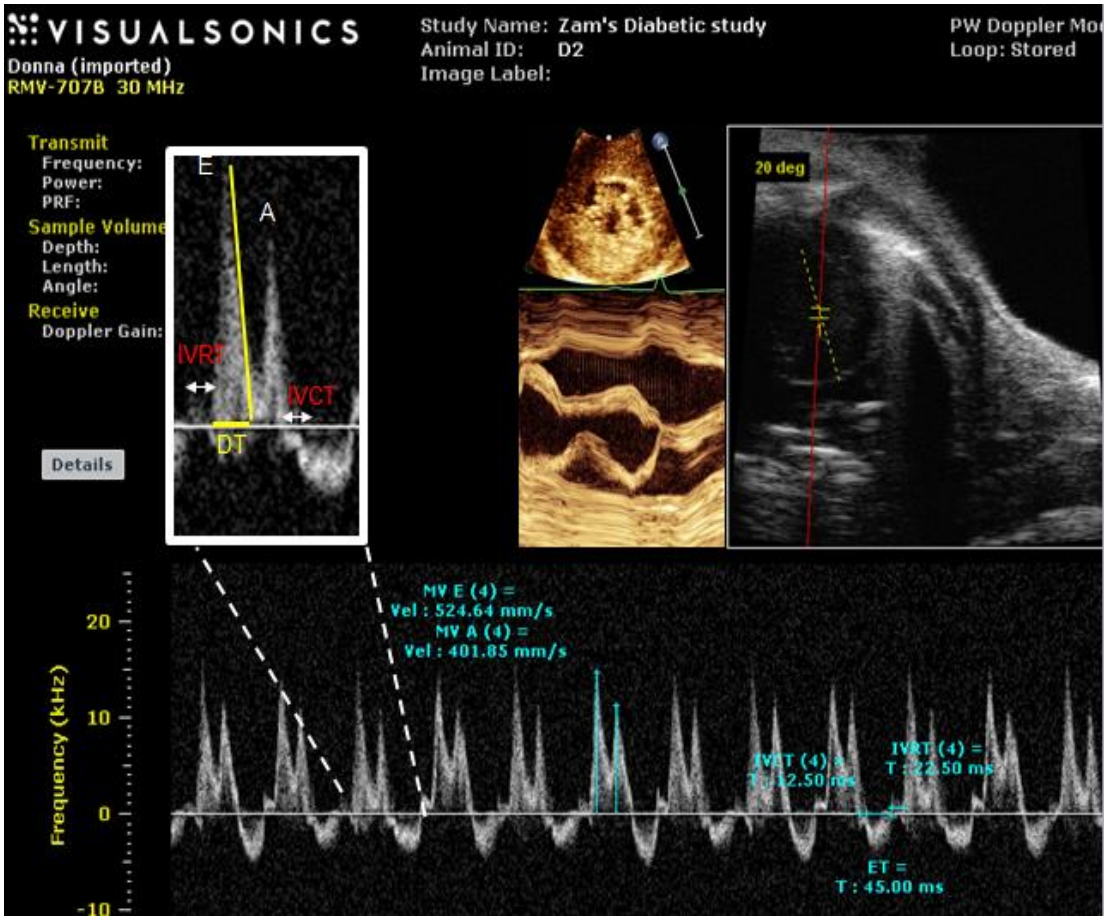

Figure 2.6 Representative image of the transmitral Doppler (TMD) imaging from a modified short axis (mitral view) in B mode.

Doppler signal of the blood traversing the mitral outlet represented in pulse wave depicting E- and A-waves. Yellow line from E to the baseline represents wave deceleration and the corresponding time shown as DT. IVRT (in red) is the isovolumetric relaxation time of LV, IVCT (in red) indicates the left ventricular isovolumetric contraction time.

Isovolumic relaxation time was calculated as the time from closure of the aortic valve to initiation of the E-wave while the deceleration time of the E-wave, was determined by measuring the time needed for the downslope of the peak of the E-wave to reach the baseline, while the rate of E-wave deceleration rate (EWDR) was calculated as the E-wave divided by the DT.

2.5.5 Tissue Doppler Imaging (TDI)

Figure 2.7 Representative image of the tissue Doppler imaging (TDI) signal detecting lateral annular motion at the mitral valve.
Corresponding E'-wave of the early filling phase, A'-wave from atrial contraction, and peak systolic annular motion (S') highlighted in a single beat.

Tissue Doppler imaging (TDI) was made at the inferolateral region in the radial short axis at the mitral valve annulus in the modified four-chamber view at the base of the heart. TDI is a novel and validated technique to assess systolic and diastolic function that is devoid to a greater extent of any compounding effect imposed by total blood volume. TDI was used to assess the early diastolic (E') and late diastolic (A') myocardial velocities (**Fig. 2.7**) in addition to peak systolic annular motion (S'). Derived parameters from TDI and mitral Doppler

represented by E/E' is considered an important marker of elevated LV filling pressure and diastolic dysfunction[8, 31, 36, 37]. The major systolic and diastolic Parameters (**Tables** 2.1 A and B) were analyzed and used to assess cardiac function.

Table 2.1 A (systolic) and B (diastolic) parameters used to analyze cardiac function.

Table 2.1.A.	Genotype
Age	
N	
HR (bpm)	
LVEF (%)	
LVFS (%)	
SV(μL)	
CO (ml/min)	
LVEDD (mm)	
LVESD (mm)	
LVPWT (mm)	
Vcfc (circ/s)	

Table 2.1.B.	Genotype
Age	
N	
E-wave (mm/s)	
A-wave (mm/s)	
E/A Ratio	
IVRT (ms)	
DT (ms)	
EWDR (mm/s^2)	
AR (mm/s)	
E′ (mm/s)	
E/E′	
LA size (mm)	

HR=heart rate; LVEF=LV ejection fraction; LVFS=LV fractional shortening; SV= stroke volume; CO=cardiac output; LVEDD=left ventricular end diastolic diameter; LVESD=left ventricular end systolic diameter; Vcfc=velocity of circumferential shortening; E wave=peak early transmitral inflow mitral E velocity; A wave=mitral Doppler A velocity; IVRT=isovolumetric relaxation time; DT=deceleration time; EWDR=E wave deceleration rate (E-wave/DT); E′=early diastolic tissue Doppler velocity.

2.5.4 Tail Cuff Blood Pressure Measurement

Tail-cuff systolic blood pressure (TC-SBP), was measured using the IITC Life science noninvasive blood pressure amplifier with built in pump for automatic cuff inflation (model 229), in conscious mice after three separate occasions of training (1-2 hours/session) prior to the experimental recordings. Blood pressure was measured every two days over three weeks, one week prior to, and two weeks after implantation of the micro-osmotic pump. These mice were placed in the acrylic restrainers and their body temperature was maintained at 34℃ by warming the restrainer chamber without any undue thermo stress. The IITC tail cuff sensor containing an inflation cuff and photoelectric sensor was placed on the tail and attached to the restrainer. The cuff was then inflated to a maximum pressure of 200 mmHg and then deflated slowly at the rate of 6mmHg.sec^{-1}. Upon reappearance of pulse signals in the form of a crescendo (as shown in **Fig. 2.8**), TC-SBP data from the IITC amplifier was recorded and analyzed by the IITC software (IITC Life Science Blood Pressure System, Woodland Hills, CA). After completion of all measurements corresponding TC-SBPs were averaged from three readings of the same sample and used for averaged systolic blood pressure data.

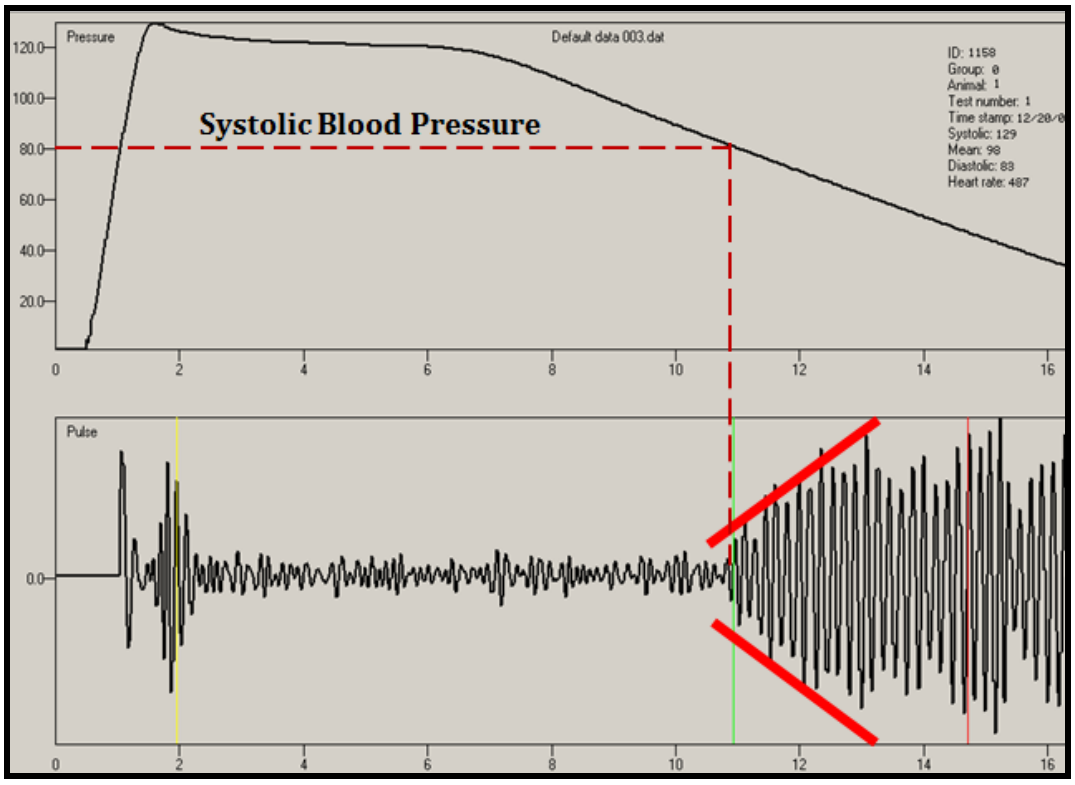

Figure 2.8 Representative image of tail cuff pressure recording.
The red lines depict the reappearance of crescendo shaped pulse signal and the corresponding systolic blood pressure shown by the dotted lines. Extracted and modified from IITC life sciences website.

2.5.5 Pressure Volume Hemodynamic Measurements

In vivo hemodynamic measurements were made invasively in 10- to 12-wk-old mice under 1% isoflurane anesthesia. The anesthetised mouse was placed on a heating pad to maintain normal body temperature at 36-37°C, the right common carotid artery was exposed and cannulated using a 1.4 French Millar pressure-volume conductance catheter (Millar Inc., Houston, TX) which was then advanced into the proximal aorta via the right carotid artery and then through the aortic valve into the left ventricle. Hemodynamic data was acquired using PowerLab data acquisition system and analyzed using the PVAN analysis

software. The parameters obtained as read outs were LV pressure in systole (LVESP) that measures peak SBP, LV end diastole pressure (LVEDP) which is a measurement of the relaxation capacity of the LV and remains high in an impaired diastolic phase, LV dP/dtmax which represents maximum acceleration in the rate of change of pressure in the LV during isovolumic contraction and measured as the first derivative of the acceleration/ time curve, LV dP/dtmin which is a measure of maximum deceleration in the rate of change pressure drop during isovolumic relaxation and acquired by the first derivate of the deceleration/time curve of the LV.

2.5.6 Ultrasound Imaging of Aortic Structure and Function

A micro-imaging system (Vevo 770; VisualSonics, Toronto, Ontario) and software analysis (VisualSonics) were used to evaluate abdominal aortic structure and function. Briefly mice were anesthetised using 1.0-1.5% isoflurane (3% induction) with 1L/min 100% oxygen and laid in supine position on a heated plate to maintain normal body temperature at 36-37°C measured by a rectal temperature probe and simultaneously monitored by ECG electrodes for heart rate and respiration monitoring. The complete procedure was performed with a single-crystal mechanical transducer with a central frequency of 40-MHz. (frame rate of 50Hz)[38] and a focal length of 6 mm to visualize the abdominal aorta using the left kidney and its ipsilateral renal branch as the reference point at the caudal end. Abdominal aorta was identified on the basis of the characteristic flow pattern and longitudinal 2 dimensional B mode images (Maximum field of

view obtained in a 15x15mm area of focal plane; spatial resolution of 100 m lateral by 40 m axial)[37] were obtained for the entire supra renal region limited by the appearance of the last rib at the cephalic end. Probe position was optimized to acquire clear vessel wall/lumen interfaces and corresponding M mode images were obtained from the abdominal aorta adjacent to the upper pole of the left kidney (**Fig 2.9**).

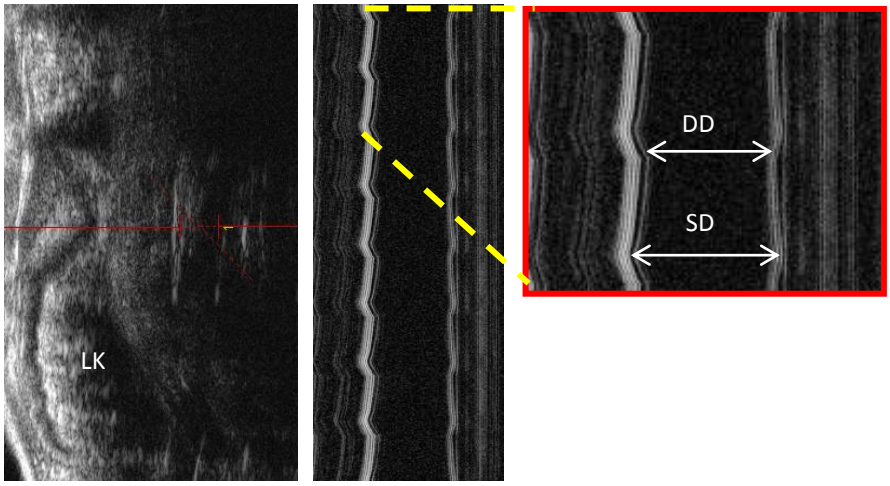

Figure 2.9 Representative ultrasound image of murine abdominal aorta.
The yellow dotted lines depict the area on m Mode image shown in an enlarged form (in red) and the corresponding systolic diameter (SD)and diastolic diameter (DD) in white; LK=Left kidney used as a reference point.

The maximum lumen diameter (systolic aortic diameter) and the minimum lumen diameter (diastolic aortic diameter) during a single cardiac cycle monitored by E.C.G were used to calculate aortic expansion index (Systolic aortic diameter- Diastolic aortic diameter)/Systolic aortic diameter*100. Doppler-flow measurements were obtained from longitudinal sections of the entire supra renal region of the abdominal aorta. Aortic dilatation was categorized in terms of percentage increase in diameter relative to its original

diastolic diameter and aneurysm was defined as dilation in the aorta greater than 50% of the original diameter.

2.6 ASSESSMENT OF VASCULAR PHYSIOLOGY (*EX VIVO)*

2.6.1 *Ex vivo* Vascular Function and Compliance

Tissue dissections were performed in ice-cold physiological saline solution (PSS), composition (in mmol/l) 10 HEPES, 5.5 glucose, 1.56 $CaCl_2$, 4.7 KCl, 142 NaCl, 1.17 $MgSO_4$, 1.18 KH_2PO_4, pH 7.5. Arteries, 1st order mesenteric or carotid, were cleaned of all surrounding adipose and connective tissues and mounted on two glass cannulas in a two-bath pressure myograph (Living Systems, Burlington, VT).

2.6.2 Vasoconstrictor and Vasodilator Responses

Vessels were given a 40-minute equilibration period during which they were exposed to a stepwise increase in pressure from 60 to 80 mmHg with regular changes of the PSS bathing solution. The pressure was set to 60 mmHg for measurement of active experimental responses, a level which was chosen since it did not cause myogenic responses. Following the equilibration period, one vessel was randomly chosen as a control while the second was incubated with *N*-nitro-L-arginine methyl ester hydrochloride (L-NAME, 100 µmol/l) for 30 minutes. A cumulative concentration-response curve (CCRC) was constructed to increasing concentrations of the adrenergic agonist phenylephrine (PE). To investigate vasodilator responses to methylcholine (MCh, 0.0001 to 100 µmol/l) in the

presence or absence of L-NAME, a CCRC was performed in PE (1 μmol/l) constricted vessels.

2.6.3 Passive Characteristics

Vessels were equilibrated in Ca^{2+}-free PSS in the presence of papaverine (0.1 μmol/l) to initiate complete dilation. Passive characteristics were then assessed using pressures from 0 to 140 mmHg in mesenteric arteries and to 180 mmHg in carotids. Corresponding circumferential wall stress was calculated using the equation: circumferential stress (dyne/cm^2) = (P*D)/2T, where P = transmural pressure (mN/mm^2, 1 mmHg = 0.133 mN/mm^2), D = internal diameter (mm) and T = wall thickness (mm). Corresponding circumferential wall strain was calculated using the equation: circumferential strain = $(D_f - D_0)/D_0$, where D_f = observed internal diameter for a given intravascular pressure (mm) and D_0 = initial diameter at 4 mmHg (mm). Arterial stiffness can be determined by Young's elastic modulus (E = stress/strain). However, since the stress-strain relationship is non-linear, a tangential or incremental elastic modulus (E_{inc}) was obtained by determining the slope of the stress-strain curve. An exponential curve was fitted to data from each animal using the equation: $Y = Y_0 \exp(k*x)$, where Y = circumferential stress, Y_0 = circumferential stress at 4 mmHg, k = the rate constant and x = circumferential strain. Deriving this equation, we find that $E_{inc} = kY$ and, therefore, for any given circumferential stress, E_{inc} is directly proportional to k, the rate constant. Any increase in the rate constant implied an

increase in E_{inc} and, therefore, an increase in arterial stiffness. Conversely, any decrease in the rate constant implied an increase in arterial elasticity.

2.7 MEASUREMENT OF RENAL PARAMETERS

2.7.1 24-Hour Urine Collection and Processing

Each experimental mouse was housed in an individual mouse metabolic cage (Nalgene; model 650-0311; Nalge Nunc International, Rochester, NY) with free access to pre-recorded volume of water and rodent chow mash and acclimatized for 1 day before the collection of experimental urine sample. Urine was collected over 24 hrs post acclimatization in a collecting funnel provided with the cage and was filtered for any mouse droppings or debris prior to measurement of urine volume and total water intake. Collected urine was centrifuged at 8,000 $\times g$ for 5 minutes at 4°C to remove unfiltered debris and was either immediately processed or flash frozen and stored at -80 °C for further analysis[39].

2.7.2 Urine Albumin Measurement

An indirect competitive ELISA kit (Albuwell M; Exocell, Philadelphia, PA) was used according to the manufacturer's instruction to measure urinary albumin concentration.[25]. Briefly, 10 µl urine sample and rabbit anti-murine albumin antibody was added to wells coated with albumin. Additionally an anti-rabbit antibody conjugated with horseradish peroxidase enzyme was added such that it labels the anti-murine antibody with the enzyme. The wells were thoroughly washed such that only the antibody-conjugate bound to the stationary phase remained in the well and detected by a chromogenic reaction where colour

intensity was inversely proportional to the logarithm of albumin in the liquid phase (Urine sample) bound competitively to the antibody against the stationary phase (well coated with albumin).

2.7.3 Glomerular Mesangial Matrix Score

Formalin-fixed, paraffin-embedded kidney tissue was used for assessment of mesangial sclerosis by light microscopy. All glomerular profiles (approximately 90) in a single 3 μm-thick periodic acid-Schiff (PAS)-stained section from each animal were scored for mesangial matrix (MM) increase. Each glomerulus was scored as 0 (normal), 1 (mild MM increase, approximately 2 times the width of a mesangial cell nucleus), 2 (moderate MM increase, 3-4 times the width of a mesangial cell nucleus), or 3 (severe MM increase, >4 times the width of a mesangial cell nucleus). The glomerular MM score for each animal was expressed as percentage MM increase ((total score/no of glomeruli) × 100).

2.8 ASSESSMENT OF RENAL ROS PRODUCTION

2.8.1 NADPH Oxidase Activity and DHE Fluorescence and Nitrotyrosine Staining

Nicotinamide adenine dinucleotide phosphate (NADPH) oxidase activity in kidney cortex of mice was quantified using a lucigenin-enhanced chemiluminescence assay using a single-tube luminometer (Berthold FB12, Berthold Technologies, Germany) with NADPH (1 mM) and lucigenin (50 μM) at 37 ℃ as previously described An indirect competitive ELISA kit (Albuwell M; Exocell, Philadelphia, PA) was used according to the manufacturer's instruction

to measure urinary albumin concentration[25]. The specific peptide inhibitor of NOX2, gp91phox ds tat (50 μM) was used to confirm superoxide generation from NADPH oxidase [40]. Dihydroethidium (DHE), an oxidative fluorescent dye, was used to measure superoxide levels in kidney samples as previously described [25]. Briefly, optimal cutting temperature (OCT)-embedded frozen kidney tissues were cut into 15 μm-thick sections, washed with Hank's balanced salt solution (HBSS), and then incubated with DHE (20 μM DHE in HBSS; Sigma-Aldrich) at 37 ℃ for 30 minutes in dark. Fluorescence images were subsequently taken with an Olympus IX81 fluorescence microscope (10). Nitrotyrosine immunofluorescence staining was performed on OCT-embedded kidney cryosections (5μm) using mouse anti-nitrotyrosine primary antibody (Santa Cruz, USA) and Alexa Fluor 594-conjugated goat anti-mouse secondary antibody (Invitrogen, USA) as previously described [41]. Quantitative measurements of DHE and nitrotyrosin fluorescence intensity were carried out using Metamorph Basic (version 7.7.0.0; Molecular Devices, Sunnyvale, CA).

2.9 MORPHOLOGICAL AND HISTOLOGICAL ANALYSES

2.9.1 Heart

2.9.1.1 Masson's Trichrome Staining for Myocardium

Excised hearts were arrested in diastole with 1M KCl, fixed in 10% neutral buffered formalin, and embedded in paraffin (Alberta Diabetes Institute Histology Core; University of Alberta, Edmonton, AB, Canada). Four micrometer sections were stained with masson trichrome for assessment of,

interstitial fibrosis and myocyte cross sectional area, and visualized using light microscopy as previously described [42, 43]. All images were captured on a Leica DM4000B microscope using Infinity Capture software (Lumenera; Ottawa, ON, Canada).

2.9.1.2 Myocyte Cross-sectional Area

Myocyte cross-sectional area were measured by tracing the cross-section of the myocytes in trichrome-stained sections that were obtained from the subendocardial region of the myocardium (Formalin-fixed, paraffin-embedded isolated LVwere cross-sectioned (4μm) and processed with Masson's trichrome stain for quantitative measurement of myocyte cross-sectional area (CSA) as an indicator of hypertrophy) under a 40× objective using Image Pro-plus software (National Institute of Health, NIH). The reported averaged values are from five hearts/group, and 200 myocytes/group. Measurements in pixels were converted to μm^2 through calibration of the system, which was done with the use of a micrometer.

2.9.2 Kidney

2.9.2.1 WT-1 Staining and Podocyte Counting

Wilms tumor protein (WT-1) is a podocyte marker [44]. WT-1 staining was performed on deparaffinized mouse kidney slides were blocked with serum for 20 minutes at room temperature. Slides were then incubated with WT-1 antibody (1:200 in 1% BSA, Santa Cruz) for 2 hours at room temperature. After 3 times washing in PBS 10 minutes each, slides were incubated with rabbit IgG

(Vectastain ABC Kit, Vector Laboratories Inc. Burlington, ON, Canada) for 1 hour. Additionally, slides were thoroughly washed in PBS for 3 times x10 minutes each, and then quenched with 1% H_2O_2 in methanol for 45 minutes. Subsequently, slides were incubated with ABC Reagent for 1 hour, then stained with DAB substrate for 1 minute. Dehydrated slides were then mounted with per-mount. All slides were scanned digitally by the Advanced Optical Microscope Facility (Princess Margaret Hospital, Toronto, ON, Canada), and Aperio ImageScope software (Aperio Technologies Inc., Vista, CA) were used to count WT-1 positive cells.

2.10 Vasculature

2.10.1 Verhoeff-van Geison (VVG) Staining for Elastin

Verhoeff-Van Geison (VVG) staining was performed (University of Alberta Department of Laboratory Medicine and Pathology; Edmonton, AB, Canada) on sections of formalin fixed and paraffin-embedded carotid and aorta to identify elastic fibres. Briefly, slides containing five micrometer paraffin-embedded sections of carotid or aorta were deparaffinised and hydrated with distilled water. Freshly made verhoeff's solution (20 ml of 5% alcoholic hematoxylin, 8 ml of 10% ferric chloride and 8 ml of weigert's iodine solution (2% potassium iodide and 1% iodine in distill water)) was used to stain the slides till the tissue turned completely black. After rinsing the slides in tap water with 2-3 changes tissues were differentiated in 2% ferric chloride for 1-2 minutes. Differentiation was stopped with several changes of tap water and treated with 5% sodium

thiosulphate for 1 minute. Sodium thiosulphate solution was discarded and the slides were washed in tap water for 5 minutes prior to counterstain in Van Geison's solution (15 ml of 1% aqueous acid fuschin, 50 ml saturated aqueous picric acid and 50 ml of distill water) for 3-5 minutes. Slides were dehydrated using 100% alcohol and cleared in two changes of xylene for 3 minutes each.

2.10.2 Gomori Trichrome Stain for Collagen

Gomori Trichrome staining was used to visualize three tissue components and stain smooth muscle tissue (red), the connective tissue (fibrillar collagen) a bluish/green colour, and the nuclei as black (Alberta Diabetes Institute Histology Core; University of Alberta, Edmonton, AB, Canada). Briefly, 5µm-thick sections of formalin fixed and paraffin-embedded carotid and aorta were deparaffinised and hydrated with distilled water prior to staining with freshly prepared Celestin blue (0.5 g of Celestin blue (CI 51050) in 100 ml of 5% ammonium ferric sulphate) for 5 minutes that stained nuclei bluish black. Sections were rinsed in distil water and additionally stained haematoxylin for 5 minutes. Subsequently, slides containing tissue sections were cleaned in running tap water for 5 minutes and finally stained with freshly prepared Gomori's stain (chromotrope 2R (CI16570) 1.2g, light green SF (CI42095) 0.6g, dodecatungstophosphoric acid 1.6g, glacial acetic acid 2ml and distil water 200 ml) for 15 minutes. Later slides were rinsed with distil water and dehydrated with alcol, cleared with xylene and mounted.

2.10.3 Scanning Electron Microscopy (SEM)

The layers of vascular wall was visualized by scanning electron microscopy (SEM)[45] at the advanced microscopy facility, department of biological sciences, Universityof Alberta. Supra renal aspect of the abdominal aorta was sliced manually into 2-3mm pieces before fixing them in 2.5% glutaraldehyde and 2% paraformaldehyde in 0.1 M PBS for 48 hrs at room temperature. Additionally samples were washed in 0.1M PBS (3×15 min), followed by quick rinse with distil water. After dehydrating the samples by a series of ethanol washes, tissue preparation was performed using hexamethyldisilazane. Samples were air dried overnight before being mounted on SEM stubs and sputter coated with Au/Pd, prior to be imaged using Phillips Scanning Electron Microscope (FEI Company, Model: XL30).

2.11 BONE MARROW RECONSTITUTION

Bone marrow (BM) reconstitution was performed to generate chimera mice as described previously [46]. Donor WT and TIMP3$^{-/-}$/MMP2$^{-/-}$ mice received 100 μg of purified anti-CD8 Ab (clone 2.43) intraperitonealy on days -2 and -1 before BM harvest to deplete CD8 T-cells. BM was harvested from the femur, tibia, and humerus in EasySep media (PBS, 2% FCS, 2 mM EDTA) and was passed through 70μm nylon cell strainers (Fisherbrand). Recipient WT and TIMP3$^{-/-}$ /MMP2$^{-/-}$ mice were sub lethally irradiated (1,000Gy), and received 10×10^6 BM cells of the opposite genotype via tail vein injection. WT bone marrow was reconstituted in TIMP3$^{-/-}$/MMP2$^{-/-}$ mice (TIMP3$^{-/-}$/MMP2$^{-/-}$-chimera mice), and

TIMP3$^{-/-}$/MMP2$^{-/-}$ bone marrow in WT (WT-chimera mice).Mice were provided with antibiotic water (40 mg neomycin, 15 mg polymyxin per 1 L) for 4 weeks post-injection, and 7 weeks were allowed for reconstitution before Alzet pumps were implanted for Ang II infusion.

2.12 IMMUNOHISTOCHEMISTRY (IHC)

2.12.1 Immunostaining for Neutrophils and Macrophages

Abdominal aortas were fixed in 10% formalin for 48 hours followed by 80% ethyl alcohol, paraffin-embedded and sectioned (4 μm thick) at the supra-renal aspect (area predominant in reproducible abdominal aortic aneurysm formation). Neutrophil and macrophage staining was performed as described previously [47] using anti-mouse neutrophil antibody with Cy3-labeled anti-rat secondary antibody, and F4/80 macrophage antibody with Cy3-labeled anti-rat secondary antibody which was pseudo-coloured to appear green for visual differentiation from neutrophil staining. We used nuclear staining by DAPI to confirm the presence of infiltrating cells in positively stained regions. Superimposed stainings for neutrophil or macrophage with DAPI appeared light greenish yellow in colour. Briefly, aortic samples in paraffin sections were deparaffinised in 5 changes of xylenes and brought down to water through graded alcohols. For neutrophil staining, sections were then pretreated with 1% pepsin in 0.01N HCl at pH 2.0 for 15 minutes at 37℃. Endogenous biotin activities were blocked using an avidin-biotin blocking kit (Lab Vision). Sections were then blocked with 10% normal rabbit serum (Vector Labs) for 10 minutes before incubating

with the rat anti mouse neutrophils antibody (Serotec: MCA771GA) overnight at 1/600 dilution. After washing well in TBS, staining was finished with 30 minutes each of a biotinylated rabbit anti-rat IgG linking antibody followed by alkaline phosphatase streptavidin (Vector Labs: SA-5100). Color development was performed using a freshly prepared solution of Vector Red from an alkaline phosphatise substrate kit (Vector Labs.: SK-5100). After washing well in tap water, sections were counterstained lightly with Mayer's hematoxylin solution. Sections were then dehydrated in alcohols, cleared in xylenes and mounted in Permount (Fisher).

For macrophage staining (Mac 3), sections were heat-retrieved using Tris-EDTA buffer at pH 9.0. Endogenous biotin activities were blocked using an avidin-biotin blocking kit (Lab Vision). Sections were then blocked with 10% normal rabbit serum (Vector Labs) for 10 minutes before incubating with the rat anti-mouse F4/80 antibody (Serotec: cat#MCA497GA, clone CI:A3-1) at 1/50 or rat anti-mouse Mac-3 antibody (BD Pharmingen: cat#550292, clone M3/84) at 1/50 overnight. After washing well in TBS, staining was finished with 30 minutes each of a biotinylated rabbit anti-rat IgG linking antibody (Vector Labs) followed by HRP conjugated streptavidin labeling reagent (ID Labs). Color development was performed using a freshly prepared solution of Nova Red (Vector Labs). After washing well in tap water, sections were counterstained lightly with Mayer's hematoxylin solution. Finally, sections were dehydrated in alcohols, cleared in xylenes and mounted in Permount (Fisher).

2.13 RNA Expression Analysis

2.13.1 RNA Extraction and Purification

Trizol (Invitrogen; Burlington, ON, Canada) was used to extract RNA from different tissues (Heart, kidney and vessels), followed by reverse transcription to make cDNA for TaqMan Realtime polymerase chain reaction (RT-PCR) for analysis of mRNA expression[45, 48]. RNA extraction involved homogenization of the tissue sample in 500 µl of Trizol reagent (Invitrogen; Burlingtion, ON, Canada) in an RNAase-free 1.5 ml (for heart and kidney) and 2 ml (for vascular tissue) microcentrifuge tube. The homogenized tissue was kept at room temperature for five minutes, and following centrifugation at 12,000 × *g* at 4 ℃ for 10 minutes the supernatant was transferred to another RNAase-free microtube. To maximize RNA yield, pellet was resuspended in another 500 µl of Trizol, with homogenization and centrifuge process repeated as explained above. To the combined supernatant, 200 µl of chloroform was added using a glass pipette. Additionally, the tubes containing supernatant with chloroform were vigorously shaken manually for 15-20 seconds to ensure a thorough dissolution and incubated at room temperature for three to five minutes. The samples were centrifuged again at 12,000 × *g* at 4 ℃ for 15 minutes that resulted in the contents being separated into three distinct layers. The RNA-containing upper colorless aqueous phase was carefully collected without and contamination from the other layers and transferred to a new RNAase-free centrifuge tube. The remaining solution with the interphase and pink organic

phenol phase was discarded. Subsequently, 500 µl of 2-propanol (isopropanol) was added to each tube and gently inverted several times and allowed to be incubated at -20 ℃ overnight for heart and kidney tissue but for at least a week for vascular tissue due to a small quantity of the tissue. Post incubation in -20 ℃, samples was centrifuged at 12,000 × *g* at 4 ℃ for 10 minutes, and 1mL of 75% ethanol (prepared from 100% ethanol and RNAase-free water) was added to the pellet (upon discarding the supernatant). The pellet was dislodged gently using a 1 ml pipette, and the sample was centrifuged at 7,500 × *g* at 4 ℃ for five minutes. The supernatant was discarded and the pellet was air-dried for 10 minutes prior to being resuspended in 12 µl of RNAase-free water for quantification. Spectrophotometer (Nanodrop 1000) (Nanodrop; Willmington, DE, USA) was used to quantify the isolated RNA using 1.5 to2 µl of the dissolved RNA.

2.13.2 Taqman RT-PCR

cDNA was made from RNA samples by reverse-transcription prior toTaqman RT-PCR experiments (All samples were run in triplicates in 384 well plates). A standard curve was generated for individual gene, using predetermined concentrations of mouse brain cDNA (0.625, 1.25, 2.5, 5, 10 and 20 µg) as a function of cycle threshold (CT). CT is the value derived by the intersectionof the amplification curve and the threshold line thereby representing a relative measure of the target concentration. The standard curve of $[cDNA]_{brain}$ as a function of CT is fit to a linear regression: Y=aX+b, where Y=cycle threshold

(CT), a=slope of the standard curve, X=[cDNA]experimental sample. The SDS2.2 software (integral to ABI7900 real-time machine) fits the CT values for the experimental samples in this formula and generates values for cDNA levels. Consequently, these values were normalized by internal controls, 18S (ribosomal RNA) or HPRT (hypoxanthine-guanine phosphoribosyltransferase-1) which appears to be a suitable house-keeping gene for myocardial[49], renal and vascular tissues. The values are expressed as relative expression (R.E.). The primers and probes of genes used in our study are listed in Table 2.2.

Table 2.2 Taqman primers and probe sequences.

Gene	Primer/ Probe	Sequence
HPRT	Forward:	5'-AGC TTG CTG GTG AAA AGG AC-3'
	Reverse:	5'-CAA CTT GCG CTC ATC TTA GG-3'
	Probe:	5'-FAM-CAA CAA AGT CTG GCC TGT ATC CAA C-TAM RA-3'
TIMP1	Forward:	5'-CAT GGA AAG CCT CTG TGG ATA TG-3'
	Reverse:	5'-AAG CTG CAG GCA CTG ATG TG-3'
	Probe:	5'-FAM-CTC ATC ACG GGC CGC CTA AGG AAC-TAM RA-3'
TIMP2	Forward:	5'-CCA GAA GAA GAG CCT GAA CCA-3'
	Reverse:	5'-GTC CAT CCA GAG GCA CTC ATC-3'
	Probe:	5'-FAM-ACT CGCT GTC CCA TGA TCC CTT GC-TAM RA-3'
TIMP3	Forward:	5'-GGC CTC AAT TAC CGC TAC CA-3'
	Reverse:	5'-CTG ATA GCC AGG GTA CCC AAA A-3'
	Probe:	5'-FAM-TGC TAC TAC TTG CCT TGT TTT GTG ACC

		TCC A-TAM RA-3'
TIMP4	Forward: Reverse: Probe:	5'-TGC AGA GGG AGA GCC TGA A-3' 5'-GGT ACA TGG CAC TGC ATA GCA-3' 5'-FAM-CCA CCA GAA CTG TGG CTG CCA AAT C-TAMRA-3'
MMP2	Forward: Reverse: Probe:	5’-AAC TAC GAT GAT GAC CGG AAG TG-3’ 5’-TGG CAT GGC CGA ACT CA-3’ 5’-FAM-TCT GTC CTG ACC AAG GAT ATA GCC TAT TCC TCG-TAM RA-3’
MMP9	Forward: Reverse: Probe:	5’-CGA ACT TCG ACA CTG ACA AGA AGT -3’ 5’- GCA CGC TGG AAT GAT CTA AGC-3’ 5’-FAM-TCT GTC CAG ACC AAG GGT ACA GCC TGT TC-TAM RA-3’
IL-1β	Forward: Reverse: Probe:	5'-AAC CTG CTG GTG TGT GAC GTT C-3’ 5'-CAG CAC GAG GCT TTT TTG TTG T-3’ 5'FAM-TAG ACA GCT GCA CTA CAG GCT CCG AGA TG-TAMRA-3’
IL-6	Forward: Reverse: Probe:	5'-ACA ACC ACG GCC TTC CCT ACT T-3’ 5'-CAC GAT TTC CCA GAG AAC ATG TG-3’ 5'FAM TTC ACA GAG GAT ACC ACT CCC AAC AGA CCT-TAMRA-3’
MCP-1	Forward: Reverse: Probe:	5’- GTT GGC TCA GCC AGA TGC A-3’ 5’-AG CCT ACT CAT TGG GAT CAT CTT G-3’ 5’-FAM-TTAACGCCCCACTCACCTGCTGCTACT-TAMRA-3’
TNF-α	Forward:	5’- ACA AGG CTG CCC CGA CTA C-3’ 5’- TTT CTC CTG GTA TGA GAT AGC AAA TC-3’

	Reverse: Probe:	5’TGC TCC TCA CCC ACA CCG TCA GC-TAMRA-3’
β-MHC	Forward: Reverse: Probe:	5'-GTGCCAAGGGCCTGAATGAG-3' 5'-GCAAAGGCTCCAGGTCTGA-3' 5'-ATCTTGTGCTACCCAGCTCTAA-3'
α- SkMA	Forward: Reverse: Probe:	5'-CAGCCGGCGCCTGTT-3' 5'-CCACAGGGCTTTGTTTGAAAA-3' 5'FAMTTGACGTGTACATAGATTGACTCGTTTTACCTCATTTTG- TAMRA-3'
pro-collagen I-α1	Forward: Reverse: Probe:	5’-CTTCACCTACAGCACCCTTGTG-3’ 5’-TGACTGTCTTGCCCCAAGTTC-3’ 5’-FAM-CTGCACGAGTCACACC-TAMRA-3’
pro-collagen III-α1 type II	Forward: Reverse: Probe:	5’- TGTCCTTTGCGATGACATAATCTG-3’ 5’- AATGGGATCTCTGGGTTGGG-3’ 5’-FAM- ATGAGGAGCCACTAGACT-TAMRA-3’
Elastin		Applied Biosystems Assay ID Mm00514670_m1 (premixed primers/probe)
WT1		Applied Biosystems Assay ID Mm01228147_m1 (premixed primers/probe)
NOX2		Applied Biosystems Assay ID Mm01287743_m1 (premixed primers/probe)
$p47^{phox}$		Applied Biosystems Assay ID Mm00447920_g1 (premixed primers/probe)

CTGF		Applied Biosystems Assay ID Mm01192933_g1 (premixed primers/probe)
TGF-ß		Applied Biosystems Assay ID Mm01178819_m1 (premixed primers/probe)
Nephrin		Applied Biosystems Assay ID Mm00497828_m1 (premixed primers/probe)
18S		Kit from Applied Biosystems (ABI; Carlsbad, CA, USA)

CTGF: connective tissue growth factor; TGF- ß transforming growth factor-beta; TNF-α: tumor necrosis factor-alpha; MCP-1: monocyte chemoattractant protein-1; IL-1ß interleukin-1 beta; IL-6: interleukin-6; WT1: Wilms tumor protein; BNP: Brain natriuretic peptide; βMHC: β-myosin heavy chain; αSkMA, α-skeletal muscle actin.

2.14 PROTEIN ANALYSES

2.14.1 Tissue Protein Extraction

Total protein was extracted from frozen tissue at -80 ℃ and (later transferred in liquid nitrogen) by gentle manual homogenization for heart and kidney tissues and by a tissue homogenizer (Omni TH$_{Q,}$ Kennesaw, GA) at 15×1000 rpm in EDTA-free RIPA buffer (please refer **Table 2.3** for western blot; **Table 2.4.** for zymography; protease inhibitor, Calbiochem, San Diego, CA, USA in **Table 2.5** and phosphatase inhibitor cocktails, Sigma-Aldrich, Oakville, ON, Canada in **Table 2.6** and Calbiochem, San Diego, CA, USA in **Table 2.7**) with variable volume depending on the amount of tissue to be homogenized. (Heart and kidney 100 µl; Aorta, carotid and mesenteric artery 60 µl). RIPA buffer was used

as it enables cell lysis and maximum protein solubilisation without any degradation. The homogenized tissue was kept on ice for 30 minutes with one minute intervals of high-speed vortex every 10 minutes. The sample was centrifuged at 14,000 × *g* for 12 minutes and the protein-containing supernatant transferred to a new 1.5 ml tube. Protein content concentration was analyzed using the Bio-Rad DC protein assay (Bio-Rad; Missisauga, ON, Canada) using a clear flat-bottom 96-well plate in a plate-reader of spectrophotometer at 750 nm. Protein extracted using Cytobuster Protein Extraction Buffer (Novagen, Madison, WI, USA) for activity assays followed the same process, except for the extraction buffer used.

Table 2.3 RIPA Protein extraction buffer pH 7.4 in ddH_2O - Western blot

RIPA Protein extraction buffer pH 7.4- Western blot				
	Chemical name	M.W. (g/mol)	$Conc._{stock}$	$Conc._{final}$
1	Tris-HCl	121.14	N/A	50 mM
2	Sodium chloride (NaCl)	58.44	N/A	120 mM
3	EDTA	372.24	N/A	1 mM
4	Triton X-100 (detergent)	624.00	N/A	1%

Table 2.4 RIPA Protein extraction buffer pH 7.4 in ddH_2O - Zymography

RIPA Protein extraction buffer pH 7.4- Zymography				
	Chemical name	M.W. (g/mol)	$Conc._{stock}$	$Conc._{final}$
1	Tris-HCl	121.14	N/A	50 mM

2	Sodium chloride (NaCl)	58.44	N/A	150 mM
3	Triton X-100 (detergent)	624.00	N/A	1%
4	SDS (detergent)	288.38	N/A	0.1%
5	NP40 (detergent)	N/A	N/A	1%
6	Sodium deoxycholate (detergent)	414.55	N/A	1%

Table 2.5 Protease inhibitor cocktail

Protease inhibitor cocktail III, EDTA-free (Calbiochem; cat# 539134)				
	Chemical name	M.W. (g/mol)	Conc.$_{stock}$	Conc.$_{final}$
1	AEBSF, hydrochloride	239.50	100x	1x
2	Aprotinin	6512.00	100x	1x
3	Bestatin	308.37	100x	1x
4	E-64	357.40	100x	1x
5	Leupeptin	475.59	100x	1x
6	Pepstatin A	685.89	100x	1x

Table 2.6 Phosphatase inhibitor cocktail- Tyr, acidic, & alkaline phosphatases

Phosphatase inhibitor cocktail 2- Tyr, acidic, & alkaline (Sigma; pdt# 5726)				
	Chemical name	M.W. (g/mol)	Conc.$_{stock}$	Conc.$_{final}$
1	Sodium-orthovanadate	183.91	100x	1x
2	Sodium-molybdate	241.95	100x	1x
3	Sodium-tartrate	230.08	100x	1x
4	Imidazole	68.08	100x	1x

Table 2.7 Phosphatase inhibitor cocktail- Ser/Thr & alkaline phosphatases

Phosphatase inhibitor cocktail IV- Ser/Thr & alkaline (Calbiochem; cat# 524628)				
	Chemical name	M.W. (g/mol)	$Conc._{stock}$	$Conc._{final}$
1	(-)-p-Bromotetramisole oxalate	373.22	100x	1x
2	Cantharidin	196.20	100x	1x
3	Calyculin A	1009.20	100x	1x

2.14.2 Western Blot

Western blot experiment comprises of sodium dodecyl sulphate-polyacrylamide (SDS) gel based transfer of protein onto a polyvinylidene fluoride (PVDF) membrane and binding of an antibody to a specific epitope on the target protein on the membrane. Each sample was prepared by combining the volume for 40 µg of sample protein with the appropriate volume of 2× protein loading buffer (**Table 2.8**) and phosphate buffered saline (PBS) (**Table 2.9**), boiled for 5 minutes to denature the protein, and allowed to traverse through the gel (variable gel percentages were selected depending upon the size of the target protein. Higher percentage allows detection of smaller size proteins with less separation as oppose to lower percent gels) driven by electrophoresis (at 100 V; Bio Rad; Mississauga, ON, Canada) in the presence of a electrophoresis running buffer solution (**Table 2.10**), and eventually transferred onto the PVDF membrane using a transfer (approximately for 1 hour) buffer solution (**Table 2.11**) (again driven by electrophoresis) for blotting. Once the transfer was complete, the membrane was blocked with 5% skim milk for two hours at room temperature

and later exposed to a primary antibody overnight at a specific dilution (ranged from 1:200 for antibodies against SERCA2a, phospho (serine16)-phospholamban, total phospholamban, TIMP3, protein kinase C (PKC) α, PKC β1, β-actin, collagen type I and alpha Elastin to 1:1000 for antibodies against of ERK1/2, p38, JNK and Akt/PKB in 5% skim milk) depending on the type and source of antibody and the target protein. The membrane was washed 3x15 minutes with Tris-based buffered solution (TBS) (**Table 2.12**) combined with 0.1% Tween (TBST), followed by the application of appropriate species-based horse radish peroxidase (HRP) linked-secondary antibody in 5% skim milk at a dilution of 1:5000 for two hours at room temperature. Membrane was meticulously washed off for another 3x15 minutes with TBST and Enhanced Chemiluminescence (ECL; GE Amersham; Baie d'Urfe, QC, Canada) was applied to the membrane according to manufacturer's instructions for 5 minutes which bound specifically to the HRP segment on the secondary antibody. An image of the membrane was taken by either developing x-ray film (Fuji Medical X-Ray Film Super Rx; Fujifilm) or by a luminescent image analyzer housing a chemiluminescence-sensitive camera (GE ImageQuant LAS 4000; GE), which was exposed to the chemiluminescent membrane. Mild stripping buffer (**Table 2.13**) was used to strip the protein in the PVDF membrane for 30 min at 55 ^{o}C and subsequently immunoblotted for a different target pretein. After the completion of all western blots, the membrane was stained with Coomassie bluedye (2% Coomassie blue, 25% methanol, 10% acetic acid and used as the

loading controls. Coomassie blue is a permanent stain that is applied to the gel after transfer to qualitatively assess the loading of the gel with the assumption of proper transfer.

Table 2.8 Sample loading buffer pH 6.8 in ddH_2O - Western blot

Sample loading buffer pH 6.8- Western blot				
	Chemical name	M.W. (g/mol)	$Conc._{stock}$	$Conc._{final}$
1	Tris-HCl	121.14	130 mM	65 mM
2	SDS	288.38	4.6%	2.3%
3	Bromophenol Blue	669.96	0.2%	0.1%
4	Glycerol	92.09	20%	10%
5	Dithiothreitol (DTT)	154.25	2%	1%

Table 2.9 Phosphate-buffered Saline (PBS) pH 7.4 in double-distilled water (ddH_2O)

Phosphate-buffered Saline (PBS) pH 7.4				
	Chemical name	M.W. (g/mol)	$Conc._{stock}$	$Conc._{final}$
1	Sodium chloride (NaCl)	58.44	1370 mM	137mM
2	Potassium chloride (KCl)	74.55	27 mM	2.7 mM
3	Sodium phosphate dibasic (Na_2HPO_4)	141.96	100 mM	10 mM
4	Potassium phosphate monobasic (KH_2PO_4)	136.09	18 mM	1.8 mM

Table 2.10 Running buffer pH 8.3 in ddH_2O

Running buffer pH 8.3				
	Chemical name	M.W. (g/mol)	$Conc._{stock}$	$Conc._{final}$

1	Tris-HCl	121.14	250 mM	25 mM
2	Glycine	75.07	1920 mM	192 mM
3	Sodium dodecyl sulfate (SDS)	288.38	10%	1%

Table 2.11 Transfer buffer pH 8.3 in ddH_2O

Transfer buffer pH 8.3				
	Chemical name	M.W. (g/mol)	Conc.$_{stock}$	Conc.$_{final}$
1	Tris- HCl	121.14	200 mM	20 mM
2	Glycine	75.07	1500 mM	150 mM
3	Methanol	32.04	N/A	20%

Table 2.12 Tris-buffered Saline (TBS) pH 8.0 in ddH_2O

Tris-buffered Saline (TBS) pH 8.0				
	Chemical name	M.W. (g/mol)	Conc.$_{stock}$	Conc.$_{final}$
1	Sodium chloride (NaCl)	58.44	1250 mM	125 mM
2	Tris-HCl	121.14	250 mM	25 mM

Table 2.13 Western blot Membrane Stripping buffer pH 6.8 in ddH_2O

Western blot Membrane Stripping buffer pH 6.8				
	Chemical name	M.W. (g/mol)	Conc.$_{stock}$	Conc.$_{final}$
1	Tris-HCl	121.14	1000 mM (pH 6.8)	62.5 mM
2	SDS	288.38	20%	2%
3	β-mercaptoethanol	78.13	14300mM	100mM

Western blotting was performed to detect phosphorylated and total levels of ERK1/2, p38, JNK, and Akt/PKB using specific antibodies (New England

Biolabs, Pickering, ON) as before[42, 43], analyses for SERCA2a, phospho (serine16)-phospholamban and total phospholamban were carried out using commercial antibodies from Santa Cruz as previously described[50, 51]. TIMP3 (30 kDa; 1:1000 dilution, monoclonal rabbit anti-mouse; Santa Cruz; Santa Cruz, CA, USA) protein levels were determined in heart and kidney tissue using a 10% polyacrylamide gel. Protein levels of protein kinase C (PKC) α, PKC β1 and β-actin (Santa Cruz and Biolabs) as an endogenous control in kidney samples were detected using 10% SDS-PAGE gels as previously described[25]. Western blot analysis was performed as previously described[52, 53] to detect the levels of mature collagen type I (COL1A1) using a 10% acrylamide gel (1:200 dilution, rabbit polyclonal affinity purified antibody raised against a peptide mapping to the N- terminus of Collagen α1Type I of human origin that detects mature Collagen of mouse, (C-18): sc-8784-R, Santa Cruz Biotechnology) and alpha Elastin (1:200 dilution, Polyclonal rabbit anti mouse alpha Elastin, Abcam Inc., Cambridge, USA) on aortic, mesenteric and carotid murine tissues.

2.14.3 Gelatin Zymography

Pro- and cleaved active MMP2 and MMP9, the classical gelatinases were detected using Gelatin zymography which represents the activation status of these proteases. Extraction of protein was carried out similarly as mentioned earlier for western blotting in section 2.14.2 except for an EDTA-free RIPA buffer used to avoid chelation by EDTA that would interfere with MMP activity. Polyacrylamide gel was prepared with gelatin at a final concentration of 2

mg/mL of the mixture. Subsequently 40 µg of protein sample, non-denaturing loading dye (**Table 2.14**) and PBS (**Table2.9**) were loaded per well.

Table 2.14 Sample loading buffer pH 6.8 in ddH_2O - Zymography

Sample loading buffer pH 6.8- Zymography				
	Chemical name	M.W. (g/mol)	Conc.$_{stock}$	Conc.$_{final}$
1	Tris-HCl	121.14	125 mM	62.5 mM
2	Glycerol	92.09	20%	10%
3	SDS	288.38	4%	2%
4	Bromophenol Blue	669.96	0.02%	0.01%

Additionally the gelatin-based polyacrylamide gel containing sample protein mixture was subjected to electrophoresis and washed in Triton-X 3 x 20 minutes prior to be washed again 3x10 minutes using incubation substrate buffer (**Table 2.15**). Finally, the gel was incubated at 37 ℃ in the incubation substrate buffer for a total of 48 hours with replaced fresh substrate buffer after the first 24 hours. After incubation the gel was stained with Coomassie Blue (2% Coomassie Blue; **Table 2.16**) overnight and further destained by a destaining solution (**Table 2.17**) until clear bands on a dark blue background were visualized. A separate 10% polyacrylamide gel with 10 µg of the protein sample used in zymography was run and stained with Coomassie-Blue eventually was used as a protein loading control.

Table 2.15 Substrate buffer in ddH_2O - Zymography

Substrate buffer- Zymography				
	Chemical name	M.W. (g/mol)	Conc.$_{stock}$	Conc.$_{final}$
1	Tris-HCl	121.14	2000 mM	50 mM

2	Calcium chloride ($CaCl_2$)•$2H_2O$	147.02	2000 mM	5 mM
3	Sodium chloride (NaCl)	58.44	N/A	150 mM
4	Sodium azide (NaN_3)	65.01	5%	0.05%

Table 2.16 Polyacrylamide Gel Staining solution in ddH_2O

Polyacrylamide Gel Staining solution				
	Chemical name	M.W. (g/mol)	Conc.$_{stock}$	Conc.$_{final}$
1	Coomassie blue	854.00	N/A	2%
2	Methanol	32.04	N/A	25%
3	Acetic acid	60.05	N/A	10%

Table 2.17 Polyacrylamide Gel Destaining solution in ddH_2O

Polyacrylamide Gel Destaining solution				
	Chemical name	M.W. (g/mol)	Conc.$_{stock}$	Conc.$_{final}$
1	Methanol	32.04	N/A	30%
2	Acetic acid	60.05	N/A	1%

2.14.4 Quantification of Protein Levels

Densitometry analysis software (ImageJ; NIH) was used to quantify protein bands detected on either the western blot or zymography. Histograms of band density relative to the background were generated by the software that allowed measurement of individual selected band density. The corresponding value obtained for individual band was normalized first to its corresponding loading control density and later normalized to one specific sample (WT sham protein band or to a specified control band of the HT1080 positive control represented

by the 64kDa cleaved MMP2). This allowed homogenization of the band density and represented as a relative value.

2.15 MMP ACTIVITY ASSAY

Total gelatinase, collagenase and elastase activities were measured using Enz-Chek fluorescent-based gelatinase/collagenase (E-12055) and elastase (E-12056) assay kit (Invitrogen; Burlington, ON, Canada) according to the manufacturer's instructions. Briefly, Cytobuster Protein Extraction Buffer was used to extract proteins for the assay that involved *in vitro* quantitative measurement of gelatinase/collagenase and elastase activity. The substrate (gelatin or collagen) heavily labelled with fluorescein isothiocyanate (FITC) and elastin labelled with BODIPY FL dye such that the fluorescence remained quenched was added to each well along with 100μg of protein sample in separate kits. The sample plate was allowed to incubate at room temperature for 6 hours (for collagenase/gelatinase) and 2 hours (for elastase) such that the proteolytic degradation of the fluorescein labelled substrate yielded fluorescence and the intensity was monitored on a fluorescence microplate reader at 495nm excitation and at 530nm emission of fluoresence. The slope of the curve generated corresponded to the proportion of the proteolytic activity.

2.16 PHARMACOLOGICAL MMP INHIBITOR (MMPI) TREATMENT

Mice of various genotypes were treated with broad-spectrum MMP inhibitor, PD-166793 (Pfizer Inc., chemical name (S)-2-(4'-bromo-biphenyl-4-

sulfonylamino)-3-methyl-butyric acid)[54] at 30 mg ŀkg^{-1} day^{-1} or doxycycline (Sigma, Aldrich) at 30 mg ŀkg^{-1} day^{-1} [55] orally by daily gavage three days before implantation of micro-osmotic pumps containing either Ang II or saline and continued for 2 or 4 weeks depending on the course of the study. PD166793 is a broad-spectrum MMP inhibitor but selective as it is not known to inhibit other families of enzymes[56].

2.17 STATISTICAL ANALYSES

All functional data in *ex vivo* vascular experiments were presented as mean ± standard error of the percentage vasoconstrictor response or the vasodilator response calculated as a percentage of constrictor tone. Stress-strain relationships were analysed by comparing the rate constants, mean ± standard error, between groups by Students'ŧ-test. All data were normally distributed as tested using the Kolmogorov-Smirnov test for Gaussian distribution. The significance of the difference in mean values of continuous variables between groups was determined by a two-way analysis of variance (ANOVA), with Bonferroni post-test for multiple comparisons. Serial blood pressure measurements were compared using 2 way ANOVA with repeated measurements followed by Bonferroni post-test. All other statistical analyses were performed using SPSS software (Chicago, Illinois, Version 19). Comparisons between different genotypes were performed using multiple ANOVA test followed by Student Neuman Keuls post-test for multiple comparison testing. Averaged values represent Mean ± SEM. Statistical significance is recognized at $p<0.05$.

2.18 REFERENCES

1. Kassiri Z, Oudit GY, Kandalam V, Awad A, Wang X, Ziou X, Maeda N, Herzenberg AM, Scholey JW. Loss of timp3 enhances interstitial nephritis and fibrosis. *J Am Soc Nephrol*. 2009;20:1223-1235

2. Itoh T, Ikeda T, Gomi H, Nakao S, Suzuki T, Itohara S. Unaltered secretion of beta-amyloid precursor protein in gelatinase a (matrix metalloproteinase 2)-deficient mice. *J Biol Chem*. 1997;272:22389-22392

3. Hsueh W, Abel ED, Breslow JL, Maeda N, Davis RC, Fisher EA, Dansky H, McClain DA, McIndoe R, Wassef MK, Rabadan-Diehl C, Goldberg IJ. Recipes for creating animal models of diabetic cardiovascular disease. *Circ Res*. 2007;100:1415-1427

4. Nozaki J, Kubota H, Yoshida H, Naitoh M, Goji J, Yoshinaga T, Mori K, Koizumi A, Nagata K. The endoplasmic reticulum stress response is stimulated through the continuous activation of transcription factors atf6 and xbp1 in ins2+/akita pancreatic beta cells. *Genes to cells : devoted to molecular & cellular mechanisms*. 2004;9:261-270

5. Wang J, Takeuchi T, Tanaka S, Kubo SK, Kayo T, Lu D, Takata K, Koizumi A, Izumi T. A mutation in the insulin 2 gene induces diabetes with severe pancreatic beta-cell dysfunction in the mody mouse. *J. Clin. Invest.* 1999;103:27-37

6. Yoshinaga T, Nakatome K, Nozaki J, Naitoh M, Hoseki J, Kubota H, Nagata K, Koizumi A. Proinsulin lacking the a7-b7 disulfide bond, ins2akita, tends to aggregate due to the exposed hydrophobic surface. *Biol. Chem.* 2005;386:1077-1085

7. Yoshioka M, Kayo T, Ikeda T, Koizumi A. A novel locus, mody4, distal to d7mit189 on chromosome 7 determines early-onset niddm in nonobese c57bl/6 (akita) mutant mice. *Diabetes*. 1997;46:887-894

8. Basu R, Oudit GY, Wang X, Zhang L, Ussher JR, Lopaschuk GD, Kassiri Z. Type 1 diabetic cardiomyopathy in the akita (ins2wt/c96y) mouse model is characterized by lipotoxicity and diastolic dysfunction with preserved systolic function. *Am J Physiol Heart Circ Physiol*. 2009;297:H2096-2108

9. Hemmeryckx B, Hoylaerts MF, Gallacher DJ, Rong Lu H, Himmelreich U, D'Hooge J, Swinnen M, Lijnen HR. Does rosiglitazone affect adiposity and cardiac function in genetic diabetic mice? *Eur J Pharmacol*. 2012

10. LaRocca TJ, Fabris F, Chen J, Benhayon D, Zhang S, McCollum L, Schecter AD, Cheung JY, Sobie EA, Hajjar RJ, Lebeche D. Na+/ca2+ exchanger-1 protects against systolic failure in the akitains2 model of diabetic cardiomyopathy via a cxcr4/nf-kappab pathway. *Am J Physiol Heart Circ Physiol*. 2012;303:H353-367

11. Lu Z, Jiang YP, Xu XH, Ballou LM, Cohen IS, Lin RZ. Decreased l-type ca2+ current in cardiac myocytes of type 1 diabetic akita mice due to reduced phosphatidylinositol 3-kinase signaling. *Diabetes*. 2007;56:2780-2789

12. Mishra PK, Chavali V, Metreveli N, Tyagi SC. Ablation of mmp9 induces survival and differentiation of cardiac stem cells into cardiomyocytes in the heart of diabetics: A role of extracellular matrix. *Can. J. Physiol. Pharmacol.* 2012;90:353-360

13. Mishra PK, Givvimani S, Metreveli N, Tyagi SC. Attenuation of beta2-adrenergic receptors and homocysteine metabolic enzymes cause diabetic cardiomyopathy. *Biochem. Biophys. Res. Commun.* 2010;401:175-181

14. Patel VB, Bodiga S, Basu R, Das SK, Wang W, Wang Z, Lo J, Grant MB, Zhong J, Kassiri Z, Oudit GY. Loss of angiotensin-converting enzyme-2 exacerbates diabetic cardiovascular complications and leads to systolic and vascular dysfunction: A critical role of the angiotensin ii/at1 receptor axis. *Circ Res*. 2012;110:1322-1335

15. Wende AR, Soto J, Olsen CD, Pires KM, Schell JC, Larrieu-Lahargue F, Litwin SE, Kakoki M, Takahashi N, Smithies O, Abel ED. Loss of bradykinin signaling does not accelerate the development of cardiac dysfunction in type 1 diabetic akita mice. *Endocrinology*. 2010;151:3536-3542

16. Alpers CE, Hudkins KL. Mouse models of diabetic nephropathy. *Curr. Opin. Nephrol. Hypertens.* 2011;20:278-284

17. Awad AS, Kinsey GR, Khutsishvili K, Gao T, Bolton WK, Okusa MD. Monocyte/macrophage chemokine receptor ccr2 mediates diabetic renal injury. *Am J Physiol Renal Physiol*. 2011;301:F1358-1366

18. Chang JH, Gurley SB. Assessment of diabetic nephropathy in the akita mouse. *Methods in molecular biology (Clifton, N.J.)*. 2012;933:17-29

19. Fujita H, Fujishima H, Takahashi K, Sato T, Shimizu T, Morii T, Shirasawa T, Qi Z, Breyer MD, Harris RC, Yamada Y, Takahashi T. Sod1, but not sod3, deficiency accelerates diabetic renal injury in

c57bl/6-ins2(akita) diabetic mice. *Metabolism: clinical and experimental*. 2012;61:1714-1724

20. Kakoki M, Kizer CM, Yi X, Takahashi N, Kim HS, Bagnell CR, Edgell CJ, Maeda N, Jennette JC, Smithies O. Senescence-associated phenotypes in akita diabetic mice are enhanced by absence of bradykinin b2 receptors. *J. Clin. Invest.* 2006;116:1302-1309

21. Koshizaka M, Takemoto M, Sato S, Tokuyama H, Fujimoto M, Okabe E, Ishibashi R, Ishikawa T, Tsurutani Y, Onishi S, Mezawa M, He P, Honjo S, Ueda S, Saito Y, Yokote K. An angiotensin ii type 1 receptor blocker prevents renal injury via inhibition of the notch pathway in ins2 akita diabetic mice. *Exp Diabetes Res*. 2012;2012:159874

22. Liu GC, Fang F, Zhou J, Koulajian K, Yang S, Lam L, Reich HN, John R, Herzenberg AM, Giacca A, Oudit GY, Scholey JW. Deletion of p47phox attenuates the progression of diabetic nephropathy and reduces the severity of diabetes in the akita mouse. *Diabetologia*. 2012;55:2522-2532

23. Lo CS, Liu F, Shi Y, Maachi H, Chenier I, Godin N, Filep JG, Ingelfinger JR, Zhang SL, Chan JS. Dual ras blockade normalizes angiotensin-converting enzyme-2 expression and prevents hypertension and tubular apoptosis in akita angiotensinogen-transgenic mice. *Am J Physiol Renal Physiol*. 2012;302:F840-852

24. Lu A, Miao M, Schoeb TR, Agarwal A, Murphy-Ullrich JE. Blockade of tsp1-dependent tgf-beta activity reduces renal injury and proteinuria in a murine model of diabetic nephropathy. *Am. J. Pathol.* 2011;178:2573-2586

25. Oudit GY, Liu GC, Zhong J, Basu R, Chow FL, Zhou J, Loibner H, Janzek E, Schuster M, Penninger JM, Herzenberg AM, Kassiri Z, Scholey JW. Human recombinant ace2 reduces the progression of diabetic nephropathy. *Diabetes*. 2010;59:529-538

26. Sanchez AP, Zhao J, You Y, Decleves AE, Diamond-Stanic M, Sharma K. Role of the usf1 transcription factor in diabetic kidney disease. *Am J Physiol Renal Physiol*. 2011;301:F271-279

27. Wong DW, Oudit GY, Reich H, Kassiri Z, Zhou J, Liu QC, Backx PH, Penninger JM, Herzenberg AM, Scholey JW. Loss of angiotensin-converting enzyme-2 (ace2) accelerates diabetic kidney injury. *Am. J. Pathol.* 2007;171:438-451

28. Yi X, Xu L, Hiller S, Kim HS, Nickeleit V, James LR, Maeda N. Reduced expression of lipoic acid synthase accelerates diabetic nephropathy. *J. Am. Soc. Nephrol.* 2012;23:103-111

29. Yu L, Su Y, Paueksakon P, Cheng H, Chen X, Wang H, Harris RC, Zent R, Pozzi A. Integrin alpha1/akita double-knockout mice on a balb/c background develop advanced features of human diabetic nephropathy. *Kidney Int.* 2012;81:1086-1097

30. Wang CH, Li F, Hiller S, Kim HS, Maeda N, Smithies O, Takahashi N. A modest decrease in endothelial nos in mice comparable to that associated with human nos3 variants exacerbates diabetic nephropathy. *Proc. Natl. Acad. Sci. U. S. A.* 2011;108:2070-2075

31. Kandalam V, Basu R, Abraham T, Wang X, Awad A, Wang W, Lopaschuk GD, Maeda N, Oudit GY, Kassiri Z. Early activation of matrix metalloproteinases underlies the exacerbated systolic and diastolic dysfunction in mice lacking timp3 following myocardial infarction. *Am J Physiol Heart Circ Physiol*. 2010;299:H1012-1023

32. Kandalam V, Basu R, Moore L, Fan D, Wang X, Jaworski DM, Oudit GY, Kassiri Z. Lack of tissue inhibitor of metalloproteinases 2 leads to exacerbated left ventricular dysfunction and adverse extracellular matrix remodeling in response to biomechanical stress. *Circulation*. 2011;124:2094-2105

33. Koonen DP, Febbraio M, Bonnet S, Nagendran J, Young ME, Michelakis ED, Dyck JR. Cd36 expression contributes to age-induced cardiomyopathy in mice. *Circulation*. 2007;116:2139-2147

34. Bose R, Kolesnick R. Measurement of ceramide levels by the diacylglycerol kinase reaction and by high-performance liquid chromatography-fluorescence spectrometry. *Methods Enzymol*. 2000;322:373-378

35. Larsen TS, Belke DD, Sas R, Giles WR, Severson DL, Lopaschuk GD, Tyberg JV. The isolated working mouse heart: Methodological considerations. *Pflugers Archiv : European journal of physiology*. 1999;437:979-985

36. Aneja A, Tang WH, Bansilal S, Garcia MJ, Farkouh ME. Diabetic cardiomyopathy: Insights into pathogenesis, diagnostic challenges, and therapeutic options. *Am J Med*. 2008;121:748-757

37. Martin-McNulty B, Vincelette J, Vergona R, Sullivan ME, Wang YX. Noninvasive measurement of abdominal aortic aneurysms in intact mice

by a high-frequency ultrasound imaging system. *Ultrasound Med Biol*. 2005;31:745-749

38. Barisione C, Charnigo R, Howatt DA, Moorleghen JJ, Rateri DL, Daugherty A. Rapid dilation of the abdominal aorta during infusion of angiotensin ii detected by noninvasive high-frequency ultrasonography. *J Vasc Surg*. 2006;44:372-376

39. Gray LW, Peng F, Molloy SA, Pendyala VS, Muchenditsi A, Muzik O, Lee J, Kaplan JH, Lutsenko S. Urinary copper elevation in a mouse model of wilson's disease is a regulated process to specifically decrease the hepatic copper load. *PLoS One*.7:e38327

40. Bodiga S, Zhong JC, Wang W, Basu R, Lo J, Liu GC, Guo D, Holland SM, Scholey JW, Penninger JM, Kassiri Z, Oudit GY. Enhanced susceptibility to biomechanical stress in ace2 null mice is prevented by loss of the p47phox nadph oxidase subunit. *Cardiovasc Res*. 2011;91:151-161

41. Patel VB, Bodiga S, Basu R, Das SK, Wang W, Wang Z, Lo J, Grant MB, Zhong J, Kassiri Z, Oudit GY. Loss of angiotensin-converting enzyme-2 exacerbates diabetic cardiovascular complications and leads to systolic and vascular dysfunction: A critical role of the angiotensin ii/at1 receptor axis. *Circulation Research*. 2012;110:1322-1335

42. Oudit GY, Kassiri Z, Patel MP, Chappell M, Butany J, Backx PH, Tsushima RG, Scholey JW, Khokha R, Penninger JM. Angiotensin ii-mediated oxidative stress and inflammation mediate the age-dependent cardiomyopathy in ace2 null mice. *Cardiovasc Res*. 2007;75:29-39

43. Oudit GY, Kassiri Z, Zhou J, Liu QC, Liu PP, Backx PH, Dawood F, Crackower MA, Scholey JW, Penninger JM. Loss of pten attenuates the development of pathological hypertrophy and heart failure in response to biomechanical stress. *Cardiovasc Res*. 2008;78:505-514

44. Sakairi T, Abe Y, Kajiyama H, Bartlett LD, Howard LV, Jat PS, Kopp JB. Conditionally immortalized human podocyte cell lines established from urine. *Am J Physiol Renal Physiol*. 2010;298:F557-567

45. Kassiri Z, Oudit GY, Sanchez O, Dawood F, Mohammed FF, Nuttall RK, Edwards DR, Liu PP, Backx PH, Khokha R. Combination of tumor necrosis factor-alpha ablation and matrix metalloproteinase inhibition prevents heart failure after pressure overload in tissue inhibitor of metalloproteinase-3 knock-out mice. *Circ Res*. 2005;97:380-390

46. Suen AY, Baldwin TA. Proapoptotic protein bim is differentially required during thymic clonal deletion to ubiquitous versus tissue-restricted antigens. *Proc Natl Acad Sci U S A*. 2010;109:893-898

47. Kandalam V, Basu R, Abraham T, Wang X, Soloway PD, Jaworski DM, Oudit GY, Kassiri Z. Timp2 deficiency accelerates adverse post-myocardial infarction remodeling because of enhanced mt1-mmp activity despite lack of mmp2 activation. *Circ Res*. 2010;106:796-808

48. Kassiri Z, Defamie V, Hariri M, Oudit GY, Anthwal S, Dawood F, Liu P, Khokha R. Simultaneous transforming growth factor beta-tumor necrosis factor activation and cross-talk cause aberrant remodeling response and myocardial fibrosis in timp3-deficient heart. *J Biol Chem*. 2009;284:29893-29904

49. Noutsias M, Rohde M, Block A, Klippert K, Lettau O, Blunert K, Hummel M, Kuhl U, Lehmkuhl H, Hetzer R, Rauch U, Poller W, Pauschinger M, Schultheiss HP, Volk HD, Kotsch K. Preamplification techniques for real-time rt-pcr analyses of endomyocardial biopsies. *BMC molecular biology*. 2008;9:3

50. Crackower MA, Oudit GY, Kozieradzki I, Sarao R, Sun H, Sasaki T, Hirsch E, Suzuki A, Shioi T, Irie-Sasaki J, Sah R, Cheng HY, Rybin VO, Lembo G, Fratta L, Oliveira-dos-Santos AJ, Benovic JL, Kahn CR, Izumo S, Steinberg SF, Wymann MP, Backx PH, Penninger JM. Regulation of myocardial contractility and cell size by distinct pi3k-pten signaling pathways. *Cell*. 2002;110:737-749

51. Flagg TP, Cazorla O, Remedi MS, Haim TE, Tones MA, Bahinski A, Numann RE, Kovacs A, Schaffer JE, Nichols CG, Nerbonne JM. Ca2+-independent alterations in diastolic sarcomere length and relaxation kinetics in a mouse model of lipotoxic diabetic cardiomyopathy. *Circ Res*. 2009;104:95-103

52. Zhong JC, Yu XY, Lin QX, Li XH, Huang XZ, Xiao DZ, Lin SG. Enhanced angiotensin converting enzyme 2 regulates the insulin/akt signalling pathway by blockade of macrophage migration inhibitory factor expression. *Br J Pharmacol*. 2008;153:66-74

53. Kassiri Z, Zhong J, Guo D, Basu R, Wang X, Liu PP, Scholey JW, Penninger JM, Oudit GY. Loss of angiotensin-converting enzyme 2 accelerates maladaptive left ventricular remodeling in response to myocardial infarction. *Circ Heart Fail*. 2009;2:446-455

54. Chancey AL, Brower GL, Peterson JT, Janicki JS. Effects of matrix metalloproteinase inhibition on ventricular remodeling due to volume overload. *Circulation*. 2002;105:1983-1988

55. Benjamin MM, Khalil RA. Matrix metalloproteinase inhibitors as investigative tools in the pathogenesis and management of vascular disease. *EXS*.103:209-279

56. Kaludercic N, Lindsey ML, Tavazzi B, Lazzarino G, Paolocci N. Inhibiting metalloproteases with pd 166793 in heart failure: Impact on cardiac remodeling and beyond. *Cardiovascular therapeutics*. 2008;26:24-37

CHAPTER THREE

TYPE 1 DIABETIC CARDIOMYOPATHY IN THE AKITA (INS2$^{WT/C96Y}$) MOUSE MODEL IS CHARACTERIZED BY DIASTOLIC DYSFUNCTION WITH PRESERVED SYSTOLIC FUNCTION

Ratnadeep Basu, MD[1,2]; Gavin Y. Oudit, MD/PhD[2,3]; Xiuhua Wang, PhD[1,2]; Liyan Zhang[2,4]; John R. Ussher, MSc[2,4]; Gary D. Lopaschuk, PhD[2,4] and Zamaneh Kassiri, PhD[1,2]

[1]Department of Physiology, University of Alberta, [2]Mazankowski Alberta Heart Institute, Edmonton, Canada, [3]Division of Cardiology, Department of Medicine, [4]Departments of Pediatrics and Pharmacology, University of Alberta, Edmonton, Canada

A modified version of this chapter has been published in *American Journal of Physiology Heart and Circulatory Physiology*, 2009 Oct 2; 297: H2096-H2108.

Author Contributions

Participated in Research Design: R.B, G.D.L, G.Y.O. and Z.K.
Conducted Experiments: R.B., X.W., L.Z., J.R.U
Performed Data Analysis: R.B., X.W., L.Z., J.R.U, G.D.L, G.Y.O. and Z.K.
Contributed to the Writing of the Manuscript: R.B., G.D.L., G.Y.O. and Z.K.

3.1 ABSTRACT

Diabetic cardiomyopathy is an important contributor to diastolic and systolic heart failure. We examined the nature and mechanism of the cardiomyopathy in Akita (*Ins2*$^{WT/C96Y}$) mice, a model of genetic non-obese type 1 diabetes which recapitulates human type 1 diabetes. Cardiac function was evaluated in male *Ins2*$^{WT/C96Y}$ and their littermate control (*Ins2*$^{WT/WT}$) mice using echocardiography and tissue Doppler imaging, *in vivo* hemodynamic measurements, as well as *ex vivo* working heart preparation. At 3- and 6-months of age, *Ins2*$^{WT/C96Y}$ mice exhibited preserved cardiac systolic function compared to *Ins2*$^{WT/WT}$ mice as evaluated by ejection fraction, fractional shortening, LV end-systolic pressure and dP/dt_{max} *in vivo*, cardiac work, cardiac power, and rate-pressure product *ex vivo*. Despite the unaltered systolic function, *Ins2*$^{WT/C96Y}$ mice exhibited significant and progressive diastolic dysfunction at 3- and 6-months of age compared to *Ins2*$^{WT/WT}$ mice. Diastolic dysfunction was assessed using tissue doppler imaging (E-wave velocity, isovolumetric relaxation time and pulmonary venous flow) and by *in vivo* hemodynamic measurements (LV end-diastolic pressure, Tau, and dP/dt_{min}). We found no evidence of myocardial hypertrophy or fibrosis in the *Ins2*$^{WT/C96Y}$ myocardium. Consistent with the lack of fibrosis, expression of pro-collagen-α type-I, pro-collagen-α type-III and fibronectin were not increased in these hearts. *Ins2*$^{WT/C96Y}$ hearts showed significantly reduced SERCA2a (cardiac sarcoplasmic reticulum Ca^{2+} pump) levels, elevated β-myosin heavy chain isoform, increased long-chain fatty acids and triacylglycerol with evidence of

lipotoxicity as indicated by a significant rise in ceramide, diacylglycerol (DAG) and lipid deposits in the myocardium. Consistent with metabolic perturbation, and a switch to fatty acid oxidation from glucose oxidation in *Ins2*$^{WT/C96Y}$ hearts, expression of mitochondrial long-chain acyl-CoA dehydrogenase (LCAD) and pyruvate dehydrogenase kinase isoform4 (PDK4) were increased. Insulin-treatment reversed the diastolic dysfunction, the elevated BNP and βMHC and the reduced SERCA2a levels with abolition of cardiac lipotoxicity. We conclude that early type 1 diabetic cardiomyopathy is characterized by diastolic dysfunction associated with lipotoxic cardiomyopathy with preserved systolic function in the absence of interstitial fibrosis and hypertrophy.

3.2 INTRODUCTION

Diabetes mellitus has become a major health concern worldwide and is predicted to be the fifth most common cause of deaths globally [1, 2]. Diabetes itself has been established to be a strong risk factor for heart failure independent of age, hypertension, dyslipidemia and coronary artery disease (CAD) [3-5]. Although type 2 diabetes is a more common form of diabetes with an early onset of hyperinsulinemia and a late onset of hyperglycemia, type 1 diabetes affects approximately 5-10% of the diabetic population globally with early onset of hyperglycemia, and both types can result in severe cardiovascular complications [6].

Diastolic heart failure is now a well-recognized clinical entity often associated with diabetes and hypertension [2, 7-9]. Several factors may contribute to the development and progression of cardiac dysfunction in diabetes mellitus,

including increased interstitial fibrosis, suppressed intracellular Ca^{2+} handling, altered contractile filament properties, and/or lipotoxicity affecting both passive and active relaxation properties of the ventricle [3, 5, 9-11]. The *Ins2*$^{WT/C96Y}$ (Akita) mouse is a well validated non-obese model of human type 1 diabetes while being free of potential confounding effects of streptozotocin (STZ) administration [12, 13]. In this study, we characterized the cardiomyopathy in *Ins2*$^{WT/C96Y}$ mice and demonstrate that these mice exhibit early and persistent diastolic dysfunction in a setting of preserved systolic function compared to their littermate control, *Ins2*$^{WT/WT}$ mice. Lack of insulin in *Ins2*$^{WT/C96Y}$ mice suppressed insulin-dependent signaling pathways such as phosphorylation of Erk1/2 and Akt/PKB in the heart. We found evidence of lipotoxicity in *Ins2*$^{WT/C96Y}$ hearts coupled with increased expression of long-chain acyl-CoA dehydrogenase (LCAD) and pyruvate dehydrogenase kinase isoform 4 (PDK4). We conclude that type 1 diabetic cardiomyopathy is characterized by diastolic dysfunction and preserved systolic function, with evidence of myocardial lipotoxicity and downregulation of the major Ca^{2+}-regulatory protein, SERCA2a, in the absence of hypertrophy or interstitial fibrosis.

3.3 OBJECTIVE

Diabetic cardiomyopathy is an important contributor to diastolic and systolic heart failure and the cardiovascular burden of patients with diabetes mellitus. In this study, we investigated the nature and mechanism of the cardiomyopathy in a

mouse model characteristic of a genetic non-obese type 1 diabetes which recapitulates human type 1 diabetes.

3.4 MATERIALS AND METHODS

3.4.1 Echocardiography and Tissue Doppler Imaging

In vivo cardiac function was measured in male Akita mice (*Ins2*$^{WT/C96Y}$, breeding detailed in Chapter 2.1.1.1) and in litter-mate wild type (*Ins2*$^{WT/WT}$) mice using Transthoracic echocardiography (Chapter 1.2.2 and 2.5) and Doppler imaging (Chapter 1.2.2, 2.5.2 and 2.5.3).

3.4.2 Hemodynamic Measurements

In vivo Hemodynamic measurements were performed invasively in 10-12 week old mice of either genotype under 1% isoflurane anesthesia. The right common carotid was exposed and cannulated using a 1.4 French Millar catheter (detailed in Chapter 2.5.5.). Hemodynamic data were acquired using PowerLab data acquisition system and analyzed.

3.4.3 Isolated Working Heart Model

Hearts were perfused using an isolated working heart preparation as described previously (Chapter 2.5)

3.4.4 Immunohistological and Molecular Analyses

Hearts were collected as described in Chapter 2.3.2 and were either formalin-fixed for immunohistological, Oil-O red staining was performed using 0.5% oil-O red as described earlier [14] and morphological analysis (Chapter 2.9.1 and 2.9.2), or

flash frozen for RNA (Chapter 2.13), protein (Chapter 2.14) and other molecular analyses associated with the metabolic status of the heart (Chapter 2.4).

3.4.5 Insulin replacement in *Ins2*$^{WT/C96Y}$ Mice

Insulin pellets (Linshin Canada) were implanted dorsally and subcutaneously in 8-wk old *Ins2*$^{WT/C96Y}$ mice. The pellets release 0.2U insulin/day for 4 weeks. Blood glucose was monitored one day prior to, and every 3 days starting one day after the implant for 4 weeks.

3.4.6 Statistical Analysis

Two-way ANOVA followed by multiple comparison test were performed to compare between the *Ins2*$^{WT/C96Y}$ and *Ins2*$^{WT/WT}$ groups at 3 months and 6months of age. Averaged values are presented as Mean ±SEM.

3.5 RESULTS

3.5.1 Diastolic Dysfunction in the Presence of Normal Systolic Function in *Ins2*$^{WT/C96Y}$ Mice

We assessed the cardiac function in *Ins2*$^{WT/C96Y}$ and littermate *Ins2*$^{WT/WT}$ mice non-invasively using a high-resolution imaging transthoracic echocardiography system equipped with a 30-MHz transducer, invasively by hemodynamic measurements, and *ex vivo* using an isolated working preparation. M-mode images from *Ins2*$^{WT/WT}$ and *Ins2*$^{WT/C96Y}$ mice at 3 months of age showed comparable LV contractility (**Fig. 3.1A**), while long-axis images from these mice show lack of LV dilation and in fact a slight reduction in the LV chamber size in the *Ins2*$^{WT/C96Y}$ mice (**Fig. 3.1B**). Consistently, parameters of cardiac systolic

function including ejection fraction, fractional shortening, stroke volume (**Table 3.1**) as well as dP/dt_{max} are comparable between *Ins2*$^{WT/C96Y}$ and their littermate *Ins2*$^{WT/WT}$ mice at 3 months and 6 months of age (**Fig. 3.1C**). Additional systolic function parameters including the systolic myocardial velocity (S') by tissue Doppler imaging are reported in Table 3.1. We further used an *ex vivo* isolated working heart model to compare the basal systolic function between the genotypes under controlled conditions. *Ins2*$^{WT/C96Y}$ mice showed unaltered systolic performance, as determined by cardiac work, cardiac power and rate pressure product, compared to *Ins2*$^{WT/WT}$ mice (**Fig. 3.1D**).

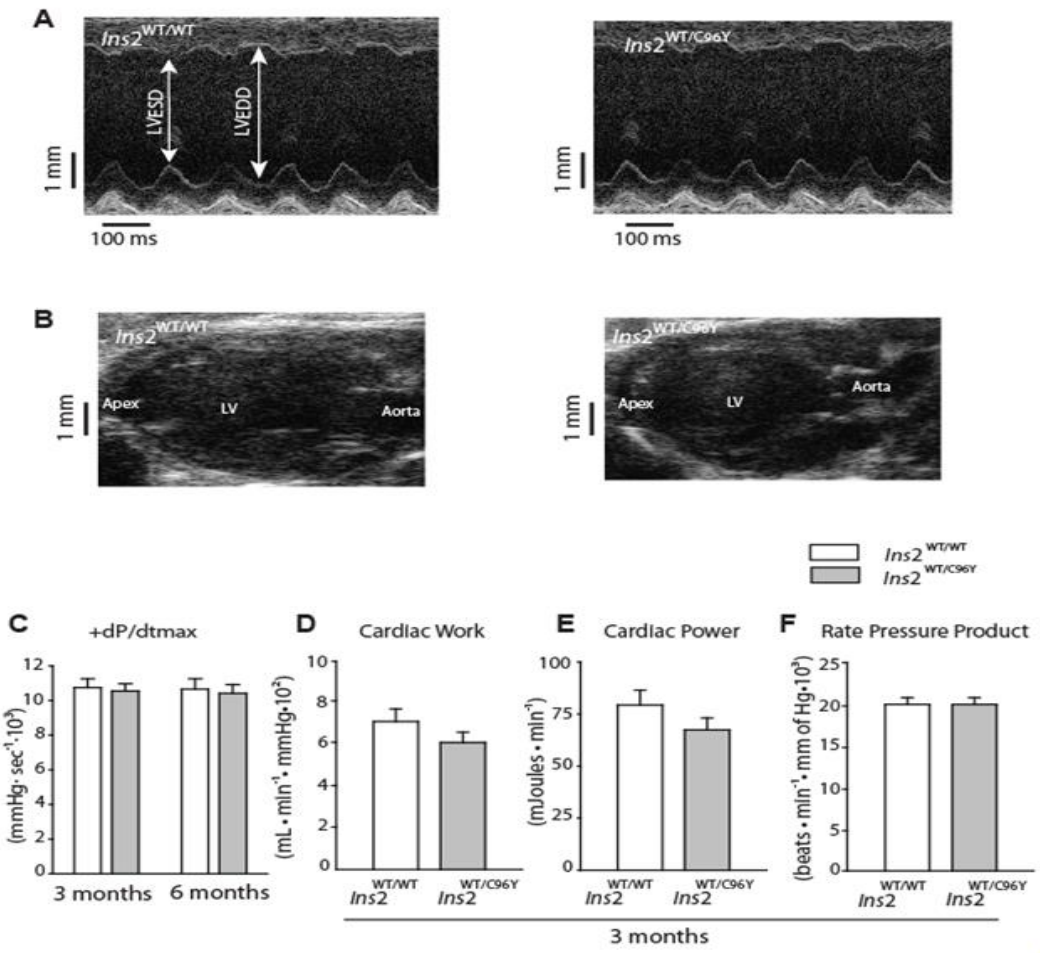

Figure 3.1 Assessment of cardiac systolic function in *Ins2*$^{WT/C96Y}$ compared to littermate *Ins2*$^{WT/WT}$ mice.

A: Representative M-mode images from *Ins2*$^{WT/WT}$ and *Ins2*$^{WT/C96Y}$ hearts at 3 months of age. *B:* Representative long-axis view of the hearts from *Ins2*$^{WT/WT}$ and *Ins2*$^{WT/C96Y}$ mice. *C-H:* Averaged parameters for *in vivo* hemodynamics *(C)*, and *ex vivo* working heart preparation *(D-F)* showing comparable systolic function between *Ins2*$^{WT/C96Y}$ and littermate *Ins2*$^{WT/WT}$ mice. LVESD = LV end-systolic diameter; LVEDD = LV end-diastolic diameter. Averaged values are presented as Mean ± SEM.

Table 3.1 Echocardiographic assessment of systolic function in 3 months and 6 months old mice.

	Ins2$^{WT/WT}$	*Ins2*$^{WT/C96Y}$	*Ins2*$^{WT/WT}$	*Ins2*$^{WT/C96Y}$
Age	3 months	3 months	6 months	6 months
n	12	12	9	9
HR (bpm)	448±11	438±12	459±16	451±13
LVEF (%)	60±1.4	59.8±1.8	54±3.4	57.4±2
LVFS (%)	28.3±1.34	29.3±0.91	27.6±2.13	29.7±1.33
SV(µL)	43.5±2.4	45±1.1	43.2±3.2	49.2±1.2
CO (ml/min)	19.5±1.26	19±0.77	19.4±1.75	19.6±0.08
LVEDD (mm)	3.81±0.07	3.68±0.07	3.82±0.05	3.71±0.04
LVESD (mm)	2.73±0.05	2.60±0.05	2.77±0.11	2.61±0.06
LVPWT (mm)	0.77±0.01	0.74±0.03	0.8±0.03	0.76±0.02
ET (ms)	50.5±2.1	44.3±2.9	54±2.5	50.3±2.2
Vcfc (circ/s)	0.56±0.04	0.67±0.1	0.51±0.05	0.59±0.03
S' (cm/s)	2.39±0.08	2.58±0.09	2.42±0.09	2.61±0.11

HR=heart rate; LVEF=LV ejection fraction; LVFS=LV fractional shortening; SV= stroke volume; CO=cardiac output; LVEDD=left ventricular end diastolic diameter; LVESD=left ventricular end systolic diameter; ET= ejection time; Vcfc=velocity of circumferential shortening, S'=systolic myocardial velocity by tissue Doppler imaging.

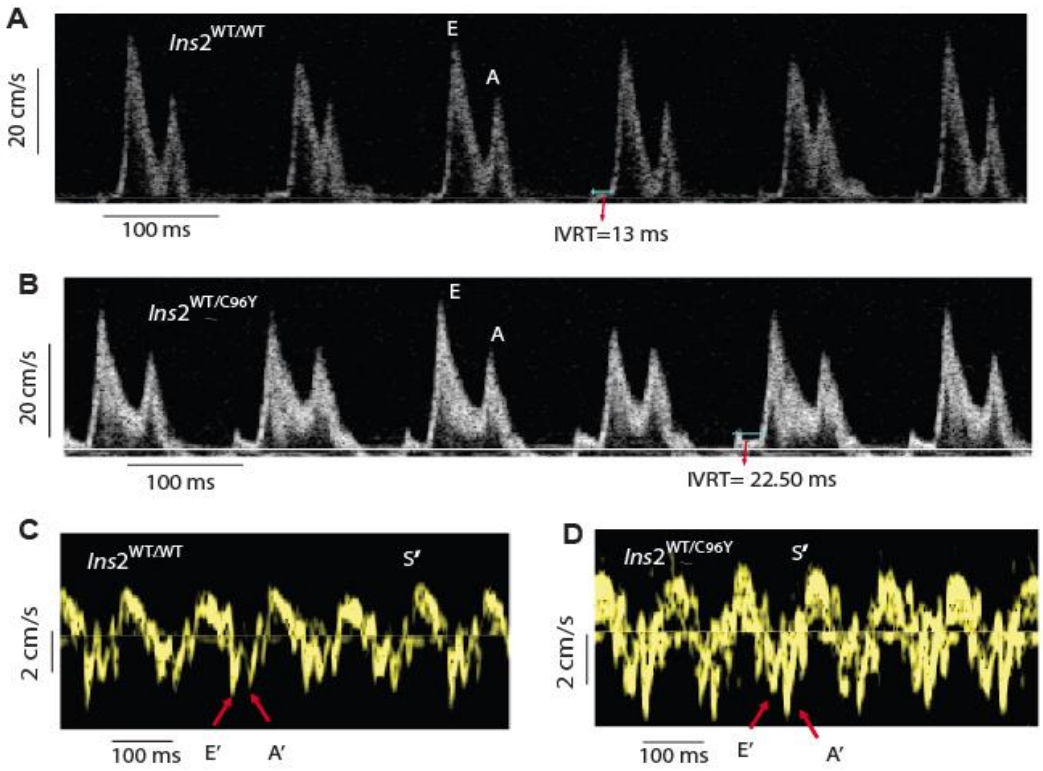

Figure 3.2 Echocardiographic assessment of diastolic function in *Ins2*$^{WT/C96Y}$ compared to *Ins2*$^{WT/WT}$ mice.

A-B: Representative transmitral Doppler flow profile showing reduced peak E-wave velocity with increased deceleration time and prolongation of isovolumetric relaxation interval (IVRT) in an *Ins2*$^{WT/C96Y}$ *(B)* compared to an *Ins2*$^{WT/WT}$ mouse *(A). C-D:* Representative tissue Doppler images of the basal inferolateral LV wall showing reduced early diastolic tissue velocity (E') in an *Ins2*$^{WT/C96Y}$ *(D)* compared to an *Ins2*$^{WT/WT}$ mouse *(C).*

We evaluated diastolic function in these mice using traditional Doppler technique coupled with TDI. Transmitral filling pattern showed reduced E-wave velocity with prolongation of deceleration time leading to a significant reduction in E-wave deceleration rates in 3-month old *Ins2*$^{WT/C96Y}$compared to littermate *Ins2*$^{WT/WT}$ mice (**Figs. 3.2A and 3.2B, Fig. 3.3A, Table 3.2**). The isovolumetric relaxation time (IVRT) was also increased markedly in *Ins2*$^{WT/C96Y}$ mice suggesting impaired relaxation (**Figs. 3.2A and 3.2B, Fig. 3.3B, Table 3.2**). Peak early tissue relaxation (E') was reduced in 3-month old *Ins2*$^{WT/C96Y}$ mice (**Figs.**

3.2C, 3.2D and Fig. 3.3C). Wet and dry lung weight in *Ins2*$^{WT/C96Y}$ and *Ins2*$^{WT/WT}$ mice showed no difference in the lung water content (WT: 0.111±0.002 mg, Akita: 0.097±0.07 mg) or dry/wet weight ratio (*Ins2*$^{WT/WT}$: 0.36±0.02, *Ins2*$^{WT/C96Y}$: 0.33±0.03) between the genotypes. These data collectively demonstrate that *Ins2*$^{WT/C96Y}$ mice exhibit early diastolic dysfunction at 3 months of age compared to their littermate *Ins2*$^{WT/WT}$ mice but have not reached clinically overt heart failure.

Impairment of diastolic function in the *Ins2*$^{WT/C96Y}$ mice is progressive. Left atrial size has been shown to positively correlate with the degree and duration of LV diastolic dysfunction [2, 15], and we found that the left atrial size in *Ins2*$^{WT/C96Y}$ mice progressively increased at 3 and 6 months of age compared to *Ins2*$^{WT/WT}$ littermates (**Table 3.2**). We also used invasive hemodynamic measurement in order to provide more definitive assessment of the diastolic dysfunction. The key hemodynamic correlates of diastolic dysfunction, LV end diastolic pressure and the time constant of LV relaxation (Tau) were increased in the *Ins2*$^{WT/C96Y}$mice (**Figs. 3.3D and 3.3E**) while dP/dt_{min} was reduced in *Ins2*$^{WT/C96Y}$mice (**Fig. 3.3F**) without alterations in baseline heart rate (524±19 bpm in *Ins2*$^{WT/WT}$ vs 539±23 bpm in *Ins2*$^{WT/C96Y}$mice; p=0.412). Overall, our data indicate that *Ins2*$^{WT/C96Y}$ mice demonstrate early and persistent diastolic dysfunction with preservation of systolic function.

Table 3.2 Echocardiographic assessment of diastolic function in 3 months and 6 months old mice.

	Ins2$^{WT/WT}$	*Ins2*$^{WT/C96Y}$	*Ins2*$^{WT/WT}$	*Ins2*$^{WT/C96Y}$
Age	3 months	3 months	6 months	6 months
n	12	12	9	9
E-wave (cm/s)	77.5±2.9	66.7±2.2*	68.5±2.5	72.6±3.2
A-wave (cm/s)	48.6±2.8	43.9±2.6	44.5±4.7	44.1±4.0
E/A Ratio	1.58±0.05	1.52±0.06	1.6±0.1	1.7±0.1
IVRT (ms)	14.7±0.72	18.87±0.94*	15.03±0.66	18.53±0.94*
DT (ms)	22.6±1.45	29.2±1.16*	25.1±2.71	23.6±1.59‡
EWDR (cm/s^2)	3.67±0.4	2.32 ±0.124*	2.9±0.4‡	3.2±0.3‡
AR (cm/s)	13.9±1.2	16.7±1.6*	7.9±0.7‡	12.8±1.5*
E′ (cm/s)	3.15±0.15	2.48±0.13*	2.63±0.17‡	2.82±0.18
E/E′	24.6±1.72	26.9±0.86	27.9±1.8	26.2±1.4
LA size (mm)	1.64±0.08	1.77±0.06*	1.85±0.07	2.17±0.05*‡

E wave=peak early transmitral inflow mitral E velocity; A wave=mitral Doppler A velocity; IVRT=isovolumetric relaxation time; DT=deceleration time; EWDR=E wave deceleration rate (E-wave/DT); E′=early diastolic tissue Doppler velocity; *p<0.05 compared with age-matched *Ins2*$^{WT/WT}$ group. ‡ P<0.05 compared with 3 month old group of the corresponding genotype.

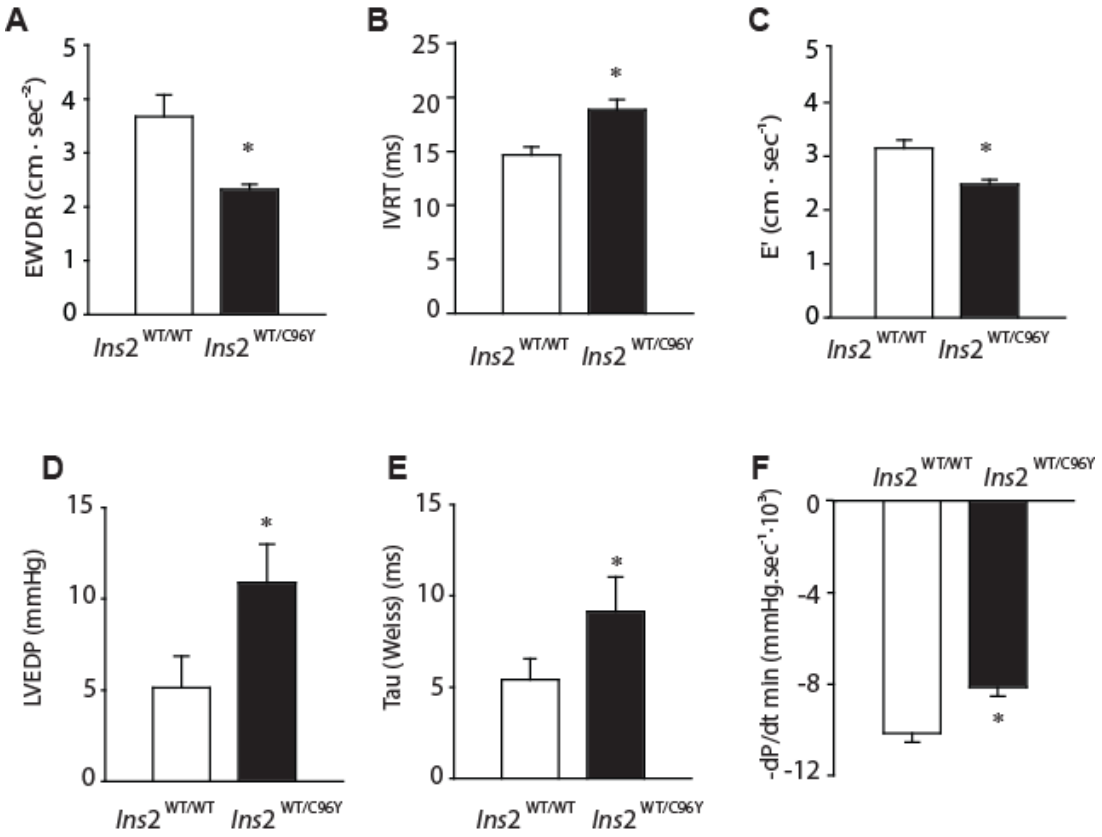

Figure 3.3 Averaged parameters of diastolic dysfunction *Ins2*$^{WT/C96Y}$ compared to *Ins2*$^{WT/WT}$ mice.

A-C: Echocardiographic assessment showing reduced E-wave deceleration rate (EWDR), prolongation of the isovolumetric relaxation time (IVRT), and reduced early tissue Doppler velocity (E') consistent with diastolic dysfunction (n=12/group). *D-F:* Hemodynamic assessment showing elevated LV end-diastolic pressure (LVEDP), prolonged LV relaxation (Tau) and reduced $-dP/dt_{min}$. *p<0.05 compared to *Ins2*$^{WT/WT}$ mice.

3.5.2 *Ins2*$^{WT/C96Y}$ Mice Exhibit No Myocardial Hypertrophy or Fibrosis

To further characterize the cardiomyopathy in this model of type 1 diabetes, we evaluated the cardiac morphometry and expression levels of disease markers. We found that *Ins2*$^{WT/C96Y}$ hearts appear smaller compared to *Ins2*$^{WT/WT}$ hearts (**Fig. 3.4A, Table 3.1**). LV weight-to-tibial length ratio was significant lower in *Ins2*$^{WT/C96Y}$hearts (Fig. 4B), and myocyte cross-sectional areas were significantly smaller in *Ins2*$^{WT/C96Y}$ hearts compared to *Ins2*$^{WT/WT}$ hearts (**Fig. 3.4C**). These

data suggest that type-1 diabetes can limit myocardial growth. The cardiomyopathy in *Ins2*$^{WT/C96Y}$ mice was further confirmed by elevated expression levels of the disease markers, B-type natriuretic peptide (BNP) (**Fig. 3.4D**) and beta-myosin heavy chain isoform (β-MHC) (**Fig. 3.4E**), further confirming the pathological nature of this phenotype.

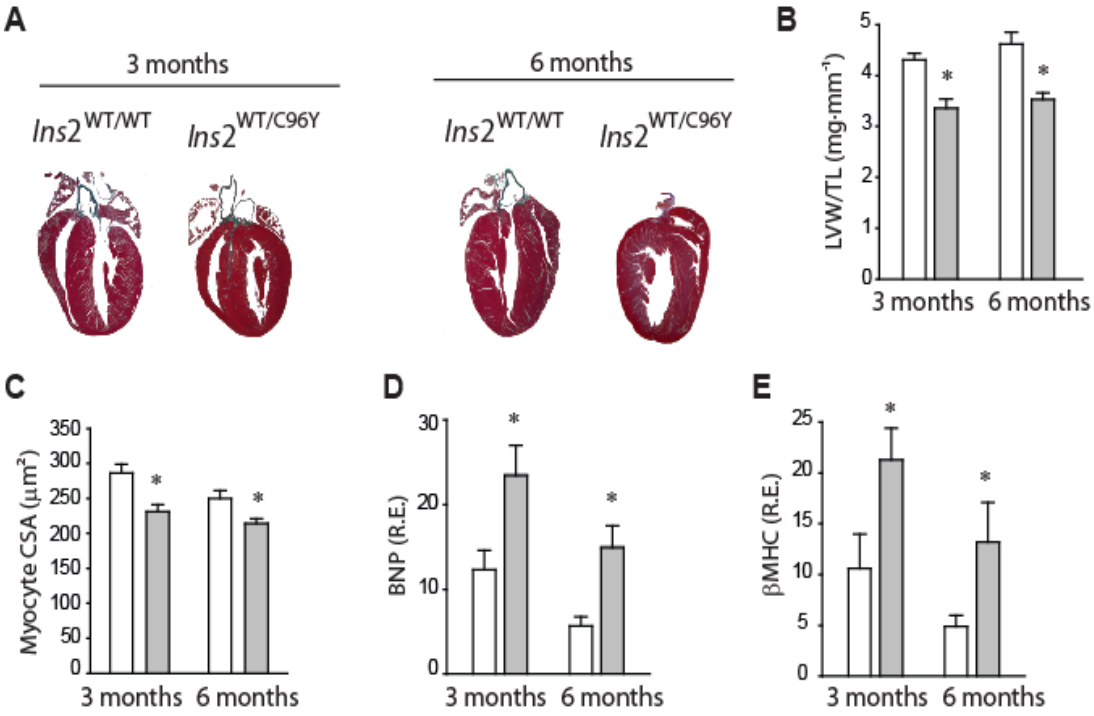

Figure 3.4 *Ins2*$^{WT/C96Y}$ hearts exhibit limited growth and no hypertrophy.
A: Trichrome-stained four-chamber views of *Ins2*$^{WT/WT}$ and *Ins2*$^{WT/C96Y}$ hearts at 3 months and at 6 months of age. *B-C:* LV weight-to-tibial ratio (LVW/TL) and myocyte cross-sectional area (CSA) show that *Ins2*$^{WT/C96Y}$ hearts are smaller than their littermate *Ins2*$^{WT/WT}$ controls. *D-E:* Disease markers for cardiomyopathy, B-type natriuretic peptide (BNP) and beta-myosin heavy chain (β-MHC) are elevated in *Ins2*$^{WT/C96Y}$ hearts.

Insulin is a tyrosine receptor kinase agonist that can activate the Erk1/2 and Akt/PKB signaling pathways in the heart [16-18]. The genetic defect in *Ins2*$^{WT/C96Y}$mice results in an early and sustained loss of the insulin-producing ß-cells resulting in very low plasma insulin levels [13, 19]. As such, we evaluated the

phosphorylation status of the Erk1/2 and Akt/PKB pathways which are known to be activated by insulin [17]. Western blot analysis showed a bimodal response of the Erk1/2 pathway in *Ins2*$^{WT/C96Y}$mice characterized by an inhibition of Erk1/2 phosphorylation at 3 months followed by increased phosphorylation at 6 months (**Fig. 3.5A**). In contrast, the phosphorylation of Akt/PKB at serine-473 (**Fig. 3.5B**) and threonine-308 (**Fig. 3.5C**) residues remained unaffected at 3 months of age but was significantly reduced at 6 months of age in the *Ins2*$^{WT/C96Y}$mice, suggesting a time-dependent loss of Erk1/2 and Akt/PKB signaling with insulin deficiency.

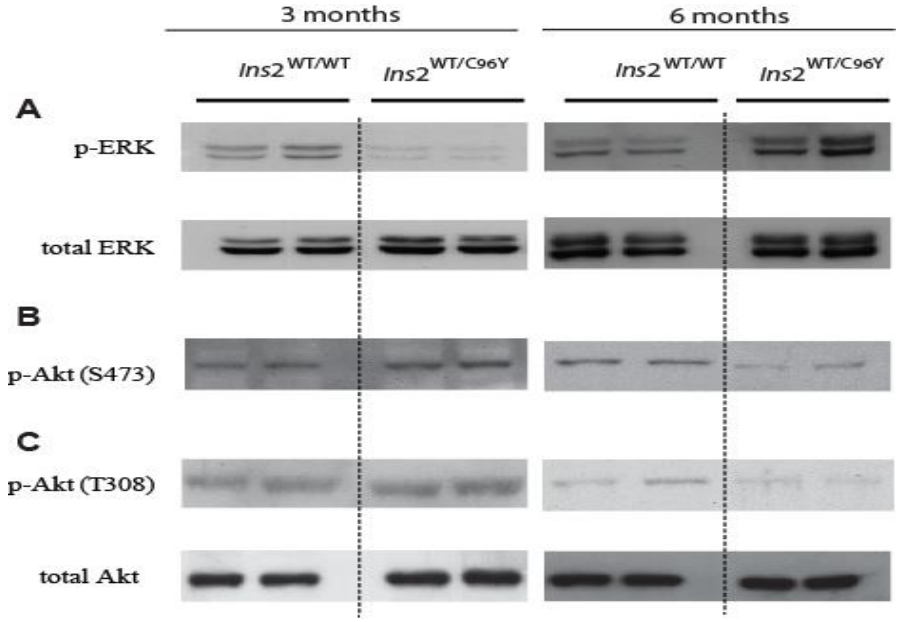

Figure 3.5 Downstream signalling pathways to insulin in 3 and 6 months old *Ins2*$^{WT/C96Y}$ hearts

A: Representative western-blots for phospho- and total ERK are shown on the left and the corresponding quantifications are shown on the right. Phosphorylation of Erk1/2 was reduced at 3 months but rebound at 6 months of age. *B-C:* Representative western blots for phospho- and total-Akt are shown on the left and the corresponding qauntifications on the right. Phosphorylation of Akt at serine-473 *(B)* and threonine-308 *(C)* residues were unchanged at 3 months but significantly decreased at 6 months of age in *Ins2*$^{WT/C96Y}$ mice. n=6/group; *p<0.05 compared to *Ins2*$^{WT/WT}$ mice. R.E= Relative expression, A.U.= Arbitrary Units.

Increased interstitial fibrosis is a characteristic phenotype in diabetic cardiomyopathy, particularly type 2 diabetic cardiomyopathy, and has been proposed to be responsible for the diastolic dysfunction observed in this condition [3, 5]. We asked if the diastolic dysfunction in *Ins2*$^{WT/C96Y}$ mice was associated with myocardial fibrosis. We assessed myocardial fibrosis using trichrome staining and light microscopy and found no evidence of increased interstitial or perivascular fibrotic tissue in *Ins2*$^{WT/C96Y}$hearts (**Fig. 3.6A**). We further confirmed the lack of fibrosis by demonstrating that mRNA expression of the extracellular matrix proteins, pro-collagen α type-I, pro-collagen α type-III and fibronectin were unaltered in *Ins2*$^{WT/C96Y}$compared to *Ins2*$^{WT/WT}$ mice at 3 months or 6 months of age (**Figs. 3.6B-D**). These results collectively indicate that insulin deficiency, characteristic of type 1 diabetes, limits myocardial growth due to attenuated insulin-dependent signaling without increased interstitial fibrosis.

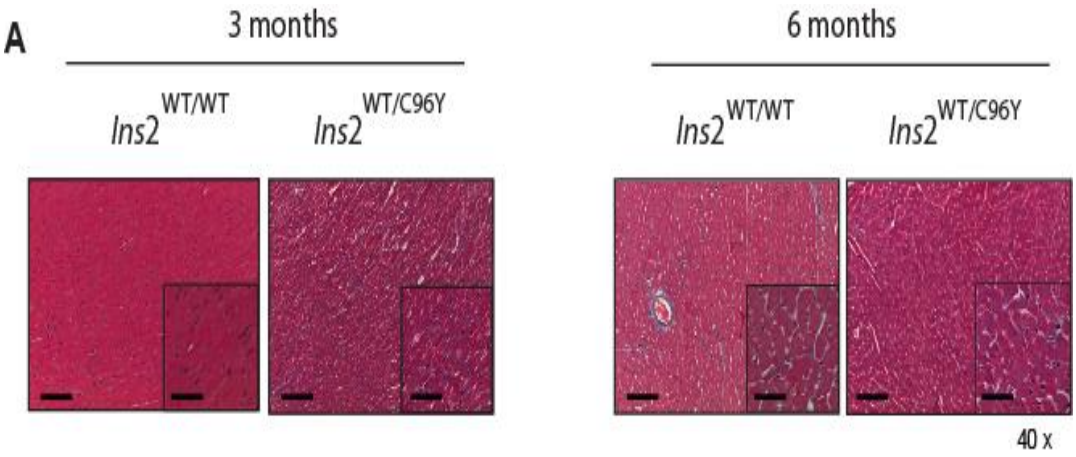

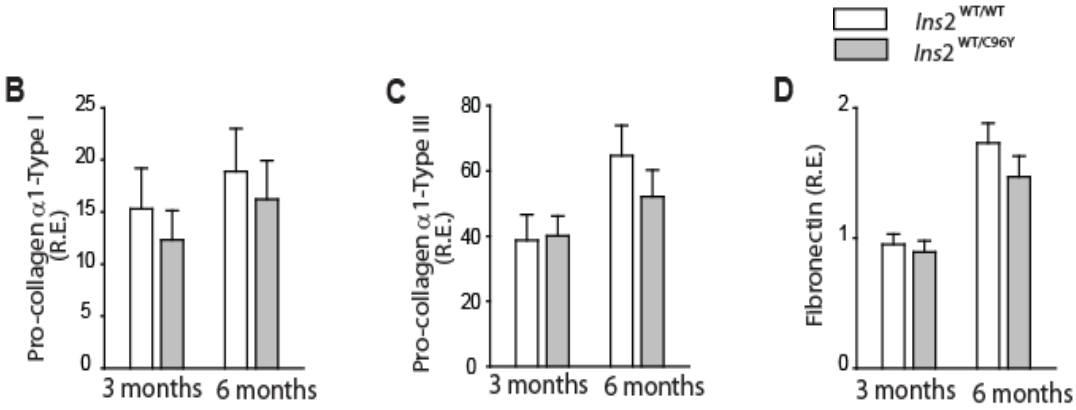

Figure 3.6 Absence of interstitial fibrosis in 3 and 6 month old *Ins2*$^{WT/C96Y}$ mice.

A: Trichrome staining shows normal myocardial architecture with no accumulation of fibrotic tissue, Scale bar=100μm (inset=50μm). *B-D:* mRNA expression levels of pro-collagen α1-type-I, pro-collagen α1-type-III, and fibronectin were comparable between *Ins2*$^{WT/C96Y}$ and *Ins2*$^{WT/WT}$ hearts (n=6/group). R.E= Relative expression.

3.5.3 Reduced SERCA2a, Metabolic Perturbation and Myocardial Lipotoxicity as Potential Mechanisms for Diastolic Dysfunction in *Ins2*$^{WT/C96Y}$ Mice

In determining the molecular cause of diastolic dysfunction in *Ins2*$^{WT/C96Y}$ mice, we examined the mechanisms that have been linked to diastolic cardiomyopathy. Downregulation of SERCA2a, the major myocardial sarcoplasmic reticulum Ca^{2+} pump, is one of the molecular alterations that has been linked to diastolic dysfunction in diabetic cardiomyopathy [3, 5, 11, 20]. Phospholamban is a negative regulator of SERCA2a, whose inhibitory function is blocked upon phosphorylation [21]. To determine if this system is altered in *Ins2*$^{WT/C96Y}$ hearts, we assayed for the phosphorylated- and total phospholamban, and SERCA2a protein levels. Our results demonstrate that in *Ins2*$^{WT/C96Y}$ mice protein levels of phospholamban and its phosphorylated form did not change (**Fig. 3.7A**), while SERCA2a showed an early and marked downregulation (**Fig. 3.7B**).

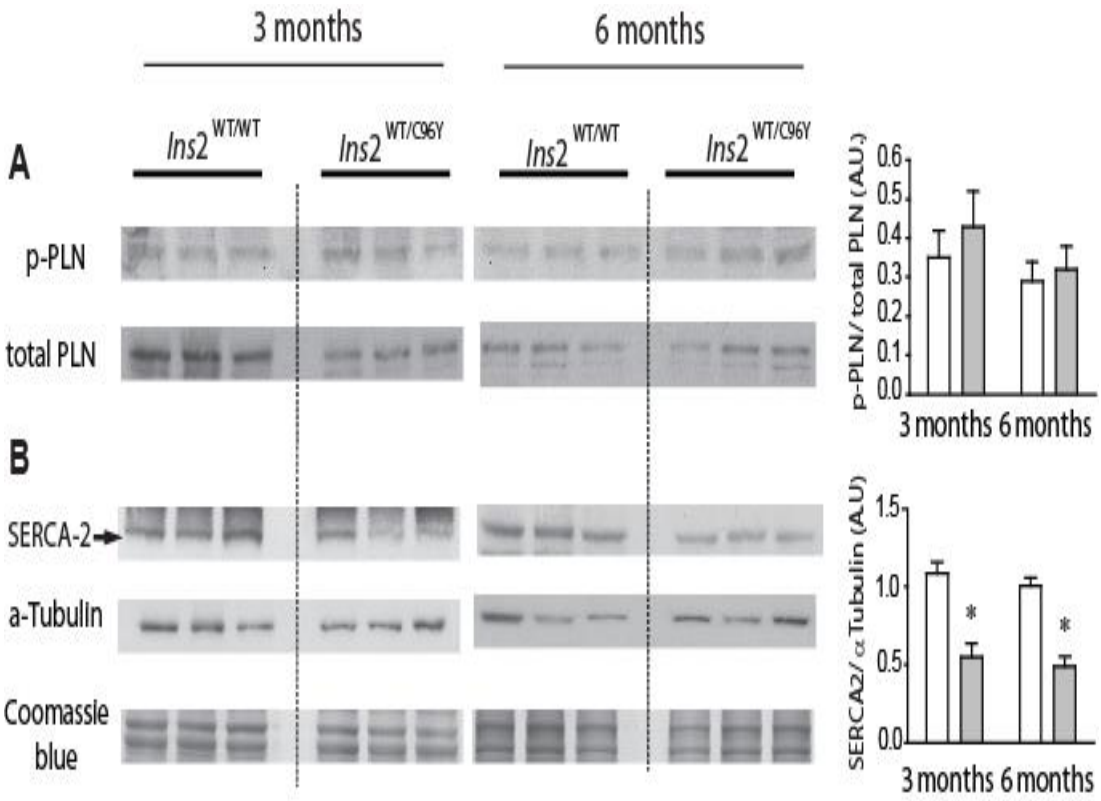

Figure 3.7 Downregulation of SERCA2a protein expression at 3 and 6 month old *Ins2*$^{WT/C96Y}$ mice.

A-B: Representative western blots are shown on the left and the corresponding quantifications are shown on the right. Phospho (serine16)-phospholamban (p-PLN)/total-phospholamban (total-PLN) ratio was comparable between the groups *(A)*, whereas SERCA2a protein levels decreased significantly in *Ins2*$^{WT/C96Y}$ hearts *(B)*. Alpha-tubulin and Coomasie blue staining were used as loading controls (n=6/group); *p<0.05 compared with *Ins2*$^{WT/WT}$ mice. A.U. = Arbitrary Units.

Altered fatty acid metabolism and lipotoxity have emerged as a unique and important mechanism by which enhanced fatty acid metabolism can generate toxic effects in the heart and lead to diastolic dysfunction [3, 11, 22, 23]. We hypothesized that myocardial fatty acid and triacylglycerol levels would be elevated in the insulin-deficient *Ins2*$^{WT/C96Y}$ hearts. Consistent with our hypothesis, myocardial levels of the major long-chain fatty acids, palmitoyl CoA, oleoyl CoA and steroyl CoA (**Fig. 3.8A**) were at least doubled in *Ins2*$^{WT/C96Y}$ mice at 3 months

of age in association with increased myocardial triacylglycerol levels (**Fig. 3.8B**). Altered cardiac fatty acid metabolism in diabetic states often correlates with changes in the expression of various key metabolic genes involved in the control of fatty acid metabolism including pyruvate dehydrogenase kinase (PDK) and the acyl-CoA dehydrogenase systems [22, 24-26]. While the expression of the medium-chain acyl-CoA dehydrogenase (MCAD) was unchanged (**Fig. 3.8C**), long-chain acyl-CoA dehydrogenase (LCAD) was significantly elevated in 6 months old *Ins2*$^{WT/C96Y}$ hearts (**Fig. 3.8D**). In addition, expression analysis showed no alteration in levels of PDK2 (**Fig. 3.8E**), but a marked early and persistent increase in mRNA levels of PDK4 (**Fig. 3.8F**) as well as in PDK4 protein levels (**Fig. 3.8G**) in *Ins2*$^{WT/C96Y}$ compared to *Ins2*$^{WT/WT}$ myocardium. These results show that *Ins2*$^{WT/C96Y}$ hearts have increased levels of long-chain fatty acids and triacylglycerol in association with increased expression of PDK4 and LCAD, providing evidence for altered fatty acid metabolism in *Ins2*$^{WT/C96Y}$ hearts.

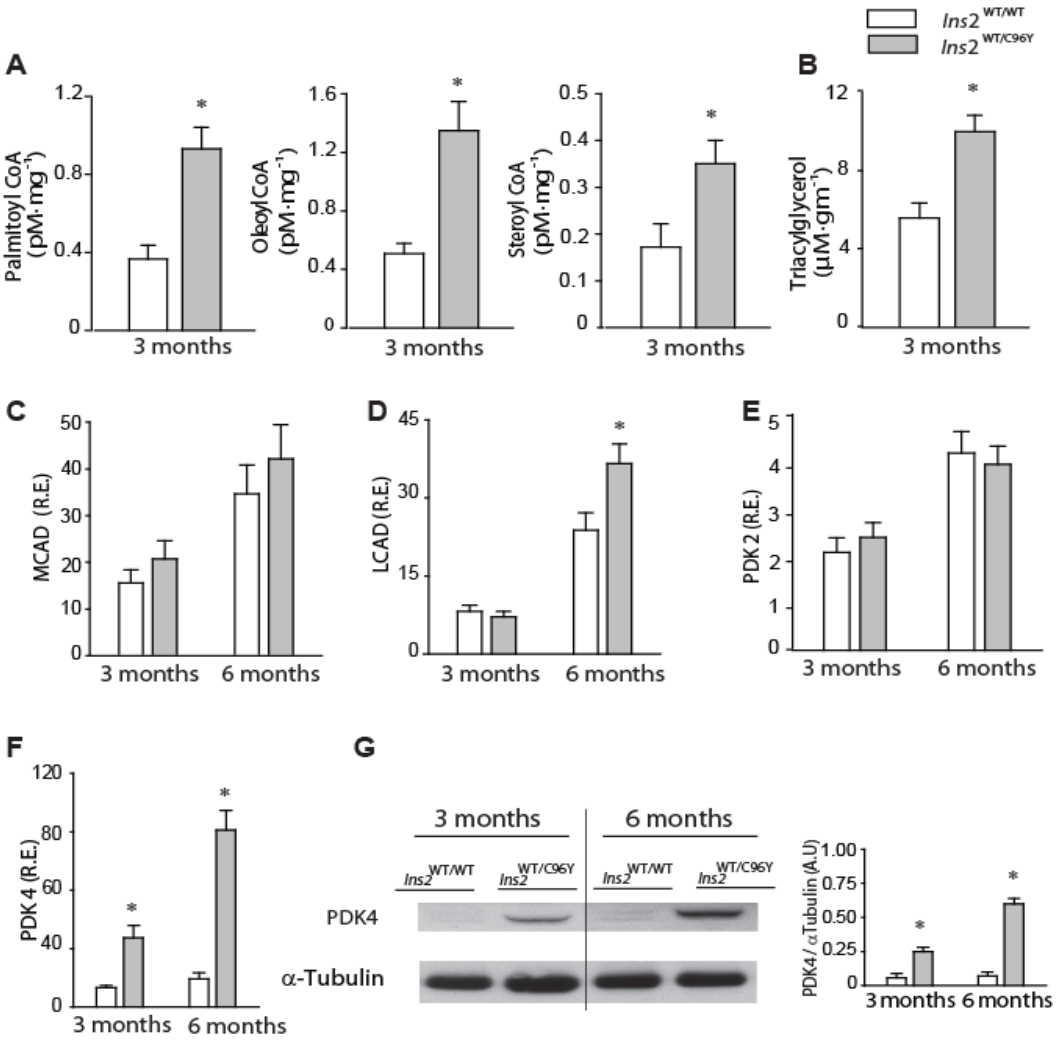

Figure 3.8 Altered fatty acid contents and metabolic gene expression in *Ins2*$^{WT/C96Y}$ hearts.

Ins2$^{WT/C96Y}$ myocardial tissue exhibit significantly elevated levels of long-chain fatty acids (palmitoyl CoA, oleoyl CoA and steroyl CoA) *(A)* and triacylglycerol *(B)* at 3 months of age (n=8/ group). *C-F:* Expression profile of mitochondrial medium-chain acyl-CoA dehydrogenase (MCAD), long-chain acyl-CoA dehydrogenase (LCAD), pyruvate dehydrogenase kinase 2 (PDK2) and pyruvate dehydrogenase kinase 4 (PDK4) by Taqman realtime RT-PCR analysis at 3 months and 6 months of age (n=6/group). *G:* Representative western blot and quantification of PDK4 protein levels at 3 and 6 months of age (n=4/group). *p<0.05 compared with *Ins2*$^{WT/WT}$ mice. R.E= Relative expression, A.U.= Arbitrary Units.

In order to determine if fatty acid metabolism was altered in *Ins2*$^{WT/C96Y}$ mice, we measured palmitate and glucose oxidation in the isolated working heart preparation. While glucose oxidation was not significantly different between the

two genotypes (**Fig. 3.9A**), palmitate oxidation was significantly increased in *Ins2*$^{WT/C96Y}$ compared to *Ins2*$^{WT/WT}$ hearts (**Fig. 3.9B**). We also found that expression of fatty acid transporters, FATP and CD36, were significantly elevated in *Ins2*$^{WT/C96Y}$ hearts (**Figs. 3.9C and 3.9D**). Increased ceramide and diacylglycerol (DAG) are markers of myocardial lipotoxicity [3, 27-30]. We found that myocardial ceramide and DAG levels are elevated in the myocardial tissue of *Ins2*$^{WT/C96Y}$ compared to *Ins2*$^{WT/WT}$ mice at 3 months of age (**Figs. 3.9C and 3.9D**). In addition, Oil-O red staining of the hearts showed presence of lipid droplets in the myocardium of *Ins2*$^{WT/C96Y}$ mice at 3months of age which became stronger and more prevalent by 6 months of age compared to the control *Ins2*$^{WT/WT}$ hearts (**Fig. 3.9E**).

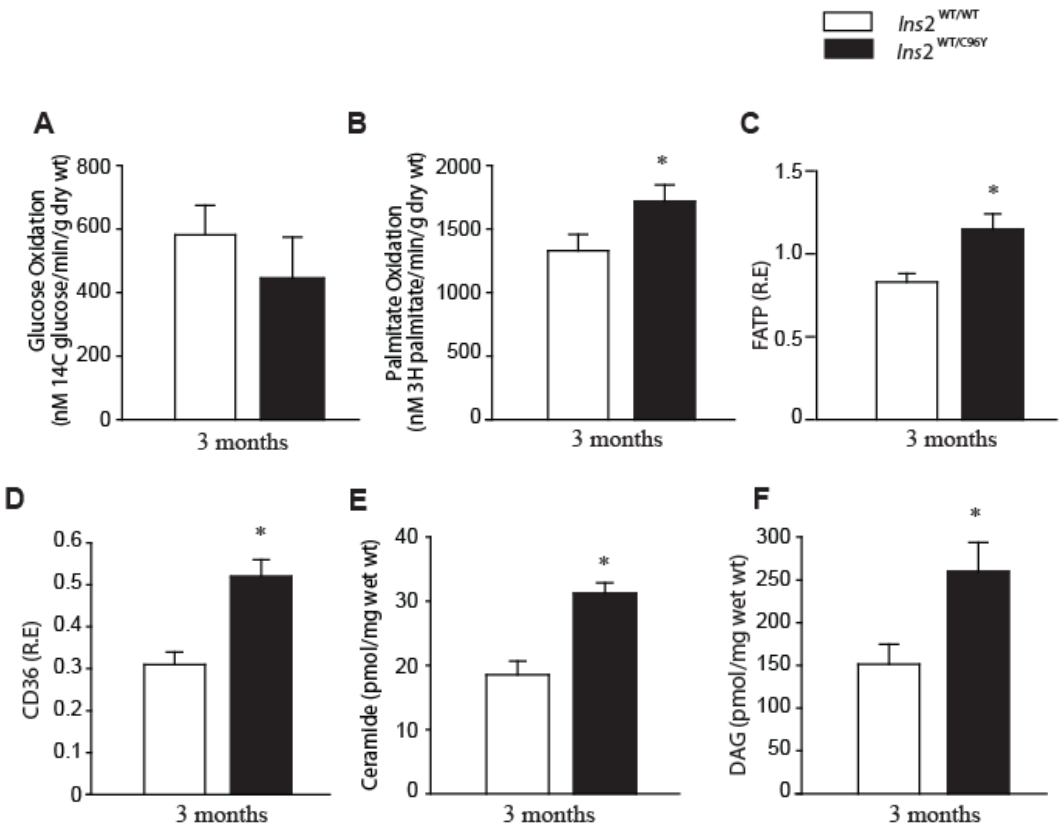

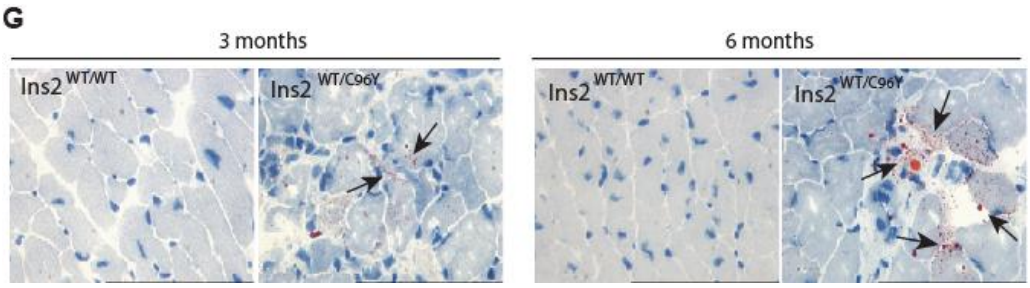

Figure 3.9 Evidence of lipotoxicity in *Ins2*$^{WT/C96Y}$ hearts.
A-B: Glucose oxidation and palmitate oxidation measured in isolated working hearts at 3 months of age (n=6/group). *C-D:* Expression of fatty acid transporter protein (FATP) and CD36 are elevated in *Ins2*$^{WT/C96Y}$ hearts. *E-F*: Ceramide and diacylglycerol (DAG) levels in the myocardium at 3 months of age (n=5/group). *G:* Oil-O red staining shows lipid deposits in *Ins2*$^{WT/C96Y}$ myocardium at 3months which intensifies by 6 months of age. Scale=100μm. R.E= Relative expression.

3.5.4 Diastolic cardiomyopathy in *Ins2*$^{WT/C96Y}$ mice reversed by insulin replacement therapy

Insulin replacement in 8-wk old *Ins2*$^{WT/C96Y}$ mice lead to a prompt and sustained normalization of the marked hyperglycemia over the ensuing 4-week period of implantation (**Fig. 8A**). At 3 months of age, we found a significant reduction in disease markers, BNP and βMHC, in insulin-treated *Ins2*$^{WT/C96Y}$ hearts to levels comparable to *Ins2*$^{WT/WT}$ hearts (**Fig. 8B**). Importantly, insulin replacement in *Ins2*$^{WT/C96Y}$ mice completely abolished the diastolic dysfunction in these mice as evident by the restoration of IVRT and DT, increased early TDI diastolic myocardial velocity (E') while improving the deceleration rate (EWDR) and A-wave reversal (**Figs. 8C-8F**). Consistent with a lack of diastolic dysfunction in insulin-treated *Ins2*$^{WT/C96Y}$ mice, SERCA2a protein levels were restored (**Fig. 8G**), while ceramide and DAG levels were reduced to levels seen in *Ins2*$^{WT/WT}$ myocardium (**Fig. 8H**) suggesting abolition of lipotoxicity.

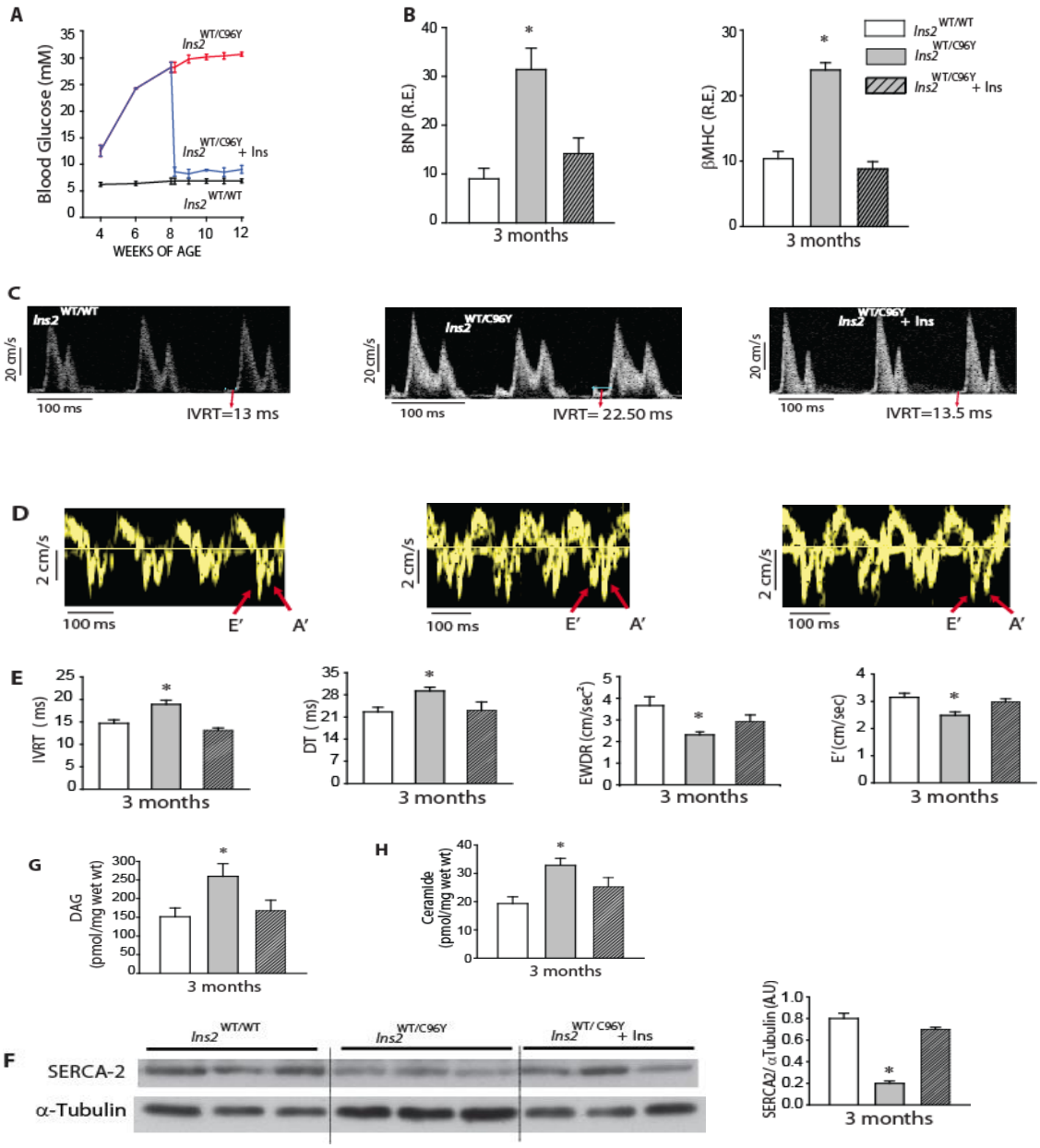

Figure 3.10 Diastolic cardiomyopathy in *Ins2*$^{WT/C96Y}$ mice is reversed following insulin-treatment.

Diastolic cardiomyopathy in *Ins2*$^{WT/C96Y}$ mice is reversed following insulin-treatment. *A-B:* Random plasma glucose *(A)*, expression of disease markers, BNP and β-MHC *(B)* in *Ins2*$^{WT/WT}$, *Ins2*$^{WT/C96Y}$ and insulin-treated *Ins2*$^{WT/C96Y}$ (+Ins) mice. *C-F:* Echocardiographic imaging showing representative transmitral Doppler flow profile (C), pulmonary venous flow (D) and tissue Doppler images (E), as well as averaged isovolumetric relaxation time (IVRT), deceleration time (DT), E-wave deceleration rate (EWDR), and tissue Doppler velocity (E') (F) in *Ins2*$^{WT/WT}$, *Ins2*$^{WT/C96Y}$ and insulin-treated *Ins2*$^{WT/C96Y}$ (+Ins) mice. *G-H:* Representative western blot and quantification of SERCA2a protein levels (G), myocardial diacylglycerol (DAG) (H) and ceramide levels (I) in *Ins2*$^{WT/WT}$, *Ins2*$^{WT/C96Y}$ and insulin-treated *Ins2*$^{WT/C96Y}$ (+Ins) mice. n=5/group, *p<0.05 compared to all other groups, R.E.=Relative Expression, A.U.= Arbitrary Units.

3.6 DISCUSSION

The *Ins2*$^{WT/C96Y}$ (Akita) mice harbor a mutation in insulin 2 gene (*Ins2*; Cys96Tyr) that results in a disruption of an intramolecular disulfide bond [12]. This affects folding of pro-insulin in the endoplasmic reticulum leading to endoplasmic reticulum stress, proteotoxicity in pancreatic β-cells and cell loss [13, 31, 32]**.** The *Ins2*$^{WT/C96Y}$ mouse provides an ideal non-obese model of type 1 diabetes that is based on a mutation described in human diabetes while being free of potential confounding effects of streptozotocin (STZ)-induced type 1 diabetes [12, 13]. Moreover, *Ins2*$^{WT/C96Y}$ mice have several advantages over inbred mouse strains that require streptozotocin treatment including a better-defined etiology, along with a more pronounced and durable hyperglycemia[3, 33]. Our study is the first to show that the predominant cardiac phenotypic abnormality in *Ins2*$^{WT/C96Y}$ mice is an early diastolic dysfunction in the absence of a systolic dysfunction. We evaluated the systolic function in *Ins2*$^{WT/C96Y}$ mice by echocardiography including tissue Doppler imaging, *in vivo* hemodynamic measurements and *ex vivo* working heart preparation, and consistent with previous studies[34], we found it to be comparable to control *Ins2*$^{WT/WT}$ mice at 3- and 6-months of age. We captured and characterized the diastolic dysfunction using a state-of-the art echocardiographic technique including tissue Doppler imaging in combination with invasive hemodynamic assessment. Our data illustrates the typical pattern of elevated LV filling pressures and/or impaired relaxation. Based on our hemodynamic measurements, -dP/dt$_{min}$,tau (relaxation time constant of LV pressure) and LVEDP

were depressed, prolonged and increased, respectively, which are all consistent with diastolic dysfunction in the *Ins2*$^{WT/C96Y}$ mice. Using tissue Doppler imaging, we have shown that the early diastolic myocardial velocity (E'), a sensitive and early marker of diastolic dysfunction[2, 35, 36], is reduced in the Akita model. The increased amplitude of the A-wave reversal in *Ins2*$^{WT/C96Y}$ mice may reflect the elevated LV filling pressure ultimately leading to LA enlargement in these mice. However, E/A ratio was not decreased in the 3-month old *Ins2*$^{WT/C96Y}$ mice which may reflect altered loading conditions due to the hyperglycemia and accompanying osmotic diuresis [33] leading to subtle changes in preload interacting with the effects of isoflurane on the cardiovascular system. In addition, *Ins2*$^{WT/C96Y}$ hearts showed no hypertrophy but with elevated BNP and βMHC levels. BNP is a disease marker for cardiomyopathy which has been reported to be elevated in patients with diastolic heart failure[37]. The smaller heart size in *Ins2*$^{WT/C96Y}$ mice is consistent with the a previous report in mice lacking cardiac-specific insulin receptor (CIRKO) which showed a similar decrease in heart size with persistent expression of βMHC [38], further supporting the role of insulin in physiological cardiac growth. Diastolic heart failure is now a well-recognized clinical entity often associated with hypertension and diabetes and can lead to marked morbidity and mortality[2, 7-9]. As such, the *Ins2*$^{WT/C96Y}$ diabetic murine model represents a clinically-relevant non-obese model of diastolic dysfunction without the confounding effects of systolic dysfunction.

Insulin is a tyrosine receptor kinase agonist triggering Erk1/2 and Akt/PKB signaling pathways in the heart[17, 18]. The genetic defect in *Ins2*$^{WT/C96Y}$ mice results in an early and sustained loss of the insulin-producing β-cells and low plasma insulin levels[13, 19]. We found that phosphorylation of ERK and Akt were suppressed in *Ins2*$^{WT/C96Y}$ hearts. We found that the changes in phosphorylation of ERK showed a bimodal pattern with a rise at 6 months. This bimodal change in pErk1/2 could be due to a number of factors. The initial decrease in ERK1/2 phosphorylation could be due to insulin-deficiency and/or hyperglycermia, while its subsequent rise could be due to progression of disease in the Akita mice, with activation of neurohumoral systems leading to increased stimulation of G-protein-coupled receptors and/or changes in biomechanical stress such as an increase in blood pressure. It has been reported that insulin-stimulated phosphorylation of serine 473-Akt is intact in *ex vivo Ins2*$^{WT/C96Y}$ hearts[34]. As such, the loss of myocardial Erk1/2 and Akt phosphorylation in *Ins2*$^{WT/C96Y}$ mice that we observed is primarily driven by reduced activation of insulin receptors secondary to insulin deficiency. The lack of a reduction in serine-473 and threonine-308 phosphorylation of Akt/PKB in *Ins2*$^{WT/C96Y}$ hearts at 3 months of age may reflect compensatory changes by other agonists such as insulin-like growth factor-1 (IGF-1) and/or adiponectin which are known to activate the Akt/PKB pathway [18, 39].

Diastolic dysfunction has been linked to increased interstitial fibrosis, SERCA2 downregulation and/or lipotoxicity affecting stiffness as well as active relaxation

of the ventricle [9, 10]. Myocardial fibrosis in diabetic hearts has been shown to be triggered by oxidative stress [40] and we found that *Ins2*$^{WT/C96Y}$ hearts exhibited no myocardial fibrosis, consistent with a lack of oxidative stress in these hearts [34]. SERCA2 levels were significantly reduced in *Ins2*$^{WT/C96Y}$ hearts, which could result in prolonged Ca^{2+} transient decay leading to delayed relaxation and subsequently diastolic dysfunction. We also found that expression of β-MHC was increased in the left ventricle of *Ins2*$^{WT/C96Y}$ mice at 3 and 6 months of age and the slower rate of ATP hydrolysis and cross-bridge cycling of β-MHC may also contribute to the diastolic dysfunction in the *Ins2*$^{WT/C96Y}$ mice. Recently, Flagg *et al.* elegantly showed that diastolic dysfunction in a mouse model of lipotoxic diabetic cardiomyopathy with cardiac specific overexpression of fatty acid transporter protein (FATP), is due to suppressed myofilament function rather than altered Ca^{2+} cycling[11]. Interestingly, these authors also observed elevated βMHC levels and decreased SERCA2 protein levels with diastolic dysfunction and preserved systolic function. In our model, other proteins involved in Ca^{2+} handling such as, Na^{+}/Ca^{2+} exchanger may also be altered as previously reported in diabetic cardiomyopathy[3]. However, the lack of systolic dysfunction despite reduced SERCA2a and elevated βMHC could be due to alterations in the properties of the $Ca^{2+/}$myofilament interaction leading to diastolic dysfunction[11, 41].

Under physiological conditions, the heart derives energy from glucose, fatty acids, and/or lactate depending upon substrate availability, circulating hormone levels, and nutritional status. We found that in *Ins2*$^{WT/C96Y}$ hearts, there is increased fatty

acid utilization consistent with previous reports[34]. Myocardial mRNA expression levels of medium chain acyl-CoA dehydrogenases (MCAD) was unchanged while the expression of long chain acyl-CoA dehydrogenase (LCAD) was significantly increased which is consistent with findings in the type 1 non-obese diabetic (NOD) mouse model [25]. Increased myocardial expression of long chain acyl-CoA synthase is sufficient to predispose the heart to lipotoxic cardiomyopathy[42]. Impaired pyruvate oxidation is a hallmark of the metabolic defect found in the diabetic heart including the *Ins2*$^{WT/C96Y}$ hearts[22, 34]. Pyruvate decarboxylation is a key irreversible step in carbohydrate oxidation mediated by pyruvate dehydrogenase (PDH) which is negatively regulated by PDH kinase (PDK)-induced phosphorylation [22, 24, 43]. The increase in PDK4 levels in *Ins2*$^{WT/C96Y}$ hearts is consistent with insulin acting as a negative regulator of PDK4[24, 43] and correlates with increased fatty acid oxidation in the *Ins2*$^{WT/C96Y}$ mice. Lipotoxicity may arise from myocardial triacylglycerol accumulation, increased use of long-chain fatty acids and increased production of ceramide and DAG, important markers of lipotoxicity in the heart [3, 27-29, 42, 44]. Indeed, we have shown that palmitate oxidation as well as myocardial levels of fatty acids, triacylglycerol, ceramide and diacylglycerol were all significantly increased in *Ins2*$^{WT/C96Y}$ compared to *Ins2*$^{WT/WT}$ hearts. In addition, we found lipid deposits in the *Ins2*$^{WT/C96Y}$ myocardium, as also reported by others using electron microscopy[34], consistent with lipotoxic cardiomyopathy in *Ins2*$^{WT/C96Y}$ hearts. The plasma triglycerol and free fatty acids in *Ins2*$^{WT/C96Y}$ mice have been shown to be lower

and similar to WT mice, respectively[45]. We observed increased expression of two key molecules, namely CD36 and FATP, involved in fatty acid uptake and cardiac lipotoxicity[11, 46] suggesting that increased uptake of fatty acids rather than increased delivery may have also contributed to the cardiac lipotoxicity observed in the *Ins2*$^{WT/C96Y}$ diabetic model.

In this study we show that in a mouse model of non-obese type 1 diabetes, cardiomyopathy is characterized by early diastolic dysfunction in the absence of systolic dysfunction. This cardiomyopathy is associated with elevated levels of disease markers, but lacks myocardial hypertrophy or fibrosis. We propose that the diastolic dysfunction in *Ins2*$^{WT/C96Y}$ mice could be brought about by a number of factors including elevated levels of β-MHC isoform and reduced SERCA2a levels leading to the observed prolonged relaxation of the LV. Additionally, the elevated levels of fatty acids, triglycerol, ceramides, diacylglycerol as well as lipid depositions in the *Ins2*$^{WT/C96Y}$ hearts strongly suggest myocardial lipotoxicity as a possible mechanism of the diastolic dysfunction in *Ins2*$^{WT/C96Y}$ mice. *Ins2*$^{WT/C96Y}$ mice develop secondary peripheral and hepatic insulin resistance[45]. In response to insulin treatment, we showed that in *Ins2*$^{WT/C96Y}$ mice hyperglycemia and lipotoxicity were normalized in association with reversal of the diastolic dysfunction and restoration of SERCA2a, BNP and βMHC levels similar to *Ins2*$^{WT/WT}$ mice. Hence, the diastolic dysfunction seen in this type I diabetic mouse model is plastic and reversible. The use of insulin therapy and improved

glycemic control is of critical importance in minimizing diabetes-induced cardiomyopathy.

3.7 CONCLUSION

We conclude that early type 1 diabetic cardiomyopathy is characterized by diastolic dysfunction related to a lipotoxicity cardiomyopathy and perhaps impaired diastolic Ca^{2+} transient due to SERCA2a downregulation, in the absence of interstitial fibrosis and hypertrophy.

3.8 REFERENCES

1. Roglic G, Unwin N, Bennett PH, Mathers C, Tuomilehto J, Nag S, Connolly V, King H. The burden of mortality attributable to diabetes: Realistic estimates for the year 2000. *Diabetes Care*. 2005;28:2130-2135

2. Paulus WJ, Tschope C, Sanderson JE, Rusconi C, Flachskampf FA, Rademakers FE, Marino P, Smiseth OA, De Keulenaer G, Leite-Moreira AF, Borbely A, Edes I, Handoko ML, Heymans S, Pezzali N, Pieske B, Dickstein K, Fraser AG, Brutsaert DL. How to diagnose diastolic heart failure: A consensus statement on the diagnosis of heart failure with normal left ventricular ejection fraction by the heart failure and echocardiography associations of the european society of cardiology. *Eur Heart J*. 2007;28:2539-2550

3. Boudina S, Abel ED. Diabetic cardiomyopathy revisited. *Circulation*. 2007;115:3213-3223

4. Ruddy TD, Shumak SL, Liu PP, Barnie A, Seawright SJ, McLaughlin PR, Zinman B. The relationship of cardiac diastolic dysfunction to concurrent hormonal and metabolic status in type i diabetes mellitus. *J Clin Endocrinol Metab*. 1988;66:113-118

5. Poornima IG, Parikh P, Shannon RP. Diabetic cardiomyopathy: The search for a unifying hypothesis. *Circ Res*. 2006;98:596-605

6. Zimmet P, Alberti KG, Shaw J. Global and societal implications of the diabetes epidemic. *Nature*. 2001;414:782-787

7. Ouzounian M, Lee DS, Liu PP. Diastolic heart failure: Mechanisms and controversies. *Nat Clin Pract Cardiovasc Med*. 2008;5:375-386

8. Lam CS, Roger VL, Rodeheffer RJ, Bursi F, Borlaug BA, Ommen SR, Kass DA, Redfield MM. Cardiac structure and ventricular-vascular function in persons with heart failure and preserved ejection fraction from olmsted county, minnesota. *Circulation*. 2007;115:1982-1990

9. van Heerebeek L, Hamdani N, Handoko ML, Falcao-Pires I, Musters RJ, Kupreishvili K, Ijsselmuiden AJ, Schalkwijk CG, Bronzwaer JG, Diamant M, Borbely A, van der Velden J, Stienen GJ, Laarman GJ, Niessen HW, Paulus WJ. Diastolic stiffness of the failing diabetic heart: Importance of fibrosis, advanced glycation end products, and myocyte resting tension. *Circulation*. 2008;117:43-51

10. Asbun J, Villarreal FJ. The pathogenesis of myocardial fibrosis in the setting of diabetic cardiomyopathy. *J Am Coll Cardiol*. 2006;47:693-700

11. Flagg TP, Cazorla O, Remedi MS, Haim TE, Tones MA, Bahinski A, Numann RE, Kovacs A, Schaffer JE, Nichols CG, Nerbonne JM. Ca2+-independent alterations in diastolic sarcomere length and relaxation kinetics in a mouse model of lipotoxic diabetic cardiomyopathy. *Circ Res*. 2009;104:95-103

12. Wang J, Takeuchi T, Tanaka S, Kubo SK, Kayo T, Lu D, Takata K, Koizumi A, Izumi T. A mutation in the insulin 2 gene induces diabetes with severe pancreatic beta-cell dysfunction in the mody mouse. *J Clin Invest*. 1999;103:27-37

13. Hsueh W, Abel ED, Breslow JL, Maeda N, Davis RC, Fisher EA, Dansky H, McClain DA, McIndoe R, Wassef MK, Rabadan-Diehl C, Goldberg IJ. Recipes for creating animal models of diabetic cardiovascular disease. *Circ Res*. 2007;100:1415-1427

14. Masserdotti C, Bonfanti U, De Lorenzi D, Ottolini N. Use of oil red o stain in the cytologic diagnosis of canine liposarcoma. *Vet Clin Pathol*. 2006;35:37-41

15. Spevack DM, Blum L, Malhotra D, Nazari R, Ostfeld RJ, Doddamani S, Bello R, Cohen HW, Sonnenblick EH. Ratio of left atrial to left ventricular size: An anatomical marker of the diastolic left ventricular pressure-volume relationship. *Echocardiography*. 2008;25:366-373

16. Oudit GY, Sun H, Kerfant BG, Crackower MA, Penninger JM, Backx PH. The role of phosphoinositide-3 kinase and pten in cardiovascular physiology and disease. *J Mol Cell Cardiol*. 2004;37:449-471

17. Bertrand L, Horman S, Beauloye C, Vanoverschelde JL. Insulin signalling in the heart. *Cardiovasc Res*. 2008;79:238-248

18. Oudit GY, Penninger JM. Cardiac regulation by phosphoinositide 3-kinases and pten. *Cardiovasc Res*. 2009;82:250-260

19. Yoshioka M, Kayo T, Ikeda T, Koizumi A. A novel locus, mody4, distal to d7mit189 on chromosome 7 determines early-onset niddm in nonobese c57bl/6 (akita) mutant mice. *Diabetes*. 1997;46:887-894

20. Vetter R, Rehfeld U, Reissfelder C, Weiss W, Wagner KD, Gunther J, Hammes A, Tschope C, Dillmann W, Paul M. Transgenic overexpression of the sarcoplasmic reticulum ca2+atpase improves reticular ca2+ handling in normal and diabetic rat hearts. *FASEB J*. 2002;16:1657-1659

21. MacLennan DH, Kranias EG. Phospholamban: A crucial regulator of cardiac contractility. *Nat Rev Mol Cell Biol*. 2003;4:566-577

22. Stanley WC, Lopaschuk GD, McCormack JG. Regulation of energy substrate metabolism in the diabetic heart. *Cardiovasc Res*. 1997;34:25-33

23. Chiu HC, Kovacs A, Blanton RM, Han X, Courtois M, Weinheimer CJ, Yamada KA, Brunet S, Xu H, Nerbonne JM, Welch MJ, Fettig NM, Sharp TL, Sambandam N, Olson KM, Ory DS, Schaffer JE. Transgenic expression of fatty acid transport protein 1 in the heart causes lipotoxic cardiomyopathy. *Circ Res*. 2005;96:225-233

24. Majer M, Popov KM, Harris RA, Bogardus C, Prochazka M. Insulin downregulates pyruvate dehydrogenase kinase (pdk) mrna: Potential mechanism contributing to increased lipid oxidation in insulin-resistant subjects. *Molecular genetics and metabolism*. 1998;65:181-186

25. Kurtz DM, Tian L, Gower BA, Nagy TR, Pinkert CA, Wood PA. Transgenic studies of fatty acid oxidation gene expression in nonobese diabetic mice. *J Lipid Res*. 2000;41:2063-2070

26. Cornelius LA, Nehring LC, Harding E, Bolanowski M, Welgus HG, Kobayashi DK, Pierce RA, Shapiro SD. Matrix metalloproteinases generate angiostatin: Effects on neovascularization. *J Immunol*. 1998;161:6845-6852

27. Park TS, Hu Y, Noh HL, Drosatos K, Okajima K, Buchanan J, Tuinei J, Homma S, Jiang XC, Abel ED, Goldberg IJ. Ceramide is a cardiotoxin in lipotoxic cardiomyopathy. *J Lipid Res*. 2008;49:2101-2112

28. Griffin ME, Marcucci MJ, Cline GW, Bell K, Barucci N, Lee D, Goodyear LJ, Kraegen EW, White MF, Shulman GI. Free fatty acid-induced insulin resistance is associated with activation of protein kinase c theta and alterations in the insulin signaling cascade. *Diabetes*. 1999;48:1270-1274

29. Xia P, Inoguchi T, Kern TS, Engerman RL, Oates PJ, King GL. Characterization of the mechanism for the chronic activation of diacylglycerol-protein kinase c pathway in diabetes and hypergalactosemia. *Diabetes*. 1994;43:1122-1129

30. Avignon A, Yamada K, Zhou X, Spencer B, Cardona O, Saba-Siddique S, Galloway L, Standaert ML, Farese RV. Chronic activation of protein kinase c in soleus muscles and other tissues of insulin-resistant type ii diabetic goto-kakizaki (gk), obese/aged, and obese/zucker rats. A

mechanism for inhibiting glycogen synthesis. *Diabetes*. 1996;45:1396-1404

31. Nozaki J, Kubota H, Yoshida H, Naitoh M, Goji J, Yoshinaga T, Mori K, Koizumi A, Nagata K. The endoplasmic reticulum stress response is stimulated through the continuous activation of transcription factors atf6 and xbp1 in ins2+/akita pancreatic beta cells. *Genes Cells*. 2004;9:261-270

32. Yoshinaga T, Nakatome K, Nozaki J, Naitoh M, Hoseki J, Kubota H, Nagata K, Koizumi A. Proinsulin lacking the a7-b7 disulfide bond, ins2akita, tends to aggregate due to the exposed hydrophobic surface. *Biol Chem*. 2005;386:1077-1085

33. Wong DW, Oudit GY, Reich H, Kassiri Z, Zhou J, Liu QC, Backx PH, Penninger JM, Herzenberg AM, Scholey JW. Loss of angiotensin-converting enzyme-2 (ace2) accelerates diabetic kidney injury. *Am J Pathol*. 2007;171:438-451

34. Bugger H, Boudina S, Hu XX, Tuinei J, Zaha VG, Theobald HA, Yun UJ, McQueen AP, Wayment B, Litwin SE, Abel ED. Type 1 diabetic akita mouse hearts are insulin sensitive but manifest structurally abnormal mitochondria that remain coupled despite increased uncoupling protein 3. *Diabetes*. 2008;57:2924-2932

35. Schaefer A, Klein G, Brand B, Lippolt P, Drexler H, Meyer GP. Evaluation of left ventricular diastolic function by pulsed doppler tissue imaging in mice. *J Am Soc Echocardiogr*. 2003;16:1144-1149

36. Yu CM, Sanderson JE, Marwick TH, Oh JK. Tissue doppler imaging a new prognosticator for cardiovascular diseases. *J Am Coll Cardiol*. 2007;49:1903-1914

37. Kitzman DW, Little WC, Brubaker PH, Anderson RT, Hundley WG, Marburger CT, Brosnihan B, Morgan TM, Stewart KP. Pathophysiological characterization of isolated diastolic heart failure in comparison to systolic heart failure. *JAMA : the journal of the American Medical Association*. 2002;288:2144-2150

38. Belke DD, Betuing S, Tuttle MJ, Graveleau C, Young ME, Pham M, Zhang D, Cooksey RC, McClain DA, Litwin SE, Taegtmeyer H, Severson D, Kahn CR, Abel ED. Insulin signaling coordinately regulates cardiac size, metabolism, and contractile protein isoform expression. *J Clin Invest*. 2002;109:629-639

39. Leth H, Andersen KK, Frystyk J, Tarnow L, Rossing P, Parving HH, Flyvbjerg A. Elevated levels of high-molecular-weight adiponectin in type

1 diabetes. *The Journal of clinical endocrinology and metabolism*. 2008;93:3186-3191

40. Aragno M, Mastrocola R, Alloatti G, Vercellinatto I, Bardini P, Geuna S, Catalano MG, Danni O, Boccuzzi G. Oxidative stress triggers cardiac fibrosis in the heart of diabetic rats. *Endocrinology*. 2008;149:380-388

41. Abraham TP, Jones M, Kazmierczak K, Liang HY, Pinheiro AC, Wagg CS, Lopaschuk GD, Szczesna-Cordary D. Diastolic dysfunction in familial hypertrophic cardiomyopathy transgenic model mice. *Cardiovasc Res*. 2009;82:84-92

42. Chiu HC, Kovacs A, Ford DA, Hsu FF, Garcia R, Herrero P, Saffitz JE, Schaffer JE. A novel mouse model of lipotoxic cardiomyopathy. *J Clin Invest*. 2001;107:813-822

43. Wu P, Sato J, Zhao Y, Jaskiewicz J, Popov KM, Harris RA. Starvation and diabetes increase the amount of pyruvate dehydrogenase kinase isoenzyme 4 in rat heart. *Biochem J*. 1998;329 (Pt 1):197-201

44. Szczepaniak LS, Victor RG, Orci L, Unger RH. Forgotten but not gone: The rediscovery of fatty heart, the most common unrecognized disease in america. *Circ Res*. 2007;101:759-767

45. Hong EG, Jung DY, Ko HJ, Zhang Z, Ma Z, Jun JY, Kim JH, Sumner AD, Vary TC, Gardner TW, Bronson SK, Kim JK. Nonobese, insulin-deficient ins2akita mice develop type 2 diabetes phenotypes including insulin resistance and cardiac remodeling. *Am J Physiol Endocrinol Metab*. 2007;293:E1687-1696

46. Yang J, Sambandam N, Han X, Gross RW, Courtois M, Kovacs A, Febbraio M, Finck BN, Kelly DP. Cd36 deficiency rescues lipotoxic cardiomyopathy. *Circ Res*. 2007;100:1208-1217

CHAPTER FOUR

LOSS OF TIMP3 SELECTIVELY EXACERBATES DIABETIC NEPHROPATHY

Ratnadeep Basu[1,2], Jiwon Lee[1,2], Zuocheng Wang[2,3], Vaibhav B. Patel[2,3], Dong Fan[1,2], Subhash K. Das[2,3], George C. Liu[4], Rohan John[5], James W. Scholey[4], Gavin Y. Oudit[1,2,3] and Zamaneh Kassiri[1,2]

[1]Department of Physiology, [2]Mazankowski Alberta Heart Institute, [3]Division of Cardiology, Department of Medicine, University of Alberta, Edmonton, Canada; [4]Division of Nephrology, Department of Medicine, [5]Department of Laboratory Medicine and Pathobiology, University of Toronto

A modified version of this chapter has been published in *American Journal of Physiology Renal Physiology*, 2012 Nov 1; 303(9): F1341-F1352.

Author Contributions

Participated in Research Design: J.W.S., G.Y.O. and Z.K.
Conducted Experiments: R.B., J.L., Z.W., V.B.P., D.F., S.K.D., G. C. L., R.J. and J.W.S.
Performed Data Analysis: R.B., Z.W., G.Y.O. and Z.K.
Contributed to the Writing of the Manuscript: R.B., Z.W., G.Y.O. and Z.K.

4.1 ABSTRACT

Diabetic nephropathy is the most common cause of end-stage renal disease. Polymorphism in the TIMP3 gene, and ECM-bound inhibitor of metalloproteinases (MMPs), has been linked to diabetic nephropathy in humans. In order to elucidate the mechanism we generated double mutant mice in which the TIMP3 gene was deleted in the genetic diabetic Akita mouse background. The aggravation of diabetic injury occurred in the absence of worsening of hypertension or hyperglycemia. In fact, myocardial TIMP3 levels were not affected and cardiac diastolic and systolic function remained unchanged in the double mutant mice. However, TIMP3 levels increased in Akita kidneys and deletion of TIMP3 exacerbated the diabetic renal injury in the Akita mouse, characterized by increased albuminuria, mesangial matrix expansion and kidney hypertrophy. The progression of diabetic renal injury was accompanied by the upregulation of fibrotic and inflammatory markers, increased production of reactive oxygen species and NADPH oxidase activity, and elevated activity of TACE (TNF-alpha converting enzyme) in the TIMP3$^{-/-}$/Akita kidneys. Moreover, while the elevated phospho-Akt (S473 and T308) and phospho-ERK1/2 in the Akita mice was not detected in the TIMP3$^{-/-}$/Akita kidneys, PKCβ1 (but not PKCα) was markedly elevated in the double mutant kidneys. Our data provide definitive evidence for a critical and selective role of TIMP3 in diabetic renal injury consistent with gene expression findings from human diabetic kidneys.

4.2 INTRODUCTION

Diabetic nephropathy and cardiomyopathy are serious long-term complications of diabetes, accounting for approximately 40% of new cases of end-stage renal disease (ESRD) in the U.S.[1-3]. Polymorphisms in tissue inhibitor of metalloproteinase-3 (TIMP3) is associated with type I diabetic nephropathy [4] and TIMP3 is differentially expressed in human diabetic glomeruli [5]. TIMP3 is one of the four identified endogenous inhibitors of matrix metalloproteinases (MMPs). The dynamic physiological equilibrium between TIMPs and MMPs determines the extracellular matrix (ECM) integrity and the tissue microenvironment. TIMP3 is ECM-bound and the most highly expressed TIMP in the kidney [6], and is also known to inhibit the ADAM (a disintegrin and metalloproteinase domain) and ADAM-TS (A disintegrin and metalloproteinase with thrombospondin motifs, also known as aggrecanase) families which are proteases controlling the bioactivity of many growth factors and cytokines [7, 8]. Loss of TIMP3 in mice enhances susceptibility to cardiomyopathy [9] and interstitial nephritis and fibrosis[6]. Given the critical role of inflammation and MMP activation in diabetic nephropathy and renal injury[10-12], we hypothesize that loss of TIMP3 will exacerbate diabetic nephropathy and cardiomyopathy.

The Akita mouse (*Ins2*$^{WT/C96Y}$) develops spontaneous hyperglycemia and reduced β-cell mass as a result of a mutation of the *insulin 2* gene (*Ins2*) (*Cys96Tyr*) that disrupts a disulfide bond between A and B chains of the insulin molecule[13-15]. The Akita model is a well established type I diabetic mouse model and the most useful

platform to study diabetic nephropathy due to less variability in renal structural responses [16-19]. We previously reported that Akita mice develop cardiac diastolic dysfunction[20]. In the present study, we cross-bred TIMP3 knockout (KO) and diabetic Akita mouse and generated the TIMP3-deficient Akita mouse model, to examine the role of TIMP3 in the progression of diabetic nephropathy. Our data revealed that lack of TIMP3 exacerbates diabetic nephropathy without altering diabetic cardiomyopathy.

4.3 OBJECTIVE

Diabetic nephropathy is an essential cause of end-stage renal disease. Here we examine the impact of TIMP3-deficiency on renal injury associated with type 1 diabetes in a well established mouse model for diabetic nephropathy.

4.4 MATERIALS AND METHODS

4.4.1 Experimental Animals and Protocol

Male Akita (*Ins2*$^{WT/C96Y}$), Akita/TIMP3$^{-/-}$ (TIMP3$^{-/-}$/*Ins2*$^{WT/C96Y}$), wild type (TIMP3$^{+/+}$/*Ins2*$^{WT/WT}$) and TIMP3$^{-/-}$ (TIMP3$^{-/-}$/ *Ins2*$^{WT/WT}$) mice at 3 and 6 months of age were used in all experiments. For breeding details please refer Chapter 2.1.2 and Fig. 2.2.

4.4.2 Blood Glucose and Tail-cuff Blood Pressure Measurements

Fasting (8 hrs) blood glucose levels were measured every month starting from 4 weeks till 24 weeks of age between 8 and 9 AM (Chapter 2.4.1). Tail-cuff systolic blood pressure (TC-SBP) at 3 and 6 months of age was measured in conscious

mice using the IITC Life Science Blood Pressure System, (Woodland Hills, CA) and detailed in Chapter 2.5.4.

4.4.3 Echocardiography and Tissue Doppler Imaging

Transthoracic echocardiography was performed and analyzed as described in Chapter 2.5. Trans-mitral flow Doppler imaging (Chapter 2.5.2), and the early diastolic (E') and late diastolic (A') peak annular velocities[20, 21] were measured using Tissue Doppler Imaging (TDI) of mitral valve annulus (Chapter 2.5.3).

4.4.4 Immunohistological, Molecular Analyses and Activity Assays

Mice were sacrificed at 3 months or 6 months or age, kidneys were collected (Chapter 2.3.2), weighed and fixed in formalin for gross morphometry, glomerular mesangial matrix scoring (Chapter 2.7.3), WT-1 staining and podocyte counting (Chapter 2.9.2.1). Whole kidney samples from mice were either embedded in OCT before being flash-frozen for DHE fluorescence and nitrotyrosine staining (Chapter 2.8.1) or used to dissect cortex in an RNA-stabilizing solution and flash frozen for RNA (Chapter 2.13), protein (Chapter 2.14) analyses, NADPH Oxidase (Chapter 2.8.1) and TACE Activity. TACE activity was assessed using an in vitro fluorogenic assay as described[22]. Briefly, 5 μg protein extracts from the cortex were incubated with 10 μM of fluorogenic substrate for TACE (7-methoxycoumarin-PLAQAV-(2,4-dinitrophenyl)-RSSSR-NH2, R&D Systems) at room temperature. The fluorescence emitted from the cleavage products of the substrate was quantified by spectrofluorometry using

excitation wavelength of 320nm, and emission wavelengths of 405nm. TACE-specific activity is expressed as RFU per minute.

4.4.5 Urine Analyses

The 24 hours urine was collected (Chapter 2.7), centrifuged at 8000 g for 5 minutes (to remove debris) and flash-frozen for further analyses. Urinary albumin concentration was measured as described in Chapter 2.7.2.

4.4.6 Statistical Analysis

Data was analyzed using either an unpaired Student's t-test (**Fig. 4.1**) or a two-way ANOVA followed by Bonferroni post-hoc testing (**Figs. 4.2-4.6**) using SPSS Statistics 19 software.

4.5 RESULTS

4.5.1 TIMP3 is Upregulated in Akita Kidneys but not in the Heart

TIMP3 is a highly expressed TIMP in the kidneys and the heart, and TIMP3-deficiency has been linked to both cardiomyopathy [9] and kidney disease [6], we assessed the expression of TIMP3 by Western blot analysis in hearts and kidneys of 3 and 6 month old Akita mice. While TIMP3 levels remained unaltered in Akita hearts (**Fig. 4.1A**), kidney levels of TIMP3 were significantly increased in the Akita model at 3 and 6 months of age (**Fig. 4.1B**). These results show that in the diabetic Akita model, TIMP3 is selectively upregulated in the kidneys.

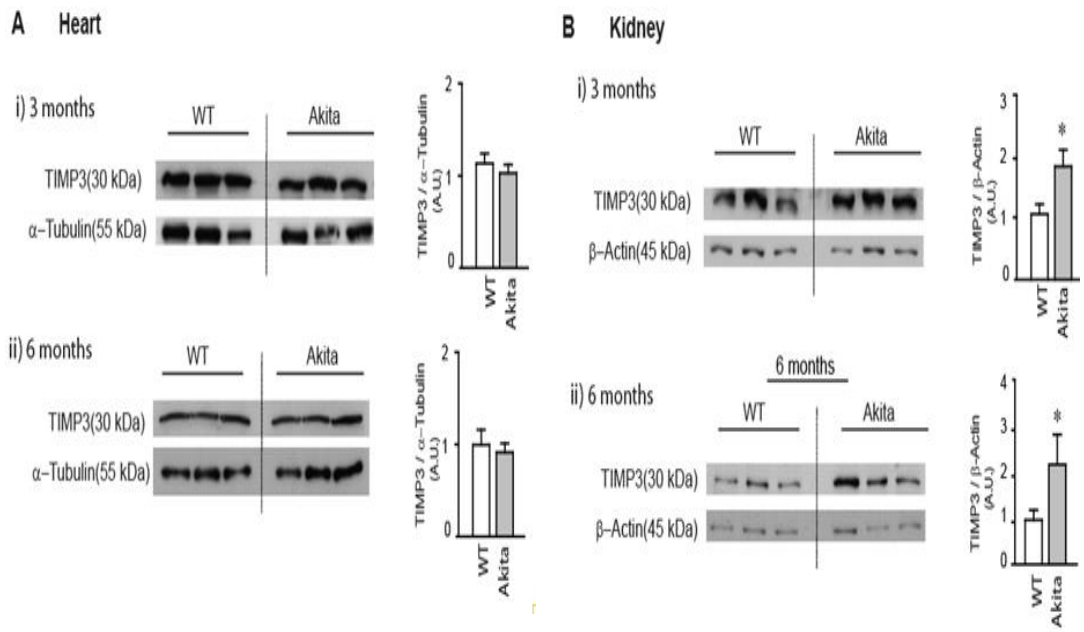

Figure 4.1 Upregulation of TIMP3 levels in the kidneys of diabetic Akita mice.

Representative Western blots and averaged protein quantification for TIMP3 protein in hearts (A) and kidneys (B) of wildtype and Akita mice at 3 months (i) and 6 months (ii) of age showing increased TIMP3 levels in the kidneys but not the hearts of Akita mice. α-tubulin and β-actin were used as loading controls for the heart and kidney, respectively. A.U. represents arbitrary units. Data are mean±SEM; n=5, **p*<0.05 vs wildtype (WT).

4.5.2 Loss of TIMP3 Does not Worsen Heart Function in Akita Mice

TIMP3 is also a critical determinant of cardiac function[9, 23] and as such we used echocardiography to assess heart function in our murine models. Our results confirmed diastolic dysfunction with preserved systolic function in Akita mice which was not altered by the loss of TIMP3 in 6 month old mice (**Fig. 4.2**). While M-mode images showed preserved systolic function (Fig. 2A), transmitral flow profile showed prolongation of isovolumetric relaxation time (IVRT) with increased deceleration time (**Fig. 4.2B**). Tissue Doppler imaging revealed a reduction in E' and an increase in A' velocities (**Fig. 4.2C**). Quantitative assessment of heart function confirmed no change in ejection fraction and

fractional shortening with equivalent reduction in the E'/A' and E/E' ratios in Akita and Akita/TIMP3 double mutant mice (**Table 4.1**). In summary, loss of TIMP3 did not alter the diastolic dysfunction in the Akita model consistent with a lack of change in TIMP3 levels in Akita hearts.

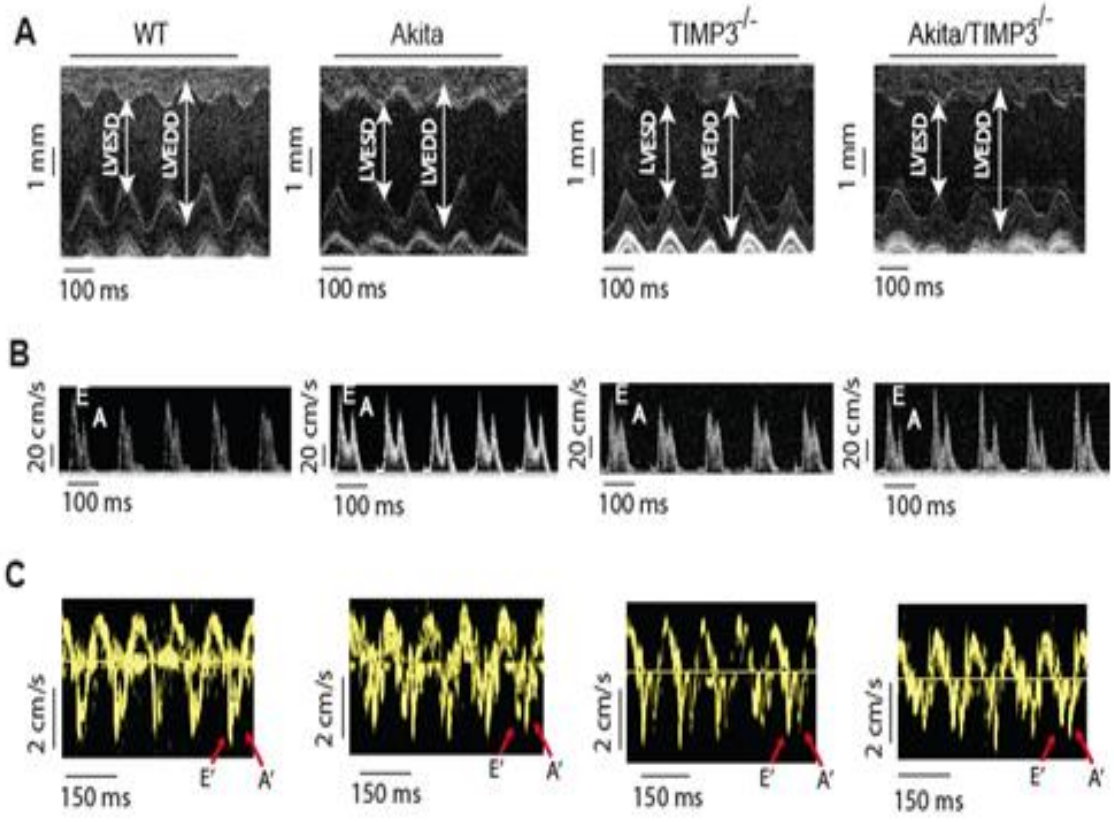

Figure 4.2 Loss of TIMP3 does not exacerbate diabetic cardiomyopathy in 6-month old Akita kidneys.

Echocardiographic assessment of heart function with representative M-mode (A), transmitral Doppler flow profile (B) and tissue Doppler imaging (C) showing normal systolic function with diastolic dysfunction in Akita and Akita/TIMP3$^{-/-}$ mice. LVEDD=left ventricular end diastolic diameter, LVESD=left ventricular end systolic diameter, E-wave=peak early transmitral inflow velocity; A-wave=transmitral inflow velocity due to atrial contraction, E'=early diastolic tissue Doppler velocity.

Table 4.1 Echocardiographic assessment of diastolic and systolic function in WT, Akita, TIMP3KO and Akita/TIMP3KO mice at 6 months of age.

	WT	Akita	TIMP3KO	Akita/TIMP3KO
n	10	12	10	12
HR (bpm)	489±16	474±13	480±20	470±20
E-wave (mm/s)	685±24.8	702±31.6	690±22.5	735±19.9
A-wave (mm/s)	445±47.3	441±40	492±37.6	494.73±14.25
E/A Ratio	1.54±0.1	1.59±0.09	1.41±0.06	1.48±0.08
IVRT (ms)	15.8±0.66	18.7±0.94*	14.5±0.75	15.4±0.82
E' (mm/s)	26.3±1.7	21.8±1.86	32.44±1.6	24.4±2.1*
E/E' Ratio	27.9±1.8	33.1±1.7*	24.54±1.07	30.1±1.7*
A'	24.4±1.4	29.2±1.5*	26.8±1.3	29.07±2.52
E'/A'	1.14±0.06	0.74±0.07*	1.23±0.07	0.84±0.08*
LVEDD (mm)	3.79±0.05	3.71±0.04	3.53±0.08	3.67±0.08
LVESD (mm)	2.59±0.06	2.52±0.05	2.27±0.12	2.43±0.11
LVFS (%)	31.6±2.1	32.1±1.9	36.02±2.17	34.09±1.83
LVEF (%)	62.7±2.4	60.4±2	62±2.13	60.21±1.01
VCFc (circ/s)	6.3±0.50	6.25±0.38	7.00±0.60	6.40±0.30
LVPWT (mm)	0.69±0.03	0.71±0.02	0.72±0.01	0.7±0.03

n=samples size; HR=heart rate; E-wave=peak early transmitral inflow mitral E velocity; A-wave=transmitral inflow velocity due to atrial contraction; IVRT=isovolumetric relaxation time; DT=deceleration time; EWDR=E-wave deceleration rate (E-wave/DT); E′=early diastolic tissue Doppler velocity; LVEDD=left ventricular end diastolic diameter; LVESD=left ventricular end systolic diameter; LVFS=LV fractional shortening; LVEF=LV ejection fraction; VCFc=Velocity of Circumferential Shortening corrected for Heart Rate; LVPWT=LV Posterior Wall Thickness. *p<0.05 compared to WT and TIMP3KO groups.

4.5.3 TIMP3-deficiency Exacerbates Diabetic Renal Injury without Altering Plasma Glucose Levels and Systolic Blood Pressure.

Gross morphological assessment of the kidneys revealed increased renal size in Akita mice as previously reported [15, 16], while the absence of TIMP3 in the Akita mice resulted in significantly greater enlargement of the kidneys (**Figs. 4.3A and 4.3B**). Moreover, the gross appearance in the double mutant that outweighed the increase in kidney weight normalized to its tibial length could be as a result of decreased mass. As diabetic injury is characterized by mesangial expansion and increased microalbuminuria, we assessed these parameters in our murine models. The mesangial matrix in the Akita/TIMP3 double mutant mice as shown using PAS staining (**Fig. 4.3C**) and mesangial matrix score was significantly greater than the Akita mice (**Fig. 4.3D**). Consistent with the expansion of the mesangium, urinary albumin excretion showed a two-fold increase in the Akita/TIMP3$^{-/-}$ mice compared to the increase in the Akita mice (**Fig. 4.3E**) which occurred in the absence of differential effects on systolic blood pressure (**Fig. 4.3F**) and hyperglycemia (**Fig. 4.3G**).

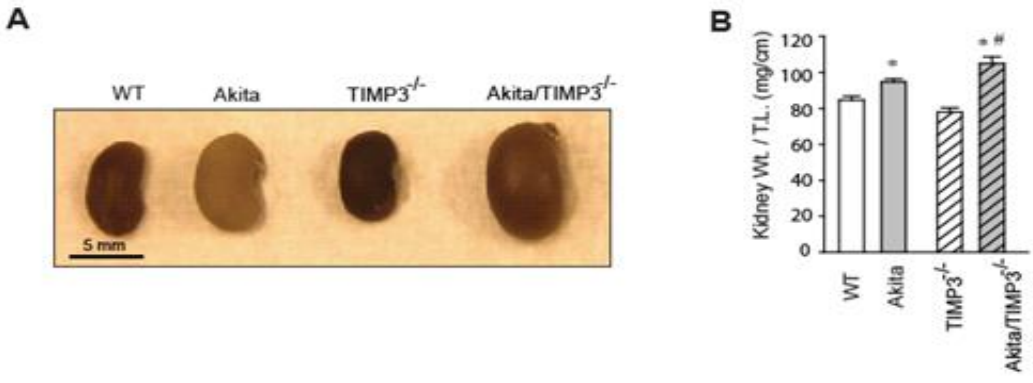

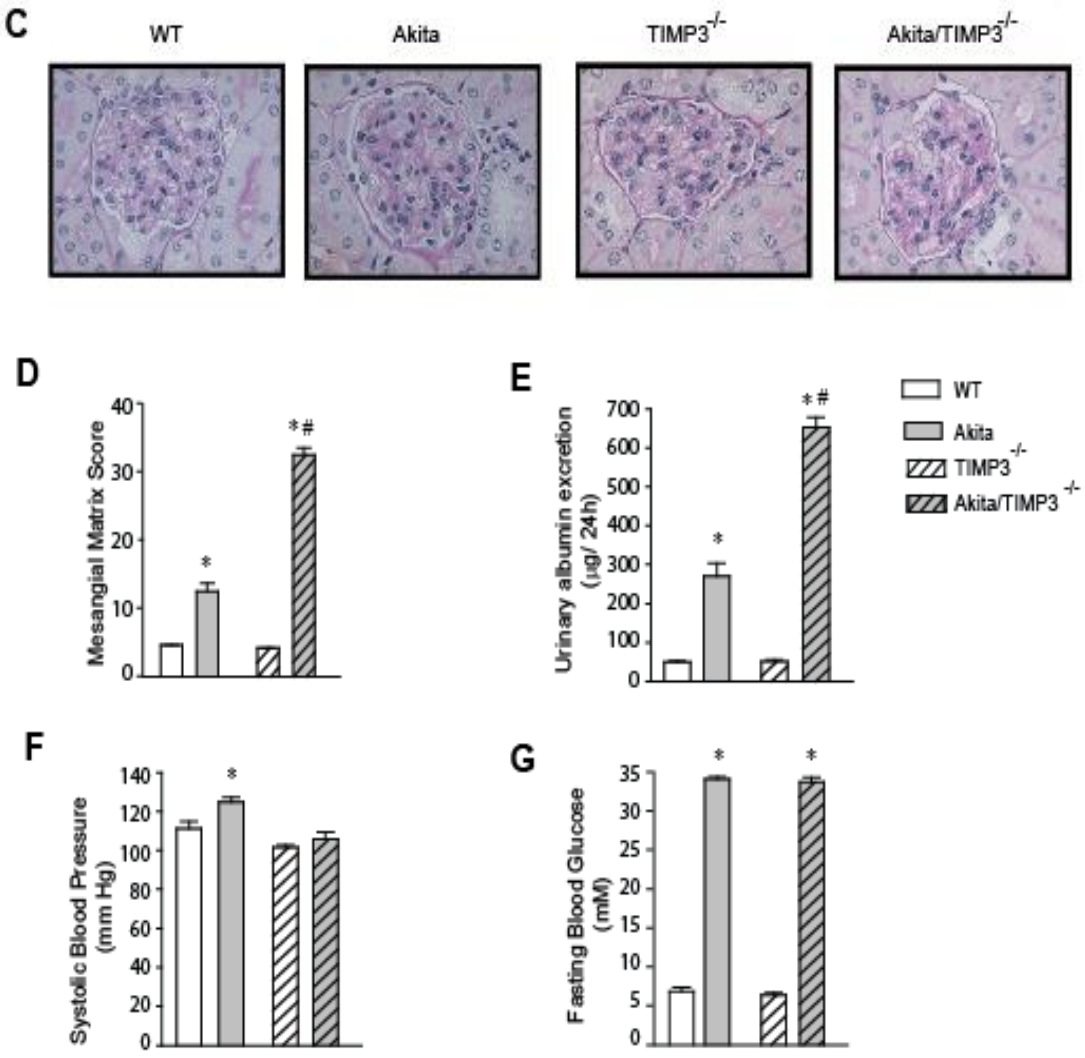

Figure 4.3 Loss of TIMP3 exacerbates diabetic renal injury in 6-month old Akita mice.

Representative images of whole kidneys (A) and averaged kidney weight-to-tibial length (TL) ratio (B) of the various genotypes showing greater enlargement of the kidneys in Akita/TIMP3$^{-/-}$ mice. Representative PAS staining (C), glomerular mesangial matrix score (D) and urinary albumin excretion (E) showing exacerbation of glomerular mesangial injury and worsening of albuminuria in the absence of a differential effect on systolic blood pressure (F) and fasting blood glucose (G) in the Akita/TIMP3$^{-/-}$ mice. Data are mean±SEM; n=10, *$p<0.05$ compared to wildtype (WT) or TIMP3$^{-/-}$, $^{\#}p<0.05$ compared to all other groups.

4.5.4 Diabetic Renal Injury Due to TIMP3 Deficiency is Not Associated with Glomerular Podocyte Loss.

Loss of glomerular podocytes has been linked to worsening diabetic nephropathy[24, 25]. However, the mRNA (**Fig. 4.4A**) and protein levels (**Fig. 4.4Bi-ii**) of nephrin, a marker of podocytes, and the average number of podocytes positively labeled with Wilms tumor protein (WT-1) or WT-1 mRNA levels (**Fig. 4.4C**) were not different among the various experimental groups mRNA expression levels (A, n=8/group), representative Western blot and averaged quantification (B, n=4/group) of nephrin protein levels in the indicated genotypes. B) Representative images of WT-1 staining (i), analysis of WT-1 positive cells per glomeruli (ii), and WT-1 mRNA expression levels (iii) in the indicated genotypes. R.E. represents relative expression. Data are presented as Mean ± SEM, n=8/group. * $p<0.05$ compared to WT, # $p<0.05$ compared to all other groups.

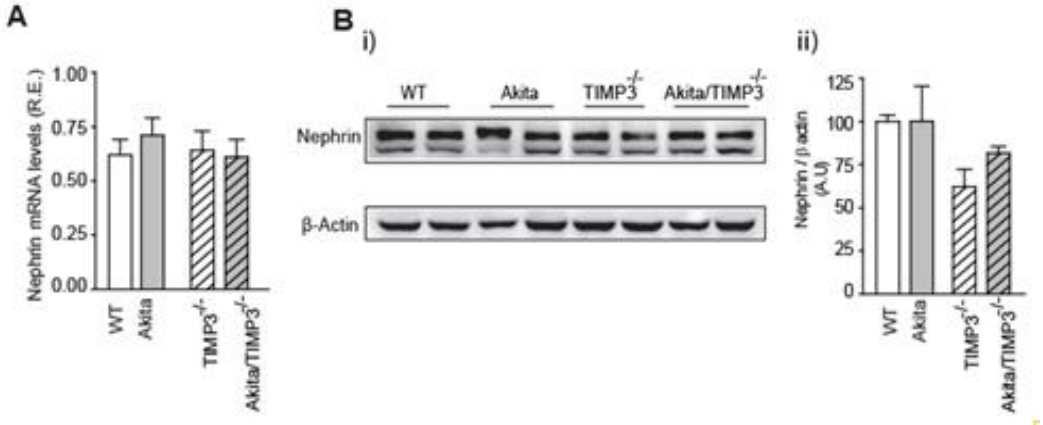

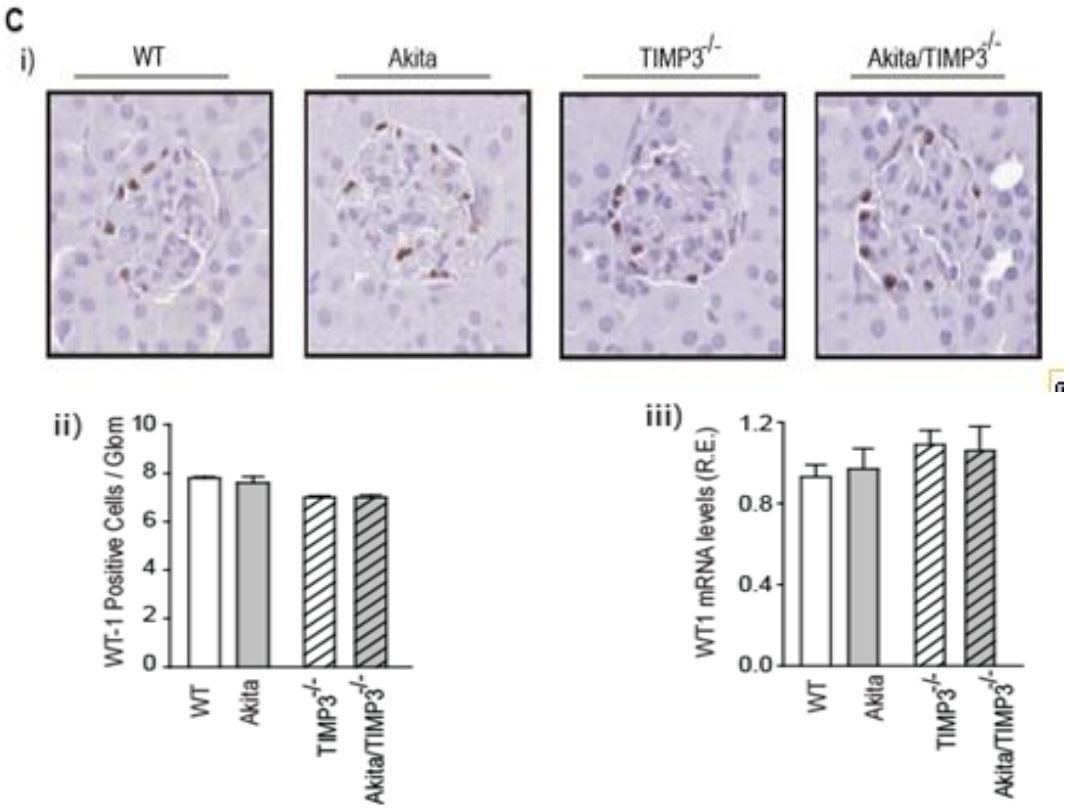

Figure 4.4 WT-1 and nephrin levels are not altered by the loss of TIMP3 in 6-month old Akita kidneys.
mRNA expression levels (A, n=8/group), representative. B) Western blot and averaged quantification, (n=4/group) of nephrin protein levels in the indicated genotypes. C) Representative images of WT-1 staining (i), analysis of WT-1 positive cells per glomeruli (ii), and WT-1 mRNA expression levels (iii) in the indicated genotypes. R.E. represents relative expression. Data are presented as Mean ± SEM, n=8/group. * $p<0.05$ compared to WT, # $p<0.05$ compared to all other groups.

4.5.5 Lack of TIMP3 Activates the PKC Pathway

Given the exacerbation of diabetic kidney injury by the loss of TIMP3, we next examined alteration in signaling pathways such as Akt, ERK1/2 and protein kinase C (PKC) in the kidneys. The phosphorylation of Akt on both serine-473 and threonine-308 were activated in Akita kidneys but not in the Akita/TIMP3-

double mutants (**Figs. 5 A and B**) with a similar trend seen for the ERK1/2 pathway (**Fig. 4.5C**).

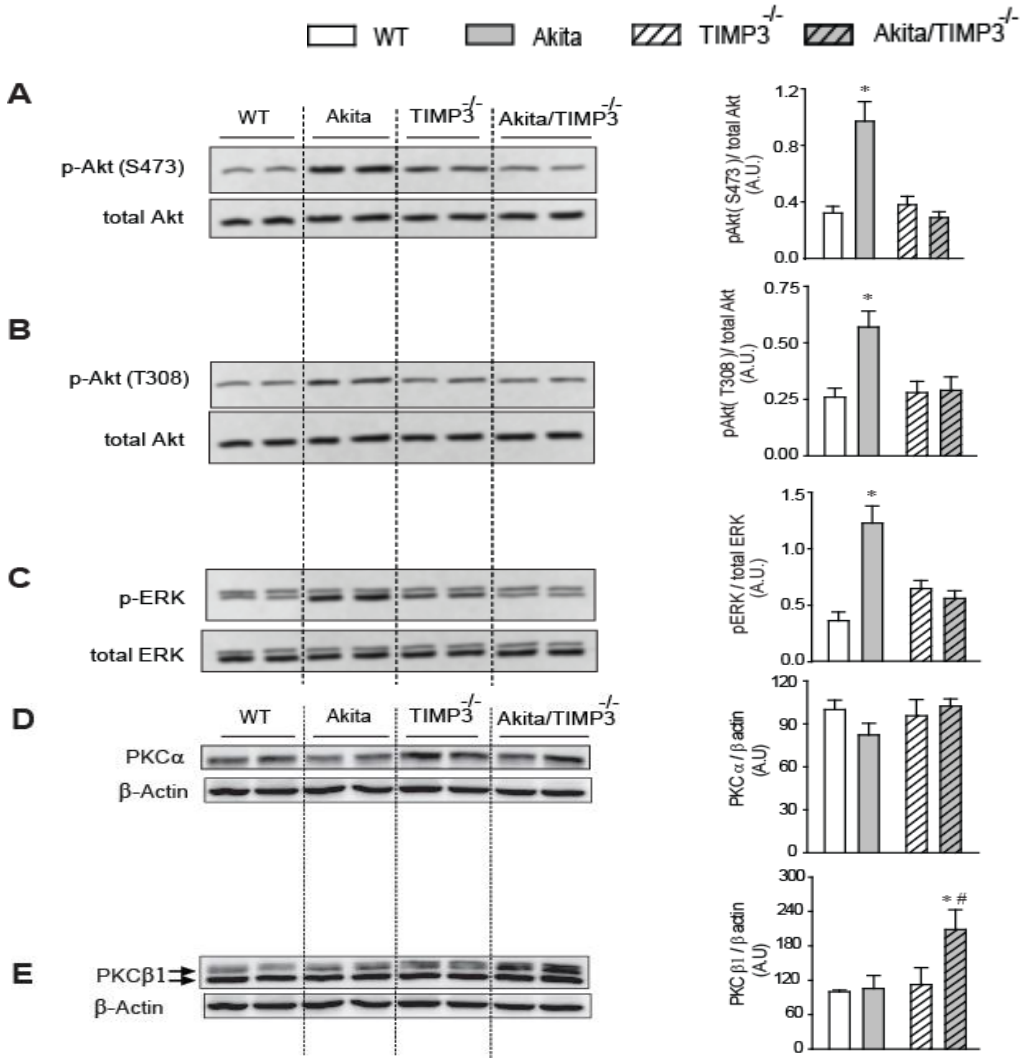

Figure 4.5 TIMP3-deficiency reverses renal protective signaling pathways and increases PKC expression in 6-month old Akita kidneys.

Representative blot and quantification of Western blot analysis of phosphorylation of Akt at serine-473 (A) and threonine-308 (B) and ERK1/2 (C) signaling pathways showing increased phosphorylation in Akita kidneys which was loss in the Akita/TIMP3 double mutant kidneys. Representative blot and quantification of Western blot analysis of PKCα (D) and PKCβ1 (E) levels showing no change in PKCα levels with an increased PKCβ1 levels in Akita/TIMP3 double mutant kidneys. A.U. represents arbitrary units. Data are mean±SEM; n=6, **p*<0.05 vs wild type (WT), #*p*< 0.05 vs all other groups.

Activation of the PKC system plays a key pathological role in diabetic nephropathy[26, 27]. While the protein expression of PKCα was unaltered (**Fig. 4.5D**), PKC β1 level was increased about 2-fold in Akita/TIMP3$^{-/-}$ kidneys (**Fig. 4.5E**). This indicates that loss of TIMP3 compromises the activation of important renoprotective signaling pathways while increasing PKCβ1 levels in diabetic kidneys.

4.5.6 TIMP3 Promotes Fibrosis and Increases Inflammation in Akita Kidneys

TIMP3 has also been shown to be involved in control of the tissue microenvironment by regulating tissue fibrosis and inflammation[6, 28]. Deletion of TIMP3 in Akita kidneys was associated with increased mRNA expression of various profibrotic markers such as pro-collagen type I-α1, connective tissue growth factor (CTGF) and transforming growth factor β (TGF-β) (**Figs. 4.6A-C**) while picrosirius red (**Fig. 4.6D**) and Masson trichrome staining (**Fig. 6E**) confirmed increased tubule-interstitial fibrosis. Expression analysis of inflammatory markers showed increased chemokine monocyte chemotactic protein-1 (MCP-1) levels while interleukin1β and tumor necrosis factor (TNF) remained unchanged (**Figs. 4.6F-H**) in Akita/TIMP3$^{-/-}$ kidneys.

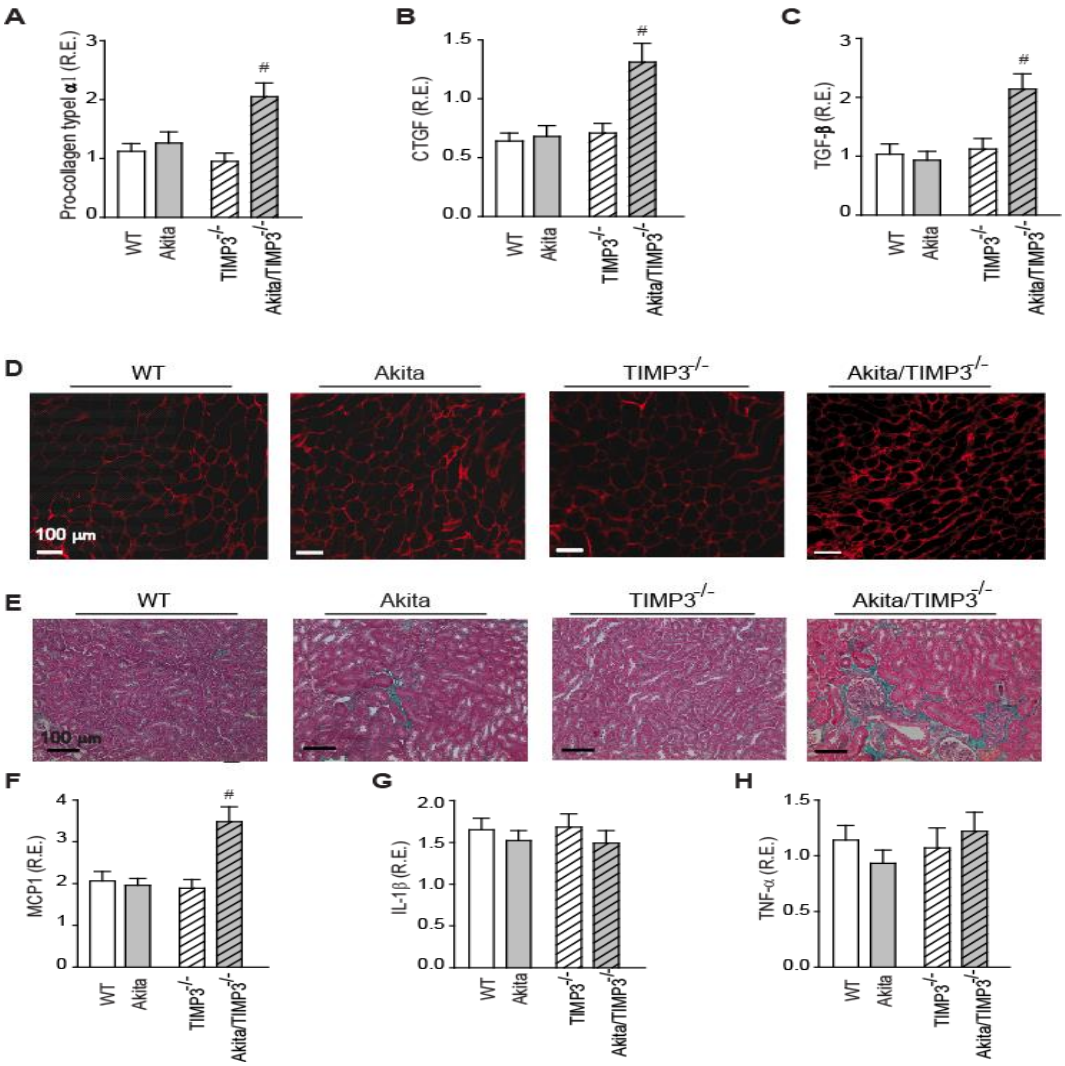

Figure 4.6 Loss of TIMP3 increases the expression of profibrotic, tubulointerstitial fibrosis and inflammatory markers in 6-month old Akita kidneys.

Expression analysis showing greater mRNA levels of profibrotic markers, pro-collagen type I α1 (A), CTGF (B) and TGFβ1 (C) while histological analysis using picrosirius red (D) and Gomori trichrome (E) staining illustrate greater tubulointerstitial fibrosis in the Akita/TIMP3$^{-/-}$ kidneys. Expression analysis showing greater mRNA levels of MCP1 (F) without altering interleukin (IL)-1β (G) and tumor necrosis factor (TNF)α (H) expression in Akita/TIMP3 double mutant kidneys. R.E. represents relative expression. Scale bar represents=100 μM. CTGF=connective tissue growth factor, TGF=transforming growth factor and MCP1=monocyte chemoattractant protein 1. Data are mean±SEM; n=8, $^{\#}p< 0.05$ vs all other groups.

4.5.7 Increased ROS Generation in the Akita/TIMP3$^{-/-}$ Kidneys.

Activation of the NADPH oxidase and generation of reactive oxygen species (ROS) plays a key role in diabetic nephropathy [19, 29, 30]. Staining for DHE (**Fig. 4.7A**) and nitrotyrosin (**Fig. 4.7B**), and the corresponding quantifications (**Figs. 4.7C and 4.7D**), confirmed higher levels of superoxide and nitrotyrosin in diabetic Akita kidneys which was increased further in the Akita/TIMP3-double mutant kidneys, indicating that loss of TIMP3 amplified ROS generation in the diabetic kidneys. The renal cortical NADPH activity based on the lucigenin chemiluminescence assay was significantly increased in Akita compared to wildtype kidneys in association with increased mRNA expression of the NADPH oxidase subunits, p47^{phox} (**Figs. 4.7E and 4.7F**). The NADPH oxidase activity was elevated further in the Akita/TIMP3$^{-/-}$ kidneys, likely driven by the greater elevation in p47^{phox} mRNA levels and increased NOX2 (gp91^{phox}) levels (**Figs. 4.7E-G**). The specific peptide inhibitor of NOX2, gp91phox ds tat (50 μM) and its inactive scrambled form (scr) were used to confirm superoxide generation from NADPH oxidase [31] (**Fig. 4.7E**).

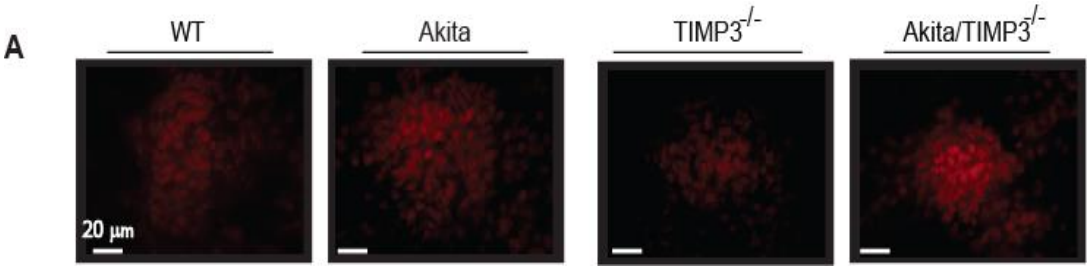

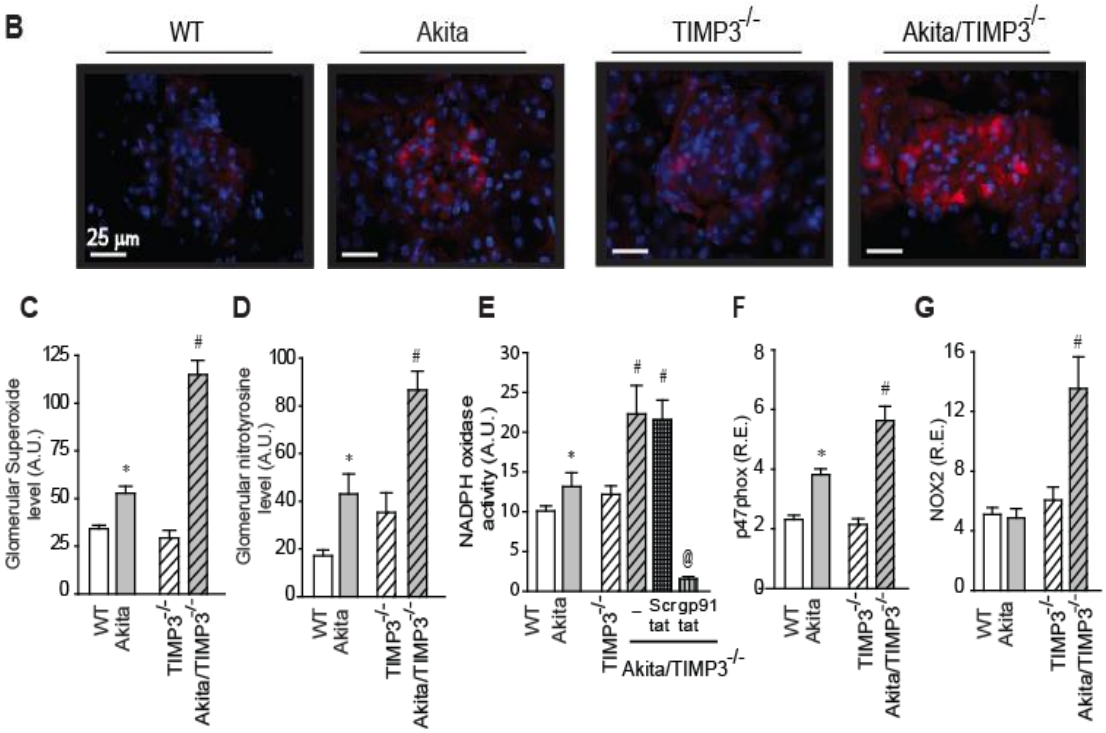

Figure 4.7 TIMP3-deficiency increases oxidative stress in 6-month old Akita diabetic kidneys.

Representative images of glomerular DHE staining (A), and nitrotyrosin staining (red) with nuclear DAPI staining (blue) (B), with quantification of superoxide (C) and nitrotyrosin levels (D) showing increased superoxide levels in the Akita/TIMP3$^{-/-}$ kidneys. Increased NADPH oxidase activity (E), p47^{phox} (F) and NOX2 (G) mRNA subunit expression in Akita/TIMP3$^{-/-}$ kidneys; n=8/group. Gp91-tat is a specific peptide inhibitor of NOX2, gp91phox ds-tat; Scr tat is an inactive scrambled form of gp91phox ds-tat. R.E. represents relative expression. A.U. represents arbitrary units. Data are mean±SEM, *p<0.05 compared to wild type (WT), $^{\#}p$<0.05 compared to all other groups; $^{@}p$<0.05 compared with scrambled (Scr) tat peptide group (using unpaired Student's t-test).

4.5.8 Lack of TIMP3 Increases TACE Activity without a Differential Effect on MMP2 Activation

Since TIMP3 is the only identified physiological inhibitor of ADAM-17 or TACE (TNF-alpha converting enzyme)[7], a key regulator of MMP2 activation [32] and MMP9 [6, 33], we next investigated whether loss of TIMP3 impacted activity of TACE, MMP2 and MMP9, the key proteases in kidney tissue remodeling in the background of type I diabetes. While mRNA expression of TACE was not

different among groups (**Fig. 8Ai**), its activity was significantly elevated with TIMP3 deficiency. The increase in TACE activity in the Akita group did not reach statistical significance, whereas when combined with TIMP3-deficiency, it was significantly elevated compared to all other groups (**Fig. 8Aii**). Gelatin zymography showed elevated pro-MMP9 levels in the TIMP3$^{-/-}$/Akita kidneys while active MMP2 band intensity was only detectable in the TIMP3$^{-/-}$ and TIMP3$^{-/-}$/Akita kidneys (**Figs. 8Bi-iii**). As such, loss of TIMP3 led to increased TACE activity and active MMP2 levels, which could contribute to oxidative stress and worsening of the diabetic nephropathy.

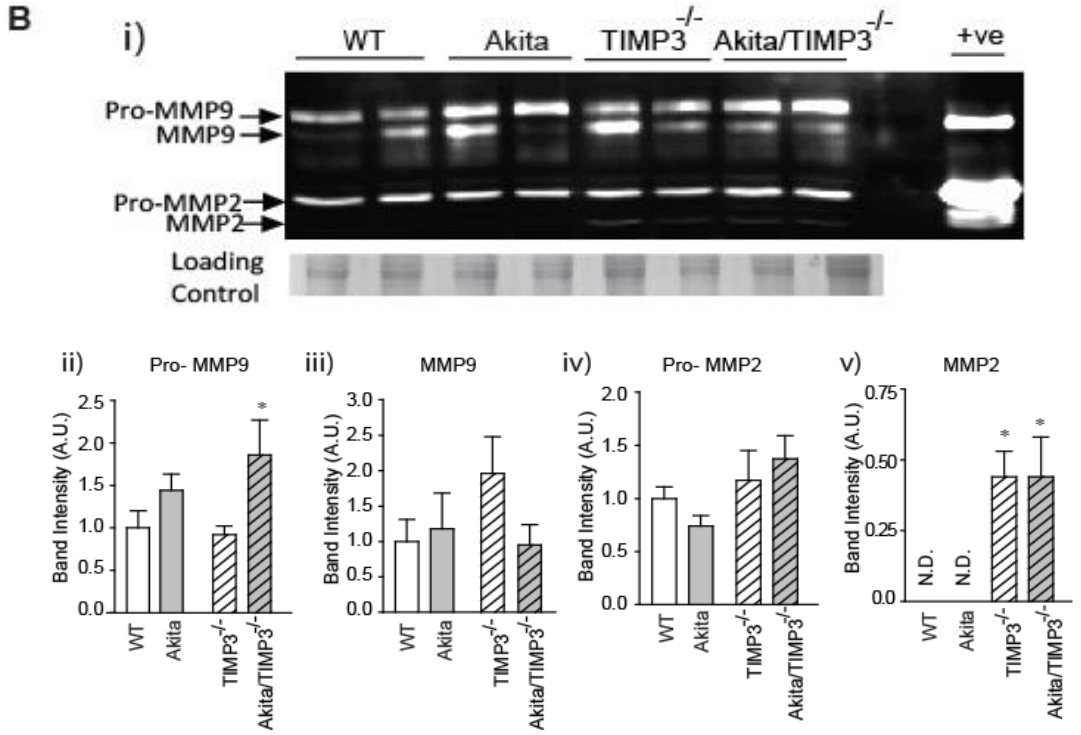

Figure 4.8 Differential alterations in TACE, MMP2 and MMP9 levels in kidneys of different genotypes.

A) TACE mRNA expression (i) and activity (ii) in all groups, n=5/group. B) Representative gelatin zymography (i), and quantification of the band intensity for pro-MMP9 (ii), MMP9 (iii), pro-MMP2 (iv), and MMP 2 (v) in each genotype; n=6/group. '+ve' indicates the positive control for MMP2 and MMP9. * $p<0.05$ compared to WT, # $p<0.05$ compared to all other groups.

4.6 DISCUSSION

Diabetic nephropathy and cardiomyopathy are well-recognized complications of diabetes and is now the most common cause of end-stage renal disease (ESRD) in the U.S. [1-3]. Studies in patients with diabetic nephropathy have implicated a possible role of TIMP3 in diabetic nephropathy[4, 5]. In this study, we demonstrate that loss of TIMP3 leads to the aggravation of diabetic renal injury as exemplified by significantly increased kidney mass, glomerular mesangial matrix score and urinary albumin excretion which are all early features of human diabetic nephropathy [34]. These changes occurred in the absence of worsening of hypertension or glycemic control. Importantly, TIMP3 levels were increased in diabetic kidneys suggesting an early compensatory role of TIMP3 in the pathogenesis of diabetic nephropathy. We previously reported that Akita mice develop cardiac diastolic dysfunction[20]. However, TIMP3-deficiency did not exacerbate this diabetic cardiomyopathy consistent with unaltered cardiac TIMP3 levels in diabetic Akita mice. These results demonstrate that TIMP3 plays a key and organ specific role in diabetic nephropathy and is consistent with observations made in human diabetic nephropathy[4, 5].

Several canonical pathways are key mediators of diabetic nephropathy including increased renal NADPH oxidase activity, and altered intracellular signaling such as activation of the PKC system and altered remodeling of the glomerular mesangium [10, 11, 26, 27, 35, 36]. Activated NADPH oxidase [19] coupled with other sources of oxidative stress such as the mitochondria-dependent [37] and

hyperglycemia-induced [29, 38] generation of ROS are clearly linked to the exacerbation of diabetic renal injury. We found increased renal cortical NADPH oxidase activity and expression of $p47^{phox}$ subunit in agreement with previous findings[19]. Exacerbation of diabetic renal injury by deletion of TIMP3 was associated with increased generation of NADPH oxidase-dependent ROS and nitrotyrosine, and increased expression of the renal cortical NADPH subunits, $p47^{phox}$ and NOX2 ($gp91^{phox}$), in Akita/TIMP3-double mutant kidneys. The peaked NADPH oxidase activity in Akita/TIMP3 double mutant kidneys was reduced dramatically by gp91phox ds tat the specific peptide inhibitor of NADPH oxidase, confirming superoxide generation from NADPH oxidase. The elevated oxidative stress could be brought about by the elevated TACE activity in the double mutant mice as TACE mediates cell surface processing of membrane-bound TNFα into its soluble form [9, 39] whereby it can activate its receptors, mainly TNFR1/p55 triggering various tissue responses including superoxide production and oxidative stress [40-44]. Loss of TIMP3 also compromised the activation of signaling pathways that have been shown to be associated with protective outcomes in diabetic nephropathy, Akt/PI3K and ERK1/2 MAPK pathways [45, 46], while increasing the expression of PKCβ1 which have been linked to exacerbation of diabetic nephropathy [26, 27].

TIMP3 is also a critical player in regulating the tissue microenvironment including control of inflammation and fibrosis[6, 28]. Inflammation has been well documented as a cardinal pathogenic mechanism in diabetic nephropathy[12]. We

investigated the role of inflammatory molecules in the deterioration of diabetic renal injury due to the lack of TIMP3 by evaluating the mRNA expression of various fibrotic and inflammatory markers. Indeed, pro-collagen type I α1, CTGF, TGF-β and MCP-1 substantially increased which was associated with increased tubuolinterstitial fibrosis in Akita/TIMP3 double mutant kidneys which is consistent with our previous findings showing that loss of TIMP3 enhances interstitial nephritis and fibrosis in a model of unilateral ureteral obstruction (9). TIMP3 is a known key suppressor of MMP2 activation[6, 23] and loss of TIMP3 led to increased active MMP2 in the diabetic Akita kidneys. Altered glomerular mesangium constituency due to relative increase in proteolysis secondary to active MMP2 may worsen glomerular injury and increase the susceptibility to diabetic nephropathy [10, 11, 36]. In summary, TIMP3 is a key player in diabetic renal injury and strategies aimed at enhancing TIMP3 levels in diabetic kidneys may minimize diabetic renal injury.

4.7 CONCLUSION

TIMP3 plays a critical role in the progression of Type I diabetic nephropathy by regulating oxidative stress and inflammation that result into tubulointerstitial fibrosis, mesangial expansion and deterioration of renal function.

4.8 REFERENCES

1. Levey AS, Andreoli SP, DuBose T, Provenzano R, Collins AJ. Chronic kidney disease: Common, harmful, and treatable--world kidney day 2007. *J Am Soc Nephrol*. 2007;18:374-378

2. Coresh J, Selvin E, Stevens LA, Manzi J, Kusek JW, Eggers P, Van Lente F, Levey AS. Prevalence of chronic kidney disease in the united states. *JAMA : the journal of the American Medical Association*. 2007;298:2038-2047

3. Grundy SM, Benjamin IJ, Burke GL, Chait A, Eckel RH, Howard BV, Mitch W, Smith SC, Jr., Sowers JR. Diabetes and cardiovascular disease: A statement for healthcare professionals from the american heart association. *Circulation*. 1999;100:1134-1146

4. Ewens KG, George RA, Sharma K, Ziyadeh FN, Spielman RS. Assessment of 115 candidate genes for diabetic nephropathy by transmission/disequilibrium test. *Diabetes*. 2005;54:3305-3318

5. Woroniecka KI, Park AS, Mohtat D, Thomas DB, Pullman JM, Susztak K. Transcriptome analysis of human diabetic kidney disease. *Diabetes*. 2011;60:2354-2369

6. Kassiri Z, Oudit GY, Kandalam V, Awad A, Wang X, Ziou X, Maeda N, Herzenberg AM, Scholey JW. Loss of timp3 enhances interstitial nephritis and fibrosis. *J Am Soc Nephrol*. 2009;20:1223-1235

7. Amour A, Slocombe PM, Webster A, Butler M, Knight CG, Smith BJ, Stephens PE, Shelley C, Hutton M, Knauper V, Docherty AJ, Murphy G. Tnf-alpha converting enzyme (tace) is inhibited by timp-3. *FEBS Lett*. 1998;435:39-44

8. Kashiwagi M, Tortorella M, Nagase H, Brew K. Timp-3 is a potent inhibitor of aggrecanase 1 (adam-ts4) and aggrecanase 2 (adam-ts5). *J Biol Chem*. 2001;276:12501-12504

9. Kassiri Z, Oudit GY, Sanchez O, Dawood F, Mohammed FF, Nuttall RK, Edwards DR, Liu PP, Backx PH, Khokha R. Combination of tumor necrosis factor-alpha ablation and matrix metalloproteinase inhibition prevents heart failure after pressure overload in tissue inhibitor of metalloproteinase-3 knock-out mice. *Circ Res*. 2005;97:380-390

10. Catania JM, Chen G, Parrish AR. Role of matrix metalloproteinases in renal pathophysiologies. *Am J Physiol Renal Physiol*. 2007;292:F905-911

11. Williams JM, Zhang J, North P, Lacy S, Yakes M, Dahly-Vernon A, Roman RJ. Evaluation of metalloprotease inhibitors on hypertension and diabetic nephropathy. *Am J Physiol Renal Physiol*. 2011;300:F983-998

12. Navarro-Gonzalez JF, Mora-Fernandez C. The role of inflammatory cytokines in diabetic nephropathy. *J Am Soc Nephrol*. 2008;19:433-442

13. Yoshioka M, Kayo T, Ikeda T, Koizumi A. A novel locus, mody4, distal to d7mit189 on chromosome 7 determines early-onset niddm in nonobese c57bl/6 (akita) mutant mice. *Diabetes*. 1997;46:887-894

14. Kayo T, Koizumi A. Mapping of murine diabetogenic gene mody on chromosome 7 at d7mit258 and its involvement in pancreatic islet and beta cell development during the perinatal period. *J Clin Invest*. 1998;101:2112-2118

15. Kakoki M, Sullivan KA, Backus C, Hayes JM, Oh SS, Hua K, Gasim AM, Tomita H, Grant R, Nossov SB, Kim HS, Jennette JC, Feldman EL, Smithies O. Lack of both bradykinin b1 and b2 receptors enhances nephropathy, neuropathy, and bone mineral loss in akita diabetic mice. *Proc Natl Acad Sci U S A*. 2010;107:10190-10195

16. Gurley SB, Clare SE, Snow KP, Hu A, Meyer TW, Coffman TM. Impact of genetic background on nephropathy in diabetic mice. *Am J Physiol Renal Physiol*. 2006;290:F214-222

17. Gurley SB, Mach CL, Stegbauer J, Yang J, Snow KP, Hu A, Meyer TW, Coffman TM. Influence of genetic background on albuminuria and kidney injury in ins2(+/c96y) (akita) mice. *Am J Physiol Renal Physiol*. 2010;298:F788-795

18. Wong DW, Oudit GY, Reich H, Kassiri Z, Zhou J, Liu QC, Backx PH, Penninger JM, Herzenberg AM, Scholey JW. Loss of angiotensin-converting enzyme-2 (ace2) accelerates diabetic kidney injury. *Am J Pathol*. 2007;171:438-451

19. Oudit GY, Liu GC, Zhong J, Basu R, Chow FL, Zhou J, Loibner H, Janzek E, Schuster M, Penninger JM, Herzenberg AM, Kassiri Z, Scholey JW. Human recombinant ace2 reduces the progression of diabetic nephropathy. *Diabetes*. 2010;59:529-538

20. Basu R, Oudit GY, Wang X, Zhang L, Ussher JR, Lopaschuk GD, Kassiri Z. Type 1 diabetic cardiomyopathy in the akita (ins2wt/c96y) mouse model is characterized by lipotoxicity and diastolic dysfunction with preserved systolic function. *Am J Physiol Heart Circ Physiol*. 2009;297:H2096-2108

21. Schaefer A, Klein G, Brand B, Lippolt P, Drexler H, Meyer GP. Evaluation of left ventricular diastolic function by pulsed doppler tissue imaging in mice. *J Am Soc Echocardiogr*. 2003;16:1144-1149

22. Rozenova KA, Deevska GM, Karakashian AA, Nikolova-Karakashian MN. Studies on the role of acid sphingomyelinase and ceramide in the regulation of tumor necrosis factor alpha (tnfalpha)-converting enzyme activity and tnfalpha secretion in macrophages. *J Biol Chem*. 2010;285:21103-21113

23. Moore L, Fan D, Basu R, Kandalam V, Kassiri Z. Tissue inhibitor of metalloproteinases (timps) in heart failure. *Heart Fail Rev*. 2011

24. Sakairi T, Abe Y, Kajiyama H, Bartlett LD, Howard LV, Jat PS, Kopp JB. Conditionally immortalized human podocyte cell lines established from urine. *Am J Physiol Renal Physiol*. 2010;298:F557-567

25. Susztak K, Raff AC, Schiffer M, Bottinger EP. Glucose-induced reactive oxygen species cause apoptosis of podocytes and podocyte depletion at the onset of diabetic nephropathy. *Diabetes*. 2006;55:225-233

26. Kelly DJ, Zhang Y, Hepper C, Gow RM, Jaworski K, Kemp BE, Wilkinson-Berka JL, Gilbert RE. Protein kinase c beta inhibition attenuates the progression of experimental diabetic nephropathy in the presence of continued hypertension. *Diabetes*. 2003;52:512-518

27. Ohshiro Y, Ma RC, Yasuda Y, Hiraoka-Yamamoto J, Clermont AC, Isshiki K, Yagi K, Arikawa E, Kern TS, King GL. Reduction of diabetes-induced oxidative stress, fibrotic cytokine expression, and renal dysfunction in protein kinase cbeta-null mice. *Diabetes*. 2006;55:3112-3120

28. Kassiri Z, Defamie V, Hariri M, Oudit GY, Anthwal S, Dawood F, Liu P, Khokha R. Simultaneous transforming growth factor beta-tumor necrosis factor activation and cross-talk cause aberrant remodeling response and myocardial fibrosis in timp3-deficient heart. *J Biol Chem*. 2009;284:29893-29904

29. Kang BP, Frencher S, Reddy V, Kessler A, Malhotra A, Meggs LG. High glucose promotes mesangial cell apoptosis by oxidant-dependent mechanism. *Am J Physiol Renal Physiol*. 2003;284:F455-466

30. Thallas-Bonke V, Thorpe SR, Coughlan MT, Fukami K, Yap FY, Sourris KC, Penfold SA, Bach LA, Cooper ME, Forbes JM. Inhibition of nadph oxidase prevents advanced glycation end product-mediated damage in

diabetic nephropathy through a protein kinase c-alpha-dependent pathway. *Diabetes*. 2008;57:460-469

31. Bodiga S, Zhong JC, Wang W, Basu R, Lo J, Liu GC, Guo D, Holland SM, Scholey JW, Penninger JM, Kassiri Z, Oudit GY. Enhanced susceptibility to biomechanical stress in ace2 null mice is prevented by loss of the p47phox nadph oxidase subunit. *Cardiovasc Res*. 2011;91:151-161

32. English JL, Kassiri Z, Koskivirta I, Atkinson SJ, Di Grappa M, Soloway PD, Nagase H, Vuorio E, Murphy G, Khokha R. Individual timp deficiencies differentially impact pro-mmp-2 activation. *J Biol Chem*. 2006;281:10337-10346

33. Moore L, Fan D, Basu R, Kandalam V, Kassiri Z. Tissue inhibitor of metalloproteinases (timps) in heart failure. *Heart Fail Rev*. 2012;17:693-706

34. Chavers BM, Bilous RW, Ellis EN, Steffes MW, Mauer SM. Glomerular lesions and urinary albumin excretion in type i diabetes without overt proteinuria. *N Engl J Med*. 1989;320:966-970

35. Furuichi K, Hisada Y, Shimizu M, Okumura T, Kitagawa K, Yoshimoto K, Iwata Y, Yokoyama H, Kaneko S, Wada T. Matrix metalloproteinase-2 (mmp-2) and membrane-type 1 mmp (mt1-mmp) affect the remodeling of glomerulosclerosis in diabetic oletf rats. *Nephrol Dial Transplant*. 2011;26:3124-3131

36. Thrailkill KM, Bunn RC, Moreau CS, Cockrell GE, Simpson PM, Coleman HN, Frindik JP, Kemp SF, Fowlkes JL. Matrix metalloproteinase-2 dysregulation in type 1 diabetes. *Diabetes Care*. 2007;30:2321-2326

37. Chacko BK, Reily C, Srivastava A, Johnson MS, Ye Y, Ulasova E, Agarwal A, Zinn KR, Murphy MP, Kalyanaraman B, Darley-Usmar V. Prevention of diabetic nephropathy in ins2(+/)(akitaj) mice by the mitochondria-targeted therapy mitoq. *Biochem J*. 2010;432:9-19

38. Craven PA, Melhem MF, Phillips SL, DeRubertis FR. Overexpression of cu2+/zn2+ superoxide dismutase protects against early diabetic glomerular injury in transgenic mice. *Diabetes*. 2001;50:2114-2125

39. Federici M, Hribal ML, Menghini R, Kanno H, Marchetti V, Porzio O, Sunnarborg SW, Rizza S, Serino M, Cunsolo V, Lauro D, Mauriello A, Smookler DS, Sbraccia P, Sesti G, Lee DC, Khokha R, Accili D, Lauro R. Timp3 deficiency in insulin receptor-haploinsufficient mice promotes

diabetes and vascular inflammation via increased tnf-alpha. *J Clin Invest*. 2005;115:3494-3505

40. Babu D, Soenen SJ, Raemdonck K, Leclercq G, De Backer O, Motterlini R, Lefebvre RA. Tnf-alpha/cycloheximide-induced oxidative stress and apoptosis in murine intestinal epithelial mode-k cells. *Curr Pharm Des*. 2012

41. Meldrum KK, Misseri R, Metcalfe P, Dinarello CA, Hile KL, Meldrum DR. Tnf-alpha neutralization ameliorates obstruction-induced renal fibrosis and dysfunction. *Am J Physiol Regul Integr Comp Physiol*. 2007;292:R1456-1464

42. Guo G, Morrissey J, McCracken R, Tolley T, Klahr S. Role of tnfr1 and tnfr2 receptors in tubulointerstitial fibrosis of obstructive nephropathy. *Am J Physiol*. 1999;277:F766-772

43. Klahr S, Morrissey J. Obstructive nephropathy and renal fibrosis. *Am J Physiol Renal Physiol*. 2002;283:F861-875

44. Awad AE, Kandalam V, Chakrabarti S, Wang X, Penninger JM, Davidge ST, Oudit GY, Kassiri Z. Tumor necrosis factor induces matrix metalloproteinases in cardiomyocytes and cardiofibroblasts differentially via superoxide production in a pi3k{gamma}-dependent manner. *Am J Physiol Cell Physiol*. 2010;298:C679-692

45. Tejada T, Catanuto P, Ijaz A, Santos JV, Xia X, Sanchez P, Sanabria N, Lenz O, Elliot SJ, Fornoni A. Failure to phosphorylate akt in podocytes from mice with early diabetic nephropathy promotes cell death. *Kidney Int*. 2008;73:1385-1393

46. Liu GC, Oudit GY, Fang F, Zhou J, Scholey JW. Angiotensin-(1-7)-induced activation of erk1/2 is camp/protein kinase a-dependent in glomerular mesangial cells. *Am J Physiol Renal Physiol*. 2012;302:F784-790

CHAPTER FIVE

TIMP3 IS THE PRIMARY TIMP TO REGULATE AGONIST-INDUCED VASCULAR REMODELING AND HYPERTENSION

Ratnadeep Basu[1,3], Jiwon Lee[1,3], Jude S. Morton[1,2,3], Abhijit Takawale[1,3], Dong Fan[1,3], Vijay Kandalam[1,3], Xiuhua Wang[1,3], Sandra T. Davidge[1,2,3], Zamaneh Kassiri[1,3]

[1]Department of Physiology, [2]Department of Obstetrics/gynaecology, [3]Cardiovascular Research Center, Mazankowski Alberta Heart Institute, University of Alberta, Edmonton, Alberta, Canada

A modified version of this chapter has been published in *Cardiovascular Research*, 2013 June 1; 98(3): 360-371.

Author Contributions

Participated in Research Design: RB., S.T.D. and Z.K.
Conducted Experiments: R.B., J.L., J.S.M., A.T., D.F., V.K., X.W. and J.W.S.
Performed Data Analysis: R.B., J.L., J.S.M., D.F.,V.K., X.W. and Z.K
Contributed to the Writing of the Manuscript: R.B., J.S.M. and Z.K.

5.1 ABSTRACT

Hypertension is accompanied by structural remodeling of vascular extracellular matrix. Tissue inhibitor of metalloproteinase (TIMPs) inhibits matrix metalloproteinases (MMPs) that degrade the matrix structural proteins. In response to a hypertensive stimulus, the balance between MMPs and TIMPs is altered. We examined the role of TIMPs in agonist-induced hypertension.

We subjected TIMP-knockout mice to Angiotensin II (Ang II) infusion, and found that Ang II-induced hypertension in TIMP1$^{-/-}$, TIMP2$^{-/-}$ and TIMP4$^{-/-}$ mice was comparable to wildtype mice, but significantly suppressed in TIMP3$^{-/-}$ mice. *Ex vivo* pressure myography analyses on carotid and mesenteric arteries revealed that Ang II-infused TIMP3$^{-/-}$ arteries were more distensible with impaired elastic recoil compared to the wildtype group. The acute response to vasoconstriction and vasodilation was intact in TIMP3$^{-/-}$ mesenteric and carotid arteries. Mesenteric arteries from TIMP3$^{-/-}$-Ang II mice exhibited a reduced media-to-lumen ratio, suppressed collagen and elastin levels, elevated elastase and gelatinase proteolytic activities compared to WT-Ang II. TIMP3$^{-/-}$-Ang II carotid arteries also showed adverse structural remodeling. Treatment of mice with Doxycycline, a matrix metalloproteinase inhibitor, improved matrix integrity in mesenteric and carotid arteries in TIMP3$^{-/-}$-Ang II and differentially regulated elastin and collagen levels in WT-Ang II versus TIMP3$^{-/-}$-Ang II.

Our study demonstrates a critical role for TIMP3, among all TIMPs, is preserving arterial extracellular matrix in response to Ang II. It is critical to acknowledge that

the suppressed Ang II-induced hypertension in TIMP3$^{-/-}$ mice is not a protective mechanism but due to adverse remodeling in arterial matrix.

5.2 INTRODUCTION

Hypertension can lead to multiple-organ complications such as chronic kidney disease, cardiac hypertrophy and stroke. Blood pressure is determined mainly by cardiac output and peripheral vascular resistance; which is regulated by the constriction and dilation of peripheral arteries. Hypertension is associated with vascular remodeling characterized by rearrangement of vascular wall components including extracellular matrix (ECM) proteins. Arterial ECM is primarily comprised of elastin and collagen which provide significant structural support and recoil properties for the arteries.[1, 2] Vascular remodeling entails degradation and reorganization of the ECM; however, an imbalance in these two processes can result in pathological remodeling.

Degradation of existing structural proteins of the ECM occurs through the proteolytic function of matrix metalloproteinases (MMPs) which is kept in check by their physiological inhibitors, tissue inhibitor of metalloproteinases (TIMPs). Among the four TIMPs identified so far, TIMP3 is the only TIMP that is ECM-bound and could thereby exert tissue-specific effects.[3, 4] Further, a polymorphysm in TIMP3 (A-915G) showed a significant association with hypertension.[5] However, the direct role of TIMP3 in hypertension remains to be understood.

In this study, we investigated the role of TIMP3 in Angiotensin II (Ang II)-induced hypertension and remodeling of resistance and small conduit arteries that

are involved in mediating the hypertensive response. Ang II exerts direct effects on vascular remodelling and function.[6, 7] Our findings indicate that TIMP3-deficiency results in adverse structural remodelling of resistance and small conduit arteries which was inhibited by Doxycycline. Therefore, while the absence of TIMP3 suppresses Ang II-induced hypertension, this was not a protective effect but was associated with degradation of the structural ECM in the vasculature which could lead to adverse long-term outcomes.

5.3 OBJECTIVE

Hypertension is accompanied by structural remodeling of vascular extracellular matrix. Tissue inhibitor of metalloproteinase (TIMPs) inhibits matrix metalloproteinases (MMPs) that degrade the matrix structural proteins. In response to a hypertensive stimulus, the balance between MMPs and TIMPs is altered. My aim is to explore the role of TIMPs and their contribution in agonist induced hypertension.

5.4 MATERIALS AND METHODS

5.4.1 Experimental Animals and Procedures

Wildtype (WT) mice were purchased from Jackson Laboratories, and TIMP1$^{-/-}$ and TIMP2$^{-/-}$ mice were purchased from Jackson Laboratories, and TIMP4$^{-/-}$ mice from Texus Institute for Genomic Medicine (TIGM). TIMP3$^{-/-}$ mice were generated as described.[8] All mice are in pure C57BL/6 background. Alzet micro-osmotic pumps containing either Ang II (Sigma-Aldrich) or saline (control) were implanted (Chapter 2.2.1) in 8-week old male mice of various genotypes for 14

days.[6, 9, 10] Doxycycline was delivered by daily oral gavage (50 mg/kg/day).[11] All experiments were conducted in accordance with the guidelines of the University of Alberta Animal Care and Use Committee (ACUC) and the Canadian Council of Animal Care.

5.4.2 Blood Pressure Measurement

Blood pressure was measured noninvasively in conscious mice using the tail-cuff method (Chapter 2.5.4.)

5.4.3 Histological Analyses

After two weeks of Ang II or saline infusion, mice were perfuse-fixed at 80 mmHg with paraformaldehyde after a PBS wash as previously described.[12] This pressure, although lower than the systolic pressure in the mice at the time of euthanasia, was used in all groups for consistency and to prevent the small arteries from collapsing during tissue collection. Subsequently, carotid and mesenteric arteries were dissected out (Chapter 2.3.3), further fixed in 10% buffered formalin for 48 hours and paraffin-embedded. Using 5 μm paraffin-embedded sections, carotid arteries were stained with Gomori Trichrome (Chapter 2.10.2) or Verhoeff-Van Geison (Chapter 2.10.10), and mesenteric arteries with Pentachrome to visualize structural changes. Media-to-lumen ratio was determined as follows. The outer cross-sectional area of the mesenteric arteries (at the outer elastic lamina) and the lumen cross-sectional area were calculated. Medial area was obtained as the difference between these two cross-sectional

areas. The ratio of medial to lumen cross-sectional area is reported as the media-to-lumen ratio.

5.4.4 *Ex vivo* Vascular Function

Mesenteric or carotid arteries, were subjected to pressure myograph to study vascular function and compliance (Chapter 2.6.1) including vasoconstrictor and dilator responses (Chapter 2.6.2) and passive charecteristics (Chapter 2.6.3).

5.4.5 Protein Extraction for Western Blot Analysis, Gelatin Zymography and Activity Assays

Mesenteric and carotid arteries from 3 mice were pooled to extract sufficient protein (Chapter 2.14.1) for one sample in *in vitro* protein analyses for immunoblotting (Chapter 2.14.2), gelatin zymography (Chapter 2.14.3) and enzymatic activity assays (Chapter 2.15).

5.4.6 mRNA Expression Analysis by TaqMan Real-time PCR

RNA was extracted from flash-frozen mesenteric or carotid arteries and mRNA expression levels of genes of interest were determined by TaqMan real-time PCR (Chapter 2.13.2.). The primers and probes for the reported genes are detailed in Table 2.2.

5.4.7 Statistical Analysis

All averaged values are represented as mean ± SEM. All data were normally distributed (Kolmogorov-Smirnov test for Gaussian distribution). Stress-strain relationships were analyzed by comparing the averaged rate constants (mean ± SEM) between groups by Student t-test. The functional data in *ex vivo* vascular

experiments are the percentage maximal vasoconstrictor or vasodilator response calculated as a percentage of constrictor tone. Statistical difference in the continuous variables between groups was determined by a two-way analysis of variance (ANOVA), with Bonferroni post-test for multiple comparisons. Comparisons between different genotypes were performed using multiple comparison ANOVA test followed by Student Neuman-Keuls post-test. Statistical significance was recognized at $p<0.05$. All other statistical analyses were performed using SPSS software (Chicago, Illinois, Version 10.1).

5.5 RESULTS

5.5.1 TIMP3-deficiency Markedly Impacts the Ang II-induced Hypertensive Response

In WT mice, Ang II triggered a rise in blood pressure within 2 days of osmotic pump implantation, which reached a plateau by day 10 (**Fig. 5.1A**). We investigated the role of each TIMP in the Ang II-induced hypertensive response by similarly subjecting TIMP1$^{-/-}$, TIMP2$^{-/-}$, TIMP3$^{-/-}$ and TIMP4$^{-/-}$ mice to 2 weeks of Ang II infusion. Body weights were comparable among genotypes after 2 weeks of saline (WT: 24.9±1.1 g; TIMP1$^{-/-}$: 24.1±0.4 g; TIMP2$^{-/-}$: 24.2±0.2 g; TIMP3$^{-/-}$: 24.6±0.9 g; TIMP4$^{-/-}$: 24.6±0.8 g) or Ang II infusion (WT: 25.3±0.4 g; TIMP1$^{-/-}$: 23.7±0.3 g; TIMP2$^{-/-}$: 24.2±0.2 g; TIMP3$^{-/-}$: 23.7±0.3 g and TIMP4$^{-/-}$: 24.7±0.3 g). We found that while mice lacking TIMP1$^{-/-}$, TIMP2$^{-/-}$ or TIMP4$^{-/-}$ exhibited a rise in blood pressure comparable to WT mice, this response was significantly suppressed in TIMP3$^{-/-}$ mice (**Fig. 5.1A**) as also evident by the

percent change in blood pressure (**Fig. 5.1B**). TIMP3$^{-/-}$ mice also showed a lower baseline blood pressure (93.8±1.7 mmHg) compared to WT (103.6±1.6 mmHg) and other TIMP-deficient mice (TIMP1$^{-/-}$: 99.2±0.8; TIMP2$^{-/-}$: 101.1±0.3; and TIMP4$^{-/-}$: 101.5±0.9 mmHg).

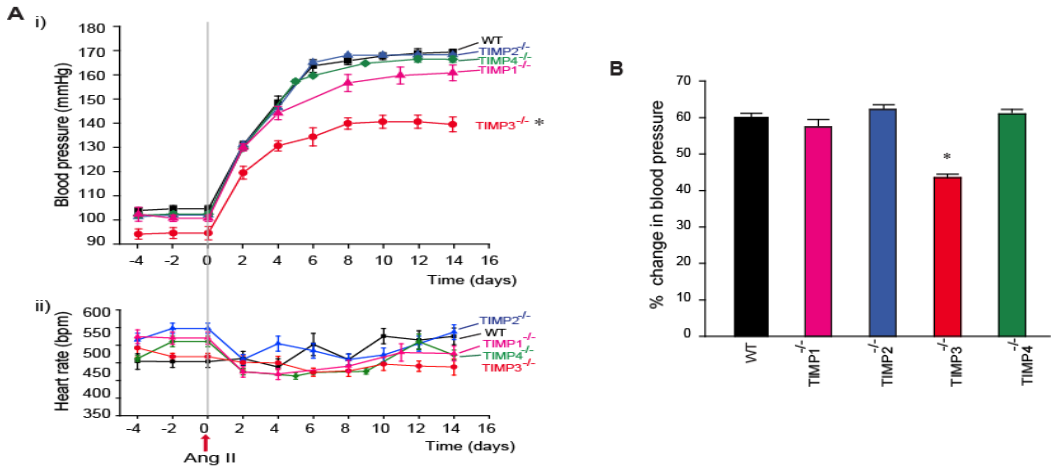

Figure 5.1 TIMP3-deficient mice exhibit suppressed hypertensive response *in vivo*, to Ang II infusion.
A) Systolic blood pressure (i) and heart rate measurements (ii) in WT, TIMP1$^{-/-}$, TIMP2$^{-/-}$, TIMP3$^{-/-}$ and TIMP4$^{-/-}$ mice before and after Ang II infusion. The arrow shows the start of Ang II infusion. B**)** Percentage change in systolic blood pressure at 14-days post-Ang II infusion in indicated genotypes. n=12/genotype. Presented values are mean±SEM. *p<0.05 compared to WT-Ang II. n=3-5/group/genotype.

5.5.2 TIMP3-deficient Mesenteric Arteries Become More Distensible Following Ang II-infusion

To understand the underlying cause of blunted Ang II-induced response in TIMP3$^{-/-}$ mice, we used the *ex vivo* pressure myography system to examine the mechanical properties of mesenteric resistance arteries in TIMP3$^{-/-}$ compared to WT mice. We measured changes in arterial diameter as a function of increasing pressure; 0 to 140 mmHg (mesenteric) in 20 mmHg increments (passive curve). After two weeks of Ang II infusion, mesenteric arteries from both genotypes showed decreased distensibility compared to their corresponding saline group

(**Figs. 5.2Ai-ii**). However, the pressure-dependent increase in diameter was significantly greater in TIMP3$^{-/-}$-Ang II mesenteric arteries (**Fig. 5.2Ci**) and was accompanied by a rightward shift in circular stress-strain relationship compared to WT-Ang II mesenteric arteries (rate constant=8.58±0.48 in TIMP3$^{-/-}$-Ang II vs. 9.56±0.89 in WT-Ang II) (**Fig. 5.2Cii**). Comparing the saline-treated mesenteric arteries showed a greater increase in passive pressure-diameter changes and a rightward shift in circular stress-strain relationship in TIMP3$^{-/-}$ compared to WT group (**Figs. 5.2Aiii and 5.2Biii**). The circumferential stress-strain relationship is a measure of mechanical changes in the vascular wall,[13, 14] and a rightward shift in this curve in the TIMP3$^{-/-}$ mesenteric arteries indicates that TIMP3$^{-/-}$ mesenteric arteries are more expandable than WT mesenteric arteries.

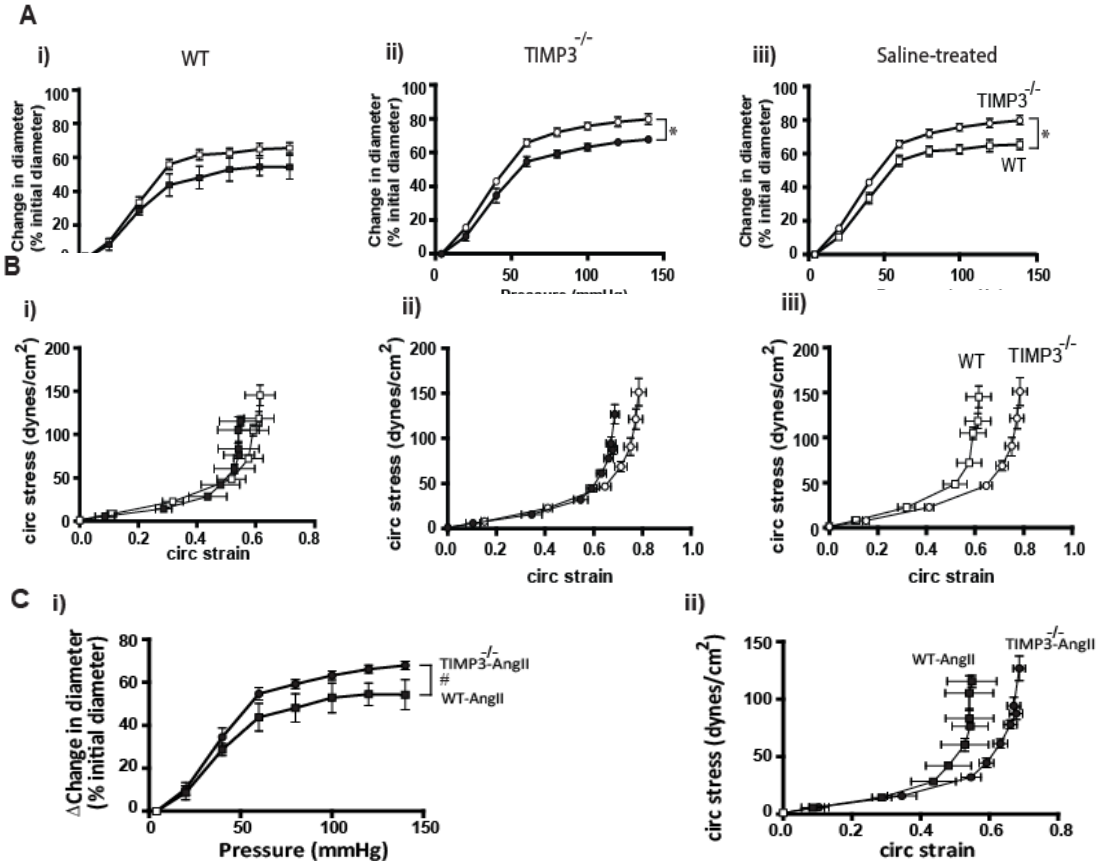

Figure 5.2 Mesenteric arteries from TIMP3-deficient mice are more expandable resistant arteries compared to WT (*ex vivo*) following Ang II-infusion.

A) *Ex vivo* analyses of the pressure-diameter of mesenteric arteries in Ang II compared to saline treated WT (i), TIMP3$^{-/-}$ (ii) and only saline treated WT and TIMP3$^{-/-}$ (iii). B) circular stress-strain relationship of mesenteric arteries in Ang II compared to saline treated WT (i), TIMP3$^{-/-}$ (ii) and only after saline treatment in WT and TIMP3$^{-/-}$. C) Passive pressure myography showing pressure-dependent changes in lumen diameter of mesenteric arteries (i) and circular stress-strain relationship of mesenteric arteries (ii) after 2-weeks of Ang II infusion in TIMP3$^{-/-}$ compared to WT group.

5.5.3 Carotid Arteries Become More Distensible Following Ang II-infusion in TIMP3-deficient Mice.

Alterations in carotid arteries have been shown to correlate with Ang II-induced changes in blood pressure in mice,[6] as such we examined the mechanical properties of the carotid arteries by measuring changes in lumen diameter as a function of increasing pressure; 0 to 180 mmHg (carotid) in 20 mmHg increments (passive curve). Two weeks of Ang II-infusion resulted in a downward shift in the pressure-diameter relationship in carotid arteries of both genotypes compared to their corresponding saline-infused group, although only in the TIMP3$^{-/-}$ group this difference reached statistical significance (**Fig. 5.3Ai-ii**), and consistently, the pressure-dependent increase in diameter was greater in TIMP3$^{-/-}$-Ang II compared to WT-Ang II carotid arteries (**Fig. 5.3Ci**). The circumferential stress-strain curve showed a significant leftward shift for carotid arteries from TIMP3$^{-/-}$-Ang II (rate constant=3.4±0.2), but not WT-Ang II (rate constant=3.7±0.2) compared to their corresponding saline group (TIMP3$^{-/-}$-saline=2.4±0.3, WT-saline=2.8±0.2) (Figure 5.3Bi-ii). However, this relationship was comparable between Ang II-infused (Figure 5.3Cii), and saline-infused (**Fig. 5.3Biii**) WT and TIMP3$^{-/-}$ carotid arteries.

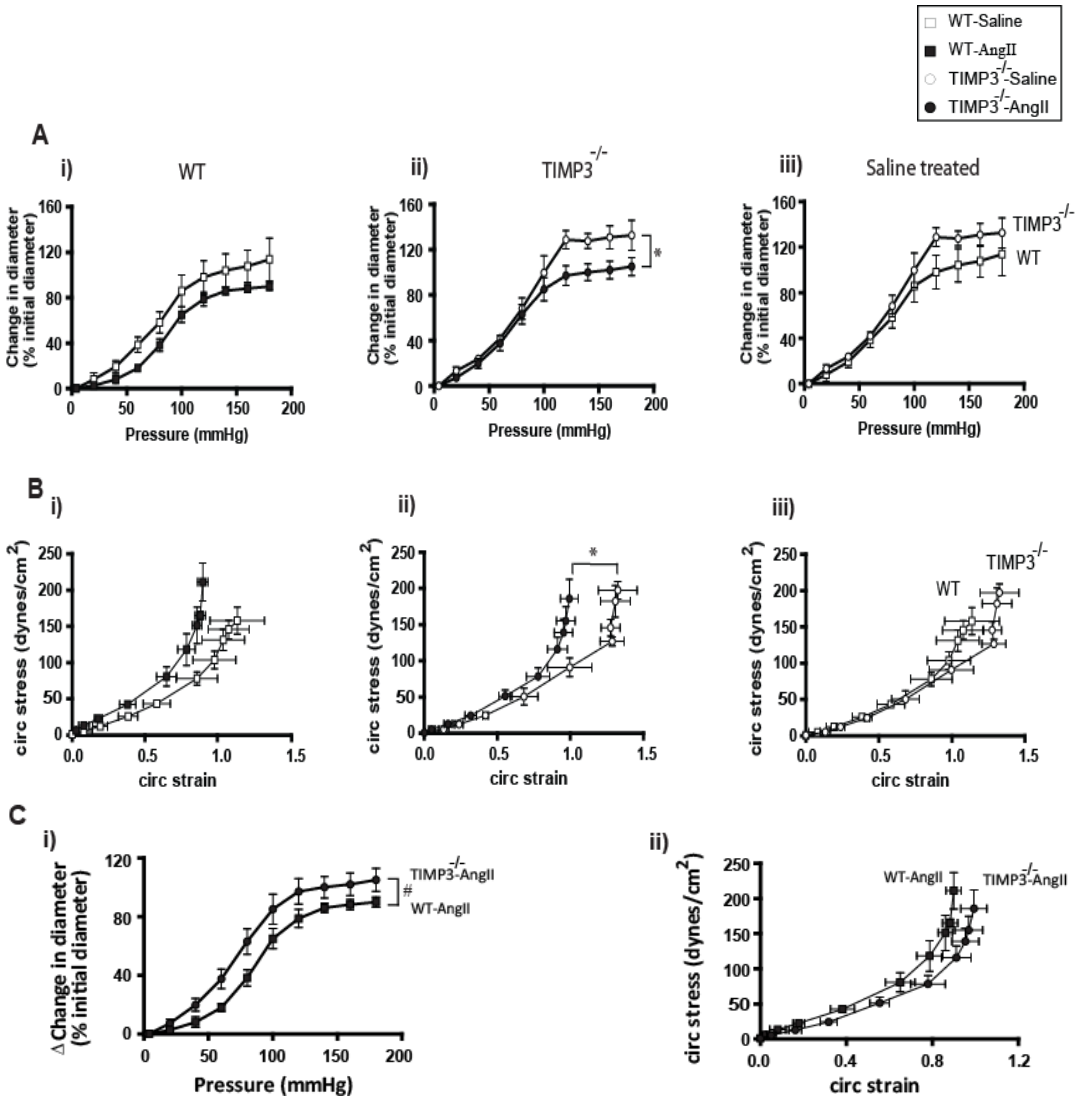

Figure 5.3 TIMP3-deficient carotid arteries become more flaccid compared to WT (*ex vivo*) after 2 weeks of Ang II infusion

A) *Ex vivo* analyses of the pressure-diameter relationship in the carotid arteries of WT-Ang II compared to WT-saline (i), TIMP3 deficient Ang II compared to saline infused group (ii) and WT-saline compared to TIMP3 deficient saline (iii). B) *Ex vivo* stress-strain relationship in WT-saline compared to WT-Ang II carotid arteries (i), TIMP3 deficient saline compared to TIMP3 deficient Ang II group (ii) and only after saline treatment in WT and TIMP3 deficient carotid arteries. C) Pressure myography (i), and the circular stress-strain relationship in carotid arteries (ii) after two weeks of Ang II infusion in TIMP3$^{-/-}$ compared to WT mice.

5.5.4 TIMP3 Deficiency Did not Affect Acute Vascular Responses to Pharmacological Induced Vasoconstriction or Dilation.

The acute vasoconstriction and vasodilation responses were unaltered in TIMP3$^{-/-}$ arteries, as evident by comparable EC_{50} and E_{max} in response to increasing doses of phenylephrine (PE) or methylcholine (MCh), respectively (**Fig.5.4**). These data collectively indicate that Ang II infusion resulted in structural changes in TIMP3$^{-/-}$ mesenteric and carotid arteries rendering them more distensible compared to WT groups.

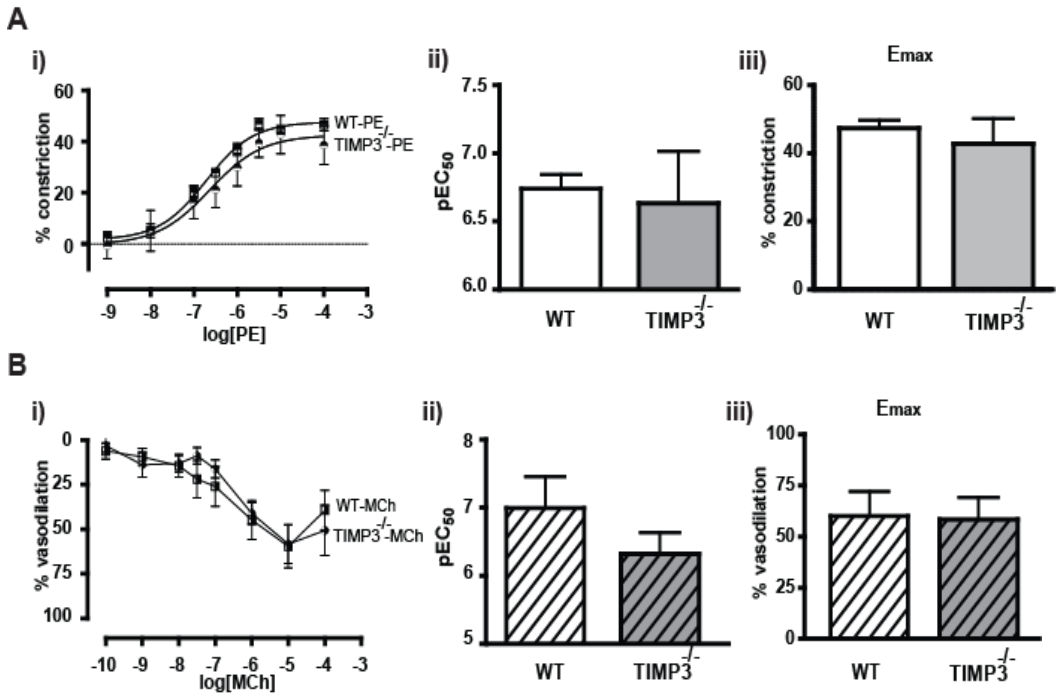

Figure 5.4 Comparable acute vasoconstriction and vasodilation responses between WT and TIMP3-deficient mesenteric arteries.

A) Dose-dependent vasoconstriction in response to increasing doses of phenylephrine (PE, 0.001 to 100 mol/L (i), peak EC50 (ii) and Emax(iii). B) *Ex vivo* stress-strain relationship in WT-saline compared to WT-Ang II carotid arteries (i), B) Dose-dependent vasodilation in response to an increasing concentration of methacholine (Mch, 0.0001 to 100 mol/L (i), and the corresponding EC50 (ii) and Emax(iii).

5.5.5 Adverse Ang II-mediated Remodeling in TIMP3-deficient Mesenteric Arteries

Hypertension is accompanied by vascular ECM remodelling.[2, 15] TIMP3 is an ECM-bound TIMP and has been demonstrated to be a key molecule in regulating ECM structure in different organs and diseases.[8, 16, 17] We examined if Ang II-mediated ECM remodeling was altered in TIMP3$^{-/-}$ mesenteric arteries. Verhoeff-Van Gieson staining of perfuse-fixed mesenteric arteries showed that Ang II infusion increased the medial thickness as shown by increased media-to-lumen ratio (**Figs. 5.5Ai-ii**). However, this ratio was significantly reduced in TIMP3$^{-/-}$-Ang II mesenteric arteries compared to WT-Ang II (**Figs. 5.5Ai-ii**) due to reduced medial thickness and increased lumen diameter (**Fig. 5.5Aiii**). Consistently, the protein levels of collagen and elastin, two major arterial ECM proteins,[2] were markedly lower in TIMP3$^{-/-}$-AngII compared to WT-Ang II mesenteric arteries (**Figs. 5.5B and 5.5C**). This reduced structural support could reduce the structural integrity of the mesenteric arteries causing them to expand.

5.5.6 Proteolysis by Elastase and Gelatinase Underlies Vascular Remodeling in TIMP3-deficient Mesenteric Arteries

In order to determine if the reduced ECM protein levels in TIMP3$^{-/-}$-Ang II mesenteric arteries were due to enhanced proteolysis, we measured the proteolytic activities in these arteries and found that Ang II infusion increased gelatinase (**Fig. 5.6Ai**) and elastase (**Fig. 5.6Aii**) activity in both genotypes; however this increase was significantly greater in TIMP3$^{-/-}$ mice. *In vitro* gelatin zymography further

showed greater MMP2 activation in TIMP3$^{-/-}$-Ang II mesenteric arteries while MMP9 levels were comparable among all groups (**Fig. 5.6B**).

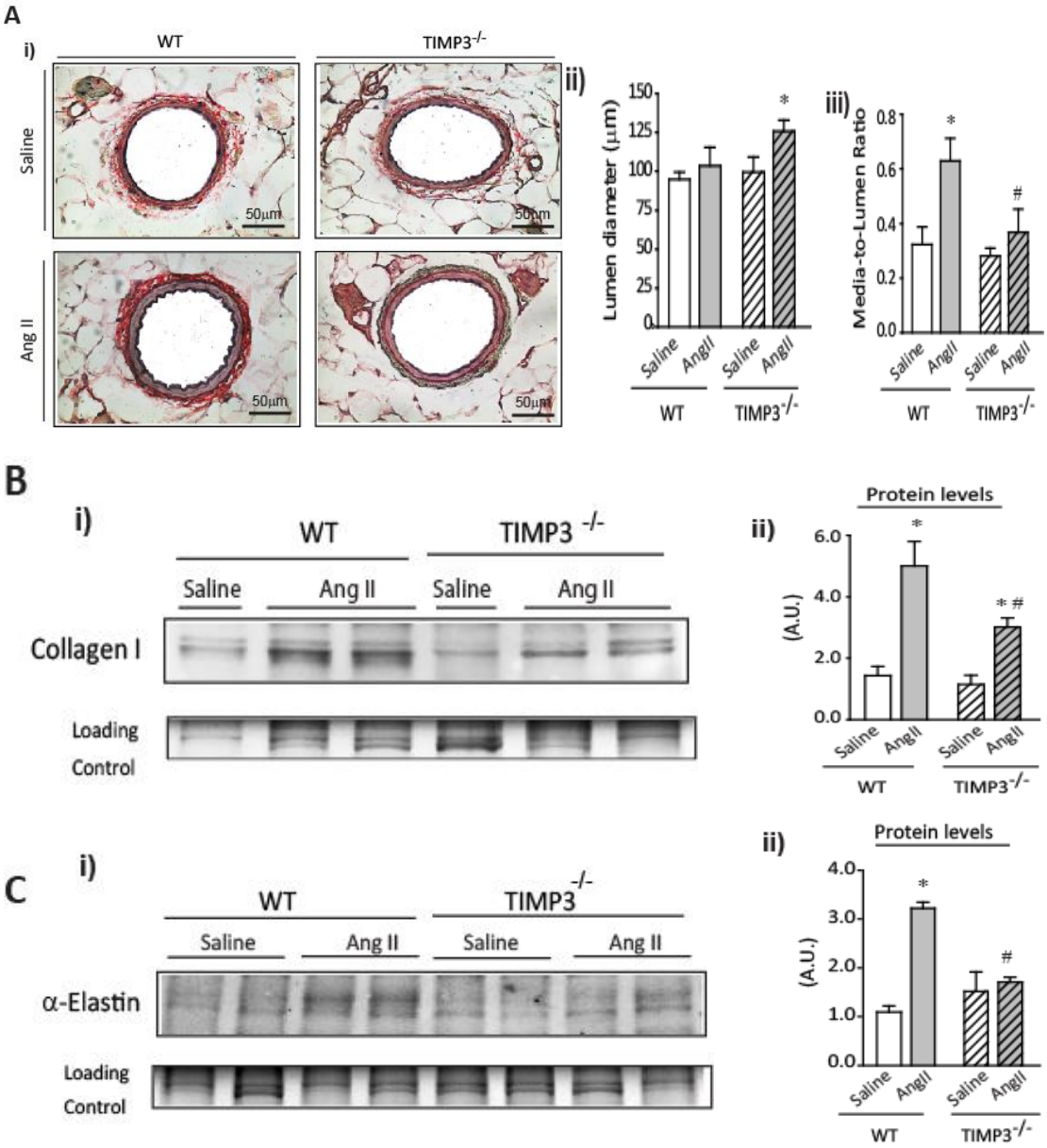

Figure 5.5 Excessive degradation of elastin and collagen in TIMP3$^{-/-}$-AngII mesenteric arteries.

A) Representative Pentachrome-stained mesenteric arteries (i), media-to-lumen ratio (ii) and lumen diameter (iii) in WT and TIMP3$^{-/-}$ mice following saline or AngII infusion. B) Representative Western blot for collagen type-1 (i), and averaged protein content (ii). C) Representative Western blot for α-elastin (i) and averaged elastin protein content (ii). For Western Blots, mesenteric arteries from 3 animals were pooled to yield sufficient protein for one sample; n=6/saline group/genotype, 12/Ang II group/genotype. Coomassie blue staining was used as the

loading control for Western blots. A.U. = Arbitrary Units. Presented values are Mean ± SEM. * p<0.05 compared to corresponding saline group. # p<0.05 compared to WT-Ang II.

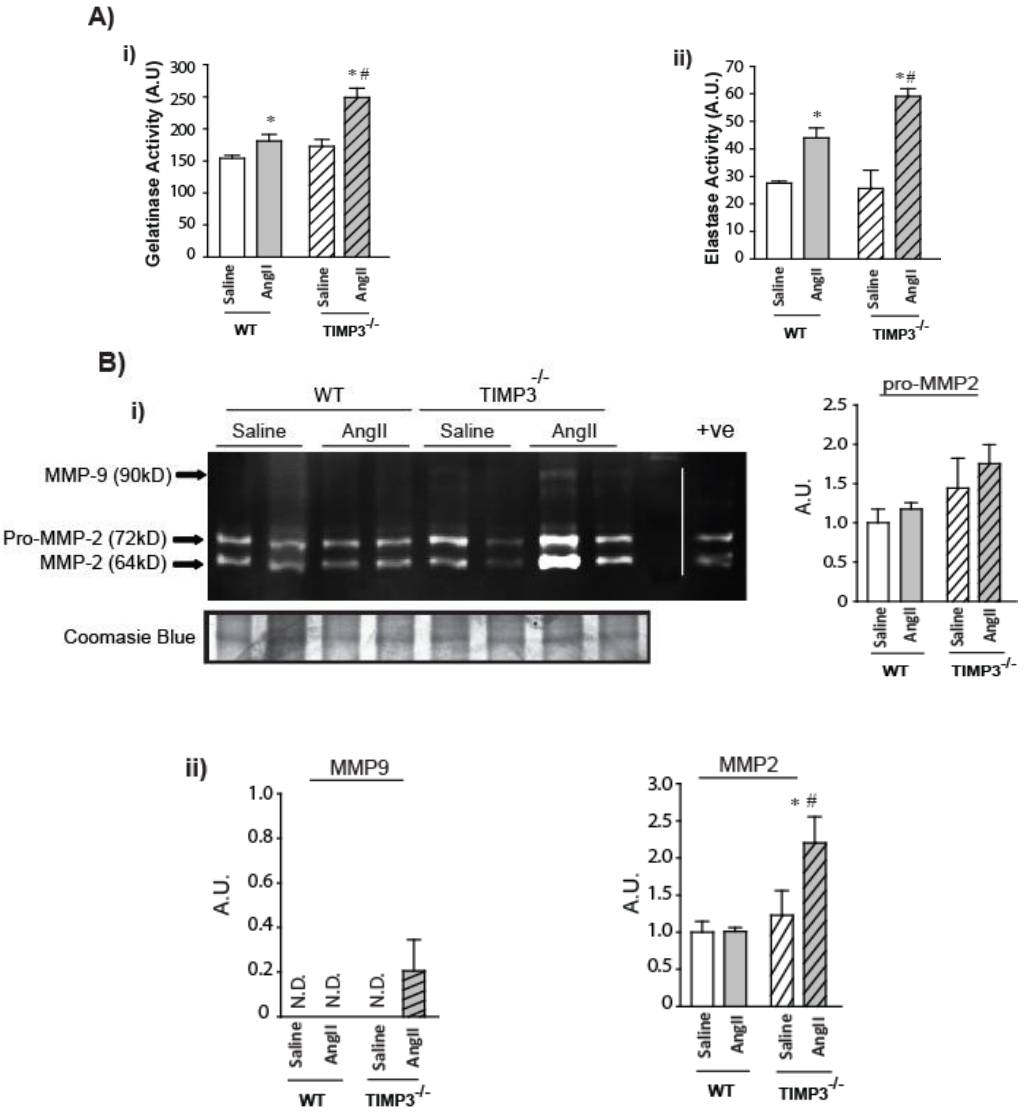

Figure 5.6 Increased proteolytic activities in TIMP3$^{-/-}$ mesenteric arteries.
A) Total gelatinase (i) and elastase activity (ii) in the mesenteric arteries of WT and TIMP3$^{-/-}$ mice after saline or Ang II infusion, n=5/genotype/group. B) Representative gelatin zymography (i) and averaged band intensities for MMP9, pro-MMP2 and cleaved MMP2 (ii) after 2 weeks of saline or Ang II infusion in WT and TIMP3$^{-/-}$ mice. n=12/group/genotype (protein from 3 animals/lane, averaged data from 4 lanes/group). A.U. = Arbitrary Units. Presented values are Mean ± SEM. * p<0.05 compared to corresponding saline group. # p<0.05 compared to WT-Ang II.

5.5.7 Ang II-mediated Remodeling in TIMP3-deficient Carotid Arteries

In order to determine if TIMP3-deficiency affected Ang II-induced remodeling in other small arteries, we studied the carotid arteries. VVG staining showed disorganized and interrupted elastin fibres in TIMP3$^{-/-}$-Ang II carotid arteries (**Fig. 4Ai**). Consistently, elastin protein levels were significantly lower (**Figs. 4Aii-iii**); although its mRNA levels were markedly greater (**Figs. 4A-iv**) in TIMP3$^{-/-}$-Ang II compared to WT-Ang II. Similarly, trichrome staining for ECM collagen fibres showed more disorganized arrangements (**Fig. 4Bi**), and reduced collagen I protein levels (**Figs. 4Bii-iii**) despite a significant elevation in mRNA levels (**Fig. 4Biv**) in TIMP3$^{-/-}$-Ang II compared to WT-Ang II carotid arteries. These data suggest that the decrease in elastin and collagen proteins in TIMP3-deficient carotid arteries is most likely due to post-translational degradation of these proteins rather than decreased synthesis.

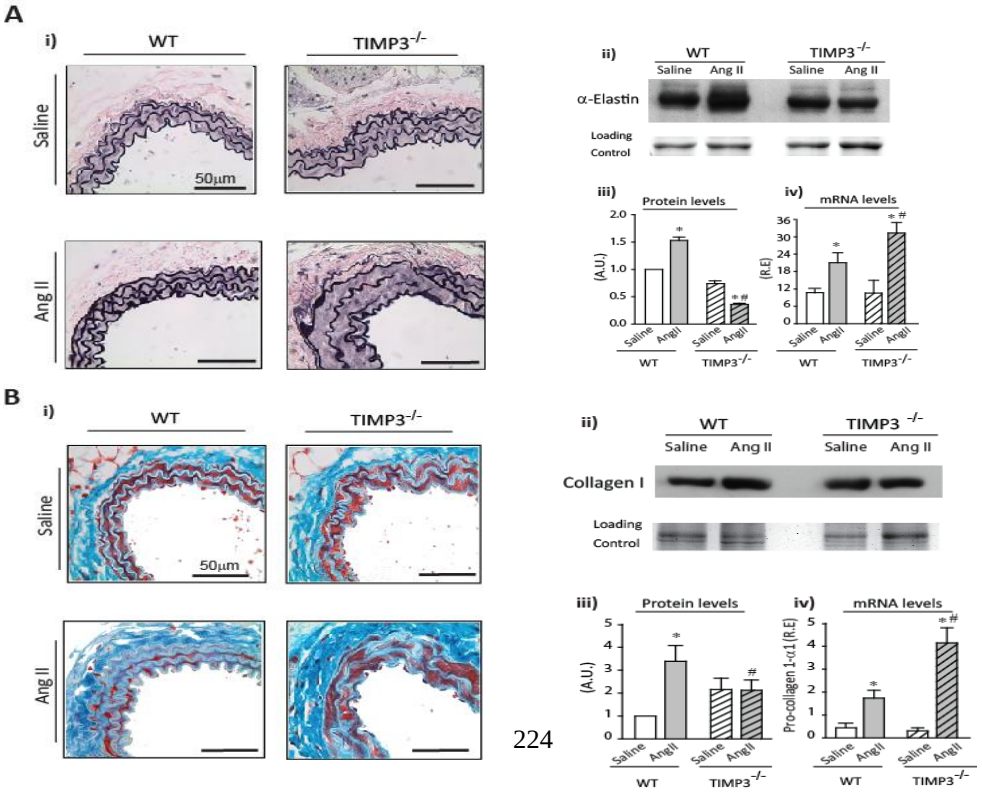

Figure 5.7 Excess degradation of vascular matrix proteins in carotid arteries of Ang II-infused TIMP3$^{-/-}$ mice.

A) Representative VVG-stained carotid arteries (i), representative Western blot for α-elastin (ii), quantification of elastin protein content (iii) and mRNA expression of elastin (iv) in WT and TIMP3$^{-/-}$ mice after saline or Ang II infusion. B) Representative Trichrome-stained carotid arteries (i), representative Western blot for collagen type I (ii), quantification of collagen protein content (n=12/group, protein from 3 animals/lane, averaged data from 4 lanes/group) (iii), and mRNA expression of pro-collagen 1-α1 (n=5/group/genotype) (iv) in WT and TIMP3$^{-/-}$ mice after saline or Ang II infusion. A.U.=Arbitrary Units, R.E.=Relative Expression. Presented values are Mean ± SEM. * $p<0.05$ compared to corresponding saline group. # $p<0.05$ compared to WT-Ang II.

5.5.8 Ang II-mediated Remodeling in TIMP3-deficient Carotid Arteries is Due to Differential Increase in Elastase Activity

In assessing the proteolytic activities in the carotid arteries, we found that gelatinase activity was comparably elevated following Ang II infusion in both genotypes (**Fig. 5.8Ai**), whereas the increase in elastase activity was significantly greater in TIMP3$^{-/-}$-Ang II compared to WT-Ang II group (**Fig. 5.8Aii**). *In vitro* gelatin zymography showed that Ang II infusion resulted in a similar rise in MMP9 levels, but a greater increase in cleaved MMP2 levels in TIMP3$^{-/-}$ carotid arteries (**Figs. 5.8Bi-ii**).

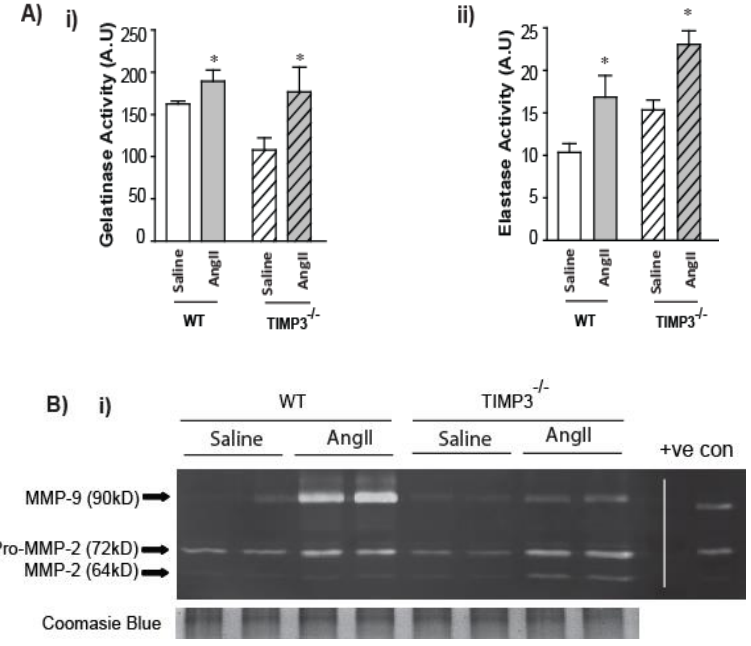

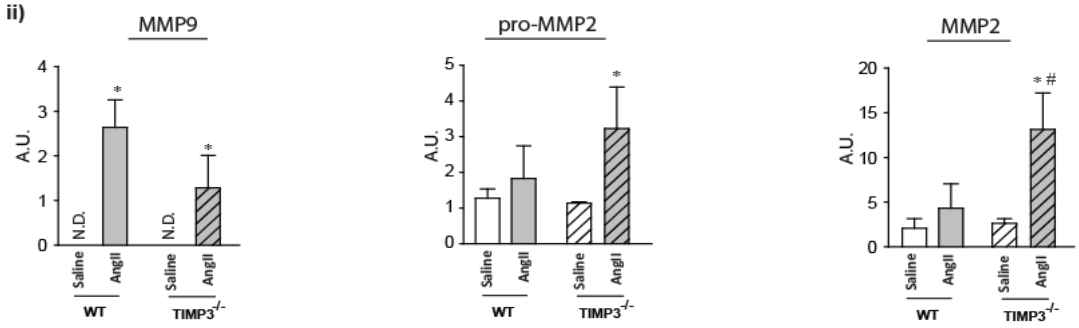

Figure 5.8 Proteolytic activities in TIMP3$^{-/-}$ carotid arteries following Ang II infusion.

A) collagenase (i) and elastase activity (ii) (n=6/group/genotype). B) Representative gelatin zymography, and C) averaged band intensity for MMP9, pro-MMP2 and cleaved MMP2 in WT and TIMP3$^{-/-}$ carotids after 2 weeks of saline or Ang II infusion (n=8/group/genotype (protein from 2 animals/lane, averaged data from 3 lanes/group). Coomassie blue was used as the loading control. A.U. = Arbitrary units. Presented values are Mean ± SEM. * $p<0.05$ compared to corresponding saline group. # $p<0.05$ compared to WT-Ang II.

5.5.9 Doxycycline Prevents the Aberrant Arterial ECM Degradation in TIMP3$^{-/-}$ mice

Next, we aimed to determine if excess proteolysis in the absence of TIMP3 is in fact the cause of the adverse ECM remodeling in TIMP3$^{-/-}$ resistance arteries following Ang II-infusion. Treatment with the well-known MMP inhibitor, Doxycycline,[18] preserved the structural integrity of mesenteric and carotid arteries in Ang II-infused TIMP3$^{-/-}$ mice (**Fig. 5.9**). The reduction in media-to-lumen ratio (**Figs. 5.9Ai-ii**) and lumen dilation (**Fig. 5.9Aiii**) observed in TIMP3$^{-/-}$-Ang II mesenteric arteries were prevented, while structural integrity of elastin and collagen fibres were preserved with Doxycycline treatment as shown by Trichrome and VVG-stained carotid arteries (**Figs. 5.9Bi-ii**) and the reduced number of elastin fibre breakage (**Fig. 5.9Biii**).

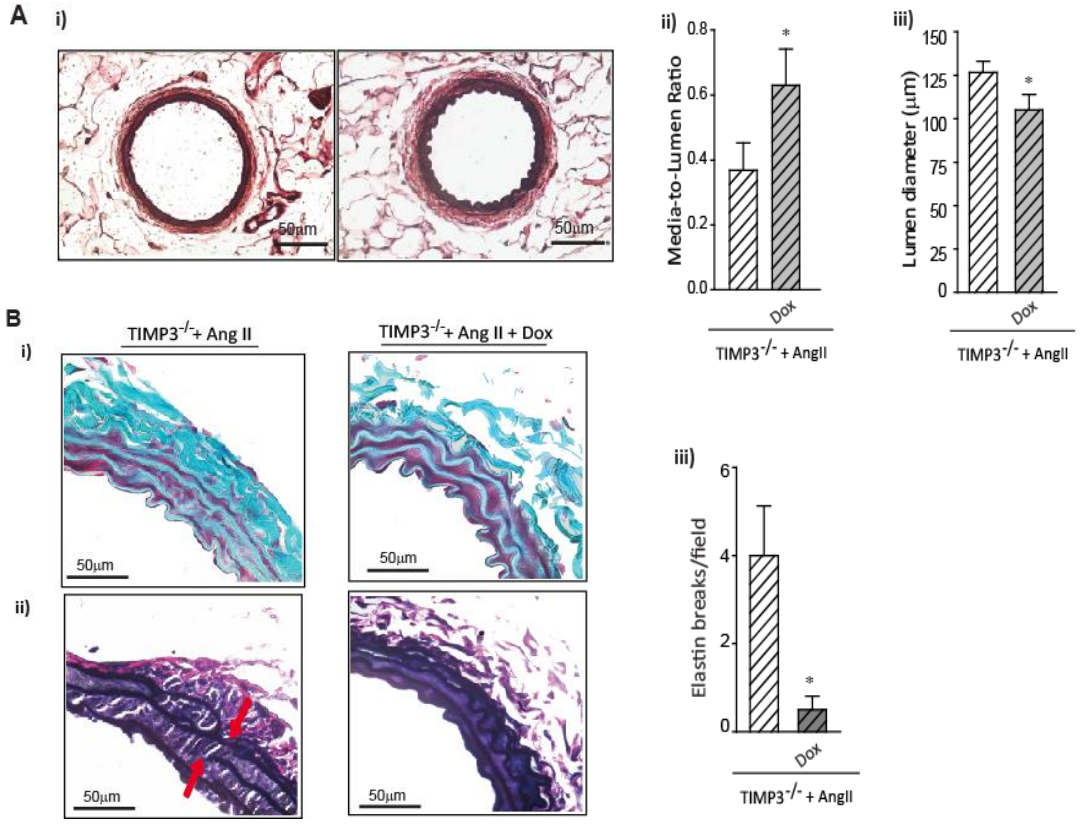

Figure 5.9 Treatment with Doxycycline, a broad spectrum MMP inhibitor, prevented the adverse remodeling in small arteries in TIMP3$^{-/-}$-Ang II mice.
A) Representative mesenteric arteries (i), media-to-lumen ratio (ii), and lumen diameter (iii) in Ang II-infused TIMP3$^{-/-}$ mice without and with doxycycline treatment, n=6/group. B) Representative trichrome staining for collagen fibers (i) and Verhoeff-Van Geison staining for elastin fibres (ii), averaged number of broken elastin fibres (iii) in TIMP3$^{-/-}$-Ang II carotid arteries from mice treated with saline or Doxycycline. * $p<0.05$ compared to TIMP3$^{-/-}$-Ang II.

5.5.10 Differential Regulation of Mesenteric and Carotid Structural Proteins by Doxycycline in WT Versus TIMP3$^{-/-}$ Mice.

Doxycycline treatment resulted in a marked increase in elastin and a significant reduction in collagen levels in WT-Ang II mesenteric arteries, whereas in TIMP3$^{-/-}$-Ang II group, collagen levels increased while elastin levels remained unchanged (**Figs. 5.10Ai and Aii**). In carotid arteries, on the other hand, doxycycline treatment markedly reduced both, elastin (**Fig. 5.10Bi**) and collagen protein levels (**Fig. 5.10Bii**) in WT-Ang II mice but not in TIMP3$^{-/-}$-Ang II mice (**Figs. 5.10Bi-**

ii). This differential impact of doxycycline on expression of vascular ECM proteins in WT versus TIMP3$^{-/-}$ mice could underlie the resulting changes in blood pressure in these two groups. Doxycycline treatment attenuated the Ang II-induced hypertension in WT mice while causing a small but significant increase in blood pressure in TIMP3$^{-/-}$ mice (**Fig.5.10C**). Overall, the protective effects of doxycline on vascular ECM integrity of TIMP3$^{-/-}$-Ang II mice indicate that the inhibitory function of TIMP3 against proteinases in the small arteries becomes more critical in the presence of a stimulus, such as elevated Ang II.

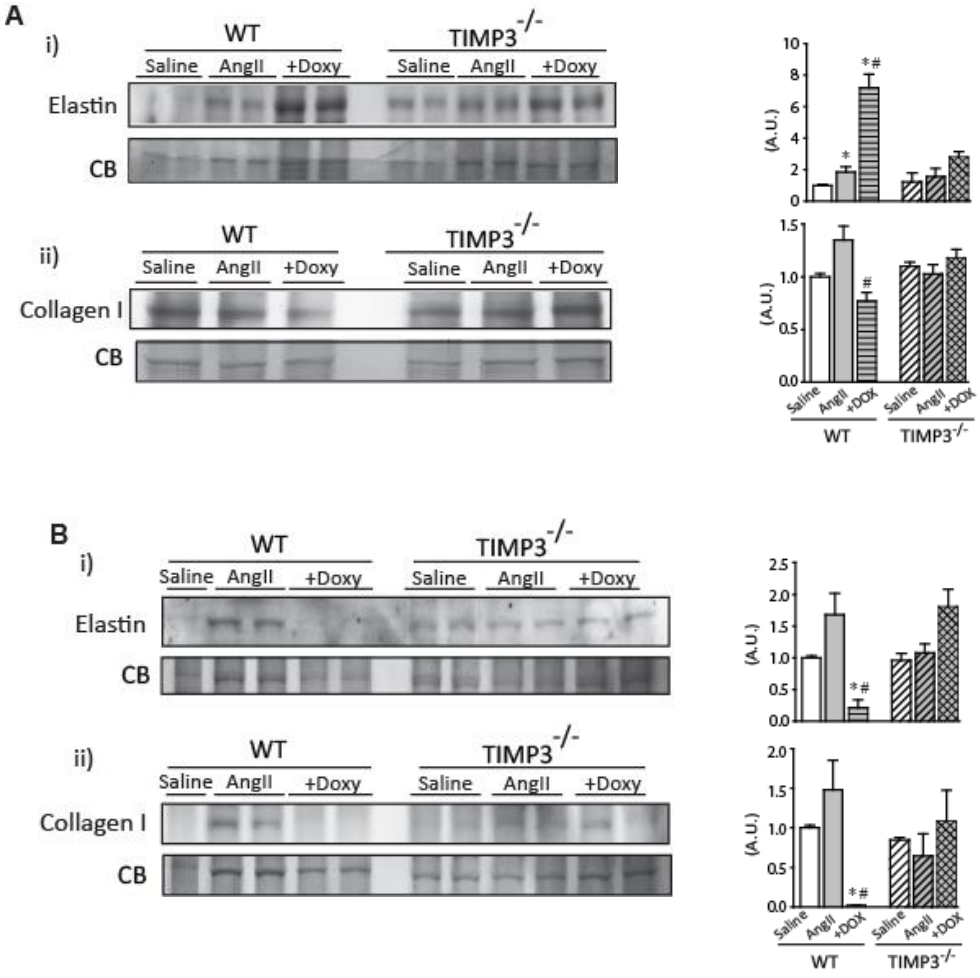

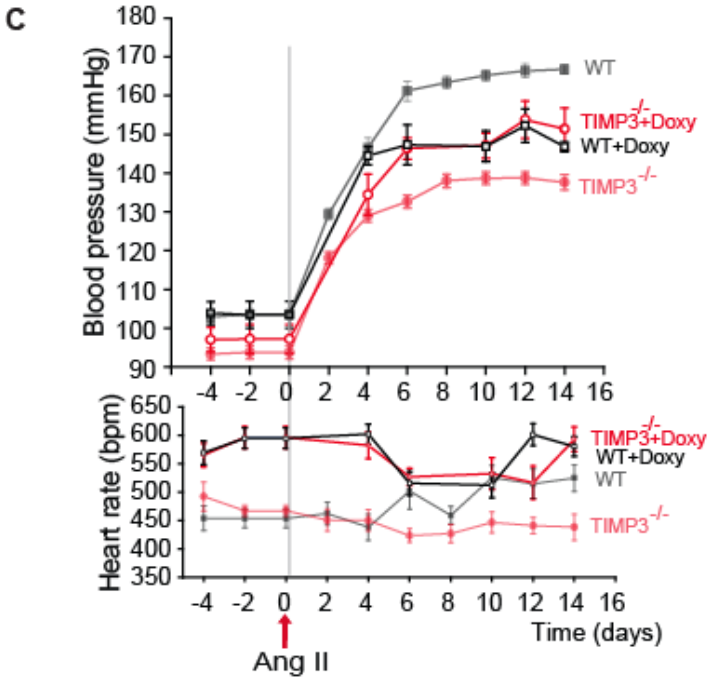

Figure 5.10 Treatment with doxycycline differentially influenced elastin and collagen proteins in WT and TIMP3$^{-/-}$ arteries.

Representative Western blot and averaged protein levels for elastin (i) and collagen (ii) in mesenteneric. A) and carotid arteries. B) in saline-, and Ang II-infused WT and TIMP3$^{-/-}$ mice without and with doxycycline treatment, n=3-6/group/genotype. C) Systolic blood pressure in doxycycline-treated WT and TIMP3$^{-/-}$ mice before and after Ang II infusion. The data presented earlier is shown in a faded shade. n=12/group, * $p<0.05$ compared to the corresponding saline group, # $p<0.0.5$ compared to corresponding group without doxycycline treatment.

5.6 DISCUSSION

Hypertension is the primary risk factor for all mortalities worldwide and contributes to approximately 7.5 million deaths annually.[19, 20] Hypertension is associated with vascular remodelling prior to the onset of clinical symptoms, and as such called the "silent killer". Vascular remodeling is an adaptive response to changes in the blood pressure-induced circumferential wall stress, elastin-dependant axial stress, and blood flow induced wall shear stress.[21] While vessel wall rigidity, which manifests as an increase in pulse wave velocity, is regarded as an independent predictor of mortality in hypertension and related diseases,[22] *ex*

vivo studies on animal models indicate that distensibility of conductance arteries (carotids) during the early stages of hypertension is associated with vascular remodelling.[21] Hypertensive vascular remodelling is an active process of structural alterations including degradation and reorganization of the vascular ECM proteins, such as collagen, elastin, proteoglycan, and fibronectin.[23] Matrix metalloproteinases (MMP) are a family of zinc dependant proteases that contribute to ECM turnover by degrading existing proteins. MMPs are well regulated at levels of expression, translation, post-translational modification, and inhibition of their activated form by TIMPs.[24, 25] Levels of MMPs and TIMPs have been shown to be altered in hypertension in animal models[6, 26-28] as well as in hypertensive patients.[29, 30] TIMP1 and TIMP2 levels were increased in rat aorta following Ang II infusion,[31, 32] TIMP2 expression was elevated in the aorta of DOCA-salt hypertensive rats,[33] while elevated plasma levels of TIMP1, MMP2 and MMP9 were detected in hypertensive patients.[34] A population study in 1000 individuals of 50-65 years of age reported that a TIMP3 polymorphism (T-1296C), but not TIMP1 or TIMP2 polymorphisms, showed a significant association with hypertension.[5] However, a direct role for TIMPs in hypertension had remained unexplored. In this study, we demonstrate that a lack of TIMP3, but not TIMP1, TIMP2 or TIMP4, results in a blunted hypertensive response following Ang II infusion due to aberrant ECM degradation in resistance arteries. It is critical to note that this reduced hypertension in TIMP3$^{-/-}$ mice is not a protective mechanism, but the degradation of the ECM in small arteries results in

pathological vasodilation which in long-term can lead to adverse outcomes such as aneurysms.[35]

Ang II is a well-known hypertensive agent that is upregulated in different cardiovascular diseases.[36-39] Majority of modern clinical antihypertensive drugs (ACEi, ARBs) target the Ang II pathway; thus it can serve as a suitable model to examine the molecular mechanisms of hypertension. In addition, we performed histological and molecular analyses in the mesenteric and carotid arteries to make a direct comparison between the hypertension phenotype and molecular alterations in arteries that are involved in blood pressure regulation.

In this study we report that among all TIMP-deficient mice, only lack of TIMP3 resulted in a suppressed hypertensive response to Ang II infusion. TIMP3 is the only ECM-bound TIMP and has the broadest spectrum of substrates among TIMPs,[40] which could explain why lack of TIMP3, but not other TIMPs, resulted in such a pronounced phenotype. Using an *in vivo* and *ex vivo* approach, we demonstrate that while acute vasocontriction and vasodilation responses are intact in TIMP3$^{-/-}$ mesenteric arteries, two weeks of Ang II infusion resulted in structural remodeling in TIMP3$^{-/-}$ small arteries making them more distensible, as evident by a rightward shift in the circular stress-strain relationship, a commonly used technique to examine the mechanical properties of vessels,[41, 42] and an upward shift in passive pressure-diameter changes in TIMP3$^{-/-}$-Ang II compared to WT-Ang II mesenteric and carotid arteries. This is consistent with a loss of the ECM structural proteins, collagen and elastin,[1, 2] that provide strength and elastic recoil

properties to the arteries, respectively,[2,43] and increased lumen-to-media ratio and lumen diameter in the mesenteric arteries from TIMP3$^{-/-}$-Ang II compared to WT-Ang II mice. The increase in mesenteric artery lumen diameter by about 20% in TIMP3$^{-/-}$-Ang II compared to WT-Ang II can markedly impact blood pressure since blood pressure is inversely related to the 4th power of the lumen radius. As such, a small change in the radius of mesenteric arteries can significantly alter the blood pressure. These data collectively demonstrate that TIMP3-deficiency leads to adverse Ang II-induced arterial ECM remodeling and impaired mechanical properties. Our findings provide evidence that vascular remodeling in the absence of TIMP3, but not other TIMPs, leads to destabilization of the vascular ECM integrity, impaired mechanical properties, and dilation of mesenteric arteries leading to impaired pressor responses. This is consistent with increased susceptibility of TIMP3$^{-/-}$ mice to abdominal aortic aneurysm following prolonged Ang II infusion[35] despite the lower blood pressure in these mice. In addition, TIMP3 could play a critical role in vascular remodeling in diseases associated with hypotension such as sepsis, as TIMP3$^{-/-}$ mice exhibited markedly compromised survival in a lipopolysaccharide model of sepsis.[44]

TIMP3 has the broadest range of substrates among TIMPs,[40] and in addition to inhibiting activated MMPs, TIMP3 can inhibit the cell surface activation of pro-MMP2 to its cleaved form,[45] consistent with the observed rise in cleaved MMP2 in Ang II-infused TIMP3$^{-/-}$ arteries. MMP2 has been shown to have substrate specificity for elastin and fibrillar collagen.[46-48] Here we demonstrate that the

elevated protease activities in TIMP3$^{-/-}$-Ang II arteries contributes to the adverse vascular ECM remodeling in these mice since treatment with Doxycycline, a broad spectrum MMP inhibitor shown to preserve vascular remodeling,[49, 50] protected the architecture and integrity of the mesenteric and carotid arteries in these mice. Doxycycline treatment markedly increased the elastin protein content and reduced collagen levels in WT-Ang II group, consistent with previous reports that doxycycline reduces collagen levels[51] and preserves elastin fibres,[52] The resulting increase in elastin-to-collagen ratio in doxycycline-treated WT-Ang II mesenteric arteries could reduce stiffness of these arteries and therefore reducing the hypertensive response. The protective effects of doxycycline on structural arrangement and organization of ECM proteins in TIMP3$^{-/-}$-Ang II small arteries was associated with increased collagen levels in the mesenteric arteries which could contribute to enhanced stiffness and therefore the rise in blood pressure in this group. It is important to note that this increase in blood pressure with preservation of the arterial ECM integrity in TIMP3$^{-/-}$ mice is indeed a beneficial outcome as inhibition of excess protease activities prevented formation of abdominal aortic aneurysm in TIMP3$^{-/-}$ mice following chronic Ang II infusion.[35]

5.7 CONCLUSION

To conclude, our study compares the causal role of the four TIMPs in agonist-induced hypertensive response and provides *in vivo* and *ex vivo* evidence that TIMP3 plays a primary role in vascular ECM remodeling thereby impacting the hypertensive response. This study also provides critical information that reduced

hypertensive response in the absence of TIMP3 is not a protective mechanism but preludes the onset of more profound vascular complications and adverse outcomes.

5.8 REFERENCES

1. Cummins PM, von Offenberg Sweeney N, Killeen MT, Birney YA, Redmond EM, Cahill PA. Cyclic strain-mediated matrix metalloproteinase regulation within the vascular endothelium: A force to be reckoned with. *Am J Physiol Heart Circ Physiol*. 2007;292:H28-42

2. Wagenseil JE, Mecham RP. Vascular extracellular matrix and arterial mechanics. *Physiol Rev*. 2009;89:957-989

3. Leco KJ, Khokha R, Pavloff N, Hawkes SP, Edwards DR. Tissue inhibitor of metalloproteinases-3 (timp-3) is an extracellular matrix-associated protein with a distinctive pattern of expression in mouse cells and tissues. *J Biol Chem*. 1994;269:9352-9360

4. Yu WH, Yu S, Meng Q, Brew K, Woessner JF, Jr. Timp-3 binds to sulfated glycosaminoglycans of the extracellular matrix. *J Biol Chem*. 2000;275:31226-31232

5. Armstrong C, Abilleira S, Sitzer M, Markus HS, Bevan S. Polymorphisms in mmp family and timp genes and carotid artery intima-media thickness. *Stroke; a journal of cerebral circulation*. 2007;38:2895-2899

6. Flamant M, Placier S, Dubroca C, Esposito B, Lopes I, Chatziantoniou C, Tedgui A, Dussaule JC, Lehoux S. Role of matrix metalloproteinases in early hypertensive vascular remodeling. *Hypertension*. 2007;50:212-218

7. Brands MW, Banes-Berceli AK, Inscho EW, Al-Azawi H, Allen AJ, Labazi H. Interleukin 6 knockout prevents angiotensin ii hypertension: Role of renal vasoconstriction and janus kinase 2/signal transducer and activator of transcription 3 activation. *Hypertension*. 2010;56:879-884

8. Kassiri Z, Oudit GY, Kandalam V, Awad A, Wang X, Ziou X, Maeda N, Herzenberg AM, Scholey JW. Loss of timp3 enhances interstitial nephritis and fibrosis. *J Am Soc Nephrol*. 2009;20:1223-1235

9. Johnson AW, Kinzenbaw DA, Modrick ML, Faraci FM. Small-molecule inhibitors of signal transducer and activator of transcription 3 protect against angiotensin ii-induced vascular dysfunction and hypertension. *Hypertension*. 2012

10. Zhong J, Guo D, Chen CB, Wang W, Schuster M, Loibner H, Penninger JM, Scholey JW, Kassiri Z, Oudit GY. Prevention of angiotensin ii-mediated renal oxidative stress, inflammation, and fibrosis by angiotensin-converting enzyme 2. *Hypertension*. 2011;57:314-322

11. Prall AK, Longo GM, Mayhan WG, Waltke EA, Fleckten B, Thompson RW, Baxter BT. Doxycycline in patients with abdominal aortic aneurysms and in mice: Comparison of serum levels and effect on aneurysm growth in mice. *J Vasc Surg*. 2002;35:923-929

12. Ju H, Gros R, You X, Tsang S, Husain M, Rabinovitch M. Conditional and targeted overexpression of vascular chymase causes hypertension in transgenic mice. *Proc Natl Acad Sci U S A*. 2001;98:7469-7474

13. Morton JS, Rueda-Clausen CF, Davidge ST. Flow-mediated vasodilation is impaired in adult rat offspring exposed to prenatal hypoxia. *J Appl Physiol*. 2011;110:1073-1082

14. Chow MJ, Zhang Y. Changes in the mechanical and biochemical properties of aortic tissue due to cold storage. *J Surg Res*. 2010;171:434-442

15. Ju H, Dixon IM. Extracellular matrix and cardiovascular diseases. *Can J Cardiol*. 1996;12:1259-1267

16. Kassiri Z, Oudit GY, Sanchez O, Dawood F, Mohammed FF, Nuttall RK, Edwards DR, Liu PP, Backx PH, Khokha R. Combination of tumor necrosis factor-alpha ablation and matrix metalloproteinase inhibition prevents heart failure after pressure overload in tissue inhibitor of metalloproteinase-3 knock-out mice. *Circ Res*. 2005;97:380-390

17. Kandalam V, Basu R, Abraham T, Wang X, Awad A, Wang W, Lopaschuk GD, Maeda N, Oudit GY, Kassiri Z. Early activation of matrix metalloproteinases underlies the exacerbated systolic and diastolic dysfunction in mice lacking timp3 following myocardial infarction. *Am J Physiol Heart Circ Physiol*. 2010;299:H1012-1023

18. Benjamin MM, Khalil RA. Matrix metalloproteinase inhibitors as investigative tools in the pathogenesis and management of vascular disease. *Exs*. 2012;103:209-279

19. Ezzati M, Lopez AD, Rodgers A, Vander Hoorn S, Murray CJ. Selected major risk factors and global and regional burden of disease. *Lancet*. 2002;360:1347-1360

20. Ezzati M, Oza S, Danaei G, Murray CJ. Trends and cardiovascular mortality effects of state-level blood pressure and uncontrolled hypertension in the united states. *Circulation*. 2008;117:905-914

21. Humphrey JD. Mechanisms of arterial remodeling in hypertension: Coupled roles of wall shear and intramural stress. *Hypertension*. 2008;52:195-200

22. Laurent S, Tropeano AI, Lillo-Lelouet A, Jondeau G, Laloux B, Boutouyrie P. Local pulse pressure is a major determinant of large artery remodelling. *Clinical and experimental pharmacology & physiology*. 2001;28:1011-1014

23. Intengan HD, Schiffrin EL. Structure and mechanical properties of resistance arteries in hypertension: Role of adhesion molecules and extracellular matrix determinants. *Hypertension*. 2000;36:312-318

24. Murphy G, Nagase H. Progress in matrix metalloproteinase research. *Molecular aspects of medicine*. 2008;29:290-308

25. Nagase H, Woessner JF, Jr. Matrix metalloproteinases. *J Biol Chem*. 1999;274:21491-21494

26. Bouvet C, Gilbert LA, Girardot D, deBlois D, Moreau P. Different involvement of extracellular matrix components in small and large arteries during chronic no synthase inhibition. *Hypertension*. 2005;45:432-437

27. Martinez ML, Castro MM, Rizzi E, Fernandes K, Demacq C, Bendhack LM, Gerlach RF, Tanus-Santos JE. Lercanidipine reduces matrix metalloproteinase-2 activity and reverses vascular dysfunction in renovascular hypertensive rats. *European journal of pharmacology*. 2008;591:224-230

28. Castro MM, Rizzi E, Figueiredo-Lopes L, Fernandes K, Bendhack LM, Pitol DL, Gerlach RF, Tanus-Santos JE. Metalloproteinase inhibition ameliorates hypertension and prevents vascular dysfunction and remodeling in renovascular hypertensive rats. *Atherosclerosis*. 2008;198:320-331

29. Ahmed SH, Clark LL, Pennington WR, Webb CS, Bonnema DD, Leonardi AH, McClure CD, Spinale FG, Zile MR. Matrix metalloproteinases/tissue inhibitors of metalloproteinases: Relationship between changes in proteolytic determinants of matrix composition and structural, functional, and clinical manifestations of hypertensive heart disease. *Circulation*. 2006;113:2089-2096

30. Yasmin, McEniery CM, Wallace S, Dakham Z, Pulsalkar P, Maki-Petaja K, Ashby MJ, Cockcroft JR, Wilkinson IB. Matrix metalloproteinase-9 (mmp-9), mmp-2, and serum elastase activity are associated with systolic

hypertension and arterial stiffness. *Arterioscler Thromb Vasc Biol*. 2005;25:372

31. Castoldi G, Di Gioia CR, Pieruzzi F, D'Orlando C, Van De Greef WM, Busca G, Sperti G, Stella A. Ang ii increases timp-1 expression in rat aortic smooth muscle cells in vivo. *Am J Physiol Heart Circ Physiol*. 2003;284:H635-643

32. Castoldi G, di Gioia CR, Travaglini C, Busca G, Redaelli S, Bombardi C, Stella A. Angiotensin ii increases tissue-specific inhibitor of metalloproteinase-2 expression in rat aortic smooth muscle cells in vivo: Evidence of a pressure-independent effect. *Clinical and experimental pharmacology & physiology*. 2007;34:205-209

33. Watts SW, Rondelli C, Thakali K, Li X, Uhal B, Pervaiz MH, Watson RE, Fink GD. Morphological and biochemical characterization of remodeling in aorta and vena cava of doca-salt hypertensive rats. *Am J Physiol Heart Circ Physiol*. 2007;292:H2438-2448

34. Derosa G, D'Angelo A, Ciccarelli L, Piccinni MN, Pricolo F, Salvadeo S, Montagna L, Gravina A, Ferrari I, Galli S, Paniga S, Tinelli C, Cicero AF. Matrix metalloproteinase-2, -9, and tissue inhibitor of metalloproteinase-1 in patients with hypertension. *Endothelium*. 2006;13:227-231

35. Basu R, Fan D, Kandalam V, Lee J, Das SK, Wang X, Baldwin TA, Oudit GY, Kassiri Z. Loss of timp3 gene leads to abdominal aortic aneurysm formation in response to angiotensin ii. *J Biol Chem*. 2012;287:44083-44096

36. Schluter KD, Wenzel S. Angiotensin ii: A hormone involved in and contributing to pro-hypertrophic cardiac networks and target of anti-hypertrophic cross-talks. *Pharmacol Ther*. 2008;119:311-325

37. Leask A. Potential therapeutic targets for cardiac fibrosis: Tgfbeta, angiotensin, endothelin, ccn2, and pdgf, partners in fibroblast activation. *Circ Res*. 2010;106:1675-1680

38. Palomeque J, Rueda OV, Sapia L, Valverde CA, Salas M, Petroff MV, Mattiazzi A. Angiotensin ii-induced oxidative stress resets the ca2+ dependence of ca2+-calmodulin protein kinase ii and promotes a death pathway conserved across different species. *Circ Res*. 2009;105:1204-1212

39. Palomeque J, Delbridge L, Petroff MV. Angiotensin ii: A regulator of cardiomyocyte function and survival. *Front Biosci*. 2009;14:5118-5133

40. Moore L, Fan D, Basu R, Kandalam V, Kassiri Z. Tissue inhibitor of metalloproteinases (timps) in heart failure. *Heart Fail Rev*. 2012;17:693-706

41. Huo Y, Cheng Y, Zhao X, Lu X, Kassab GS. Biaxial vasoactivity of porcine coronary artery. *Am J Physiol Heart Circ Physiol*. 2012;302:H2058-2063

42. Khamdaeng T, Luo J, Vappou J, Terdtoon P, Konofagou EE. Arterial stiffness identification of the human carotid artery using the stress-strain relationship in vivo. *Ultrasonics*. 2012;52:402-411

43. Ikonomidis JS, Jones JA, Barbour JR, Stroud RE, Clark LL, Kaplan BS, Zeeshan A, Bavaria JE, Gorman JH, 3rd, Spinale FG, Gorman RC. Expression of matrix metalloproteinases and endogenous inhibitors within ascending aortic aneurysms of patients with marfan syndrome. *Circulation*. 2006;114:I365-370

44. Smookler DS, Mohammed FF, Kassiri Z, Duncan GS, Mak TW, Khokha R. Tissue inhibitor of metalloproteinase 3 regulates tnf-dependent systemic inflammation. *J Immunol*. 2006;176:721-725

45. English JL, Kassiri Z, Koskivirta I, Atkinson SJ, Di Grappa M, Soloway PD, Nagase H, Vuorio E, Murphy G, Khokha R. Individual timp deficiencies differentially impact pro-mmp-2 activation. *J Biol Chem*. 2006;281:10337-10346

46. Aimes RT, Quigley JP. Matrix metalloproteinase-2 is an interstitial collagenase. Inhibitor-free enzyme catalyzes the cleavage of collagen fibrils and soluble native type i collagen generating the specific 3/4- and 1/4-length fragments. *J Biol Chem*. 1995;270:5872-5876

47. Shipley JM, Doyle GA, Fliszar CJ, Ye QZ, Johnson LL, Shapiro SD, Welgus HG, Senior RM. The structural basis for the elastolytic activity of the 92-kda and 72-kda gelatinases. Role of the fibronectin type ii-like repeats. *J Biol Chem*. 1996;271:4335-4341

48. Murphy G, Nguyen Q, Cockett MI, Atkinson SJ, Allan JA, Knight CG, Willenbrock F, Docherty AJ. Assessment of the role of the fibronectin-like domain of gelatinase a by analysis of a deletion mutant. *J Biol Chem*. 1994;269:6632-6636

49. Pires PW, Rogers CT, McClain JL, Garver HS, Fink GD, Dorrance AM. Doxycycline, a matrix metalloprotease inhibitor, reduces vascular remodeling and damage after cerebral ischemia in stroke-prone

spontaneously hypertensive rats. *Am J Physiol Heart Circ Physiol*. 2011;301:H87-97

50. Castro MM, Tanus-Santos JE, Gerlach RF. Matrix metalloproteinases: Targets for doxycycline to prevent the vascular alterations of hypertension. *Pharmacological research : the official journal of the Italian Pharmacological Society*. 2011;64:567-572

51. Fujita H, Sakamoto N, Ishimatsu Y, Kakugawa T, Hara S, Hara A, Amenomori M, Ishimoto H, Nagata T, Mukae H, Kohno S. Effects of doxycycline on production of growth factors and matrix metalloproteinases in pulmonary fibrosis. *Respiration*. 2011;81:420-430

52. Ennis T, Jin J, Bartlett S, Arif B, Grapperhaus K, Curci JA. Effect of novel limited-spectrum mmp inhibitor xl784 in abdominal aortic aneurysms. *Journal of cardiovascular pharmacology and therapeutics*. 2012;17:417-426

CHAPTER SIX

LOSS OF TIMP3 LEADS TO ABDOMINAL AORTIC ANEURYSM FORMATION IN RESPONSE TO ANGIOTENSIN II

Ratnadeep Basu[1,4], Dong Fan[1,4], Vijay Kandalam[1,4], Jiwon Lee[1,4], Subhash Das[2,4], Xiuhua Wang[1,4], Troy A Baldwin[3], Gavin Y. Oudit[2,4], Zamaneh Kassiri[1,4]

[1]Department of Physiology, [2]Department of Medicine/Division of Cardiology,
[3]Dept. of Medical Microbiology & Immunology, University of Alberta, Edmonton, AB, Canada.
[4]Cardiovascular Research Center, Mazankowski Alberta Heart Institute, Edmonton, AB, Canada

A modified version of this chapter has been published in *Journal of Biological Chemistry*, 2012 December 28; 287(53): 44083-96.

Author Contributions

Participated in Research Design: RB., G.Y.O. and Z.K.
Conducted Experiments: R.B., D.F., V.K., J.L., S.D., X.W., T.A.B.
Performed Data Analysis: R.B., D.F.,V.K., J.L., S.D., X.W., T.A.B. and Z.K
Contributed to the Writing of the Manuscript: R.B., G.Y.O and Z.K.

6.1 ABSTRACT

Aortic aneurysm is dilation of the aorta primarily due to degradation of the vascular wall extracellular matrix (ECM). Tissue inhibitor of metalloproteinases (TIMPs) inhibit MMPs, the proteases that degrade the ECM. TIMP3 is the only ECM-bound TIMP and its levels are altered in the aorta from patients with abdominal aortic aneurysm (AAA). We investigated the causal role of TIMP3 in AAA formation. Infusion of angiotensin II (Ang II), using micro-osmotic (Alzet) pumps, in TIMP3$^{-/-}$ male mice but not wild type (WT) mice led to adverse remodeling of the abdominal aorta, reduced collagen and elastin proteins, and elevated MMP2 activation indicative of excess protein degradation within 2 weeks, and formation of abdominal aortic aneurysm (AAA) by 4 weeks. Intriguingly, TIMP3$^{-/-}$/MMP2$^{-/-}$ mice exhibited exacerbated AAA, compromised survival due to aortic rupture, inflammation and elevated MMP9. We determined that MMP2 is produced by cells intrinsic to the aorta, while the predominant source of MMP9 is the infiltrating inflammatory cells. Consistently, reconstitution of WT bone marrow reconstitution in TIMP3$^{-/-}$/MMP2$^{-/-}$ mice reduced inflammation, MMP9 production and prevented AAA in these animals. Treatment with a broad-spectrum MMP inhibitor (PD166793) prevented the Ang II-induced AAA in TIMP3$^{-/-}$ as well as in TIMP3$^{-/-}$/MMP2$^{-/-}$ mice. Our study demonstrates that the regulatory function of TIMP3 is critical in preventing adverse vascular remodeling and AAA. Hence, replenishing TIMP3, a physiological inhibitor of a

number of metalloproteinases, could serve as a therapeutic approach in limiting AAA development or expansion.

6.2 INTRODUCTION

Abdominal aortic aneurysm (AAA) is a degenerative vascular disorder characterized by dilation of the aorta due to destructive remodeling of the aortic wall and degradation of the fibrillar proteins of the vascular extracellular matrix (ECM). AAA has remained an unresolved clinical problem since β-blockers [1, 2], statin therapy [3], and angiotensin converting enzyme (ACE) inhibitors have been ineffective in controlling AAA expansion, and AAA remains as the 13th leading cause of death in Western countries [4-6]. Surgical and mechanical interventions are the only effective treatments to prevent AAA rupture, but that is only recommended in severe AAA cases where the inherent risk of surgery is less than the risk of aortic rupture [1, 6]. The ten-year survival for patients deemed unfit for surgical repair is less than 25% [7]. Additionally, the recent Tromsø study indicates that the incident of AAA is greater in males compared to female patients [8, 9], while similar findings have been reported in animal models [10]. As such understanding the molecular mechanism underlying AAA development, expansion and rupture is critical in developing effective therapies for this disease.

Arterial ECM is primarily comprised of collagen and elastin fibres which provide significant structural support and recoil properties for the arteries [11, 12]. Matrix metalloproteinases (MMPs) degrade the ECM structural proteins while their inhibitors, tissue inhibitor of metalloproteinases (TIMPs) keep their activity in

check. An imbalance in the interaction between MMPs and TIMPs has been reported in the aorta of patients with abdominal aneurysm [13]. Among the four TIMPs identified in mammals, TIMP3 is ECM-bound whereby it can exert tissue-specific effects [14, 15]. TIMP3 protein levels are reduced in the aorta of patients with Marfan syndrome with increased rate of aortic rupture [16]. TIMP3 mRNA levels are increased in dilated aorta from patients with aortic aneurysm whereas other TIMPs were not altered [17], however, TIMP3 protein levels were not measured in this study. In addition, a significant interaction between polymorphism of TIMP3, but not TIMP1 or TIMP2, occurs in patients with AAA and with a positive family history of AAA [18]. Hence, the causal role of TIMP3 in AAA development remains to be determined.

Our study examined the role of TIMP3 in angiotensin II (Ang II)-induced vascular remodeling and the formation of AAA.

6.3 OBJECTIVE

To find the long term MMP-inhibitory role of TIMP3 in agonist induced vascular ECM remodeling.

6.4 MATERIALS AND METHODS

6.4.1 Experimental Animals and Procedures

Wildtype (WT) mice were purchased from Jackson Laboratories, $TIMP3^{-/-}$ mice were generated as described.[19] We cross-bred $TIMP3^{-/-}$ [19] and $MMP2^{-/-}$ [20] mice to generate $TIMP3^{-/-}/MMP2^{-/-}$ mice (Chapter 2.1.3). All mice are in pure C57BL/6 background. Alzet micro-osmotic pumps containing either Ang II (Sigma-Aldrich)

or saline (control) were implanted for 4 weeks (Chapter 2.2.1) in 8-week old male mice of various genotypes for 14 days.[21-23] MMP inhibitor (PD166793, MMPi) was administered (Chapter 2.16) orally by daily gavage as before (30 mg/kg/d) [24, 25]. All experiments were conducted in accordance with the guidelines of the University of Alberta Animal Care and Use Committee (ACUC) and the Canadian Council of Animal Care.

6.4.2 Bone Marrow Reconstitution

Bone marrow reconstitution was performed to generate chimera mice as described previously [26] and detailed in Chapter 2.11.

6.4.3 Histological analyses and Scanning Electron Microscopy

Abdominal aortas were fixed in 10% formalin, parafin-embedded and used for Gomori Trichrome (Chapter 2.10.2), Verhoeff-Van Geison (2.10.1). Tissue processing and scanning electron microscopy (Chapter 2.10.3) was done as before [25]. Neutrophil and macrophage staining (Chapter 2.12.) was performed as described previously [27]

6.4.4 Ultrasonic Imaging of Abdominal Aorta

Ultrasonic images of the abdominal aorta were obtained in mice anesthetized with isoflurane, using the Vevo 770 high resolution imaging system (Chapter 2.5.6)

6.4.5 Protein Extraction for Western Blot Analysis, Gelatin Zymography and Activity Assays

Abdominal aorta at the suprarenal aspect was excised to extract sufficient protein (Chapter 2.14.1) for immunoblotting (Chapter 2.14.2), gelatin zymography (Chapter 2.14.3) and enzymatic activity assays (Chapter 2.15).

6.4.6 mRNA Expression Analysis by TaqMan Real-time PCR

RNA was extracted from flash-frozen aorta and mRNA expression were measured by TaqMan real-time PCR Chapter 2.13.2.). The primers and probes for the reported genes are detailed in Table 2.2.

6.4.7 Statistical Analysis

The statistical analyses were performed using SPSS software (Chicago, Illinois, Version 10.1). We performed normality test (Shapiro-Wilk) and homogeneity of variance test (Levene) to confirm normal distribution of all data. To compare data sets with two factors (genotype and treatment) we performed two-way analysis of variance (ANOVA) (Fig. 1-6). In Figures 5-8, to compare 3 levels of the genotype, two-way ANOVA was followed by Bonferroni post hoc testing if the results attained statistical significance ($p<0.05$). In Figure 7B, the effects of MMPi in each genotype was tested using unpaired t-test. Survival data (Fig. 4B) were compared using Kaplan-Meier survival curves followed by the log rank test adjusted with the Bonferroni method. Averaged values represent mean ± SEM. Statistical significance was recognized at $p<0.05$.

6.5 RESULTS

6.5.1 Increase in TIMP3 Protein Levels in WT Aaorta after 2 Weeks of Angiotensin II Infusion

In WT mice, 2 weeks of Ang II infusion significantly elevated TIMP3 mRNA and protein levels in the abdominal aorta (**Figs. 6.1i and 6.1ii**).

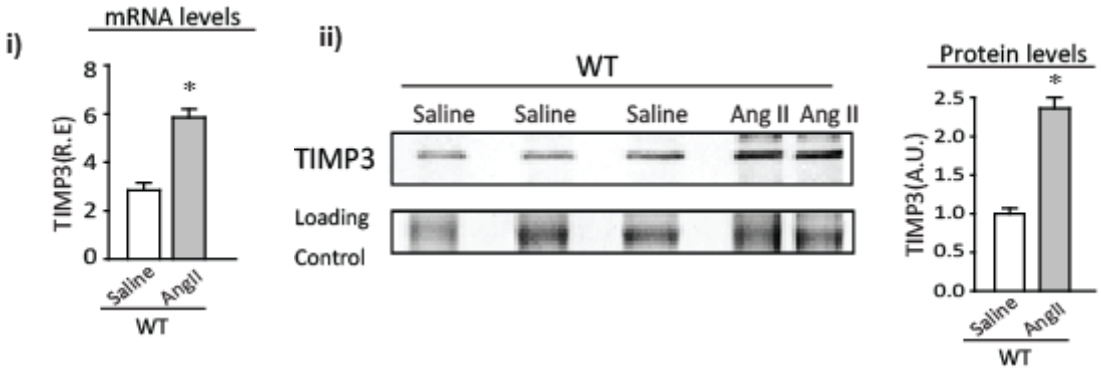

Figure 6.1 Elevated TIMP3 expression and protein levels in WT aorta post Ang II infusion for 2 weeks.
mRNA expression (i) representative Western Blot and averaged TIMP3 protein levels (ii) in the abdominal aorta of WT mice after 2 weeks of Ang II or saline infusion.

6.5.2 TIMP3-deficient Mice Exhibit Adverse Aortic Remodelling after 2 Weeks of Angiotensin II Infusion

To examine the role of TIMP3 in Ang II-induced aortic remodeling, we subjected mice lacking TIMP3 to Ang II infusion, we assessed the predominant arterial structural proteins, elastin and fibrillar collagen type I [12]. Verhoeff-Van Gieson staining showed disorganized and disrupted elastin fibres with a greater frequency of elastin fibre disruption in the abdominal aorta of $TIMP3^{-/-}$-Ang II compared to WT-Ang II mice (**Figs. 6.2A, 6.2B**). The Ang II-induced reduction in elastin protein content was greater in $TIMP3^{-/-}$ abdominal aorta (**Fig. 6.2Ci-ii**) despite a larger increase in mRNA synthesis of elastin in these mice (**Fig. 6.2Ciii**). Gomori

Trichrome staining similarly revealed disorganized collagen structures (greenish-blue, **Fig. 6.2D**), and a drastic decrease in collagen type I protein levels (**Figs. 6.2Ei-ii**) despite a marked rise in its mRNA synthesis (**Fig. 6.2Eiii**) in TIMP3$^{-/-}$-Ang II compared to WT-Ang II abdominal aortas. These data suggest that the decrease in elastin and collagen protein levels in TIMP3-deficient aorta is most likely due to post-translational degradation of these proteins and not reduced

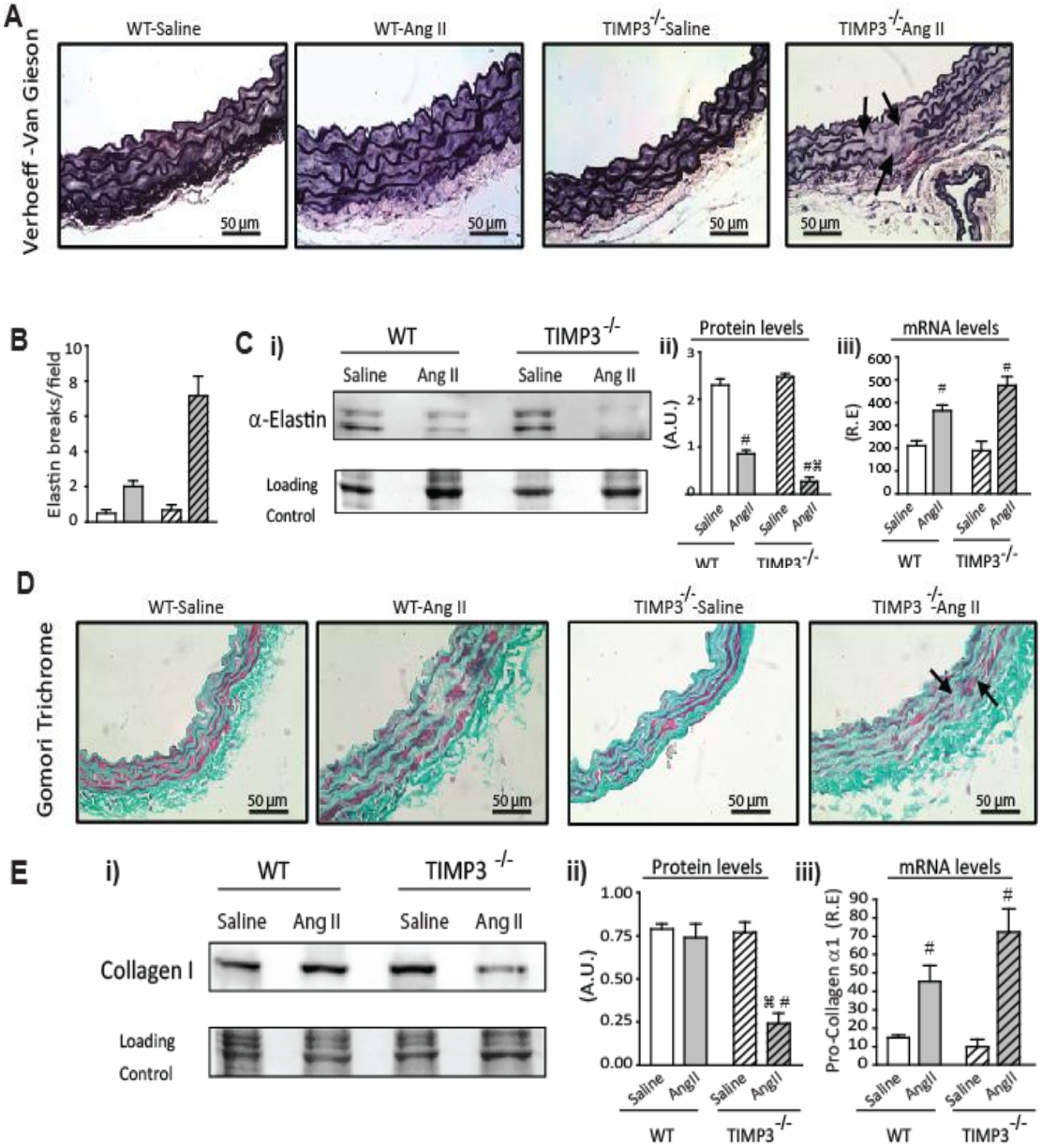

Figure 6.2 Adverse remodeling of ECM structure in TIMP3$^{-/-}$ abdominal aorta following 2 weeks of Ang II infusion.

A) Verhoeff-Van Gieson staining shows elastin fibres. B) number of elastin breaks per field under 40x magnification. C) representative Western blots and averaged elastin protein levles (i-ii), and elastin mRNA levels (iii) in saline- and Ang II-infused WT and TIMP3$^{-/-}$ mice. D) Collagen staining by Gomori trichrome. E) representative Western blot and averaged collagen protein ontent (i-ii), and mRNA expression levels (iii) in saline- and Ang II-infused WT and TIMP3$^{-/-}$ mice. Coomassie blue-stained gel was used as the loading control for the Western blots. A.U.=Arbitrary Units, R.E=Relative Expression, n=5/group (protein); 5/group (mRNA). *$p<0.05$ compared to corresponding saline, #$p<0.05$ compared to WT-Ang II. Arrows point to disrupted collagen or elastin structure. Averaged data represent mean ± S.E (error bars).

6.5.3 Enhanced MMP2 Activation in TIMP3$^{-/-}$ Mice Following 2 Weeks of Angiotensin II Infusion

TIMP3 is a potent inhibitor of a number of active MMPs, and can inhibit cell-surface activation of MMP2 [28], hence its absence can lead to uncontrolled proteolytic activities [29]. *In situ* gelatin zymography showed that Ang II-infusion resulted in a stronger gelatinase activity in TIMP3$^{-/-}$ compared to WT aorta (**Fig. 6.3A**). To determine the contribution of individual gelatinases, namely MMP2 and MMP9, we performed *in vitro* gelatin zymography which revealed a markedly greater MMP2 activation in TIMP3$^{-/-}$-Ang II abdominal aorta, as indicated by a stronger 64 kDa band, while MMP9 levels rose similarly in both genotypes (**Figs. 6.3Bi-ii**). The increase in MMP2 activation was also associated with increased mRNA expression (**Fig. 6.3Ci**), while MMP9 mRNA did not increase (**Fig. 6.3Cii**). Expression analysis of other MMPs showed a greater increase in MMP13 levels in TIMP3$^{-/-}$-Ang II group (**Fig. 6.3Ciii**) while membrane type MMP (MT1-MMP) was elevated similarly in both genotypes (**Fig. 6.3Civ**).

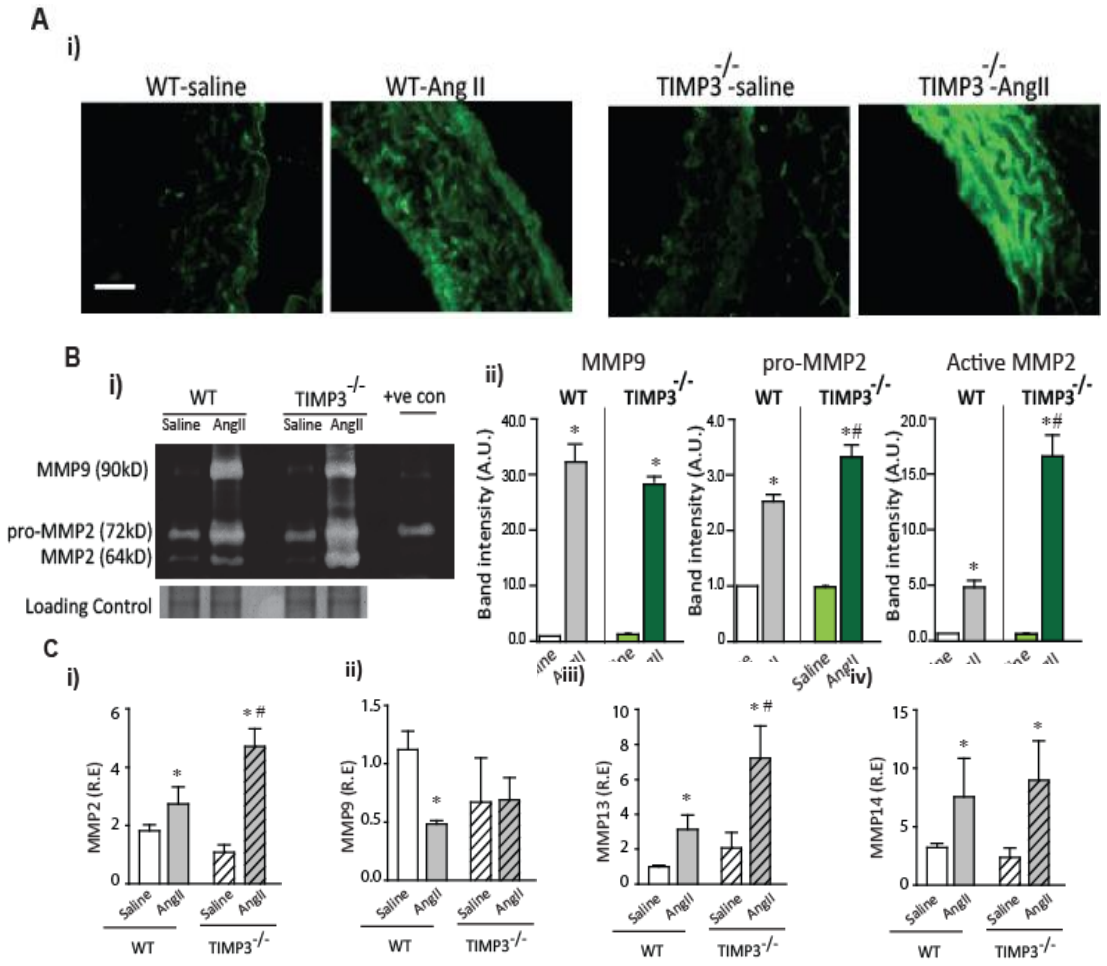

Figure 6.3 Elevated protease activity in Ang II-infused TIMP3-deficient aorta

A) *In situ* gelatin zymography in aorta from saline- or Ang II-infused WT and TIMP3$^{-/-}$ mice. Scale=50 μM. B) *In vitro* gelatin zymography (i) and band-intensiy for MMP9, pro-MMP2 and active MMP2 (ii). C) mRNA expression levels of MMP2 (i), MMP9 (ii), MMP13 (iii) and MT1-MMP (iv) in abdominal aorta from saline- or Ang II-infused WT and TIMP3$^{-/-}$ mice. Coomassie blue-stained gel was used as the loading control for the gelatin zymography. n=5/group/genotype. A.U=Arbitrary Units. *p<0.05 compared to corresponding saline, #p<0.05 compared to WT-Ang II.

6.5.4 TIMP3-deficient Mice are Susceptible to Abdominal Aortic Aneurysm (AAA)

Next, we examined the long term outcome of these structural remodelling in the TIMP3$^{-/-}$ aorta. After 4 weeks of Ang II infusion, TIMP3$^{-/-}$ mice, but not WT mice, developed an aneurysm in the abdominal aorta but not in the ascending or

descending thoracic aorta (**Fig. 6.4A**). Aneurysm was defined as a dilation of 50% or more in the abdominal aortic diameter[1, 30] measured by ultrasound imaging. In WT mice, Ang II-induced dilation of the abdominal aorta did not exceed 20% of the original aortic diameter, whereas 55% of TIMP3$^{-/-}$ mice exhibited greater than 50% aortic dilation in the supra-renal region. Representative ultrasonic images (**Fig. 6.4B**) and averaged diameter of the abdominal aorta (**Figs. 6.4Ci-ii**) demonstrate marked aortic dilation at the supra-renal region in Ang II-infused TIMP3$^{-/-}$ compared to parallel WT group. Aortic systolic expansion index, a measure of aortic elasticity and recoil property during systole and diastole [31], was also significantly suppressed in the aneurysmal aorta in TIMP3$^{-/-}$-Ang II mice (**Fig. 6.4Ciii**) confirming the compromised structural and functional integrity of the TIMP3-deficient aorta.

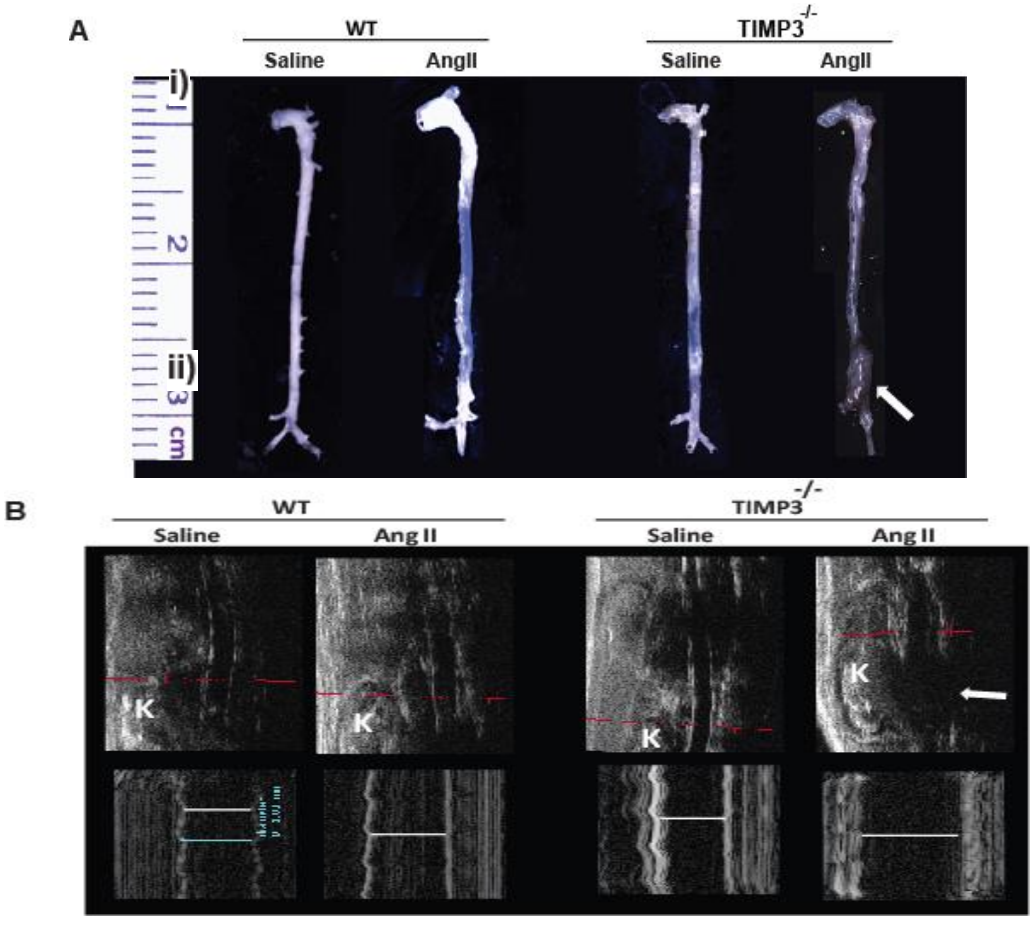

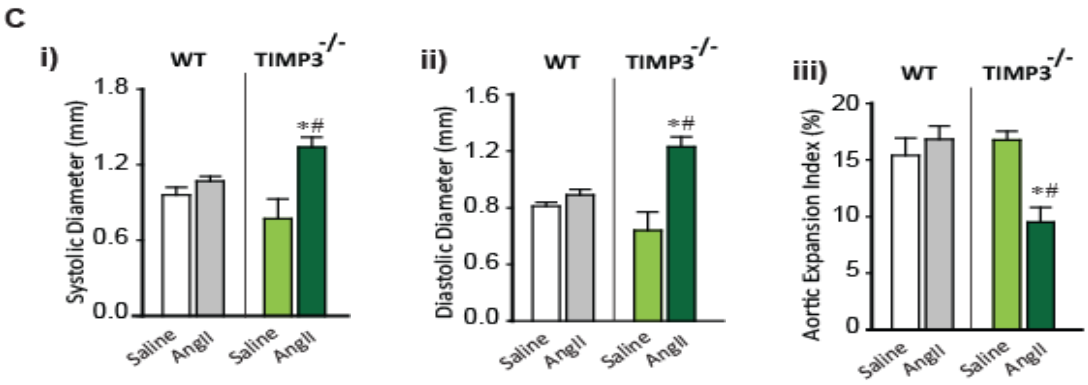

Figure 6.4 TIMP3-deficient mice developed AAA after 4 weeks of Ang II infusion.

A) Representative photographs of the entire aorta showing macroscopic features of aneurysm induced by Ang II in TIMP3-deficient mice. B) Ultrasonographic B-mode (i) and M-mode (ii) images of the abdominal arota in saline- and Ang II-infused WT and TIMP3$^{-/-}$ mice. C) Averaged aortic systolic (i) and diastolic (ii) diameters, and aortic systolic expansion index (iii) of abdominal aorta in saline- or AngII-infused WT and TIMP3-deficient mice (n=9/group/genotype). *P<0.05 compared to corresponding saline group, #p<0.05 compared to WT-Ang II. 'K' indicates the top of the left kidney as a point of reference.

6.5.5 Deletion of MMP2 in TIMP3$^{-/-}$ Mice Led to Exacerbated AAA

In order to determine the contribution of the elevated MMP2 activation in development of AAA in TIMP3$^{-/-}$-Ang II mice, we generated TIMP3$^{-/-}$ mice that also lacked MMP2. Intriguingly, TIMP3$^{-/-}$/MMP2$^{-/-}$ mice exhibited more severe AAA after 4 weeks of Ang II-infusion compared to TIMP3$^{-/-}$ mice (**Fig. 6.5A**) as dilation of the abdominal aorta exceeded 50% of the original aortic diameter in 75% of these mice. In addition, while TIMP3$^{-/-}$ mice exhibited compromised survival post-Ang II infusion, mortality was increased further in TIMP3$^{-/-}$/MMP2$^{-/-}$ mice (**Fig. 6.5Bi**). Routine autopsy examination revealed that aortic rupture at the supra-renal region of the aorta where aneurysmal dilation was detected (**Fig. 6.5Bii**), was the cause of the increased mortality in these mice. Morphometric analysis of the full cross-section of abdominal aorta in saline-infused WT

compared to Ang II-infused WT, TIMP3$^{-/-}$ and TIMP3$^{-/-}$/MMP2$^{-/-}$ mice clearly shows the dilation in abdominal aorta in TIMP3$^{-/-}$ mice, and a strikingly greater dilation in the TIMP3$^{-/-}$/MMP2$^{-/-}$ mice (**Fig. 6.5C**). Histological analyses at higher magnifications further revealed deterioration of the aortic wall at the site of aneurysm as indicated by disrupted elastin fibres (VVG staining) and collagen structure (GT staining) which were more severe in TIMP3$^{-/-}$/MMP2$^{-/-}$ mice (**Fig. 6.5C**).

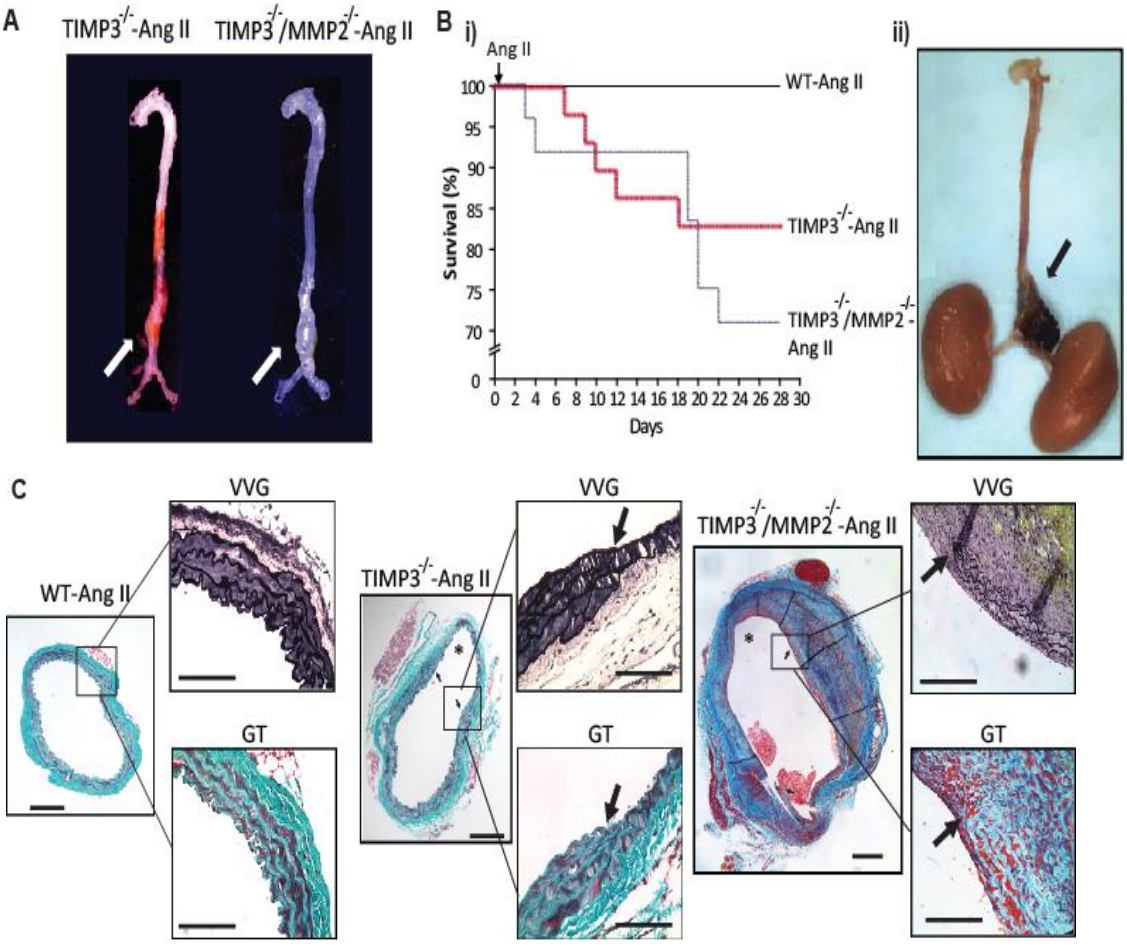

Figure 6.5 MMP2 deletion in TIMP3-deficient mice led to exacerbated AAA.
A) Photographs of full aortas from Ang II-infused TIMP3$^{-/-}$ and TIMP3$^{-/-}$/MMP2$^{-/-}$ mice. Arrows point to the aneurysmal area. N=20/WT, n=30/TIMP3$^{-/-}$, n=30/ TIMP3$^{-/-}$/MMP2$^{-/-}$. B) Survival curve reflecting mortalities due to aortic rupture i), Image of an aortic rupture (arrow) at the supra-

renal region ii). The kidney was left in place as a point of reference. C) Microscopic images of full cross-sections of abdominal aorta (Scale bar=100mm, note the different scale bar size in double-deficient group), and VVG- and GT-staining at a higher magnification (scale bar=50 μm). Arrows point to areas of structural degradation, *indicates the area of aneurysm

6.5.6 Scanning Electron Microscopy Revealed the Disrupted and Disarrayed Aortic Wall of TIMP3$^{-/-}$/MMP2$^{-/-}$ Mice at a Higher Magnification

Scanning electron microscopy allowed us to perform a more detailed evaluation of the structural remodelling of the abdominal aortic walls. Ang II infusion led to remodelling of the aortic wall in WT mice as indicated by compactly folded elastin lamellae (**Fig. 6.6i**) which was more evident at a higher magnification (**Fig. 6.6ii**). TIMP3-deficient mice, on the other hand, exhibited disrupted medial elastic lamellae and disrupted fibrillar structures (open arrows in **Fig. 6.6i**) and this structural deterioration was worsened in TIMP3$^{-/-}$/MMP2$^{-/-}$-Ang II mice (Fig. 6.6i-ii). Structure and diameter of the abdominal aorta in saline-infused mice were comparable among the genotypes (data not shown). These findings demonstrate that although the increase in MMP2 activity is significantly greater in TIMP3$^{-/-}$-Ang II aorta, its deletion indeed aggravated the structural deterioration and the adverse remodeling in the abdominal aorta which resulted in worsened AAA.

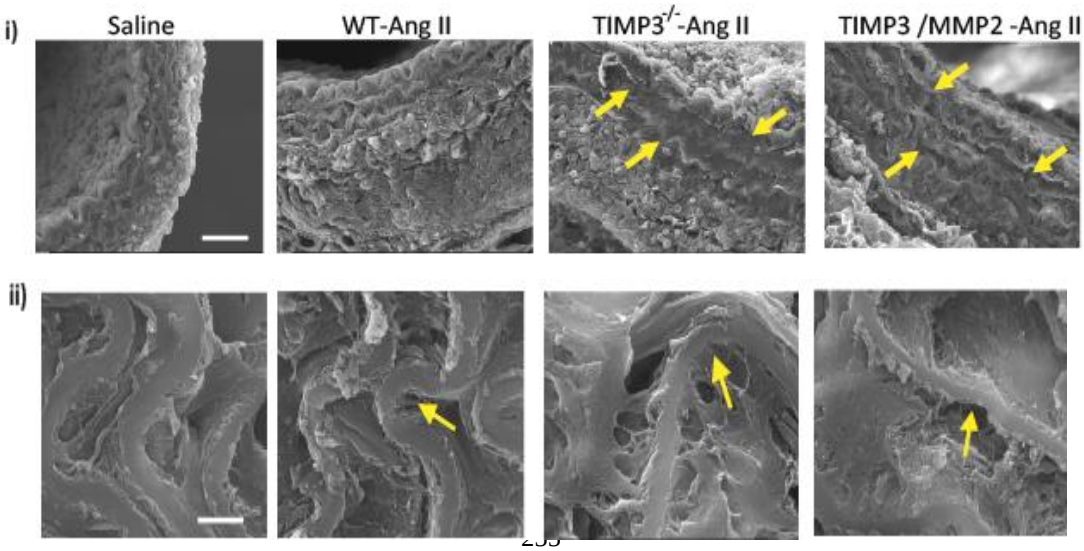

Figure 6.6 Adverse remodeling at a higher magnification using scanning electron microscopy.
Scanning electron microscopy of abdominal aorta in saline- or Ang II-infused mice of different genotypes, at two different magnifications (i, scale bar=40mm; ii, scale bar=4 μM). Yellow arrows point to the elastin lamella structures.

6.5.7 TIMP3$^{-/-}$/MMP2$^{-/-}$-Ang II Mice Exhibited Upregulated MMP9 and Total Gelatinase Activity in Abdominal Aorta

Further examination of the TIMP3$^{-/-}$/MMP2$^{-/-}$ mice revealed that Ang II-induced total collagenase activity was the largest in the abdominal aorta of TIMP3$^{-/-}$ mice and was reduced significantly in TIMP3$^{-/-}$/MMP2$^{-/-}$ group (**Fig. 6.7Ai**). This is consistent with MMP2 also being a potent collagenase [32]. However, the Ang II-induced rise in gelatinase activity was markedly greater in TIMP3$^{-/-}$/MMP2$^{-/-}$ compared to TIMP3$^{-/-}$ abdominal aorta despite the absence of MMP2 (**Fig. 6.7Aii**). MMP2 and MMP9 are the classically known gelatinases, as such the rise in total gelatinase activity in the absence of MMP2 would imply an increase in MMP9 activity. *In vitro* gelatin zymography confirmed a striking upregulation in MMP9 levels in Ang II-infused TIMP3$^{-/-}$/MMP2$^{-/-}$ abdominal aortas compared to all other groups (**Figs. 6.7Bi-ii**) which was also accompanied by elevated mRNA expression of MMP9 (**Fig. 6.7Biii**).

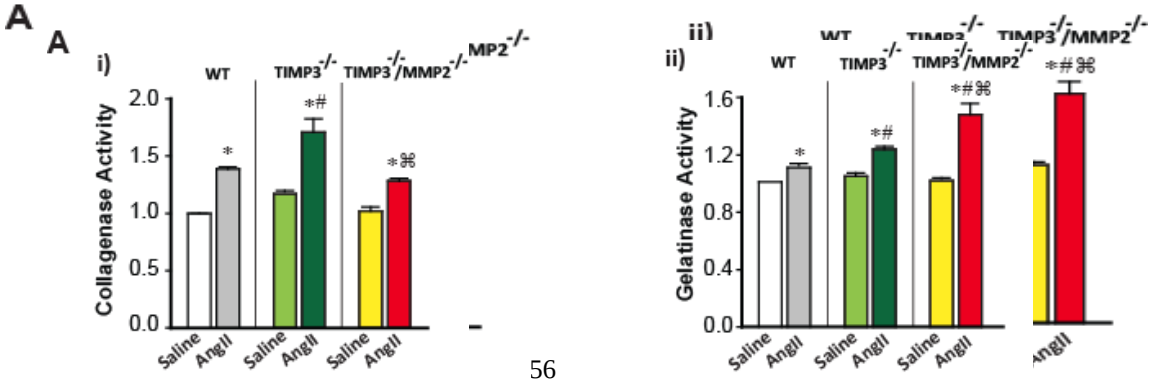

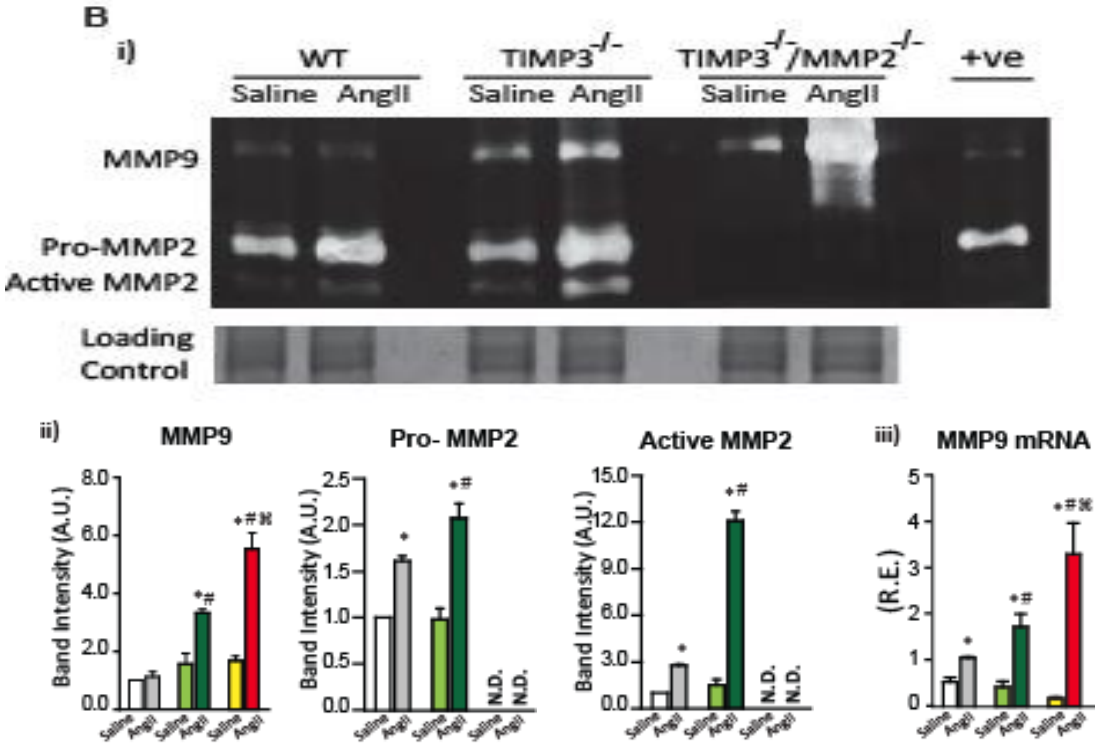

Figure 6.7 Aneursymal aorta from TIMP3$^{-/-}$/MMP2$^{-/-}$ mice exhibit marked MMP9 levels and gelatinase activity.

A) Total collagenase (i) and gelatinase (ii) activity in saline- or Ang II-infused mice of indicated genotypes (normalized to WT-saline group) n=6/group. B) *In vitro* gelatin zymography showing MMP9, pro- and active MMP2 levels (i-ii) and MMP9 mRNA expression levels (iii) in all groups.. Coomassie blue-stained gel is used as the loading control. n=4-6/group/genotype, A.U.=Arbitrary Units, R.E.=Relative Expression. *P<0.05 compared to corresponding saline group, #p<0.05 compared to WT-Ang II, ⌘p<0.05 compared to TIMP3-deficient-Ang II group.

6.5.8 Inflammation in Abdominal Aorta of TIMP3$^{-/-}$/MMP2$^{-/-}$-Ang II Mice

MMP9 is a well-known elastase that can degrade vascular elastin lamella [33] leading to invasion of inflammatory cells and inflammation [34] and exacerbation of AAA [35]. Immunofluorescent staining for inflammatory cells, neutrophils and macrophages (superimposed with DAPI-nucleus staining), showed enhanced infiltration of neutrophils and macrophages in the abdominal aorta of Ang II-

infused TIMP3$^{-/-}$/MMP2$^{-/-}$ mice (**Fig. 6.8A**). TIMP3$^{-/-}$-Ang II group showed a less severe macrophage infiltration, no infiltrating cells were detected in WT-Ang II abdominal aorta (**Fig. 6.8A**). Consistently, mRNA levels of inflammatory markers, interleukin-1β (IL-1β), interleukin-6 (IL-6), and monocyte chemotactic protein-1 (MCP-1) were significantly elevated in the aneurysmal aorta of TIMP3$^{-/-}$/MMP2$^{-/-}$ mice compared to parallel WT and TIMP3$^{-/-}$ groups (**Figs. 6.8Bi-iii**).

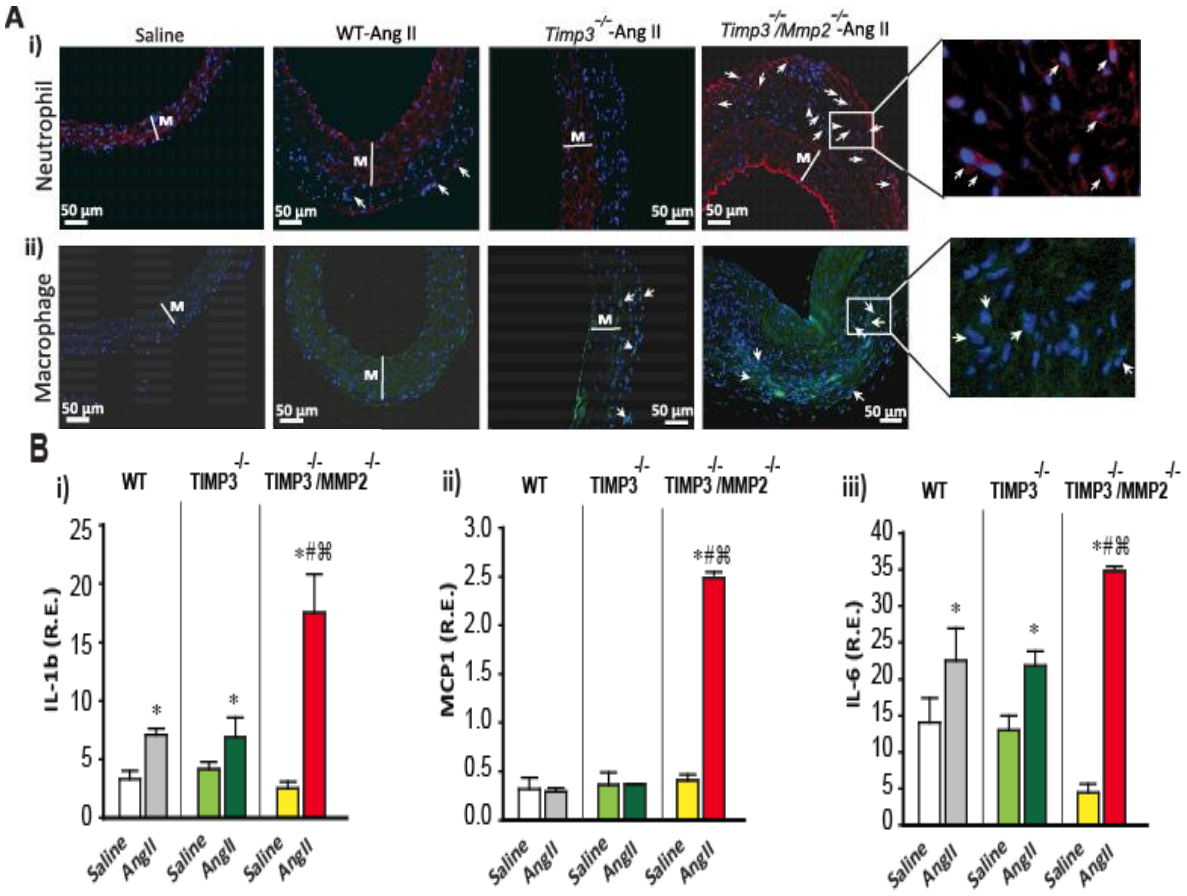

Figure 6.8 TIMP3$^{-/-}$/MMP2$^{-/-}$ aorta with increased infiltrating inflammatory cells and elevated expression levels of cytokines after 4 weeks of Ang II infusion.

A) Immunofluorescent staining for neutrophil and macrophage superimposed with DAPI nucleus staining (blue) in abdominal aorta of indicated groups. "M" indicates the medial thickness. Arrows point to positively stained neutrophils or macrophages. B) Expression levels of inflammatory markers, interleukin-1beta (IL-1b) , interleukin-6 (IL-6) and monocyte chemoattractant protein-1

(MCP1), in the abdominal aorta of WT, TIMP3$^{-/-}$ and TIMP3$^{-/-}$/MMP2$^{-/-}$ mice after 4 weeks of saline or Ang II-infusion. *P<0.05 compared to all other groups. R.E; relative expression.

6.5.9 Inflammation is A Key Factor in Exacerbated AAA in TIMP3$^{-/-}$/MMP2$^{-/-}$-Ang II Mice

In order to determine the mechanism underlying the worsening of AAA in TIMP3$^{-/-}$/MMP2$^{-/-}$-Ang II mice, and the contribution of the observed heightened inflammation in these aortas, we reconstituted WT bone marrow in TIMP3$^{-/-}$/MMP2$^{-/-}$ mice, and vice versa. We generated TIMP3$^{-/-}$/MMP2$^{-/-}$-chimera mice by reconstituting WT bone marrow in these mice, and WT-chimera mice by reconstituting TIMP3$^{-/-}$/MMP2$^{-/-}$ bone marrow in WT mice. After 7 weeks of reconstitution, and 4 weeks of Ang II infusion, we found that TIMP3$^{-/-}$/MMP2$^{-/-}$-chimera mice did not develop aortic aneurysm (**Fig. 6.9A**). In addition, the diameter of abdominal aorta (**Figs. 6.9Bi-ii**) and aortic expansion index (**Fig. 6.9Bii**i) in these mice were comparable to saline-infused animals. Consistently, minimal infiltration of neutrophils and macrophages were detected (**Fig. 6.9Cii**), while MMP9 levels were significantly reduced (**Fig. 6.9D**) in the TIMP3$^{-/-}$/MMP2$^{-/-}$-chimera-Ang II mice.

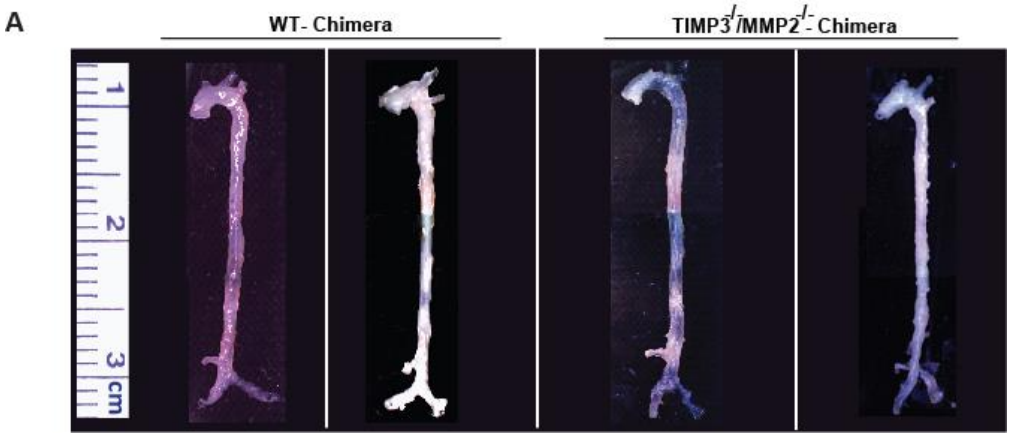

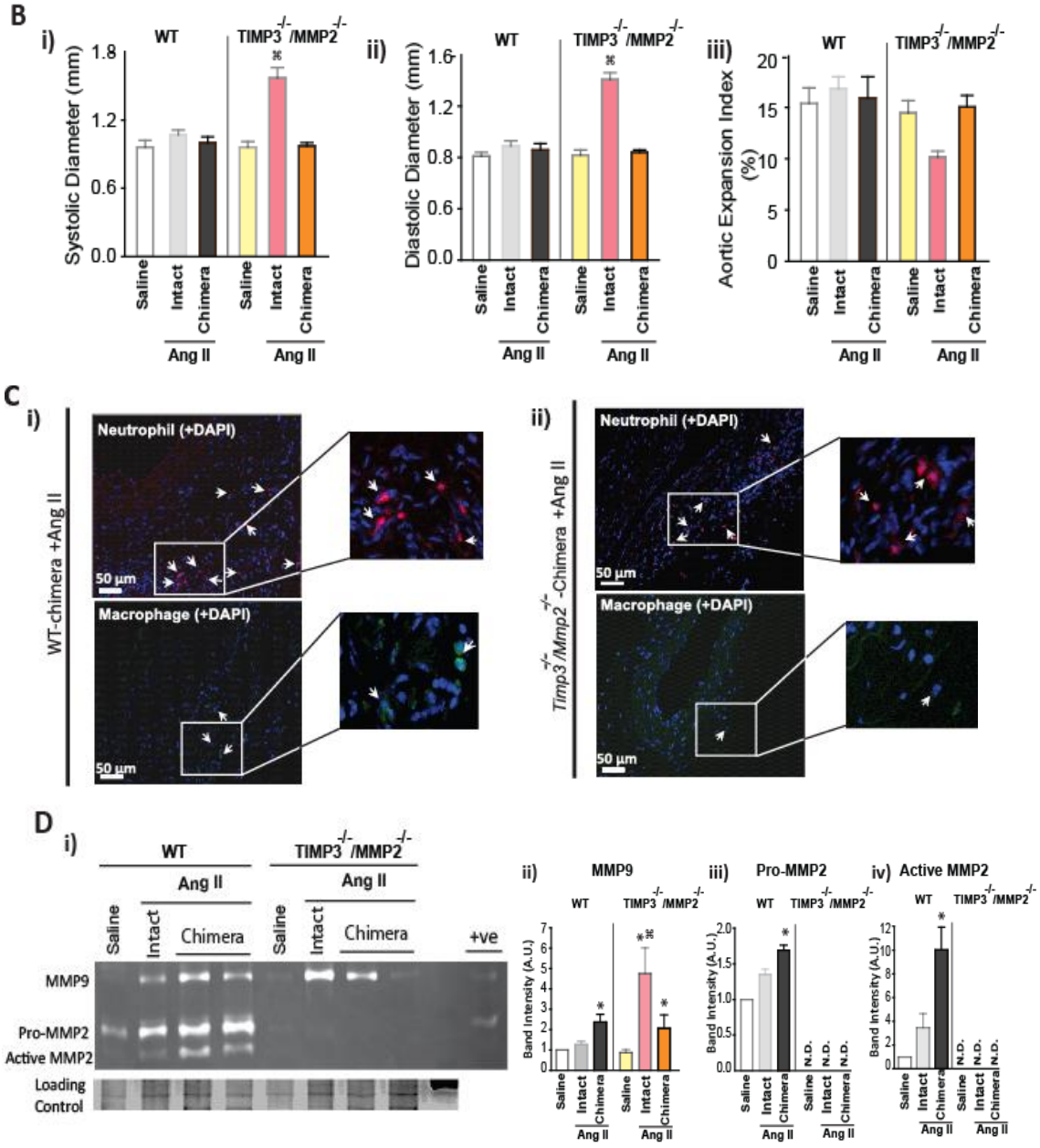

Figure 6.9 WT bone marrow reconstitution alleviated inflammation and AAA in TIMP3$^{-/-}$/MMP2$^{-/-}$ mice.

A) representative images of the entire aorta of WT that received TIMP3$^{-/-}$/MMP2$^{-/-}$ bone marrow (WT-chimera) and TIMP3$^{-/-}$/MMP2$^{-/-}$ mice that received WT bone marrow (TIMP3$^{-/-}$/MMP2$^{-/-}$-chimera) after 7 weeks of bone marrow reconstitution followed by 4 weeks of Ang II infusion. B) Averaged systolic (i) and diastolic abdominal aortic diameters (ii), and expansion index of abdominal aorta (iii) in indicated groups (n=9/genotype/group). The data presented in earlier figures (WT-Ang II and TIMP3$^{-/-}$-Ang II) are shown here in a faded shade. C) Immunofluorescent staining for neutrophil (red) and macrophage (green) superimposed with DAPI nucleus staining (blue) in abdominal aorta of indicated groups. Arrows point to positively stained neutrophils or

macrophages. D) representative *In vitro* gelatin zymography (i), and averaged band intensities for MMP9 and MMP2 (ii) in Ang II-infused chimera groups compared to saline control; *P<0.05 compared to all other groups. N.D; not detectable; A.U.; arbitrary units.

6.5.10 Multiple MMP Inhibition Prevented AAA in TIMP3$^{-/-}$ and TIMP3$^{-/-}$ /MMP2$^{-/-}$ Mice

To investigate the contribution of the elevated protease activity as the underlying mechanism for AAA in TIMP3$^{-/-}$ and the exacerbated AAA formation in TIMP3$^{-/-}$ /MMP2$^{-/-}$ mice, we treated these mice with a broad-spectrum MMP inhibitor, PD166793 (MMPi) [24, 36] during the course of Ang II infusion. Interestingly, simultaneous inhibition of a number of MMPs with this inhibitor blocked AAA development in TIMP3$^{-/-}$ and significantly suppressed AAA formation in TIMP3$^{-/-}$ /MMP2$^{-/-}$ mice (**Fig. 6.10A**). Ultrasonic measurement of abdominal aortic diameter showed that MMPi-treatment was strongly effective in preventing the Ang II-induced dilation of the abdominal aorta in TIMP3$^{-/-}$ and TIMP3$^{-/-}$/MMP2$^{-/-}$ mice (**Figs. 6.10Bi-ii**). Moreover, aortic recoil property, as measured by systolic expansion index, was significantly restored in MMPi-treated TIMP3$^{-/-}$-Ang II mice and to a lesser extent in TIMP3$^{-/-}$/MMP2$^{-/-}$-Ang II mice (**Fig. 7Biii**). These improvements were well reflected in the abdominal aortic wall structure as shown by intact elastin (VVG) and collagen (GT) structures (**Fig. 6.11A**), and preserved elastin lamella organization as seen scanning electron microscopy images (**Fig. 6.11B**). Consistently, MMPi treatment prevented the elevation of collagenase and gelatinase activities in the abdominal aorta of Ang II-infused TIMP3$^{-/-}$ and TIMP3$^{-/-}$/MMP2$^{-/-}$ mice (**Fig. 6.11C**). These data demonstrate the protective

function of MMPi against Ang II-induced aortic wall deterioration which otherwise leads to AAA in TIMP3$^{-/-}$ and TIMP3$^{-/-}$/MMP2$^{-/-}$ mice.

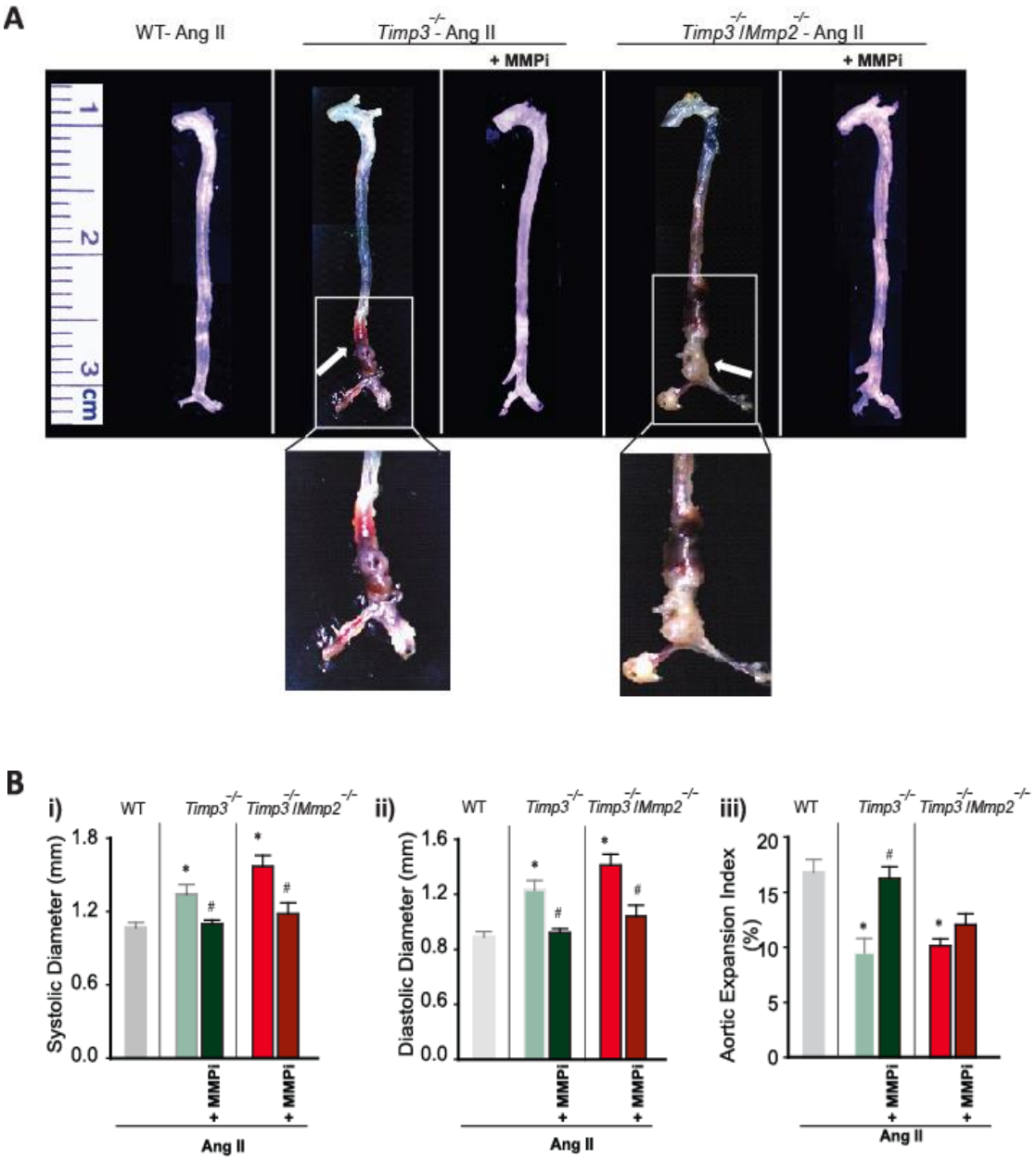

Figure 6.10 Broad spectrum MMP-inhibitor (MMPi, PD166793) prevented Ang II induced AAA in TIMP3$^{-/-}$ and in TIMP3$^{-/-}$/MMP2$^{-/-}$ mice.

A) Macroscopic images of the entire aorta from Ang II-infused WT compared to TIMP3$^{-/-}$ and TIMP$^{-/-}$/MMP2$^{-/-}$ mice without (left) and with (right) MMPi-treatment.. B) averaged systolic (i) diastolic diameters (ii) and systolic expansion index (iii) of abdominal aorta in the indicated

groups. N=9/genotype/group. The data shown earlier are in faded colour bars for comparision. *P<0.05 compared to WT. #P<0.05 compared with corresponding non-MMPi treated group.

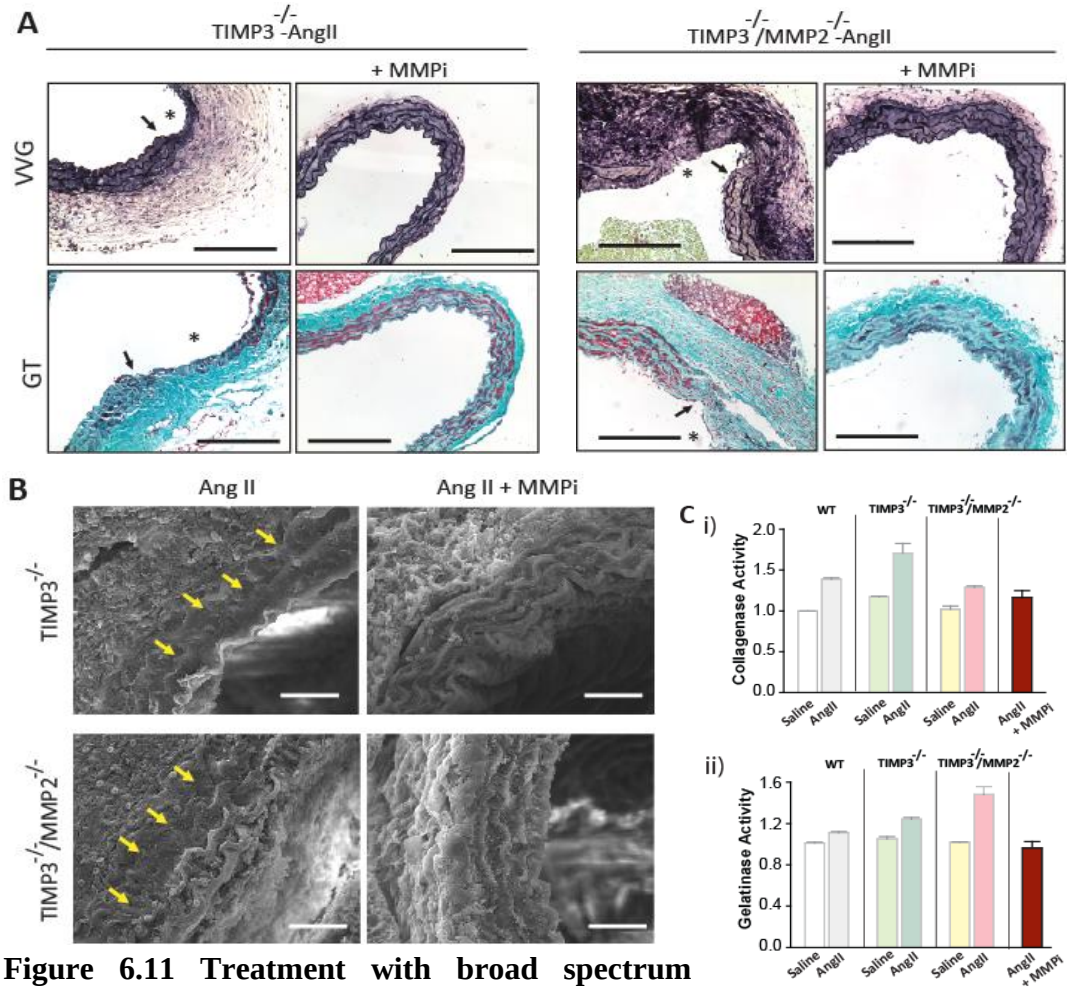

Figure 6.11 Treatment with broad spectrum PD166793) prevented the structural degradation in the abdominal aorta in TIMP3$^{-/-}$ and in TIMP3$^{-/-}$/MMP2$^{-/-}$ mice.

A) Histoligical analysis showing elastin (VVG) and collagen (GT) structure and arrangement in Ang II-infused TIMP3$^{-/-}$ and TIMP$^{-/-}$/MMP2$^{-/-}$ mice after without (left) and with (right) MMPi-treatment. Scale bar=200 µm. B) Scanning electron microscopy of the abdominal aorta in indicated groups showing the improved structural arrangement following MMPi-treatment. Scale bar=40 µm. The arrows point to the disrupted elastin lamella and wall structure. VVG=Verhoeff-Van Gieson staining, GT=Gomori Trichrome staining. *indicates the site of aneurysm in untreated groups

6.6 DISCUSSION

Abdominal aortic aneurysm (AAA) is a common and lethal vascular disorder as about 6-9% of the elderly population have an AAA [6, 37]. While small aneurysms can be managed conservatively with imaging and controlling of risk factors such

as smoking and hypertension, patients continue to experience significant morbidity and mortality from ruptured aneurysms [4, 6]. Development and expansion of AAA result from disruption of the orderly structure of the aortic wall and ECM. Elastin and collagen fibres are the main structural proteins of the aortic ECM, which underlie the recoil properties and impart strength to the vessel wall, respectively [11, 12]. TIMP3 is the only ECM-bound TIMP, and its altered levels have been linked to aortic rupture [16] and aortic aneurysm [17] while its polymorphism showed strong association with AAA in patients with a family history of AAA [18]. In this study we provide evidence for the causal role of TIMP3-deficiency in development of AAA by demonstrating that mice lacking TIMP3 are more susceptible to Ang II-induced AAA. We found a temporal and transient rise in TIMP3 levels in the abdominal aorta of WT mice following Ang II infusion. This is consistent with the finding in patients with aortic aneurysm which reported that the increase in TMP3 mRNA was a compensatory response to the augmented MMP activity [17].

We used the Ang II-infused model of aortic aneurysm formation in the absence of dyslipidemia and/or metabolic syndrome commonly associated with high fat-fed models of AAA where aneurysm forms under atherosclerotic lesions [37]. Ang II is a physiological hormone that is elevated in patients with cardiovascular diseases [38-40] and has been shown to exert direct effects on vascular remodelling and function in numerous studies [23, 35, 41]. The Ang II infusion model allowed us to examine the role of TIMP3 in the adverse remodeling of the aortic wall leading to

aortic aneurysm formation, in the absence of complications associated with atherosclerosis, and in the entire aorta rather than a targeted region. In this study we report that, first, the regulatory function of TIMP3 is essential in preventing AAA development; second, despite the greater increase in MMP2 activation in the aneurysmal TIMP3$^{-/-}$ aorta, specific deletion of MMP2 led to compensatory upregulation of MMP9, inflammation and exacerbated AAA; third, MMP2 is produced by the cells intrinsic to the aorta while inflammatory cells are the main source of MMP9; fourth simultaneous inhibition of a number of ECM-degrading proteinases (MMPs) could be a more effective approach in treating AAA.

The saline-infused TIMP3$^{-/-}$ mice showed comparable MMP activities and aortic structure to WT-saline group and did not develop AAA, suggesting that under normal conditions, the remaining TIMPs (-1, -2 and -4) are sufficient to keep the activity of MMPs under control in the absence of TIMP3. However, in the presence of a pathological stimulus such as Ang II, TIMP3 is critical in regulating the proteolytic activities for optimal remodeling in the abdominal aortic wall. TIMP3 has been reported to hinder the activation of pro-MMP2 (72kDa) into its cleaved (64 kDa) form [28], and consistently, we found that absence of TIMP3 promoted activation of pro-MMP2 into its 64kDa form in the TIMP3$^{-/-}$-AngII aortas. However, TIMP3$^{-/-}$/MMP2$^{-/-}$ mice revealed that MMP2 activation is not the deriving factor in AAA formation in these mice. The more severe AAA in TIMP3$^{-/-}$/MMP2$^{-/-}$-Ang II mice is particularly interesting since MMP2 has been strongly linked to AAA in patients [42, 43], and MMP2$^{-/-}$ mice are protected against

$CaCl_2$-induced AAA [44]. However in the absence of TIMP3, MMP2 deletion resulted in adverse outcomes such as inflammation and MMP9 upregulation. MMP2 has been shown to play a role in early stages of vascular remodeling such as in aneurysm formation [42, 43], while MMP9 is suggested to be involved in later stages such as aneurysm expansion [42, 45]. MMP9 has been identified as the key elastase involved in vascular degeneration and aneurysm [33, 46] which can also degrade other vascular ECM proteins such as the basement membrane collagen type IV [47]. Mice lacking MMP9 are protected against elastase-induced AAA [33], as well as $CaCl_2$-induced AAA [44]. In this study, we demonstrate that reconstitution of WT bone marrow in $TIMP3^{-/-}/MMP2^{-/-}$ mice suppressed infiltration of inflammatory cells, reduced MMP9 levels and prevented the Ang II-induced AAA formation, while no MMP2 was detected in $TIMP3^{-/-}/MMP2^{-/-}$-chimera mice. In agreement with our findings, it has been reported that reconstitution of WT macrophages in $MMP9^{-/-}$ mice, but not in $MMP2^{-/-}$ mice, led to development of AAA in the $MMP9^{-/-}$ mice which are otherwise resistant to $CaCl_2$-induced AAA, therefore, the macrophage-derived MMP9 and the MMP2 produced by mesenchymal cells were proposed to work in concert to mediate AAA [44]. Further, production of MMP2 by mysenchymal cells has been shown to be enhanced by the presence of inflammatory cells [48]. This is consistent with our observation of elevated MMP2 levels in WT-chimera mice (containing $TMP3^{-/-}/MMP2^{-/-}$ bone marrow) as the only possible source of MMP2 in these animals is in fact the native cells and not the $TMP3^{-/-}/MMP2^{-/-}$ inflammatory cells. Elastin degradation

products in AAA samples from patients exhibit chemotactic activity that attracts macrophages to the site of AAA leading to inflammation [49]. Since the inflammatory cells such as neutrophils and macrophages produce MMP9 [50, 51] and other ECM-degrading metalloproteinases [52, 53], this initiates a vicious cycle leading to further destruction of the aortic wall structure, aortic expansion and more severe AAA. TIMP1 has been shown be protective against aortic aneurysm [54-56], whereas TIMP2-deficiency posed beneficial outcomes in a $CaCl_2$ model of AAA [57].

6.7 CONCLUSION

The current study is the first report on the role of TIMP3, the only ECM-bound TIMP, and AAA. In this study we demonstrate that lack of TIMP3 triggers adverse remodeling of aortic wall and AAA formation in response to Ang II. In addition, inhibition of one specific MMP did not provide beneficial outcomes in limiting AAA progression, whereas inhibition of a number of ECM-targeting MMPs was a more effective approach. Consistent with our findings, doxycycline, a broad spectrum MMP inhibitor, has been a promising treatment in preventing AAA expansion and rupture [58-61], whereas other treatments including β-blockers, ACE inhibitors and statins have been ineffective[1-4, 6]. Overall, our study demonstrates that TIMP3 is critical in constructive vascular remodeling and and as such, targeted overexpression of TIMP3 could serve as a promising therapeutic approach in preventing aneurysm formation or controlling its expansion.

6.8 REFERENCES

1. Baxter BT, Terrin MC, Dalman RL. Medical management of small abdominal aortic aneurysms. *Circulation*. 2008;117:1883-1889

2. Investigators TPAT. Propranolol for small abdominal aortic aneurysms: Results of a randomized trial. *J Vasc Surg*. 2002;35:72-79

3. Ferguson CD, Clancy P, Bourke B, Walker PJ, Dear A, Buckenham T, Norman P, Golledge J. Association of statin prescription with small abdominal aortic aneurysm progression. *Am Heart J*. 2010;159:307-313

4. Golledge J, Norman PE. Current status of medical management for abdominal aortic aneurysm. *Atherosclerosis*. 2011

5. Isselbacher EM. Thoracic and abdominal aortic aneurysms. *Circulation*. 2005;111:816-828

6. Danyi P, Elefteriades JA, Jovin IS. Medical therapy of thoracic aortic aneurysms: Are we there yet? *Circulation*. 2011;124:1469-1476

7. Greenhalgh RM, Brown LC, Powell JT, Thompson SG, Epstein D. Endovascular repair of aortic aneurysm in patients physically ineligible for open repair. *N Engl J Med*. 2010;362:1872-1880

8. Singh K, Bonaa KH, Jacobsen BK, Bjork L, Solberg S. Prevalence of and risk factors for abdominal aortic aneurysms in a population-based study : The tromso study. *Am J Epidemiol*. 2001;154:236-244

9. Forsdahl SH, Solberg S, Singh K, Jacobsen BK. Abdominal aortic aneurysms, or a relatively large diameter of non-aneurysmal aortas, increase total and cardiovascular mortality: The tromso study. *Int J Epidemiol*. 2010;39:225-232

10. Zhang X, Thatcher SE, Rateri DL, Bruemmer D, Charnigo R, Daugherty A, Cassis LA. Transient exposure of neonatal female mice to testosterone abrogates the sexual dimorphism of abdominal aortic aneurysms. *Circ Res*. 2012;110:e73-85

11. Cummins PM, von Offenberg Sweeney N, Killeen MT, Birney YA, Redmond EM, Cahill PA. Cyclic strain-mediated matrix metalloproteinase regulation within the vascular endothelium: A force to be reckoned with. *Am J Physiol Heart Circ Physiol*. 2007;292:H28-42

12. Wagenseil JE, Mecham RP. Vascular extracellular matrix and arterial mechanics. *Physiol Rev*. 2009;89:957-989

13. Knox JB, Sukhova GK, Whittemore AD, Libby P. Evidence for altered balance between matrix metalloproteinases and their inhibitors in human aortic diseases. *Circulation*. 1997;95:205-212

14. Leco KJ, Khokha R, Pavloff N, Hawkes SP, Edwards DR. Tissue inhibitor of metalloproteinases-3 (timp-3) is an extracellular matrix-associated protein with a distinctive pattern of expression in mouse cells and tissues. *J Biol Chem*. 1994;269:9352-9360

15. Yu WH, Yu S, Meng Q, Brew K, Woessner JF, Jr. Timp-3 binds to sulfated glycosaminoglycans of the extracellular matrix. *J Biol Chem*. 2000;275:31226-31232

16. Ikonomidis JS, Jones JA, Barbour JR, Stroud RE, Clark LL, Kaplan BS, Zeeshan A, Bavaria JE, Gorman JH, 3rd, Spinale FG, Gorman RC. Expression of matrix metalloproteinases and endogenous inhibitors within ascending aortic aneurysms of patients with marfan syndrome. *Circulation*. 2006;114:I365-370

17. Tsarouhas K, Soufla G, Apostolakis S, Zaravinos A, Panagiotou M, Khoury M, Hassoulas JA, Tsatsakis AM, Spandidos DA. Transcriptional regulation of timps in ascending aorta aneurysms. *Thromb Res*. 2010;126:399-405

18. Ogata T, Shibamura H, Tromp G, Sinha M, Goddard KA, Sakalihasan N, Limet R, MacKean GL, Arthur C, Sueda T, Land S, Kuivaniemi H. Genetic analysis of polymorphisms in biologically relevant candidate genes in patients with abdominal aortic aneurysms. *J Vasc Surg*. 2005;41:1036-1042

19. Kassiri Z, Oudit GY, Kandalam V, Awad A, Wang X, Ziou X, Maeda N, Herzenberg AM, Scholey JW. Loss of timp3 enhances interstitial nephritis and fibrosis. *J Am Soc Nephrol*. 2009;20:1223-1235

20. Itoh T, Ikeda T, Gomi H, Nakao S, Suzuki T, Itohara S. Unaltered secretion of beta-amyloid precursor protein in gelatinase a (matrix metalloproteinase 2)-deficient mice. *J Biol Chem*. 1997;272:22389-22392

21. Johnson AW, Kinzenbaw DA, Modrick ML, Faraci FM. Small-molecule inhibitors of signal transducer and activator of transcription 3 protect against angiotensin ii-induced vascular dysfunction and hypertension. *Hypertension*. 2012

22. Zhong J, Guo D, Chen CB, Wang W, Schuster M, Loibner H, Penninger JM, Scholey JW, Kassiri Z, Oudit GY. Prevention of angiotensin ii-mediated renal oxidative stress, inflammation, and fibrosis by angiotensin-converting enzyme 2. *Hypertension*. 2011;57:314-322

23. Flamant M, Placier S, Dubroca C, Esposito B, Lopes I, Chatziantoniou C, Tedgui A, Dussaule JC, Lehoux S. Role of matrix metalloproteinases in early hypertensive vascular remodeling. *Hypertension*. 2007;50:212-218

24. Kandalam V, Basu R, Abraham T, Wang X, Awad A, Wang W, Lopaschuk GD, Maeda N, Oudit GY, Kassiri Z. Early activation of matrix metalloproteinases underlies the exacerbated systolic and diastolic dysfunction in mice lacking timp3 following myocardial infarction. *Am J Physiol Heart Circ Physiol*. 2010;299:H1012-1023

25. Kandalam V, Basu R, Moore L, Fan D, Wang X, Jaworski DM, Oudit GY, Kassiri Z. Lack of tissue inhibitor of metalloproteinases 2 leads to exacerbated left ventricular dysfunction and adverse extracellular matrix remodeling in response to biomechanical stress. *Circulation*. 2011;124:2094-2105

26. Suen AY, Baldwin TA. Proapoptotic protein bim is differentially required during thymic clonal deletion to ubiquitous versus tissue-restricted antigens. *Proc Natl Acad Sci U S A*. 2010;109:893-898

27. Kandalam V, Basu R, Abraham T, Wang X, Soloway PD, Jaworski DM, Oudit GY, Kassiri Z. Timp2 deficiency accelerates adverse post-myocardial infarction remodeling because of enhanced mt1-mmp activity despite lack of mmp2 activation. *Circ Res*. 2010;106:796-808

28. English JL, Kassiri Z, Koskivirta I, Atkinson SJ, Di Grappa M, Soloway PD, Nagase H, Vuorio E, Murphy G, Khokha R. Individual timp deficiencies differentially impact pro-mmp-2 activation. *J Biol Chem*. 2006;281:10337-10346

29. Moore L, Fan D, Basu R, Kandalam V, Kassiri Z. Tissue inhibitor of metalloproteinases (timps) in heart failure. *Heart Fail Rev*. 2012;17:693-706

30. Lederle FA, Johnson GR, Wilson SE, Chute EP, Littooy FN, Bandyk D, Krupski WC, Barone GW, Acher CW, Ballard DJ. Prevalence and associations of abdominal aortic aneurysm detected through screening. Aneurysm detection and management (adam) veterans affairs cooperative study group. *Ann Intern Med*. 1997;126:441-449

31. Bezerra Lira-Filho E, Campos O, Lazaro Andrade J, Henrique Fischer C, Godoy Nunes C, Cavalcanti Lins A, Hata F, Carvalho AC. Thoracic aorta evaluation in patients with takayasu's arteritis by transesophageal echocardiography. *J Am Soc Echocardiogr*. 2006;19:829-834

32. Aimes RT, Quigley JP. Matrix metalloproteinase-2 is an interstitial collagenase. Inhibitor-free enzyme catalyzes the cleavage of collagen fibrils and soluble native type i collagen generating the specific 3/4- and 1/4-length fragments. *J Biol Chem*. 1995;270:5872-5876

33. Thompson RW, Holmes DR, Mertens RA, Liao S, Botney MD, Mecham RP, Welgus HG, Parks WC. Production and localization of 92-kilodalton gelatinase in abdominal aortic aneurysms. An elastolytic metalloproteinase expressed by aneurysm-infiltrating macrophages. *J Clin Invest*. 1995;96:318-326

34. Gong Y, Hart E, Shchurin A, Hoover-Plow J. Inflammatory macrophage migration requires mmp-9 activation by plasminogen in mice. *J Clin Invest*. 2008;118:3012-3024

35. Satoh K, Nigro P, Matoba T, O'Dell MR, Cui Z, Shi X, Mohan A, Yan C, Abe J, Illig KA, Berk BC. Cyclophilin a enhances vascular oxidative stress and the development of angiotensin ii-induced aortic aneurysms. *Nat Med*. 2009;15:649-656

36. Kassiri Z, Oudit GY, Sanchez O, Dawood F, Mohammed FF, Nuttall RK, Edwards DR, Liu PP, Backx PH, Khokha R. Combination of tumor necrosis factor-alpha ablation and matrix metalloproteinase inhibition prevents heart failure after pressure overload in tissue inhibitor of metalloproteinase-3 knock-out mice. *Circ Res*. 2005;97:380-390

37. Ruddy JM, Jones JA, Spinale FG, Ikonomidis JS. Regional heterogeneity within the aorta: Relevance to aneurysm disease. *J Thorac Cardiovasc Surg*. 2008;136:1123-1130

38. Tomaschitz A, Pilz S, Ritz E, Morganti A, Grammer T, Amrein K, Boehm BO, Marz W. Associations of plasma renin with 10-year cardiovascular mortality, sudden cardiac death, and death due to heart failure. *Eur Heart J*. 2011;32:2642-2649

39. Javed U, Deedwania PC. Angiotensin receptor blockers: Novel role in high-risk patients. *Cardiol Clin*. 2008;26:507-526

40. Bohm M. Angiotensin receptor blockers versus angiotensin-converting enzyme inhibitors: Where do we stand now? *Am J Cardiol*. 2007;100:38J-44J

41. Brands MW, Banes-Berceli AK, Inscho EW, Al-Azawi H, Allen AJ, Labazi H. Interleukin 6 knockout prevents angiotensin ii hypertension: Role of renal vasoconstriction and janus kinase 2/signal transducer and activator of transcription 3 activation. *Hypertension*. 2010;56:879-884

42. Goodall S, Crowther M, Hemingway DM, Bell PR, Thompson MM. Ubiquitous elevation of matrix metalloproteinase-2 expression in the vasculature of patients with abdominal aneurysms. *Circulation*. 2001;104:304-309

43. Crowther M, Goodall S, Jones JL, Bell PR, Thompson MM. Localization of matrix metalloproteinase 2 within the aneurysmal and normal aortic wall. *Br J Surg*. 2000;87:1391-1400

44. Longo GM, Xiong W, Greiner TC, Zhao Y, Fiotti N, Baxter BT. Matrix metalloproteinases 2 and 9 work in concert to produce aortic aneurysms. *J Clin Invest*. 2002;110:625-632

45. Freestone T, Turner RJ, Coady A, Higman DJ, Greenhalgh RM, Powell JT. Inflammation and matrix metalloproteinases in the enlarging abdominal aortic aneurysm. *Arterioscler Thromb Vasc Biol*. 1995;15:1145-1151

46. Pyo R, Lee JK, Shipley JM, Curci JA, Mao D, Ziporin SJ, Ennis TL, Shapiro SD, Senior RM, Thompson RW. Targeted gene disruption of matrix metalloproteinase-9 (gelatinase b) suppresses development of experimental abdominal aortic aneurysms. *J Clin Invest*. 2000;105:1641-1649

47. Murphy G, Cockett MI, Ward RV, Docherty AJ. Matrix metalloproteinase degradation of elastin, type iv collagen and proteoglycan. A quantitative comparison of the activities of 95 kda and 72 kda gelatinases, stromelysins-1 and -2 and punctuated metalloproteinase (pump). *Biochem J*. 1991;277 (Pt 1):277-279

48. Davis V, Persidskaia R, Baca-Regen L, Itoh Y, Nagase H, Persidsky Y, Ghorpade A, Baxter BT. Matrix metalloproteinase-2 production and its binding to the matrix are increased in abdominal aortic aneurysms. *Arterioscler Thromb Vasc Biol*. 1998;18:1625-1633

49. Hance KA, Tataria M, Ziporin SJ, Lee JK, Thompson RW. Monocyte chemotactic activity in human abdominal aortic aneurysms: Role of elastin degradation peptides and the 67-kd cell surface elastin receptor. *J Vasc Surg*. 2002;35:254-261

50. Cuadrado E, Ortega L, Hernandez-Guillamon M, Penalba A, Fernandez-Cadenas I, Rosell A, Montaner J. Tissue plasminogen activator (t-pa)

promotes neutrophil degranulation and mmp-9 release. *Journal of leukocyte biology*. 2008;84:207-214

51. Lambert JM, Lopez EF, Lindsey ML. Macrophage roles following myocardial infarction. *International journal of cardiology*. 2008;130:147-158

52. Shapiro SD, Campbell EJ, Senior RM, Welgus HG. Proteinases secreted by human mononuclear phagocytes. *The Journal of rheumatology. Supplement*. 1991;27:95-98

53. Shapiro SD, Campbell EJ, Welgus HG, Senior RM. Elastin degradation by mononuclear phagocytes. *Ann N Y Acad Sci*. 1991;624:69-80

54. Ikonomidis JS, Gibson WC, Butler JE, McClister DM, Sweterlitsch SE, Thompson RP, Mukherjee R, Spinale FG. Effects of deletion of the tissue inhibitor of matrix metalloproteinases-1 gene on the progression of murine thoracic aortic aneurysms. *Circulation*. 2004;110:II268-273

55. Eskandari MK, Vijungco JD, Flores A, Borensztajn J, Shively V, Pearce WH. Enhanced abdominal aortic aneurysm in timp-1-deficient mice. *J Surg Res*. 2005;123:289-293

56. Allaire E, Forough R, Clowes M, Starcher B, Clowes AW. Local overexpression of timp-1 prevents aortic aneurysm degeneration and rupture in a rat model. *J Clin Invest*. 1998;102:1413-1420

57. Xiong W, Knispel R, Mactaggart J, Baxter BT. Effects of tissue inhibitor of metalloproteinase 2 deficiency on aneurysm formation. *J Vasc Surg*. 2006;44:1061-1066

58. Baxter BT, Pearce WH, Waltke EA, Littooy FN, Hallett JW, Jr., Kent KC, Upchurch GR, Jr., Chaikof EL, Mills JL, Fleckten B, Longo GM, Lee JK, Thompson RW. Prolonged administration of doxycycline in patients with small asymptomatic abdominal aortic aneurysms: Report of a prospective (phase ii) multicenter study. *J Vasc Surg*. 2002;36:1-12

59. Mosorin M, Juvonen J, Biancari F, Satta J, Surcel HM, Leinonen M, Saikku P, Juvonen T. Use of doxycycline to decrease the growth rate of abdominal aortic aneurysms: A randomized, double-blind, placebo-controlled pilot study. *J Vasc Surg*. 2001;34:606-610

60. Hackmann AE, Rubin BG, Sanchez LA, Geraghty PA, Thompson RW, Curci JA. A randomized, placebo-controlled trial of doxycycline after endoluminal aneurysm repair. *J Vasc Surg*. 2008;48:519-526; discussion 526

61. Lindeman JH, Abdul-Hussien H, van Bockel JH, Wolterbeek R, Kleemann R. Clinical trial of doxycycline for matrix metalloproteinase-9 inhibition in patients with an abdominal aneurysm: Doxycycline selectively depletes aortic wall neutrophils and cytotoxic t cells. *Circulation*. 2009;119:2209-2216

CHAPTER SEVEN

DISCUSSION

Rise in the aging population is concomitant with the increase in prevalence of patients suffering from multiple chronic diseases as oppose to single disease[1]. The significant global death due to NCDs (63% of all deaths globally) is associated with an increase in the risk of developing diseases such as CVD, diabetes and CKD in the same person as co-morbid states. Diabetes is a well-established risk factor for CVD (including hypertension and dyslipidemia)[2] and diabetic nephropathy, a leading cause of end stage kidney disease. On the contrary CKD alone increases the risk factor for CVD and vice versa[3]. Prolonged untreated hypertension leads to CKD due to damage of renal blood vessels. Moreover, commonalities in risk factors (ageing, obesity, sedentary lifestyle, unhealthy food habits, smoking)[4] associated with these diseases further encourage occurrence of cardio metabolic syndrome (a constellation of insulin resistance/hyperinsulinemia, central obesity, dyslipidemia, hypertension and microalbuminuria)[5]. However, the high risk of developing CVD, diabetes and CKD in the midst of cardiometabolic syndrome (3 times more compared to absence of cardiometabolic syndrome)[6, 7]clearly suggests the presence of unknown, complex mechanisms and molecules that bind these diseases. In view of such complexity associated with these diseases, transgenic murine models serve as an invaluable tool to study and better understand the pathogenesis by replicating these diseases or pathological states.

The question arises as what determines the normal as opposed to pathological state of an organ? Normal function of an organ is maintained by the metabolic and structural homeostasis of its cellular as well as extracellular matrix (ECM) components. Metabolic homeostatic imbalance involves changes in substrate for cellular energetics, oxidative stress (mitochondrial derived ROS) and accumulation of cytotoxic by-products metabolic imbalance together with dynamic changes in the ECM impacts the spatio-temporal onset of a disease and its complications.

Generally, the ECM consists of fibrous structural proteins (collagen and elastin predominantly) embedded in a gel like consistent ground substance made up of polysaccharide (glycosaminoglycan). Differential proportion of these two ECM components determines the type of ECM required for an organ (for example ECM of tendons are high in fibrous proteins whereas abundant polysaccharides make up cartilages) to maintain its normal function. Integrity of the ECM is maintained by a balance between a group of proteinases, MMPs and their endogenous physiological inhibitors, TIMPs. TIMP3 is a potent inhibitor of a number of MMPs, and is the only TIMP directly bound to the ECM. Thus, my interest to study diseases such as diabetic cardiomyopathy, diabetic nephropathy, hypertension and aortic aneurysm was directed on either subtle changes in metabolism and/or the causal role of TIMP3 underlying a small but an essential part in the pathogenesis and the observed phenotype.

7.1 SYNOPSIS OF IMPORTANT AND NOVEL FINDINGS

Our study is the first to show that the predominant cardiac phenotypic abnormality in Akita (*Ins2*$^{WT/C96Y}$) mice is an early diastolic dysfunction in the absence of any systolic dysfunction. We captured and characterized the diastolic dysfunction using a state-of-the art echocardiographic technique including tissue Doppler imaging in combination with invasive hemodynamic assessment. We evaluated the systolic function in Akita mice by echocardiography, hemodynamic measurement and *ex vivo* working heart preparation, and found it to be comparable to the control WT (*Ins2*$^{WT/WT}$) mice at 3- and 6-month of age. Moreover, the genetic defect in Akita mice resulted in an early and sustained loss of the insulin-producing β-cells and low plasma insulin levels [8, 9] associated with suppressed Erk1/2 and serine-473 and threonine-308 phosphorylation of Akt/PKB phosphorylation at 6 months but not at 3 months owing to early compensatory changes by other agonists such as insulin-like growth factor-1 (IGF-1) and/or adiponectin which are known to activate the Akt/PKB pathway [10, 11]. The presence of heart disease in Akita heart was associated with increased expression of the disease markers, B-type natriuretic peptide (BNP) which is a disease marker for cardiomyopathy and has been reported to be elevated in patients with diastolic heart failure[12] and beta-myosin heavy chain (β-MHC) without any signs of LV hypertrophy. Akita hearts were devoid of any myocardial fibrosis contrary to earlier findings where myocardial fibrosis in diabetic hearts has been shown to be triggered by oxidative stress[13].

Our findings were consistent with a recent study reporting absence of oxidative stress in these hearts[14]. Apart from interstitial fibrosis diastolic dysfunction in diabetic cardiomyopathy has been linked to impaired cytosolic calcium handling via SERCA2 downregulation and/or lipotoxicity affecting both passive (compliance) and active relaxation in the ventricle.[15, 16] We found reduced levels of SERCA2 without any change in protein levels of phospholamban or its serine-16 phosphorylation status in Akita hearts. However, these changes were associated with prolonged IVRT and relaxation time constant (tau) and reduced $-dP/dt_{min}$ in diabetic hearts. Moreover, our findings revealed an impaired fatty acid metabolism leading to accumulation of lipid intermediates (myocardial triacylglycerol accumulation, increased use of long-chain fatty acids and increased production of ceramide) together with elevated expression of long chain acyl-CoA dehydrogenase (LCAD) in Akita hearts as a predisposing factor towards lipotoxic cardiomyopathy.[17]

In addition to cardiomyopathy diabetic nephropathy is a well-recognized complication of diabetes and the most common cause of end-stage renal disease (ESRD) in the U.S. [18-20] Studies in patients with diabetic nephropathy have implicated a possible role of TIMP3 in diabetic nephropathy [21, 22]. Moreover, TIMP3 levels were increased in diabetic kidneys with a relative lack of alteration in cardiac TIMP3 levels of Akita mice. TIMP3 deficiency in Akita mice led to an excacerbated form of diabetic renal injury as exemplified by significantly increased kidney mass, glomerular mesangial matrix score and urinary albumin

excretion which are all early features of human diabetic nephropathy [23]. These changes occurred in the absence of worsening of hypertension and glycemic control. Consistent with the lack of relative change in TIMP3 levels in Akita compared to WT cardiac tissue, TIMP3 deficiency did not exacerbate this diabetic cardiomyopathy.

Our findings for the first time demonstrated the early compensatory role of TIMP3 in diabetic nephropathy and are consistent with observations made in human diabetic nephropathy [21, 22]. We further determined that deficiency of TIMP3 led to the loss of early compensation which resulted in increased oxidative stress secondary to increased TACE activity, induction of mRNA expression of various fibrotic and inflammatory markers and altered glomerular mesangium matrix due to relative increase in proteolysis secondary to active MMP2. Although activation of MMP2 was comparable in TIMP3 deficient and Akita/TIMP3 double mutant kidneys, it affected only the diabetic kidney and resulted in the worsening of the nephropathy together with an increased renal oxidative stress.

These findings highlighted organ specific role of TIMP3, as well as differential function based on the type of insult within an individual organ. While the level of TIMP3 was unaffected in diabetic mouse heart, other studies have reported that its deficiency exacerbated heart disease in different murine models[24-26]. However, organ and disease specific role of TIMP3 were further exemplified by a blunted hypertensive response in mice lacking TIMP3, but not TIMP1, TIMP2 or TIMP4,

following Ang II infusion for 2 weeks. It is critical to note that this reduced hypertension in TIMP3 deficient mice was primarily due to degradation of the ECM in small arteries and cannot be regarded as a protective antihypertensive mechanism. Although, acute vasoconstrictive and vasodilatory responses of mesenteric arteries were intact in TIMP3 deficient mice using an *ex vivo* approach, two weeks of Ang II infusion resulted in structural remodeling in small arteries making them more distensible. A similar pattern of upward shift in pressure-diameter relationship was observed in TIMP3$^{-/-}$-Ang II compared to WT-Ang II mesenteric and carotid arteries that was consistent with a loss of the ECM structural proteins, collagen and elastin,[27, 28]. Moreover, prolonged exposure of the agonist for 4 weeks resulted in pathological dilation of the aortic lumen and led to adverse outcomes such as abdominal aortic aneurysm.

The adverse remodelling in the abdominal aorta of TIMP3 deficient mice was associated with increased proteolytic activity of MMP2. TIMP3 has been earlier reported to hinder the activation of pro-MMP2 (72kDa) into its cleaved (64 kDa) form[29]. Surprisingly, upon additional deletion of MMP2 in the absence of TIMP3 resulted in increased MMP9 activation in association with elastase activity in response to Ang II infusion which led to a more severe AAA. This detoriation in the aneurysmal growth in the double deficient mice was associated with increased infiltration of inflammatory cells such as macrophages and neutrophils. However, reconstitution of WT bone marrow in TIMP3 and MMP2 double deficient mice suppressed infiltration of inflammatory cells and reduced MMP9 levels that

prevented the Ang II-induced AAA formation. Consistently, inhibition of excess protease activities in TIMP3 deficient mice prevented suppressed hypertensive response at 2 weeks as well as abrogated the formation of AAA post 4 weeks of Ang II infusion. These findings collectively demonstrate the critical role of TIMP3 in maintaining a delicate balance with MMPs that is specific to an organ system and the type of stimulus triggering the disease process.

7.2 DISCRETE RESPONSE OF INSULIN DEFICIENCY AND IMPAIRED SERCA IN DIABETIC CARDIOMYOPATHY

The dual action of insulin as a stimulant of lipogenesis and an inhibitor of lipolysis is a well-known phenomenon[30]. Lack of insulin in type 1 diabetes promotes increase availability of FFA in the plasma resulting in elevated intracellular levels of FA. In streptozotocin-treated rats, insulin administration suppressed the expression and activity of cardiac PDK4,[31] while in an insulin-resistance state, insulin suppresses PDK expression.[32] Consistent with these reports we found insufficient downregulation of PDK4 mRNA in an insulin-deficient state that could be a cause of increased PDK expression leading to impaired glucose oxidation and increased fatty acid oxidation as reported in Akita mice.[14] Chronic exposure of the heart to high levels of free fatty acids may cause accumulation of toxic lipid intermediates within the heart.[33] Cardiomyopathy due to myocardial di and tri-acylglycerol accumulation, increased use of long-chain fatty acids and increased production of ceramide, occurs secondary to lipotoxicity in the heart.[17, 34, 35] Earlier studies have shown that increased myocardial ceramide

leads to increase cytosolic Ca^{2+} due to impaired flux from the endoplasmic reticulum[36]. However, Akita hearts were associated with decreased SERCA levels that may lead to impaired uptake of cytosolic Ca^{2+} resulting in diastolic dysfunction during the early stages of diabetic cardiomyopathy.

7.3 DIFFERENTIAL ROLE OF TIMP3 IN HEART AND KIDNEY PATHOLOGY

TIMP3 is one of the highest expressed TIMPs in the mouse heart and is decreased in patients with ischemic cardiomyopathy[25]. In addition, TIMP3 is most highly expressed in the kidneys[37]. Chronic hyperglycemia has been shown to increase MMP activities [38-40] at differential cellular levels such as vascular ECM, coronary endothelial cells and renal cells which could be partly linked to altered expression of their inhibitors, TIMPs[41]. Moreover, earlier studies have demonstrated that TIMP3 deficiency exacerbated myocardial hypertrophy, fibrosis and inflammation in different murine models of heart disease such as myocardial infarction and pressure overload by transverse aortic constriction [24-26, 42]. Additionally, different cardiomyopathies including diabetic cardiomyopathy are often associated with structural remodeling of the heart, a major component of which is remodeling of the extracellular matrix (ECM) [43]. Direct evidence of ECM remodelling in diabetic cardiomyopathy was shown in streptozotocin treated rats associated with suppressed MMP2 activity and elevated expression of TIMP2 [44]. In Akita hearts the TIMP3 protein levels were comparable to WT hearts at 3 and 6 months of age suggesting lack of any role played by this endogenous MMP

inhibitor in the myocardial ECM of diabetic heart. While, TIMP3-deficiency in insulin receptor haplosufficiency background lead to overt hyperglycemia and hyperinsulinemia in all I*nsr*$^{+/-}$ mice [45], its deficiency did not alter the glycemic status or exacerbate diabetic cardiomyopathy in Akita mice.

Howover, association of TIMP3 in renal disease have been recognised in earlier reports.TIMP3 was found as a significant candidate gene for diabetic nephropathy in humans [21]. Besides, TIMP3 has been linked to a variety of other kidney diseases. Our lab reported that TIMP3-deficient mice subjected to unilateral ureteral obstruction have enhanced interstitial fibrosis and nephritis[26]. We found that TIMP3 protein levels were elevated significantly in diabetic kidneys of Akita mice at 3 and 6 months of age. This selective upregulation of TIMP3 in the diabetic nephropathy plays a key role and consistent with observations made in human diabetic nephropathy[21, 22] Moreover, TIMP3 deficiency in Akita kidneys resulted in an intensified renal injury illustrated by increased renal mass and size, mesangial expansion and elevated urinary albumin excretion, suggesting an early compensatory role of this only ECM bound TIMP in diabetic nephropathy.

7.4 ROLE OF TIMP3 IN REGULATING INFLAMMATION AND FIBROSIS IN DIABETIC NEPHROPATHY

TIMP3 is also a critical player in regulating the tissue microenvironment including control of inflammation and fibrosis[26, 42] Inflammation has been well documented as a cardinal pathogenic mechanism in diabetic nephropathy[46]. Lack of TIMP3 in diabetic kidney induced mRNA expression of various fibrotic and

inflammatory markers such as pro-collagen type I α1, CTGF, TGF-β and MCP-1 significantly which was associated with increased tubuolinterstitial fibrosis in Akita/TIMP3 double mutant kidneys. These findings were directly contributed to TIMP3 deficiency as Akita kidneys did not exhibit such elevation of fibrosis and its markers. It was also consistent with our previous findings showing that loss of TIMP3 enhances interstitial nephritis and fibrosis in a model of unilateral ureteral obstruction[26]. Additionally, TIMP3 is a known physiological inhibitor of TNFα converting enzyme (TACE) and thereby inhibits shedding of membrane bound tumor necrosis factor alpha (TNFα)[47]. We found TIMP3 deficiency in Akita kidney resulted in an increase in the activity of TACE.

7.5 THE ROLE OF TIMP3 IN CANONICAL PATHWAYS MEDIATED RENAL INJURY IN DIABETIC NEPHROPATHY

Hyperglycemia induced generation of ROS via advanced glycation end products (AGE) and cytokine such as TGF-β1 is a well-established phenomenon in neonatal mesangial and proximal tubular epithelial cells [48]. However, we found that TIMP3 deficiency exacerbated renal injury without altering the glycemic status in diabetic mice. Therefore detoriation in nephropathy symptoms in Akita /TIMP3 double mutant mice is directly attributed to the effects of TIMP3 in the modulation of the canonical pathways mediating renal injury. Several canonical pathways are key mediators of diabetic nephropathy including increased renal NADPH oxidase activity, and altered intracellular signaling such as activation of the PKC system and altered remodeling of the glomerular mesangium [49-54].

Activated NADPH oxidase [55] coupled with other sources of oxidative stress such as the mitochondria-dependent [56] and hyperglycemia-induced [57, 58] generation of ROS are clearly linked to the exacerbation of diabetic renal injury. Additionally, increased renal cortical NADPH oxidase activity and expression of $p47^{phox}$ subunit has been linked to renal injury previously[55].

Exacerbation of diabetic renal injury by deletion of TIMP3 was associated with upregulation of TGF-β1 expression, increased generation of NADPH oxidase-dependent ROS and increased expression of the renal cortical NADPH subunits, $p47^{phox}$ and NOX2 ($gp91^{phox}$), in Akita/TIMP3 double mutant kidneys. The peaked NADPH oxidase activity in Akita/TIMP3 double mutant kidneys was reduced dramatically by gp91phox ds tat the specific peptide inhibitor of NADPH oxidase, confirming superoxide generation from NADPH oxidase. Loss of TIMP3 also compromised the activation of renoprotective signaling pathways including the Akt/PI3K and ERK1/2 MAPK pathways[59, 60] while increasing the expression of PKCβ1 which have been linked to exacerbation of diabetic nephropathy [51, 52].

7.6 TIMP3 MEDIATED REGULATION OF MMP2 IN DIABETIC NEPHROPATHY AND AGONIST INDUCED VASCULAR REMODELLING.

TIMP3 has the broadest range of substrates among TIMPs,[61] and in addition to inhibiting activated MMPs, TIMP3 can inhibit the cell surface activation of pro-MMP2 to its cleaved form[29] . Besides, TIMP3 being the only TIMP which is bound to the ECM, it has been identified earlier as a link between diabetes type 2

and vascular inflammation[62]. Earlier studies have implicated differential expression of MMPs predominantly MMP2 and progression of disease process in various rodent models of diabetic nephropathy[63-65]. Besides, expression of MMPs in the nephron is species specific nevertheless; only MMP2 is expressed almost in all segments (glomerulus, proximal tubule, descending loop of Henle, ascending loop of Henle, distal convoluted tubule and collecting duct) of the nephron considering different mammalian species characterized so far [49]. Although, these studies have associated increased ECM accumulation due to decreased expression and activity of MMPs along with earlier report of elevated expression of TIMP2 [66] in the progression of diabetic nephropathy, TIMP3 mRNA expression was suppressed in a rat model of lithium induced diabetic nephropathy [67].

This earlier observation, however suggest differential role of TIMP3 in addition to proteolytic modulation of renal ECM via MMPs in diabetic nephropathy. Despite the fact that MMP2 activation was elevated in TIMP3 deficient and Akita/TIMP3 double mutant kidneys, adverse renal injury and worsening of an existing nephropathy was observed only in the double mutants. However, loss of TIMP3 increased oxidative stress in the setting of active MMP2 which aggravated the pre-existing diabetic nephropathy without affecting baseline TIMP3 deficient mice. Surprisingly, among all TIMP-deficient mice, only lack of TIMP3 resulted in a suppressed hypertensive response to Ang II infusion for 2 weeks. TIMP3 deficiency resulted in elevated activation of cleaved MMP2 in the mesenteric and carotid arteries in response to Ang II. While, TIMP3 has the broadest range of

substrates among TIMPs,[61] and in addition to inhibiting activated MMPs, TIMP3 can inhibit the cell surface activation of pro-MMP2 to its cleaved form,[29] consistent with the observed rise in cleaved MMP2 in Ang II-infused TIMP3$^{-/-}$ arteries. However, increase in cleaved MMP2 was observed in renal tissues of control TIMP3 deficient mice as oppose to baseline TIMP3 deficient aorta suggesting organ specific differential pattern of MMP2 regulation by TIMP3 at baseline.

7.7 MMP2 MEDIATED PROTEOLYSIS IN AGONIST INDUCED VASCULAR REMODELLING IN THE ABSENCE OF TIMP3.

Agonist induced hypertensive vascular remodelling is an active process of structural alterations including degradation and reorganization of the arterial wall ECM proteins, such as collagen, elastin, proteoglycan, and fibronectin.[68] Matrix metalloproteinase (MMP) are a family of zinc dependant proteases that contribute to ECM turnover by degrading existing proteins. MMPs are well regulated at levels of expression, translation, post-translational modification, and inhibition of their activated form by TIMPs.[69, 70] Upon 2 weeks of Ang II infusion we found decreased collagen type I and elastin protein levels in TIMP3 deficient carotid arteries compared to WT despite a significant elevation in its mRNA levels. These findings of decreased elastin protein associated with corresponding increase in mRNA levels suggested post translational degradation rather an impaired synthesis of elastin. Further, evaluating the proteolytic activities that may explain the post translational degradation of structural proteins secondary to agonist

infusion in the wall of carotid arteries, elevated activity of gelatinase comparable in both TIMP3 deficient and WT was observed. However, the elastase activity post agonist infusion was found to be significantly higher in TIMP3 deficient relative to WT carotid walls. Even though MMP2 and 9 are regarded as classical gelatinases, based on early findings of desired substrate, they possess the ability to degrade ECM proteins other than gelatin. Besides, being a classical gelatinase, MMP2 has been shown in several studies to have substrate specificity for elastin and fibrillar collagen.[71-73].

Nevertheless, Ang II infusion for 2 weeks resulted in similar increase in activation of MMP9 but led to a significant elevation of MMP2 in carotids and mesenteric arteries of TIMP3 deficient mice compared to WT mice. This increased levels of activated MMP2 corresponded to elevated elastase activity that resulted in degradation and loss of elastin in carotid and mesenteric arteries of TIMP3 deficient mice. Moreover, in a TIMP3 deficient state the loss of structural proteins secondary to Ang II infusion were not restricted only to mesenteric and carotid arteries and involved larger conduit artery such as aorta. Elevated levels of MMP2 (protein as well as mRNA expression) in TIMP3 deficient aorta were associated with proteolytic degradation of fibrillar collagen and elastin despite an increase in their expression. Long term effects of MMP2 mediated degradation of structural proteins in the TIMP3 deficient aorta after 4 weeks of Ang II infusion resulted in development in abdominal aneurysm (defined by a dilatation of more than 50% from its baseline diameter) as opposed to merely 20% dilatation in WT

aorta. These findings collectively suggest a causal role of elevated MMP2 activation and activity in the absence of TIMP3 in the degradation of structural proteins of small as well as large arteries that underlies agonist induced arterial remodelling and pathological consequences that may lead to refractory hypotension and abdominal aortic aneurysm.

7.8 COMPENSATORY ROLE OF MMP9 IN THE ABSENCE OF MMP2 IN AGONIST INDUCED VASCULAR REMODELLING IN THE ABSENCE OF TIMP3

While, MMP2 mediated proteolytic degradation of vascular structural proteins secondary to 4 weeks of Ang II infusion in the absence of TIMP3 resulted in development of AAA, its absence in TIMP3 deficient mice did not abrogate the phenotype. On the contrary the TIMP3/MMP2 double deficient mice exhibited an exacerbated form of AAA after infusion of Ang II for 4 weeks. The exacerbated form of aneurysm was associated with adverse vascular remodelling and a more severe form than seen in TIMP3 deficient aorta after 4 weeks of agonist infusion. However, in the presence of a pathological stimulus such as Ang II, TIMP3 is critical in regulating the proteolytic activities for optimal remodelling in the abdominal aortic wall. TIMP3 deficiency steadily promoted activation of pro-MMP2 into its 64kDa form in the aorta after Ang II infusion that was consistent with earlier study that reported inhibition of pro-MMP2 (72kDa) by TIMP3[29]. However in the absence of TIMP3, MMP2 deletion resulted in adverse outcomes such as inflammation and MMP9 upregulation. However, upregulation of MMP9 in the absence of MMP2 in TIMP3 deficient mice was observed only secondary to

Ang II infusion but not at baseline levels in the aorta. Moreover earlier reports of increased activation of MMP9 was observed in MMP2 deficient lymphocyte from spleen derived cultured media and resulted in increased severity of experimental autoimmune encephalomyelitis in the brain [74].

Additionally, TIMP3 deficient heart subjected to myocardial infarction resulted in severe inflammation and upregulation of MMP9 in the presence of MMP2 which was not observed in TIMP3 deficient aorta infused with Ang II. All these studies reveal organ specific upregulation of MMP9 secondary to differential stimuli and associated with variable infiltration of inflammatory cells related to these conditions.

7.9 INFLAMMATORY CELLULAR SOURCE OF MMP9 IN TIMP3 DEFICIENT STATE AND ITS ROLE IN AGONIST INDUCED ECM REMODELLING IN AAA

MMP2 has been shown to play a role in early stages of vascular remodeling such as in aneurysm formation [75, 76], while MMP9 is suggested to be involved in later stages such as aneurysm expansion [75, 77].

MMP9 has been identified as the key elastase involved in vascular degeneration and aneurysm [78, 79] which can also degrade other vascular ECM proteins such as the basement membrane collagen type IV [80]. Mice lacking MMP9 are protected against elastase-induced AAA [78], as well as $CaCl_2$-induced AAA [81]. Moreover, severity of inflammation associated with inflammatory diseases including sepsis has often been gauged by levels of MMP9[82]. We found upregulation of MMP9

levels concomitant with increased infiltration of lymphocytes and macrophages in aortas of TIMP3/MMP2 double deficient mice post Ang II infusion. Furthermore, we determined inflammatory cells as a source of upregulated MMP9 in these mice by demonstrating that reconstitution of WT bone marrow in TIMP3/MMP2 double deficient mice suppressed infiltration of inflammatory cells, reduced MMP9 levels and prevented the Ang II-induced AAA formation, without any detection of MMP2 in these chimera mice. Consistent with our findings, it has been reported that reconstitution of WT macrophages in MMP9 deficient, but not in MMP2 deficient mice, led to development of AAA which are otherwise resistant to $CaCl_2$-induced AAA, therefore, the macrophage-derived MMP9 and the MMP2 produced by mesenchymal cells were proposed to work in concert to mediate AAA [81].

Further, production of MMP2 by mesenchymal cells has been shown to be enhanced by the presence of inflammatory cells [83]. This is consistent with our observation of elevated MMP2 levels in WT-chimera mice (containing TMP3/MMP2 double deficient bone marrow) as the only possible source of MMP2 in these animals is in fact the native cells and not the TMP3/MMP2 double deficient inflammatory cells.

Elastin degradation products in AAA samples from patients exhibit chemotactic activity that attracts macrophages to the site of AAA leading to inflammation [84]. Since the inflammatory cells such as neutrophils and macrophages produce MMP9 [85, 86] and other ECM-degrading metalloproteinases [87, 88], this initiates a

vicious cycle leading to further destruction of the aortic wall structure, aortic expansion and more severe AAA.

7.10 CONCLUSION

My thesis comprises of studies involving metabolic perturbation and TIMP3 in the pathognomic role of proteolysis underlying the development of diabetic complications and aortic aneurysm. These investigation presented in preceding chapters proves the multifaceted role of TIMP3 in various diseases that continues to plague humans in this 21st century. However a long path remains to be traversed to validate these novel findings in relevance to humans for appropriate clinical trials and potential therapies.

7.11 REFERENCES

1. Marengoni A, Winblad B, Karp A, Fratiglioni L. Prevalence of chronic diseases and multimorbidity among the elderly population in sweden. *Am J Public Health*. 2008;98:1198-1200

2. Diabetes mellitus: A major risk factor for cardiovascular disease. A joint editorial statement by the american diabetes association; the national heart, lung, and blood institute; the juvenile diabetes foundation international; the national institute of diabetes and digestive and kidney diseases; and the american heart association. *Circulation*. 1999;100:1132-1133

3. Go AS, Chertow GM, Fan D, McCulloch CE, Hsu CY. Chronic kidney disease and the risks of death, cardiovascular events, and hospitalization. *N Engl J Med*. 2004;351:1296-1305

4. Huang PL. A comprehensive definition for metabolic syndrome. *Dis Model Mech*. 2009;2:231-237

5. Manrique C, Lastra G, Whaley-Connell A, Sowers JR. Hypertension and the cardiometabolic syndrome. *J Clin Hypertens (Greenwich)*. 2005;7:471-476

6. Dekker JM, Girman C, Rhodes T, Nijpels G, Stehouwer CD, Bouter LM, Heine RJ. Metabolic syndrome and 10-year cardiovascular disease risk in the hoorn study. *Circulation*. 2005;112:666-673

7. Stern MP, Williams K, Gonzalez-Villalpando C, Hunt KJ, Haffner SM. Does the metabolic syndrome improve identification of individuals at risk of type 2 diabetes and/or cardiovascular disease? *Diabetes Care*. 2004;27:2676-2681

8. Yoshioka M, Kayo T, Ikeda T, Koizumi A. A novel locus, mody4, distal to d7mit189 on chromosome 7 determines early-onset niddm in nonobese c57bl/6 (akita) mutant mice. *Diabetes*. 1997;46:887-894

9. Hsueh W, Abel ED, Breslow JL, Maeda N, Davis RC, Fisher EA, Dansky H, McClain DA, McIndoe R, Wassef MK, Rabadan-Diehl C, Goldberg IJ. Recipes for creating animal models of diabetic cardiovascular disease. *Circ Res*. 2007;100:1415-1427

10. Oudit GY, Sun H, Kerfant BG, Crackower MA, Penninger JM, Backx PH. The role of phosphoinositide-3 kinase and pten in cardiovascular physiology and disease. *J Mol Cell Cardiol*. 2004;37:449-471

11. Leth H, Andersen KK, Frystyk J, Tarnow L, Rossing P, Parving HH, Flyvbjerg A. Elevated levels of high-molecular-weight adiponectin in type 1 diabetes. *The Journal of clinical endocrinology and metabolism*. 2008;93:3186-3191

12. Kitzman DW, Little WC, Brubaker PH, Anderson RT, Hundley WG, Marburger CT, Brosnihan B, Morgan TM, Stewart KP. Pathophysiological characterization of isolated diastolic heart failure in comparison to systolic heart failure. *JAMA : the journal of the American Medical Association*. 2002;288:2144-2150

13. Aragno M, Mastrocola R, Alloatti G, Vercellinatto I, Bardini P, Geuna S, Catalano MG, Danni O, Boccuzzi G. Oxidative stress triggers cardiac fibrosis in the heart of diabetic rats. *Endocrinology*. 2008;149:380-388

14. Bugger H, Boudina S, Hu XX, Tuinei J, Zaha VG, Theobald HA, Yun UJ, McQueen AP, Wayment B, Litwin SE, Abel ED. Type 1 diabetic akita mouse hearts are insulin sensitive but manifest structurally abnormal mitochondria that remain coupled despite increased uncoupling protein 3. *Diabetes*. 2008;57:2924-2932

15. Asbun J, Villarreal FJ. The pathogenesis of myocardial fibrosis in the setting of diabetic cardiomyopathy. *J Am Coll Cardiol*. 2006;47:693-700

16. van Heerebeek L, Hamdani N, Handoko ML, Falcao-Pires I, Musters RJ, Kupreishvili K, Ijsselmuiden AJ, Schalkwijk CG, Bronzwaer JG, Diamant M, Borbely A, van der Velden J, Stienen GJ, Laarman GJ, Niessen HW, Paulus WJ. Diastolic stiffness of the failing diabetic heart: Importance of fibrosis, advanced glycation end products, and myocyte resting tension. *Circulation*. 2008;117:43-51

17. Chiu HC, Kovacs A, Ford DA, Hsu FF, Garcia R, Herrero P, Saffitz JE, Schaffer JE. A novel mouse model of lipotoxic cardiomyopathy. *J Clin Invest*. 2001;107:813-822

18. Levey AS, Andreoli SP, DuBose T, Provenzano R, Collins AJ. Chronic kidney disease: Common, harmful, and treatable--world kidney day 2007. *Clinical journal of the American Society of Nephrology : CJASN*. 2007;2:401-405

19. Coresh J, Selvin E, Stevens LA, Manzi J, Kusek JW, Eggers P, Van Lente F, Levey AS. Prevalence of chronic kidney disease in the united states. *JAMA : the journal of the American Medical Association*. 2007;298:2038-2047

20. Grundy SM, Benjamin IJ, Burke GL, Chait A, Eckel RH, Howard BV, Mitch W, Smith SC, Jr., Sowers JR. Diabetes and cardiovascular disease: A statement for healthcare professionals from the american heart association. *Circulation*. 1999;100:1134-1146

21. Ewens KG, George RA, Sharma K, Ziyadeh FN, Spielman RS. Assessment of 115 candidate genes for diabetic nephropathy by transmission/disequilibrium test. *Diabetes*. 2005;54:3305-3318

22. Woroniecka KI, Park AS, Mohtat D, Thomas DB, Pullman JM, Susztak K. Transcriptome analysis of human diabetic kidney disease. *Diabetes*. 2011;60:2354-2369

23. Chavers BM, Bilous RW, Ellis EN, Steffes MW, Mauer SM. Glomerular lesions and urinary albumin excretion in type i diabetes without overt proteinuria. *N Engl J Med*. 1989;320:966-970

24. Kassiri Z, Oudit GY, Sanchez O, Dawood F, Mohammed FF, Nuttall RK, Edwards DR, Liu PP, Backx PH, Khokha R. Combination of tumor necrosis factor-alpha ablation and matrix metalloproteinase inhibition prevents heart failure after pressure overload in tissue inhibitor of metalloproteinase-3 knock-out mice. *Circ Res*. 2005;97:380-390

25. Kandalam V, Basu R, Abraham T, Wang X, Awad A, Wang W, Lopaschuk GD, Maeda N, Oudit GY, Kassiri Z. Early activation of matrix metalloproteinases underlies the exacerbated systolic and diastolic dysfunction in mice lacking timp3 following myocardial infarction. *Am J Physiol Heart Circ Physiol*. 2010;299:H1012-1023

26. Kassiri Z, Oudit GY, Kandalam V, Awad A, Wang X, Ziou X, Maeda N, Herzenberg AM, Scholey JW. Loss of timp3 enhances interstitial nephritis and fibrosis. *J Am Soc Nephrol*. 2009;20:1223-1235

27. Cummins PM, von Offenberg Sweeney N, Killeen MT, Birney YA, Redmond EM, Cahill PA. Cyclic strain-mediated matrix metalloproteinase regulation within the vascular endothelium: A force to be reckoned with. *Am J Physiol Heart Circ Physiol*. 2007;292:H28-42

28. Wagenseil JE, Mecham RP. Vascular extracellular matrix and arterial mechanics. *Physiol Rev*. 2009;89:957-989

29. English JL, Kassiri Z, Koskivirta I, Atkinson SJ, Di Grappa M, Soloway PD, Nagase H, Vuorio E, Murphy G, Khokha R. Individual timp deficiencies differentially impact pro-mmp-2 activation. *J Biol Chem*. 2006;281:10337-10346

30. Sonksen P, Sonksen J. Insulin: Understanding its action in health and disease. *Br J Anaesth*. 2000;85:69-79

31. Wu P, Sato J, Zhao Y, Jaskiewicz J, Popov KM, Harris RA. Starvation and diabetes increase the amount of pyruvate dehydrogenase kinase isoenzyme 4 in rat heart. *Biochem J*. 1998;329 (Pt 1):197-201

32. Majer M, Popov KM, Harris RA, Bogardus C, Prochazka M. Insulin downregulates pyruvate dehydrogenase kinase (pdk) mrna: Potential mechanism contributing to increased lipid oxidation in insulin-resistant subjects. *Molecular genetics and metabolism*. 1998;65:181-186

33. Chess DJ, Stanley WC. Role of diet and fuel overabundance in the development and progression of heart failure. *Cardiovasc Res*. 2008;79:269-278

34. Szczepaniak LS, Victor RG, Orci L, Unger RH. Forgotten but not gone the rediscovery of fatty heart, the most common unrecognized disease in america. *Circulation Research*. 2007;101:759-767

35. Park TS, Hu Y, Noh HL, Drosatos K, Okajima K, Buchanan J, Tuinei J, Homma S, Jiang XC, Abel ED, Goldberg IJ. Ceramide is a cardiotoxin in lipotoxic cardiomyopathy. *J Lipid Res*. 2008;49:2101-2112

36. Demaurex N, Distelhorst C. Cell biology. Apoptosis--the calcium connection. *Science*. 2003;300:65-67

37. Nuttall RK, Sampieri CL, Pennington CJ, Gill SE, Schultz GA, Edwards DR. Expression analysis of the entire mmp and timp gene families during mouse tissue development. *FEBS Lett*. 2004;563:129-134

38. Uemura S, Matsushita H, Li W, Glassford AJ, Asagami T, Lee KH, Harrison DG, Tsao PS. Diabetes mellitus enhances vascular matrix metalloproteinase activity: Role of oxidative stress. *Circ Res*. 2001;88:1291-1298

39. Federici M, Menghini R, Mauriello A, Hribal ML, Ferrelli F, Lauro D, Sbraccia P, Spagnoli LG, Sesti G, Lauro R. Insulin-dependent activation of endothelial nitric oxide synthase is impaired by o-linked glycosylation modification of signaling proteins in human coronary endothelial cells. *Circulation*. 2002;106:466-472

40. Chung AW, Yang HH, Sigrist MK, Brin G, Chum E, Gourlay WA, Levin A. Matrix metalloproteinase-2 and -9 exacerbate arterial stiffening and angiogenesis in diabetes and chronic kidney disease. *Cardiovasc Res*. 2009;84:494-504

41. Cardellini M, Menghini R, Martelli E, Casagrande V, Marino A, Rizza S, Porzio O, Mauriello A, Solini A, Ippoliti A, Lauro R, Folli F, Federici M. Timp3 is reduced in atherosclerotic plaques from subjects with type 2 diabetes and increased by sirt1. *Diabetes*. 2009;58:2396-2401

42. Kassiri Z, Defamie V, Hariri M, Oudit GY, Anthwal S, Dawood F, Liu P, Khokha R. Simultaneous transforming growth factor beta-tumor necrosis factor activation and cross-talk cause aberrant remodeling response and myocardial fibrosis in timp3-deficient heart. *J Biol Chem*. 2009;284:29893-29904

43. Schenke-Layland K, Stock UA, Nsair A, Xie J, Angelis E, Fonseca CG, Larbig R, Mahajan A, Shivkumar K, Fishbein MC, MacLellan WR. Cardiomyopathy is associated with structural remodelling of heart valve extracellular matrix. *Eur Heart J*. 2009;30:2254-2265

44. Li Q, Sun SZ, Wang Y, Tian YJ, Liu MH. The roles of mmp-2/timp-2 in extracellular matrix remodelling in the hearts of stz-induced diabetic rats. *Acta Cardiol*. 2007;62:485-491

45. Federici M, Hribal ML, Menghini R, Kanno H, Marchetti V, Porzio O, Sunnarborg SW, Rizza S, Serino M, Cunsolo V, Lauro D, Mauriello A, Smookler DS, Sbraccia P, Sesti G, Lee DC, Khokha R, Accili D, Lauro R. Timp3 deficiency in insulin receptor-haploinsufficient mice promotes diabetes and vascular inflammation via increased tnf-alpha. *J Clin Invest*. 2005;115:3494-3505

46. Navarro-Gonzalez JF, Mora-Fernandez C. The role of inflammatory cytokines in diabetic nephropathy. *J Am Soc Nephrol*. 2008;19:433-442

47. Zheng Y, Saftig P, Hartmann D, Blobel C. Evaluation of the contribution of different adams to tumor necrosis factor alpha (tnfalpha) shedding and of the function of the tnfalpha ectodomain in ensuring selective stimulated shedding by the tnfalpha convertase (tace/adam17). *J Biol Chem*. 2004;279:42898-42906

48. Scivittaro V, Ganz MB, Weiss MF. Ages induce oxidative stress and activate protein kinase c-beta(ii) in neonatal mesangial cells. *Am J Physiol Renal Physiol*. 2000;278:F676-683

49. Catania JM, Chen G, Parrish AR. Role of matrix metalloproteinases in renal pathophysiologies. *Am J Physiol Renal Physiol*. 2007;292:F905-911

50. Williams JM, Zhang J, North P, Lacy S, Yakes M, Dahly-Vernon A, Roman RJ. Evaluation of metalloprotease inhibitors on hypertension and diabetic nephropathy. *Am J Physiol Renal Physiol*. 2011;300:F983-998

51. Kelly DJ, Zhang Y, Hepper C, Gow RM, Jaworski K, Kemp BE, Wilkinson-Berka JL, Gilbert RE. Protein kinase c beta inhibition attenuates the progression of experimental diabetic nephropathy in the presence of continued hypertension. *Diabetes*. 2003;52:512-518

52. Ohshiro Y, Ma RC, Yasuda Y, Hiraoka-Yamamoto J, Clermont AC, Isshiki K, Yagi K, Arikawa E, Kern TS, King GL. Reduction of diabetes-induced oxidative stress, fibrotic cytokine expression, and renal dysfunction in protein kinase cbeta-null mice. *Diabetes*. 2006;55:3112-3120

53. Furuichi K, Hisada Y, Shimizu M, Okumura T, Kitagawa K, Yoshimoto K, Iwata Y, Yokoyama H, Kaneko S, Wada T. Matrix metalloproteinase-2 (mmp-2) and membrane-type 1 mmp (mt1-mmp) affect the remodeling of glomerulosclerosis in diabetic oletf rats. *Nephrol Dial Transplant*. 2011;26:3124-3131

54. Thrailkill KM, Bunn RC, Moreau CS, Cockrell GE, Simpson PM, Coleman HN, Frindik JP, Kemp SF, Fowlkes JL. Matrix metalloproteinase-2 dysregulation in type 1 diabetes. *Diabetes Care*. 2007;30:2321-2326

55. Oudit GY, Liu GC, Zhong J, Basu R, Chow FL, Zhou J, Loibner H, Janzek E, Schuster M, Penninger JM, Herzenberg AM, Kassiri Z, Scholey JW. Human recombinant ace2 reduces the progression of diabetic nephropathy. *Diabetes*. 2010;59:529-538

56. Chacko BK, Reily C, Srivastava A, Johnson MS, Ye Y, Ulasova E, Agarwal A, Zinn KR, Murphy MP, Kalyanaraman B, Darley-Usmar V. Prevention of diabetic nephropathy in ins2(+/)(-)(akitaj) mice by the mitochondria-targeted therapy mitoq. *Biochem J*. 2010;432:9-19

57. Kang BP, Frencher S, Reddy V, Kessler A, Malhotra A, Meggs LG. High glucose promotes mesangial cell apoptosis by oxidant-dependent mechanism. *Am J Physiol Renal Physiol*. 2003;284:F455-466

58. Craven PA, Melhem MF, Phillips SL, DeRubertis FR. Overexpression of cu2+/zn2+ superoxide dismutase protects against early diabetic glomerular injury in transgenic mice. *Diabetes*. 2001;50:2114-2125

59. Tejada T, Catanuto P, Ijaz A, Santos JV, Xia X, Sanchez P, Sanabria N, Lenz O, Elliot SJ, Fornoni A. Failure to phosphorylate akt in podocytes from mice with early diabetic nephropathy promotes cell death. *Kidney Int*. 2008;73:1385-1393

60. Liu GC, Oudit GY, Fang F, Zhou J, Scholey JW. Angiotensin-(1-7)-induced activation of erk1/2 is camp/protein kinase a-dependent in glomerular mesangial cells. *Am J Physiol Renal Physiol*. 2012;302:F784-790

61. Moore L, Fan D, Basu R, Kandalam V, Kassiri Z. Tissue inhibitor of metalloproteinases (timps) in heart failure. *Heart Fail Rev*. 2012;17:693-706

62. Menghini R, Menini S, Amoruso R, Fiorentino L, Casagrande V, Marzano V, Tornei F, Bertucci P, Iacobini C, Serino M, Porzio O, Hribal ML, Folli F, Khokha R, Urbani A, Lauro R, Pugliese G, Federici M. Tissue inhibitor of metalloproteinase 3 deficiency causes hepatic steatosis and adipose tissue inflammation in mice. *Gastroenterology*. 2009;136:663-672.e664

63. Inada A, Nagai K, Arai H, Miyazaki J, Nomura K, Kanamori H, Toyokuni S, Yamada Y, Bonner-Weir S, Weir GC, Fukatsu A, Seino Y. Establishment of a diabetic mouse model with progressive diabetic nephropathy. *Am J Pathol*. 2005;167:327-336

64. McLennan SV, Kelly DJ, Cox AJ, Cao Z, Lyons JG, Yue DK, Gilbert RE. Decreased matrix degradation in diabetic nephropathy: Effects of ace inhibition on the expression and activities of matrix metalloproteinases. *Diabetologia*. 2002;45:268-275

65. Wu K, Setty S, Mauer SM, Killen P, Nagase H, Michael AF, Tsilibary EC. Altered kidney matrix gene expression in early stages of experimental diabetes. *Acta Anat (Basel)*. 1997;158:155-165

66. Han SY, Jee YH, Han KH, Kang YS, Kim HK, Han JY, Kim YS, Cha DR. An imbalance between matrix metalloproteinase-2 and tissue inhibitor of matrix metalloproteinase-2 contributes to the development of early diabetic nephropathy. *Nephrol Dial Transplant*. 2006;21:2406-2416

67. Rojek A, Nielsen J, Brooks HL, Gong H, Kim YH, Kwon TH, Frokiaer J, Nielsen S. Altered expression of selected genes in kidney of rats with lithium-induced ndi. *Am J Physiol Renal Physiol*. 2005;288:F1276-1289

68. Intengan HD, Schiffrin EL. Structure and mechanical properties of resistance arteries in hypertension: Role of adhesion molecules and extracellular matrix determinants. *Hypertension*. 2000;36:312-318

69. Murphy G, Nagase H. Progress in matrix metalloproteinase research. *Molecular aspects of medicine*. 2008;29:290-308

70. Nagase H, Woessner JF. Matrix metalloproteinases. *Journal of Biological Chemistry*. 1999;274:21491-21494

71. Aimes RT, Quigley JP. Matrix metalloproteinase-2 is an interstitial collagenase. Inhibitor-free enzyme catalyzes the cleavage of collagen fibrils and soluble native type i collagen generating the specific 3/4- and 1/4-length fragments. *J Biol Chem*. 1995;270:5872-5876

72. Shipley JM, Doyle GA, Fliszar CJ, Ye QZ, Johnson LL, Shapiro SD, Welgus HG, Senior RM. The structural basis for the elastolytic activity of the 92-kda and 72-kda gelatinases. Role of the fibronectin type ii-like repeats. *J Biol Chem*. 1996;271:4335-4341

73. Murphy G, Nguyen Q, Cockett MI, Atkinson SJ, Allan JA, Knight CG, Willenbrock F, Docherty AJ. Assessment of the role of the fibronectin-like domain of gelatinase a by analysis of a deletion mutant. *J Biol Chem*. 1994;269:6632-6636

74. Esparza J, Kruse M, Lee J, Michaud M, Madri JA. Mmp-2 null mice exhibit an early onset and severe experimental autoimmune encephalomyelitis due to an increase in mmp-9 expression and activity. *FASEB J*. 2004;18:1682-1691

75. Goodall S, Crowther M, Hemingway DM, Bell PR, Thompson MM. Ubiquitous elevation of matrix metalloproteinase-2 expression in the vasculature of patients with abdominal aneurysms. *Circulation*. 2001;104:304-309

76. Crowther M, Goodall S, Jones JL, Bell PR, Thompson MM. Localization of matrix metalloproteinase 2 within the aneurysmal and normal aortic wall. *Br J Surg*. 2000;87:1391-1400

77. Freestone T, Turner RJ, Coady A, Higman DJ, Greenhalgh RM, Powell JT. Inflammation and matrix metalloproteinases in the enlarging abdominal aortic aneurysm. *Arterioscler Thromb Vasc Biol*. 1995;15:1145-1151

78. Thompson RW, Holmes DR, Mertens RA, Liao S, Botney MD, Mecham RP, Welgus HG, Parks WC. Production and localization of 92-kilodalton gelatinase in abdominal aortic aneurysms. An elastolytic metalloproteinase expressed by aneurysm-infiltrating macrophages. *J Clin Invest*. 1995;96:318-326

79. Pyo R, Lee JK, Shipley JM, Curci JA, Mao D, Ziporin SJ, Ennis TL, Shapiro SD, Senior RM, Thompson RW. Targeted gene disruption of matrix metalloproteinase-9 (gelatinase b) suppresses development of

experimental abdominal aortic aneurysms. *J Clin Invest*. 2000;105:1641-1649

80. Murphy G, Houbrechts A, Cockett MI, Williamson RA, O'Shea M, Docherty AJ. The n-terminal domain of tissue inhibitor of metalloproteinases retains metalloproteinase inhibitory activity. *Biochemistry*. 1991;30:8097-8102

81. Longo GM, Xiong W, Greiner TC, Zhao Y, Fiotti N, Baxter BT. Matrix metalloproteinases 2 and 9 work in concert to produce aortic aneurysms. *J Clin Invest*. 2002;110:625-632

82. Lorente L, Martin MM, Labarta L, Diaz C, Sole-Violan J, Blanquer J, Orbe J, Rodriguez JA, Jimenez A, Borreguero-Leon JM, Belmonte F, Medina JC, Lliminana MC, Ferrer-Aguero JM, Ferreres J, Mora ML, Lubillo S, Sanchez M, Barrios Y, Sierra A, Paramo JA. Matrix metalloproteinase-9, -10, and tissue inhibitor of matrix metalloproteinases-1 blood levels as biomarkers of severity and mortality in sepsis. *Critical care (London, England)*. 2009;13:R158

83. Davis V, Persidskaia R, Baca-Regen L, Itoh Y, Nagase H, Persidsky Y, Ghorpade A, Baxter BT. Matrix metalloproteinase-2 production and its binding to the matrix are increased in abdominal aortic aneurysms. *Arterioscler Thromb Vasc Biol*. 1998;18:1625-1633

84. Hance KA, Tataria M, Ziporin SJ, Lee JK, Thompson RW. Monocyte chemotactic activity in human abdominal aortic aneurysms: Role of elastin degradation peptides and the 67-kd cell surface elastin receptor. *J Vasc Surg*. 2002;35:254-261

85. Cuadrado E, Ortega L, Hernandez-Guillamon M, Penalba A, Fernandez-Cadenas I, Rosell A, Montaner J. Tissue plasminogen activator (t-pa) promotes neutrophil degranulation and mmp-9 release. *Journal of leukocyte biology*. 2008;84:207-214

86. Lambert JM, Lopez EF, Lindsey ML. Macrophage roles following myocardial infarction. *International journal of cardiology*. 2008;130:147-158

87. Shapiro SD, Campbell EJ, Welgus HG, Senior RM. Elastin degradation by mononuclear phagocytesa. *Annals of the New York Academy of Sciences*. 1991;624:69-80

88. Shapiro SD, Campbell EJ, Senior RM, Welgus HG. Proteinases secreted by human mononuclear phagocytes. *The Journal of rheumatology. Supplement*. 1991;27:95-98

CHAPTER EIGHT

LIMITATIONS AND FUTURE DIRECTIONS

8.1 LIMITATIONS

8.1.1 Mechanistic Limitation in the Study of Diabetic Cardiomyopathy

Insulin treatment reversed the early diastolic dysfunction of type I diabetic cardiomyopathy, however, it remains unclear whether the improvement was due to the direct effects of insulin or due to the correction of hyperglycaemia. Cultured rat cardiac myocytes and fibroblasts showed differential responses to high glucose and high insulin concentrations[1]. High glucose concentrations increased collagen synthesis and mRNA expression of fibronectin and transforming growth factor-β1 (TGF-β1) only in cardiac fibroblast, whereas high insulin concentrations increased DNA and collagen synthesis in fibroblasts and elevated protein synthesis and ANP secretion in cardiomyocytes[1]. To dissect the role of insulin versus hyperglycaemia we need *in vitro* studies with cardiomyocyte and fibroblast cultures and subjected to separate conditions simulating either high insulin or high glucose levels conditions found in diabetes. Moreover, the majority of the world's diabetic population is comprised of type 2 and the cardiomyopathy associated with diabetes type 2 is characterized by increased myocardial interstitial fibrosis, inflammation, vasoconstriction and endothelial dysfunction[2-4]. Hence findings of cardiomyopathy related to type 2 diabetic model would be more relevant in the setting of insulin resistance and hyperglycemia. Moreover, alterations in SERCA protein levels in the Akita hearts indicated an indirect evidence of impaired calcium handling without providing an explicit

underlying mechanism of diastolic dysfunction. Additional investigations such as measurements of calcium transients in isolated cardiac myocyte in a hyperglycemic environment would further enrich our understanding of the impaired calcium regulation in diabetic cardiomyopathy. Although the majority of the cytosolic calcium uptake is due to SERCA protein in murine cardiomyocyte, alterations of other proteins such as sodium-calcium exchanger (NCX) underlying decreased calcium transient in diabetic cardiomyopathy has been reported earlier[5]. My study lacks any additional contributions of other Ca^{2+} transport proteins but was restricted to SERCA in the understanding of diastolic dysfunction.

8.1.2 Organ Specific and Conditional Gene Deletion in Experimental Disease Models

In our studies we utilized whole body knockout for TIMP3 and MMP2 deficiency. Additionally, to dissect the causal role of a protein in a disease process, organ or even cell specific deletion of the gene responsible for transcription would be more relevant. The advantages of murine models in our study over many large animals include a small gestation period, large litter size and above all the ease in genetic manipulation of an already sequenced genome. However, a whole body gene knock out from birth is not devoid of compounding effects of its deletion from other organs and still remains far from being physiological or mimic pathological conditions seen in humans. .However, conditional and organ specific gene knockout of TIMP3 from mesangial, tubulointerstitial cells of kidneys in our diabetic nephropathy project would have been a more relevant approach thus limiting the effects of TIMP3 deletion in renal specific cells.

Unfortunately, it still remains unknown as which cell type is responsible for expression of TIMP3 for its compensatory role in diabetic renal injury. Moreover, deletion of TIMP3 in glomerular specific cells in the background of Akita would more explicitly explain the role of this protein in diabetic glomerular injury. Additionally, inflammatory processes involving immune derived cells such as macrophage infiltration are recognized as potential factors in the progression of diabetic nephropathy[6, 7]. Moreover, TIMP3 deletion in these immune derived cells in the background of diabetes and any alterations of their migration and proliferative properties in association of diabetic nephropathy needs to be explored that was out of scope in our studies. Similarly, compounding effects of TIMP3 deletion in endothelial cells would allow a more specific role of TIMP3 in the agonist induced vascular remodelling projects if vascular smooth muscle cell specific knock outs were used instead of whole body deletion.

8.1.3 Lack of Temporal Changes in the Pathogenesis of Vascular Disease

Tissues were harvested in studies involving agonist infusion after 2 or 4 weeks from the day of infusion for molecular work. As all the changes in protein levels and the enzymatic activities were assessed either at 2 or 4 weeks post Ang II pump implantation that lacked to reveal any molecular perturbation during the course of infusion. A time course analysis of these parameters would provide insight into the order of events that may lead to better understanding of the subtle changes that would be essential in developing any potential therapeutic intervention. The time course of development of aneurysm may involve early

events such as aortic dissection [8] that could not be captured in ultrasound performed at 2 and 4 week post implantation of osmotic pumps.

8.1.4 MMP Inhibitors as Prevention and not as Treatment

In our vascular studies, we used doxycycline and PD166793 as a broad spectrum inhibitor for 2 and 4 weeks respectively. However these MMP inhibitors were provided in the form of daily gavage during the course of Ang II infusion. Although, they provided essential insight into the proteolytic mechanism of MMPs underlying the disease processes, they cannot be regarded as a true treatment procedure. Moreover, these broad spectrum MMP inhibitors were administered prior to the pathological proteolytic degradation of the arterial ECM and provide good evidence for prevention rather than abrogation of a preformed pathology. Further investigation involving treatment with these broad spectrum MMP inhibitors after establishment of aortic pathology via ultrasonography would definitely prove more physiologically relevant approach in the therapeutics of vascular pathology.

8.2 FUTURE DIRECTIONS

8.2.1 The Role of TIMP3 in Type 2 Diabetic Cardiomyopathy

TIMP3 is one of the highest expressed TIMPs in the mouse heart. Apart from being altered in several heart diseases [9-11] its role in metabolic diseases are yet to be explored. However, a study investigating candidate genetic association for metabolic disease revealed TIMP3 gene among quantitative trait loci associated with diabetes and dyslipidemia [12]. Previous study involving heterozygosity for

null insulin receptor allele (I*nsr*$^{+/-}$) showed variable degrees of insulin resistance due to different environmental factors and genetic modifiers [13]. Additionally, sub-population of I*nsr*$^{+/-}$ mice that develop diabetes type 2 (I*nsr*$^{+/-}$D, hyperglycaemic and hyperinsulinemic) show down regulation of TIMP3 expression compared to the non-diabetic sub-population of these mice (I*nsr*$^{+/-}$ N, Normoglycaemic)[14]. Furthermore, TIMP3-deficiency in insulin receptor haplosufficiency background leads to overt hyperglycemia and hyperinsulinemia in all I*nsr*$^{+/-}$ mice[14]. Deficiency of TIMP3 resulted in dilated cardiomyopathy with contractile dysfunction and progressive cardiac remodelling in 21 months aged mice comparable to human heart failure[15]. Nevertheless, the role of TIMP3 in cardiomyopathy secondary to diabetes type 2 has not been investigated. I intend to study further the role of TIMP3 in an experimental animal model of diabetes associated with obesity and traits of metabolic abnormalities due to impairment in leptin signaling such as *db/db* mice. This mice harbour a point mutation in the gene responsible for leptin receptor isoform (ObRb) that is ubiquitously expressed in mamalian tissue with abundance in the hypothalamus[16]. Moreover, db/db mice is accompanied by insulin resistance[17], dyslipidemia[18] and impaired glucose tolerance, thus mimics the disease processes in humans associated with metabolic syndrome. In addition to cardiac dysfunction, TIMP3 has been identified as the link between insulin resistance and vascular inflammation[19]. I would further investigate the role of TIMP3 in remodeling of vascular ECM and inflammatory processes associated with vasculopathy in diabetes type 2.

8.2.2 The Role of TIMP3 in Agonist Induced Fibrosis

Adult mouse fibroblast (FB) are known to express at least six different types of MMPs of which four belong to the family of secreted collagenases (MMP-2, MMP-8, MMP-9, MMP-13) and the membrane bound MMPs (MT1-MMP, MT3-MMP) [20]. MMPs are the key molecules of fibroblast-mediated collagen degradation. Fibroblasts also have the ability to degrade collagen type I, the predominant fibrillar proteins in the ECM, via secreted collagenases [21, 22] and to invade tissues due to the membrane bound MT1-MMP[23]. Previous study has shown that TIMP3 deficient mice exhibit severe myocardial fibrosis following pressure overload[11]. However, complete characterization of fibrosis after agonist infusion such as Ang II which is a well-known fibrogenic agonist [24] in heart, vessels and kidneys is still lacking in the literature. We will use cultured adult cardiofibroblast to determine the mechanism of fibrogenic potency of TIMP3-deficient fibroblasts in response to Ang II. Additionally, it would be explanatory to examine if cultured cardiac FB lacking TIMP3 express greater levels of ECM proteins. Previous study from our lab has explicitly shown that TIMP3 deficiency resulted in increased peritubular interstitial fibrosis and enhanced collagen I accumulation in the renal fibrotic lesion after unilateral ureteric obstruction mimicking human obstructive nephropathy[25]. While, fibroblasts remains the main source of excessive interstitial collagen produced in renal injury [26] it is essential to determine if the greater collagen production in TIMP3 deficient renal FB is due to higher rate of proliferation of these fibroblasts which can lead to increased collagen production in these mice.

8.2.3 TIMP3 Replenishment in the Treatment of Diabetic Nephropathy and AAA

Establishment of the critical role of TIMP3 in diabetic nephropathy and agonist induced AAA in TIMP3 deficient mice has paved the way for an exciting arena of replenishing this protein in order to investigate its therapeutic potentiality. Conventional approach of introducing TIMP3 in the diseased organ stems from futile methods of delivery and a lack of prolong effect due to its short half-life in the tissue. Gene base therapy with replication defective adenoviral and adeno-associated viral vector has been used in earlier studies of vascular gene transfer with significant success[27, 28]. However, non-viral vectors such cationic liposomes and naked plasmid DNA have proved safer than viral vectors but resulted in restricted efficiency. Nonetheless, combined forms of replication defective adeno virus with conjugated vectors are designed to overcome efficiency and specificity issues[28]. The primary effect of TIMP3 gene therapy either in the aorta for AAA and in the kidney of diabetic animal models would be based on the enhancement of endogenous TIMP3 specific to these organs and sparing rest of the body. Many clinical trials regarding gene therapy involving humans are under way, however only a hand full of them is associated with vascular disease[29, 30]. Although systemic gene therapy in the cardiovascular system has shown promising results in areas of atherosclerosis and hyperlipidemia, most of the adenoviral vector infusion resulted in hepatic accumulation and expression. Treatment of AAA using gene therapy would need local expression of TIMP3 gene at the aneurysmal site as oppose to systemic therapy to avoid iatrogenic effects at other healthy and

prevent dilution of the therapeutic concentration of the vector[31]. One of the simplest methods of local gene transfer in the artery is known as the "dwell method"[32-34]. This method comprises of surgical isolation of the arterial segment of interest held between 2 temporary ligatures. Solution containing the vector is introduced after withdrawal of blood from the lumen of the target segment. The solution is further allowed to incubate before being withdrawn and circulation restored in the area[28]. However,, replenishment of a gene of interest in the area of vascular gene therapy depends on the efficiency of delivery. Ironically, delivery efficiency is amplified in vascular pathology with a breached endothelium. Histopathological evidence from murine aortic aneurysmal samples in our study has shown focal degradation of structural proteins in the media and a breached endothelial layer. Hence effective medial gene transfer may be more efficiently achieved due an impaired endothelial barrier in diseases like AAA[31]. Besides, to overcome the difficulties in delivery efficiency, approaches such as indirect and direct gene transfer in the arterial system has been performed previously. The indirect transfer involves the transfection of vascular cells with the virus *in vitro* before being transplanted into the arterial area of interest[35]and specific to smooth muscle cells[36]. The direct method on the contrary involves direct introduction of the transgene via catheter[37] or surgically[38]. However, the endothelium and the internal elastic lamina proves the main barrier for adequate arterial gene transfer[39]. Renal specific gene transfer share many commonalities with vascular gene therapy as discussed above and has proven successful in abrogating kidney disease in animal model of experimental glomerulonephritis[40].

8.2.4 Aortic Aneurysm Studies on Females

Our study on AAA was primarily aimed to investigate the causal role of TIMP3 and experiments were performed using male mice as AAA is approximately 6 times more prevalent in men than women[41, 42]. However, once the disease develops females are known to have a severe course of the disease with increased rate of rupture and poor prognosis[43]. The female sex specific protection and detoriated prognosis of AAA needs further investigation in terms of the roleof TIMP3 and a possible effect of oestrogen.

8.3 REFERENCES

1. Tokudome T, Horio T, Yoshihara F, Suga S, Kawano Y, Kohno M, Kangawa K. Direct effects of high glucose and insulin on protein synthesis in cultured cardiac myocytes and DNA and collagen synthesis in cardiac fibroblasts. *Metabolism*. 2004;53:710-715

2. Aragno M, Mastrocola R, Alloatti G, Vercellinatto I, Bardini P, Geuna S, Catalano MG, Danni O, Boccuzzi G. Oxidative stress triggers cardiac fibrosis in the heart of diabetic rats. *Endocrinology*. 2008;149:380-388

3. King GL. The role of inflammatory cytokines in diabetes and its complications. *Journal of periodontology*. 2008;79:1527-1534

4. Hotamisligil G. Inflammatory pathways and insulin action. *International Journal of Obesity*. 2003;27:S53-S55

5. Pereira L, Matthes J, Schuster I, Valdivia HH, Herzig S, Richard S, Gomez AM. Mechanisms of [ca2+]i transient decrease in cardiomyopathy of db/db type 2 diabetic mice. *Diabetes*. 2006;55:608-615

6. Furuta T, Saito T, Ootaka T, Soma J, Obara K, Abe K, Yoshinaga K. The role of macrophages in diabetic glomerulosclerosis. *Am J Kidney Dis*. 1993;21:480-485

7. Chow F, Ozols E, Nikolic-Paterson DJ, Atkins RC, Tesch GH. Macrophages in mouse type 2 diabetic nephropathy: Correlation with diabetic state and progressive renal injury. *Kidney Int*. 2004;65:116-128

8. Cao RY, Amand T, Ford MD, Piomelli U, Funk CD. The murine angiotensin ii-induced abdominal aortic aneurysm model: Rupture risk and inflammatory progression patterns. *Front Pharmacol*.1:9

9. Kassiri Z, Oudit GY, Sanchez O, Dawood F, Mohammed FF, Nuttall RK, Edwards DR, Liu PP, Backx PH, Khokha R. Combination of tumor necrosis factor-alpha ablation and matrix metalloproteinase inhibition prevents heart failure after pressure overload in tissue inhibitor of metalloproteinase-3 knock-out mice. *Circ Res*. 2005;97:380-390

10. Kandalam V, Basu R, Abraham T, Wang X, Awad A, Wang W, Lopaschuk GD, Maeda N, Oudit GY, Kassiri Z. Early activation of matrix metalloproteinases underlies the exacerbated systolic and diastolic dysfunction in mice lacking timp3 following myocardial infarction. *Am J Physiol Heart Circ Physiol*. 2010;299:H1012-1023

11. Kassiri Z, Defamie V, Hariri M, Oudit GY, Anthwal S, Dawood F, Liu P, Khokha R. Simultaneous transforming growth factor beta-tumor necrosis factor activation and cross-talk cause aberrant remodeling response and myocardial fibrosis in timp3-deficient heart. *J Biol Chem*. 2009;284:29893-29904

12. Su Z, Tsaih SW, Szatkiewicz J, Shen Y, Paigen B. Candidate genes for plasma triglyceride, ffa, and glucose revealed from an intercross between inbred mouse strains nzb/b1nj and nzw/lacj. *J Lipid Res*. 2008;49:1500-1510

13. Kido Y, Philippe N, Schaffer AA, Accili D. Genetic modifiers of the insulin resistance phenotype in mice. *Diabetes*. 2000;49:589-596

14. Federici M, Hribal ML, Menghini R, Kanno H, Marchetti V, Porzio O, Sunnarborg SW, Rizza S, Serino M, Cunsolo V, Lauro D, Mauriello A, Smookler DS, Sbraccia P, Sesti G, Lee DC, Khokha R, Accili D, Lauro R. Timp3 deficiency in insulin receptor-haploinsufficient mice promotes diabetes and vascular inflammation via increased tnf-alpha. *J Clin Invest*. 2005;115:3494-3505

15. Fedak PW, Smookler DS, Kassiri Z, Ohno N, Leco KJ, Verma S, Mickle DA, Watson KL, Hojilla CV, Cruz W, Weisel RD, Li RK, Khokha R. Timp-3 deficiency leads to dilated cardiomyopathy. *Circulation*. 2004;110:2401-2409

16. Tartaglia LA. The leptin receptor. *J Biol Chem*. 1997;272:6093-6096

17. Koranyi L, James D, Mueckler M, Permutt MA. Glucose transporter levels in spontaneously obese (db/db) insulin-resistant mice. *J Clin Invest*. 1990;85:962-967

18. Kobayashi K, Forte TM, Taniguchi S, Ishida BY, Oka K, Chan L. The db/db mouse, a model for diabetic dyslipidemia: Molecular characterization and effects of western diet feeding. *Metabolism*. 2000;49:22-31

19. Menghini R, Menini S, Amoruso R, Fiorentino L, Casagrande V, Marzano V, Tornei F, Bertucci P, Iacobini C, Serino M, Porzio O, Hribal ML, Folli F, Khokha R, Urbani A, Lauro R, Pugliese G, Federici M. Tissue inhibitor of metalloproteinase 3 deficiency causes hepatic steatosis and adipose tissue inflammation in mice. *Gastroenterology*. 2009;136:663-672.e664

20. Sabeh F, Ota I, Holmbeck K, Birkedal-Hansen H, Soloway P, Balbin M, Lopez-Otin C, Shapiro S, Inada M, Krane S, Allen E, Chung D, Weiss SJ. Tumor cell traffic through the extracellular matrix is controlled by the

membrane-anchored collagenase mt1-mmp. *The Journal of cell biology*. 2004;167:769-781

21. Lee H, Overall CM, McCulloch CA, Sodek J. A critical role for the membrane-type 1 matrix metalloproteinase in collagen phagocytosis. *Molecular biology of the cell*. 2006;17:4812-4826

22. Madsen DH, Engelholm LH, Ingvarsen S, Hillig T, Wagenaar-Miller RA, Kjoller L, Gardsvoll H, Hoyer-Hansen G, Holmbeck K, Bugge TH, Behrendt N. Extracellular collagenases and the endocytic receptor, urokinase plasminogen activator receptor-associated protein/endo180, cooperate in fibroblast-mediated collagen degradation. *J Biol Chem*. 2007;282:27037-27045

23. Sabeh F, Li XY, Saunders TL, Rowe RG, Weiss SJ. Secreted versus membrane-anchored collagenases: Relative roles in fibroblast-dependent collagenolysis and invasion. *J Biol Chem*. 2009;284:23001-23011

24. Zhong J, Basu R, Guo D, Chow FL, Byrns S, Schuster M, Loibner H, Wang XH, Penninger JM, Kassiri Z, Oudit GY. Angiotensin-converting enzyme 2 suppresses pathological hypertrophy, myocardial fibrosis, and cardiac dysfunction. *Circulation*. 2010;122:717-728, 718 p following 728

25. Kassiri Z, Oudit GY, Kandalam V, Awad A, Wang X, Ziou X, Maeda N, Herzenberg AM, Scholey JW. Loss of timp3 enhances interstitial nephritis and fibrosis. *J Am Soc Nephrol*. 2009;20:1223-1235

26. Cook HT. The origin of renal fibroblasts and progression of kidney disease. *Am J Pathol*.176:22-24

27. DeYoung MB, Zamarron C, Lin AP, Qiu C, Driscoll RM, Dichek DA. Optimizing vascular gene transfer of plasminogen activator inhibitor 1. *Hum Gene Ther*. 1999;10:1469-1478

28. Feldman LJ, Steg G. Optimal techniques for arterial gene transfer. *Cardiovasc Res*. 1997;35:391-404

29. Anderson WF. Human gene therapy. *Nature*. 1998;392:25-30

30. Mann MJ, Whittemore AD, Donaldson MC, Belkin M, Conte MS, Polak JF, Orav EJ, Ehsan A, Dell'Acqua G, Dzau VJ. Ex-vivo gene therapy of human vascular bypass grafts with e2f decoy: The prevent single-centre, randomised, controlled trial. *Lancet*. 1999;354:1493-1498

31. Ballermann BJ. Gene therapy in the vasculature and the kidney. *Nefrologia*. 2000;20 Suppl 2:19-24

32. Lemarchand P, Jones M, Yamada I, Crystal RG. In vivo gene transfer and expression in normal uninjured blood vessels using replication-deficient recombinant adenovirus vectors. *Circ Res*. 1993;72:1132-1138

33. Guzman RJ, Lemarchand P, Crystal RG, Epstein SE, Finkel T. Efficient and selective adenovirus-mediated gene transfer into vascular neointima. *Circulation*. 1993;88:2838-2848

34. Riessen R, Isner JM. Prospects for site-specific delivery of pharmacologic and molecular therapies. *J Am Coll Cardiol*. 1994;23:1234-1244

35. Nabel EG, Plautz G, Boyce FM, Stanley JC, Nabel GJ. Recombinant gene expression in vivo within endothelial cells of the arterial wall. *Science*. 1989;244:1342-1344

36. Plautz G, Nabel EG, Nabel GJ. Introduction of vascular smooth muscle cells expressing recombinant genes in vivo. *Circulation*. 1991;83:578-583

37. Nabel EG, Plautz G, Nabel GJ. Site-specific gene expression in vivo by direct gene transfer into the arterial wall. *Science*. 1990;249:1285-1288

38. Feldman LJ, Pastore CJ, Aubailly N, Kearney M, Chen D, Perricaudet M, Steg PG, Isner JM. Improved efficiency of arterial gene transfer by use of poloxamer 407 as a vehicle for adenoviral vectors. *Gene Ther*. 1997;4:189-198

39. Rome JJ, Shayani V, Flugelman MY, Newman KD, Farb A, Virmani R, Dichek DA. Anatomic barriers influence the distribution of in vivo gene transfer into the arterial wall. Modeling with microscopic tracer particles and verification with a recombinant adenoviral vector. *Arterioscler Thromb*. 1994;14:148-161

40. Basile DP. Toward an effective gene therapy in renal disease. *Kidney Int*. 1999;55:740-741

41. Scott RA, Bridgewater SG, Ashton HA. Randomized clinical trial of screening for abdominal aortic aneurysm in women. *Br J Surg*. 2002;89:283-285

42. Pleumeekers HJ, Hoes AW, van der Does E, van Urk H, Hofman A, de Jong PT, Grobbee DE. Aneurysms of the abdominal aorta in older adults. The rotterdam study. *Am J Epidemiol*. 1995;142:1291-1299

43. Norman PE, Powell JT. Abdominal aortic aneurysm: The prognosis in women is worse than in men. *Circulation*. 2007;115:2865-2869